Dissertation
submitted to
the Combined Faculties for the Natural Sciences
and for Mathematics
of the Ruperto-Carola University of Heidelberg,
Germany
for the degree of
Doctor of Natural Sciences

presented by

Ibrahim Murathan Sektioglu (M.Sc.)
born in Bursa, Turkey

Oral-examination:
16.07.2015

Control of
T cell infiltration and tumor rejection by regulatory T cells, basophils and macrophages

First examiner: Prof. Dr. Hans-Reimer Rodewald

Second Examiner: Prof. Dr. Günter J. Hämmerling

ACKNOWLEDGEMENTS

This PhD thesis was completed in the Division of Molecular Immunology at German Cancer Research Center (DKFZ) in Heidelberg, Germany with the priceless help of many people.

Foremost, I would like to express my sincere gratitude to my supervisor Prof. Dr. Günter J. Hämmerling for the continuous support of my PhD study and research, for his patience, motivation, enthusiasm, and immense knowledge. His guidance helped me in all the time of research and writing of this thesis.

I also thank Dr. Rafael Carretero-Coca for his valuable ideas and stimulating discussions throughout my time as a PhD student. I also thank him sharing his vast experience in laboratory techniques with me.

I am very grateful to Nadja Bulbuc, who contributed to this project as an expert technician. I also would like to thank Sabine Schmidt, Elke Deibel and Barbara Goedecke for their help in animal experiments.

Special thanks go to Prof. Dr. Hans-Reimer Rodewald, Prof. Dr. Michael Brunner and Dr. Grant Hansman , who agreed to be members of my PhD defence committee.

Finally, I want to thank Carolin for her selfless support and encouragement.

Biricik annem ve babama sonsuz sevgileri ve destekleri için teşekkür ediyorum. Sizleri çok seviyorum!

ABSTRACT

Most solid tumors are intrinsically resistant to immune rejection due to immunosuppressive mechanisms operative within the tumor microenvironment. Cancer patients frequently harbor elevated numbers of regulatory T cells (Tregs), which inhibit efficient anti-tumor T cell responses. We employed different mouse models for Treg depletion in order to study the mechanisms that control tumor rejection. Depletion of about 99% Tregs in Foxp3^{DTR} knock-in mice resulted in complete rejection of transplanted HCmel 1274 and B16 melanomas in a CD8$^+$ T cell-dependent way. In contrast, about 90% Treg depletion in BAC transgenic Foxp3.LuciDTR4 mice failed to induce complete rejection of HCmel 1274 and B16, demonstrating that low numbers of Tregs were able to control CD8$^+$ T cell responses against the tumor. Treg depletion provoked drastic changes within tumor microenvironment, such as cytokine storm and strong infiltration of CD8$^+$ T cells. In addition, substantial infiltration of basophils was observed. This study reported for the first time that tumor-associated basophils play a crucial role in tumor rejection. These intratumoral basophils produced large amounts of chemokines such as CCL3 and CCL4 that were found to be responsible fo the infiltration of tumor-specific CD8$^+$ T cells into the tumor. IFN-γ produced by these CD8$^+$ T cells resulted in skewing of tumor-associated macrophages from a M2-like phenotype to a M1-like phenotype. In a feedback mechanism, the M1-like macrophages potentiated infiltration of CD8$^+$ T cells by secreting potent CD8$^+$ T cell chemoattractants, including CCL2, CXCL9 and CXCL10, and by inducing normalization of the tumor vasculature.

The mechanisms of tumor rejection were also investigated in a second tumor model. Rip1-Tag5 (RT5) mice develop spontaneously pancreatic cancer, which precisely reflects the clinical development of pancreatic neuroendocrine tumors. Like almost all human and rodent tumors, these insulinomas contain an abnormal tumor vasculature, which acts as a barrier for T cell migration into the tumor. Thus, treatment of Rip1-Tag5 mice with adoptively transferred T cells failed to eradicate the tumors. However, when T cell transfer was combined with CpG-ODN as an inducer of pro-inflammatory signals, upregulation of T cell adhesion molecules such as VCAM-1 on the tumor endothelium was observed, as well as strong infiltration of T

cells, prolonged survival of tumor-bearing mice. Of note, CpG-ODN was found to bind to $CD206^+$ $iNOS^-$ M2-like macrophages and to polarize them into $CD206^-$ $iNOS^+$ M1-like macrophages. Depletion of macrophages and blockade of iNOS revealed that the iNOS activity by the M1-skewed tumor macrophages was responsible for the increased VCAM-1 expression on the tumor endothelium and for the subsequent T cell infiltration and tumor rejection. Notably, transfer of pre-activated $iNOS^+$ macrophages in combination with tumor-specific $CD8^+$ T cells, in the absence of additional CpG-ODN, was also able to promote VCAM-1 expression and T cell infiltration. In contrast, iNOS-deficient macrophages failed to do so, highlighting the critical role of NO production by M1-polarized tumor macrophages. In vitro, incubation of human endothelial cells with iNOS-expressing human macrophages or with the NO donor GTN induced expression of adhesion molecules, such as VCAM-1, ICAM-1 and E-selectin, but only with low doses of GTN, whereas higher doses resulted in inhibition. Thus, these results indicate that NO production by M1-polarized tumor macrophages is a critical step in tumor therapy.

Together, the data from both mouse models show that adoptive T cell therapy and basophil/macrophage targeting strategies, or co-transfer of M1-polarized macrophages are able to evoke efficient T cell infiltration and tumor rejection. These findings have implications for immunotherapeutic interventions in cancer patients.

ZUSAMMENFASSUNG

Der Großteil solider Tumoren besitzt aufgrund immunsuppressiver Mechanismen, die ihre Aktivitäten in der Mikroumgebung des Tumors entfalten, eine intrinsische Resistenz gegenüber immunologischen Abstoßungsmechanismen. Tumorpatienten weisen häufig eine erhöhte Anzahl an regulatorischen T-Zellen auf, die effiziente T-Zell-Reaktionen gegenüber dem Tumor verhindern. Um die Mechanismen zu untersuchen, die die Tumorabstoßung kontrollieren, wurden von uns unterschiedliche Mausmodelle zur Depletion regulatorischer T-Zellen eingesetzt. In $Foxp3^{DTR}$ knock-in Mäusen, deren Tregs zu circa 99 % entfernt worden waren, konnte eine vollständige $CD8^+$ T-Zell abhängige Abstoßung transplantierter HCmel 1274 und B16 Melanoma erzielt werden. Im Gegensatz dazu gab es, nach einer circa 90%igen Depletion der Tregs in BAC transgenen Foxp3.LuciDTR4 Mäusen, keine vollständige Abstoßung der HCmel 1274 und B16 Tumore. Dies zeigt, dass bereits eine geringe Anzahl an Tregs genügt, um die $CD8^+$ T-Zell-Antworten gegen den Tumor zu kontrollieren. Durch die Depletion der Tregs kam es zu sehr großen Veränderungen in der Tumormikroumgebung, die durch durch eine enorme Zytokinausschüttung und einer vermehrten Infiltration an $CD8^+$T-Zellen ausgelöst wurde. Zusätzlich konnte eine erhebliche Infiltration basophiler Granulozyten beobachtet werden.

In dieser Forschungsarbeit konnte zum ersten Mal gezeigt werden, dass die tumorassoziierten Basophilen eine signifikante Rolle bei der Tumorabstoßung besitzen. Diese im Tumor vorhandenen Basophile produzierten große Mengen an Zytokinen wie CCL3 und CCL4. Wir konnten nachweisen, dass diese Zytokinen für die Infiltration tumorspezifischer $CD8^+$ T-Zellen verantwortlich sind. Das von den $CD8^+$ T-Zellen produzierte IFN-γ verursacht eine Änderung bei den tumorassoziierten Makrophagen vom M2-ähnlichen hin zum M1-ähnlichen Phänotyp. Über einen Rückkopplungsmechanismus verstärken die M1-ähnlichen Makrophagen die Infiltration der $CD8^+$ T-Zellen indem sie stark chemotaktisch auf $CD8^+$ T-Zellen wirkende Stoffe, einschließlich CCL2, CXCL9 und CXCL10, sezernieren und eine Normalisierung der Gefäßversorgung des Tumors induzieren.

Die Mechanismen der Tumorabstoßung wurden in einem weiteren Tumormodell untersucht. Rip1-Tag5 Mäuse entwickeln spontan Bauchspeicheldrüsenkrebs, was sich auch in der klinischen Entwicklung neuroendokriner Pankreastumoren wiederspiegelt. Wie nahezu alle Tumoren bei Mensch und Nager, besitzen auch diese Insulinome eine veränderte Gefäßstruktur, welche sich als Barriere für die Infiltration von T-Zellen in dem Tumor auswirkt. Demzufolge führt eine Behandlung der Rip1-Tag5 Mäuse durch einen adoptiven T-Zell Transfer zu keiner Tumoreradikation. Wurde aber der T-Zell Transfer mit CpG-ODN, einem Auslöser proinflammotorischer Signale, kombiniert, konnte im endothelialen Tumorgewebe eine Hochregulation von T-Zell Adhäsionsmolekülen wie zum Beispiel VCAM-1 beobachtet werden, sowie eine starke Infiltration von T-Zellen und eine verlängerte Überlebenszeit der tumortragenden Mäuse. Bemerkenswerterweise stellte sich heraus, dass CpG-ODN an $CD206^+$ $iNOS^+$ M2-ähnlichenMakrophagen bindet und sie zu $CD206^-$ $iNOS^+$ M1-ähnlichen Makrophagen polarisiert. Durch die Depletion der Makrophagen und die Blockade von iNOS wurde gezeigt, dass die iNOS Aktivität der zu M1-gewandelten Tumor Makrophagen für die vermehrte Expression vonVCAM-1 auf dem Tumorendothelien sowie die nachfolgende T-Zell Infiltration und Tumorabstoßung verantwortlich waren. Beachtenswert ist ebenfalls, dass der Transfer voraktivierter $iNOS^+$ Makrophagen zusammen mit tumorspezifischen $CD8^+$ T-Zellen, auch in Abwesenheit von CpG-ODN, in der Lage waren die VCAM-1 Expression und die Einwanderung der T-Zellen zu fördern. Im Gegensatz dazu fehlte diese Eigenschaft iNOS defizienten Makrophagen, was die wesentliche Rolle der NO Produktion durch M1-polarisierte Tumor Makrophagen hervorhebt. Mittels in vitro Experimenten konnte demonstriert werden, dass die Inkubation humaner Endothelzellen mit iNOS exprimierenden humanen Makrophagen oder mit dem NO Spender Glyceroltrinitrat (GTN) die Expression von Adhäsionsmolekülen wie VCAM-1, ICAM-1 und E-Selectin induzierte. Allerdings konnte dieser Effekt nur mit niederen Dosen GTN erzielt werden. Höhere Dosen führten zu einer Inhibition. Diese Ergebnisse machen deutlich, dass die NO Produktion durch M1-polarisierte Tumor Makrophagen einen kritischen Punkt einer Tumortherapie darstellt.

Zusammengefasst zeigen die Daten beider Mausmodelle, dass adoptive T-Zelltherapie und zielgerichtete Strategien bezüglich Basophile/ Makrophagen oder

auch der Transfer von M1-polarisierten Makrophagen eine effiziente T-Zell Infiltration und Tumorabstoßung bewirken. Diese neuen Erkenntnisse können die immuntherapeutischen Behandlungsstrategien bei Tumortherapien beeinflussen.

CONTENTS

LIST OF FIGURES

LIST OF TABLES

1 INTRODUCTION

1.1 Tumor Immunity

Cancer is one of the biggest health problem in the world. In 2012, there were an estimated 14.1 million new cancer cases diagnosed and 8.2 million cancer deaths worldwide[1]. Cancer is characterized by the accumulation of mutations in various genes that results in the loss of normal cellular regulatory processes and, consequent transformation of normal cells into malignant cells with unlimited proliferation capacity. Nevertheless, the host develops various defenses against the growth of transformed cells. These defenses include the immune system.

More than a five decades ago, Lewis Thomas and Frank Macfarlane Burnett proposed the "immune surveillance" theory stating that the immune system can confer protection against cancer by recognizing and eliminating transformed cells[2, 3, 4, 5]. Since then, the idea that the immune system can control cancer has been a matter of great debate. Over the last two decades, findings from gene-targeted mouse models that selectively lack key components of the immune system have reinforced the immune surveillance theory. Recombination activating gene 2 (RAG2)-deficient mice that lack both T and B cells were shown to be more susceptible to spontaneous or carcinogen-induced carcinomas[6]. In addition, mice lacking γδ T cells showed increased susceptibility to developing cutaneous tumors[7]. Strikingly, mice deprived of cytokines interferon-α/β (IFN-α/β) or IFN-γ were found to be more susceptible to spontaneous tumor induction as well as tumor induction by chemical carcinogen[5, 6, 8,9]. Further evidence for the immunosurveillance theory was provided by the mice deficient of perforin[10], which is used by cytotoxic T cells to kill target cells. These mice exhibited elevated incidence of spontaneous lymphoma[10]. All together, these data indicate that the immune system does indeed confer protection against cancer in mice. However, a study, showing the importance of IFN- γ in tumor rejection, suggested that the immune system can also promote tumor progression by shaping tumor immunogenicity[6]. This caused a considerable revision of immunosurveillance

hypothesis and gave rise to a relatively extended hypothesis termed "cancer immunoediting", which is divided into three sequential phases. The first phase is called "elimination" phase in which the immune system acts to destroy transformed cells long before they develop to clinically apparent tumors. If the elimination is complete, this phase represents the full extent of the process. However, if rare tumor cell variants survive the elimination phase, they may enter the "equilibrium" phase in which the immune system is still able to control the outgrowth of tumor cells but, meanwhile, shapes the tumor immunogenecitiy. The constant immune selection pressure placed on genetically unstable tumor cells in the equilibrium phase may yield variants with new mutations that confer them escape mechanisms, including antigen loss, defects in antigen processing and presentation (i.e. loss of major histocompatibility complex (MHC) expression), and induction of anti-apoptotic mechanisms. Alternatively, tumors may escape immune attacks by establishing immunosupressive tumor microenvironment. Then, these tumor cells in "escape" phase may multiply to generate clinically apparent tumors.

In addition to evidence compiled in mice, there are clear indications that the human immune system does indeed naturally protect against cancer. The main evidence in human comes from observations that primary (inborn) immunodeficiencies are correlated with increased risk of malignancy. For example, patients with common variable immunodeficiency (CVID), who have defective humoral immunity, are far more susceptible than the general population to lymphoma, stomach, breast, bladder and cervix cancer[11, 12]. Patients with immunoglobulin A (IgA) deficiency showed higher incidence of gastric carcinoma[12]. Furthermore, patients, who have a mutation in the CD40 ligand molecule, had an increased incidence of developing pancreas and liver tumors[13]. All these findings reveal a consistent correlation between primary immunodeficiency and elavated risk of developing various types of tumors.

Histopathologic data has demonstrated that many solid tumors are infiltrated by immune cells including T and B lymphocytes, natural killer (NK) cells and macrophages. Several studies indicate an association between immune cell infiltrates and the clinical outcome for many cancer types. For instance, the presence of $CD3^+$ T cells in ovarian and colorectal cancers was shown to be correlated with increased

survival of patients[14, 15]. $CD4^+$ T cell infiltrates were found to predict positive clinical outcome in non-small cell lung cancer[16]. $CD8^+$ T cell infiltration into colon, lung and breast tumors represents a positive prognostic marker[16, 17, 18, 19]. $CD4^+$ and $CD8^+$ T infiltrates, together, were shown to be associated with prolonged survival in esophageal squamous cell carcinoma and non-small cell lung cancer[20, 21]. As compared to other subsets of $CD4^+$ T cells, T-helper (Th)-1 phenotype was reported to be beneficial for colorectal, liver and breast cancer patients[14, 22, 23, 24]. Infiltration by $NKp46^+$ NK cells was also found to predict positive clinical outcome in patients with gastrointestinal stromal tumors (GIST)[25]. Moreover, the number of intratumoral $CD68^+$ macrophages was demonstrated to be linked to longer survival of patients with prostate, lung and colon cancers[17, 25, 26, 27, 28]. This association between immune cell infiltration and clinical outcome is intriguing but does not provide a direct evidence for the generation of an effective anti-tumor immune responses in cancer patients.

Today, it is well established that tumor cells can express antigens that can be recognized by B and T lymphocytes. So far, a variety of tumor antigens have been discovered in both mouse and human cancers, especially ones recognized by cytotoxic $CD8^+$ T cells. Tumor antigens can be classified into two group based their expression patterns. Antigens that are expressed solely on tumor cells are called "tumor-specific antigens" and have the potential to induce tumor-specific immune responses. This class of antigens includes viral antigens, antigens that result from mutations, deletions, chromosomal translocations or viral gene insertions affecting proto-oncogens and tumor-suppressor genes, and antigens that are encoded by cancer-germline genes. The majority of these antigens is unique to individual tumors, whereas few of them are shared by different tumors. Another class of antigens are called "tumor-associated antigens" which are expressed on both normal and tumor cells. Most of these antigens are strongly overexpressed in tumor cells in comparison to normal cells. Besides, some antigens are unique to particular lineage but expressed on both malignant and normal cells.

The molecular identification of human tumor antigens has provided the basis for the development of immunotherapies for cancer patients. In principle, two treatment concepts have emerged on the basis that tumors express antigens, which can be recognized by T cells. Antigen-specific "vaccination therapy" is designed to

stimulate and augment anti-tumor activity of patient's T cells whereas "adoptive T cell therapy" involves infusion of ex vivo-expanded tumor antigen-specific T cells into cancer patients for elimination of cancer cells.

1.1.1 Evasion of immune responses by tumors

The generation of an anti-tumor immune response is a multi-step process that involves several components of the immune system. In the first step, antigens released from tumor cells are taken up by antigen-presenting cells (APCs). APCs, mainly dendritic cells, process the tumor antigens and present them to $CD4^+$ T cells or $CD8^+$ T cells on MHC-II or MHC-I molecules, respectively, in regional lymph nodes. This step results in priming and activation of effector T cells directed against tumor antigens. Next, activated T cells have to traffic to the tumor site and cross the tumor endothelial barrier in order to obtain access to the tumor bed, where they can kill the tumor cells.

Tumors possess multiple mechanisms to evade and resist T cell-mediated immune attacks. These mechanisms enable tumor cells to interfere with almost every step needed for effective immune responses, from deregulation of APCs that prevents efficient T cell priming to establishment of aberrant endothelial barrier that blocks T cell infiltration and to generation of immunosuppresive microenvironment that abolishes T cell activity in the tumor.

1.1.1.1 Progressive loss of tumor-specific T cells

Central tolerance mechanism presents a challange to the generation of anti-tumor T cell responses while protecting against autoimmunity. Medullary thymic epithelial cells (mTECs) contribute to central tolerance through expression of a broad range of self antigens, which is largely dependent on autoimmune regulator (AIRE). During thymic maturation, developing T cells that responds to self-antigens on mTECs are deleted by negative selection or assume regulatory T (Treg) cell phenotype. Since many tumor antigens are self-antigens, many tumor-specific T cells are potentially deleted as well. However, central tolerance is sometimes incomplete,

allowing maturation and survival of low numbers of tumor-specific T cells with T cell receptors (TCRs) that have low-to-intermediate affinity for antigen recognition[29]. In fact, transient depletion of mTECs or modulation of AIRE ecpression were shown to enhance anti-tumor immunity by increasing the pool and affinity of effector T cells recognizing tumor/self-antigens[30, 31].

1.1.1.2 Inefficient priming of tumor-reactive T cells

Tumors can impair tumor antigen presentation to T cells mainly by modulating dendritic cells (DCs), which are the most efficient APCs. DCs capture tumor-derived antigens, process them into peptides, migrate into the tumor-draining lymph nodes, where they present peptide-MHC complexes to T cells, thereby generating antigen-specific T cell responses. Antigens may also directly travel to draining lymph nodes through lymph and can be taken up by lymph node-resident DCs[32]. Non-activated (immature) DCs are highly phagocytic and can process antigens for presentation to T cells but often induce immune tolerance through T cell deletion, T cell anergy or expansion of regulatory T cells[33, 34, 35, 36]. In contrast, mature DCs, which are activated by a variety of factors including pathogen-associated molecular patterns (PAMPs)[37, 38, 39], danger-associated molecular patterns (DAMPs)[40, 41, 42, 43], cytokines[44, 45] and CD40 ligand[46, 47, 48, 49], elicit effective T cell responses. Typically, tumor microenvironment lacks the factors required for DC activation, and, therefore, tumor-infiltrating DCs often show functionally impaired phenotype[50]. In addition, tumors produce factors that prevent DC maturation. Such factors include vascular endothelial growth factor (VEGF)[51, 52, 53], interleukin (IL)-10[54], transforming growth factor (TGF)-β[55]. Hypoxia and lactic acid, which are frequently present in the tumor microenvironment, can also influence DC maturation[56, 57]. Immature DCs or incompletely matured DCs assume regulatory phenotype and secrete immunosuppresive molecules, including IL-10, indoleamine 2,3-dioxygenase (IDO) and prostagladin E_2 (PGE_2)[56, 57, 58, 59, 60]. Moreover, tumors affect differentiation of DC precursors. For example, tumor-derived IL-6 and macrophage colony-stimulating factor (M-CSF) have been reported to promote differentiation of monocytes to macrophages rather than DCs[61], hence contributing to reduced APC activity in cancer patients.

1.1.1.3 Impaired infiltration of tumor-reactive T cells into the tumor

The control of T-cell trafficking to tumors are coordinated by chemokines. It seems that inefficient levels of intratumoral chemokine expression contribute to tumor escape from T cell responses. Of note, tumors with high-level T cell infiltration are characterized by high-level expression of T cell-attracting chemokines, including chemokine (C-C motif) ligand 2 (CCL2), CCL3, CCL4, CCL5, chemokine (C-X-C motif) ligand 9 (CXCL9) and CXCL10[62]. Chemokine activity can be disrupted by abnormal post-translational modifications, and alterations in proteolytic cleavage, glycosylation, or deamination[63, 64], which are common processes in the tumor microenvironment. For instance, reactive nitrogen species (RNS) in the tumor microenvironment cause nitrosylation of CCL2, which, therefore loses the ability to recruit tumor-specific T cells into tumor bed[65].

T cells must cross the tumor endothelium in order to be able to recognize and kill tumor cells. However, accumulating evidence indicates that the tumor endothelium actually represents a physical barrier to T cell penetration into the tumor[66, 67, 68].

The angiogenic switch is a critical step in tumor progression. It induces formation of new vessels from pre-existing capillaries and post-capillary venules to provide oxygenation, nutrition and waste disposal for the growing tumor mass. Importantly, the angiogenic switch leads to an aberrant tumor vasculature that is characterized by structural abnormalities, including heterogenous distribution, tortuosity, dilation, inadequate perivascular cell coverage and funtional abnormalities, such as insufficient blood flow and leakiness[69]. This aberrant phenotype is driven via production of angiogenic factors, such as VEGF, by tumor itself[70, 71] and/or by tumor-infiltrating macrophages[72, 73] and/or by tumor-infiltrating Tregs[74]. Our group has shown that the abnormal tumor vasculature itself can also act as a major barrier to T cell infiltration[75]. Gene expression profiling data demonstrated that regulator of G-protein signaling (RGS)-5 was overexpressed in aberrant tumor vasculature[76]. Genetic deletion of RGS-5 resulted in normalization of the vasculature, pericyte maturation and striking decreases in tumor hypoxia and vessel leakiness[75]. These vascular changes, in turn, augmented the influx of tumor-specific effector T cells into tumor

and enhanced survival of tumor-bearing mice[75]. Angiogenic factors in the tumor microenvironment, such as VEGF and fibroblast growth factor (FGF), were shown to hinder the endothelial expression of intracellular adhesion molecule (ICAM)-1/2 and vascular cell adhesion molecule (VCAM)-1[77, 78], which are critical for adhesion of T cells to tumor endothelium. T cell infiltration-blocking nature of tumor endothelium might be determined by the quantity of these adhesion molecules. Moreover, an aberrant vasculature causes a tumor microenvironment, which is a hostile milieu for T cells. For example, an abnormal tumor vasculature is associated with hypoxia in the tumor[69], which is known to limit T cell functions[79, 80, 81]. Tumor endothelial cells can also produce immunosuppressive molecules, including programmed death ligand (PD-L) 1 and 2[82, 83, 84], B7-H3[85], T cell immunoglobulin mucin (TIM)-3[86], IL-10[87, 88], TGF-β[87, 88] and PGE_2[87, 88]. A recent study demonstrated that Fas ligand (FasL) expression on tumor endothelial cells induces the death of effector T cells, thus limiting T cell infiltration into tumor[89].

1.1.1.4 Immunosuppressive mechanisms in the tumor microenvironment

Upon penetration into tumors, T cells will encounter an immunosuppressive microenvionment characterized by tumor stroma and immunosuppresive immune cells such as Tregs, tumor-associated macrophages (TAMs) and myeloid-derived suppressor cells (MDSCs). The tumor stroma is composed of fibroblasts, myeloid-lineage cells and endothelial cells with variable extent of extracellular matrix (ECM). They all appear to play crucial roles in tumor progression by providing an environment for tumor grrowth[90, 91, 92] or by curbing anti-tumor immune responses[93,94]. Carcinoma-associated fibroblasts (CAFs) comprises a major portion of tumor stroma and exhibit altered functions in comparison to normal fibroblasts[91,92,95,96,97,98]. Elimination of fibroblasts with a genetic model that lacks fibroblast-activating protein (FAP) was shown to induce tumor regression by a mechanism that relied on host IFN-γ and tumor necrosis factor (TNF) production[94].

$CD4^+$ $CD25^+$ (IL-2 $receptor^+$) forkhead box P_3^+ ($Foxp3^+$) Tregs are enriched in the tumors of several cancer types, including melanoma[99], ovarian[100], breast[101], colorectal[102], lung[100], gastric[103] and pancreatic[101] cancers. Of particular interest is the observation that elevated numbers of Tregs in tumors predict poor clinical outcome in

some cancers, such as breast[104], gastric[103] and ovarian[105, 106] cancers. Natural Tregs (nTregs), which originate in the thymus like other T cells, can be recruited to tumors via several factors. CCL22 production by tumors and TAMs was reported to induce infiltration of chemokine (C-C motif) receptor (CCR)4^+ Tregs in ovarian cancer[105] and Hodgkin's lymphoma[107]. Recently, hypoxia was found to favor $CCR10^+$ Treg recruitment into ovarian tumors by upregulating CCL28 expression in the tumor microenvironment[74]. In addition to chemokine-mediated attraction of Tregs, tumors promote the expansion nTregs[108] and the generation of inducible Tregs (iTregs) from naive $CD4^+$ T cell precursors[109]. This conversion can be achieved by enhanced expression of IL-10[110], TGF-β[111] and adenosine[112] in the tumor microenvironment. Tregs exert immunosuppresive functions that result in immunologic tolerance and ignorance of tumors. Tregs are known to inhibit efficient priming of T cells in lymph nodes[113, 114], thereby preventing expansion of tumor-specific $CD8^+$ T cell clones. This is probably the most important mechanism by which Tregs block efficient T cell responses against tumors. Tregs also secrete IL-10, TGF-β, IL-35, which are known to inhibit immune responses by supressing expansion of T cells and cytokine production by T cell [115, 116]. Of importance, IL-10 and TGF-β have been shown to mediate tumor progression by limiting anti-tumor immunity[117, 118]. An additional mechanism of Treg-mediated immunosuppression is the induction of effector T cell apoptosis, which is executed via expression of granzyme B[119, 120], tumor necrosis factor-related apoptosis-inducing ligand (TRAIL)[121] and galectin-1[122]. Tregs induce effector T cell apoptosis also by depleting local resources of IL-2[123], which is essential for survival of both Tregs and effector T cells. Further, Tregs suppress T cell functions through the generation of adenosine[124, 125]. Tregs can limit anti-tumor immune responses not only by acting on effector T cells but also by acting on DCs, impairing antigen presentation to tumor-specific T cells. They can engage in crosstalk with DCs through cell-cell interaction mediated by cytotoxic T lymphocyte antigen (CTLA)-4 on Tregs and CD80 and/or CD86 on DCs[126]. This interaction induces IDO expression by DCs, which, in turn, suppress T cell functions through tryptophan catabolism[126]. Tregs have been shown to restrict DCs' ability to stimulate T cell priming and activation by some other mechanisms, including inhibition of costimulatory molecules, tolerogenic polarization of DCs by IL-10 and TGF-β[127] and Treg-DC interactions via lymphocyte-activation gene (LAG)-3[128]. A recent study has defined a new role for Tregs in tumor progression[74]. Beyond their immunosuppressive

activities, Tregs have been demonstrated to promote angiogenesis in ovarian cancer by VEGF expression[74].

Macrophages and MDSCs are abundantly present in solid tumors and can contribute to immune evasion. Macrophages are specialized phagocytic cells that engulf and digest invading microbes, cell debris and foreign substances[129]. In addition to their phagocytic activity, they can modulate adaptive immune responses through antigen presentation or through the release of various cytokines and chemokines[129]. Macrophages can acquire distinct phenotypes depending on the local tissue microenvironment[129]. The conventional classification divides activated macrophages into M1 macrophages (classically activated macrophages) and M2 macrophages (alternatively activated macrophages)[129]. Importantly, macrophage polarization is usually temporary and can be altered by changes in the tissue microenvironment[129], indicating a high degree of plasticity. M1 polarization can be driven by bacterial moeties, such as toll-like receptor (TLR) ligands and Th1 cytokines, including IFN-γ and TNF-α[129]. Upon activation, M1-polarized macrophages secrete pro-inflammatory cytokines that orchestrate Th1-type immune responses, and chemokines that attract other Th1-related immune cells[129]. In contrast, M2 macrophages are mainly induced by Th2 cytokines IL-4, IL-13 and IL-10[129]. Upon activation, they produce cytokines and chemokines that are involved in Th2-type immune responses[129]. M2 macrophages can also exert immunoregulatory functions and take part in tissue homeostasis[129]. Importantly, macrophage polarization in vivo rarely results in pure M1 or M2 populations but usually into populations that are skewed only to a certain extend towards the M1 or M2 phenotype. For instance, tumor macrophages show M2-like phenotype due to abundant presence of cytokines and growth factors, such as IL-4, IL-13, IL-10 and M-CSF, in the tumor microenvironment[130, 131, 132, 133]. Clinical evidence show that increased numbers of TAM is associated with poor prognosis and resistance to therapies in many cancer types, such as breast cancer[134, 135], Hodgkin's lymphoma[136, 137], T cell lymphoma[138, 139], B cell lymphoma[140], cervical cancer[141], uveal melanoma[142] and lung cancer[143].

TAMs also play an essential role in regulating tumor angiogenesis. Clinical studies have reported a positive correlation between blood vessel density and the

number of TAMs in vessel areas in human tumors[144, 145]. Mouse models further supported the role of TAMs in tumor angiogenesis. It has been shown that TAM depletion in mice reduced tumor angiogenesis[146, 147] whereas TAM enrichment augmented tumor angiogenesis[148]. Moreover, hypoxia in the tumor microenvironment modulates macrophages to produce large amounts of VEGF via hypoxia-inducible factor (HIF)-1 and HIF-2 signaling[149, 150, 151]. Indeed, VEGF production by TAMs has been demonstrated to regulate angiogenesis in the spontaneous mammary carcinoma model and in some transplantable tumor models[73, 152]. TAMs also produce and secrete number of other pro-angiogenic factors such as placental growth factor (PlGF), basic-fibroblast growth factor (b-FGF), M-CSF, platelet-derived growth factor (PDGF), heparin-binding epidermal growth factor (HB-EGF), macrophage-inhibitory factor (MIF), platelet activating factor (PAF), semaphorin 4D (Sema4D) and TGF-β[153, 154, 155].

TAMs release a variety cytokines that can suppress effector T cells. TAMs have been reported to produce IL-10 and TGF-β in human and animal cancers[156], which are implicated in tumor progression by hindering anti-tumor immune responses. In addition, macrophages have been shown to cause Treg recruitment to tumors by chemokine production[105, 157] and induce conversion of naive $CD4^+$ T cell into iTregs in the tumor[158]. TAM-derived arginase I (ARGI) can curb T cell activity by depleting local L-arginine resources in the tumor microenvironment[81, 159, 160, 161].

MDSCs are immature myeloid-cell lineage cells, which are often found in large numbers in cancer patients and correlated with tunor progression[58]. They can potently suppress effector T cells through functional activity of ARGI[160] and nitrosylation of TCR on infiltrating T cells by RNS[162].

T cell-mediated tumor killing requires the recognition of target tumor antigen through MHC-TCR interactions. However, many tumors develop resistance to T cell attacks through loss of antigen and MHC expression, and deregulation of antigen-processing[163, 164, 165, 166, 167]. These resistance mechanims possibly stem from selection pressures of host immunity and can be acquired by mutations, genetic loss or epigenetic silencing[164]. In fact, loss of MHC expression is linked to poor clinical outcome in cancer patients[163]. Tumors may produce molecules, such as FasL and

TRAIL[168], that can directly kill T cells. They can also express surface molecules PD-L1 and PD-L2[169], which, in turn, binds to programmed death receptor (PD)-1 receptor on activated T cells and prevents T cell proliferation, cytokine production and cytolytic activity[170]. Of importance, PD-L1 and PD-L2 are also highly expressed on tumor-infiltrating DCs and macrophages[171, 172, 173].

In summary, tumors employ a variety of intrinsic and extrinsic strategies to impair immune responses and to promote their progression. In the field of tumor immunology, major efforts now concentrate on attenuating immune escape mechanims of tumor to improve efficacy of immunotherapies against cancer.

1.1.2 Clinical immunotherapies for cancer

The potential for treating cancer patients by immunotherapies is now becoming a clinical reality. Current therapies for cancer, including chemotherapy and radiotherapy, are designed to block cell division or kill proliferating cells but they may have severe side effects on normal cells. In contrast, immunotherapy has the potential of being the most tumor-restricted treatment modality since immune responses to tumors are usually against the antigens that are specific to tumors.

The earliest attempts to boost cancer patient's immune responses against tumor cellls include antigen-based vaccination. Cancer vaccines are typically composed of tumor antigens and adjuvants, such as toll-like receptor (TLR) ligands poly I:C, monophoshoryl lipid A (MPL), flagellin, Aldara (Imiquimod), Resiquimod and CpG[174]. They are designed to stimulate antigen-specific T cell responses to eliminate tumors and to generate memory T cells that will serve to impede relapse. Indeed, vaccination of cancer patients based on purified tumor antigen-associated peptides or whole tumor cells leads to expansion of antigen-specific $CD4^+$ and/or $CD8^+$ T cells in the blood[175, 176, 177, 178, 179, 180], however the clinical success is limited (objective response rate = 3.8%)[177, 180, 181].

The adoptive transfer of tumor-specific T cells into cancer patients is one of the main treatment modalities within cancer immunotherapy. In this therapy, T cells

are isolated from patients' blood or tumor, and then expanded in vitro in the presence of appropriate T cell growth factors such as IL-2. T cell populations that are reactive against tumor antigens can be specifically selected and expanded, then adoptively infused into cancer patients. When combined with lymphodepletion by chemotherapy alone or chemotherapy in combination with total body irradiation, adoptive T cell therapy (ACT) of patients with metastaic melanoma resulted in objective response rate around 48%[182, 183, 184]. It seems that the availability of naturally occuring tumor-infiltrating cells for ACT is restricted to melanoma[185]. Therefore, in order to expand the range of cancers potentialy susceptible to ACT therapy, T cells are engineered to express appropriate T cell receptor that is specific for particular tumor antigen by several techniques. The most developed technique is the use of chimeric antigen receptors (CARs), in which T cells from patients are transfected or transduced with a construct encoding a single chain variable fragment of an antibody that specifically recognize target tumor antigen[185]. Thanks to CAR technology, the range of cancer amenable to ACT now includes B-cell acute lymphoblastic leukemia (against CD19)[186], renal carcinoma (against carbonic anhydrase)[187] and neuroblastoma (against L1 adhesion molecule)[188]. The most promising results have been achieved in blood cancers[189, 190], where T cells do not have to penetrate a stromal barrier to recognize and kill tumor cells.

Despite the considerable successes with vaccination and ACT, some patients fail to respond favourably to these treatments, probably due to the presence of immunosuppresive elements within the tumor microenvironment. The tumors in these patients may have tumor vasculature that is nonpermisive for entry by T cells. Proangiogenic signals are known to drive abnormalization of tumor vasculature that is characterized by reduced expression of adhesion molecules for T cell penetration[191, 192]. In addition, dysregulated tumor angiogenesis creates a hostile microenvironment for T cells[191]. Interestingly, treatment of tumor-bearing mice and cancer patients with anti-angiogenic agents resulted in a normalized vasculature and a more immunosupportive tumor microenvironment[191]. The United States Food and Drug Administration (FDA)-approved anti-VEGF antibody, bevacizumab, has shown its effectiveness in normalizing tumor vasculature in several clinical trials[193, 194, 195]. Several animal studies have shown that vessel-targeted therapies improve the efficacy of immunotherapies by augmenting T cell infiltration into the tumor[75, 196, 197, 198].

One of the immunosuppresive mechanisms present in the tumor microenvironment is the negative regulation of T cell activation by cytotoxic T lymphocyte activation marker 4 (CTLA-4), which is an coinhibitory receptor expressed on activated T cells and binds to costimulatory molecules B7.1 and B7.2 on antigen presenting cells[199]. The use of ipilimumab, a monoclonal antibody directed against CTLA-4, in clinical trials has shown an overall survival benefit for patients with advanced melanoma[200, 201]. Programmed death (PD)-1 is another coinhibitory receptor expressed on T cells and binds to PD-L1 and PD-L2 expressed on tumor cells, stromal cells or other immune cells[202]. Blocking of PD-1 signaling has been shown to enhance T cell responses against tumors in animal studies[173, 203]. In addition, clinical trials using either anti-PD-1 or or anti-PD-L1 antibodies resulted in objective clinical responses in patients with melanoma, renal cell cancer or lung cancer[204, 205]. Importantly, dual blockade of PD-1 and CTLA-4 were demonstrated to further augment T cell responses in a preclinical model with transplantable tumors[206] whereas clinical trials with dual blockade is underway (trial number NCT01024231).

In summary, multiple approaches to cancer immunotherapy exist and few are able to generate significant clinical responses. One attractive approach is to combine potent vaccines or adoptive T cell therapy with therapeutic agents targeting immunosuppressive cells or molecules in the tumor microenvironment.

1.2 Treg Depletion as A Model to Study Anti-Tumor Immune Responses

The role of Tregs in cancer progression has mentioned above in **section 1.1.1.4**. Several groups have examined whether Treg depletion can improve anti-tumor immunity. It was reported that Treg depletion with PC-61 antibody (anti-CD25 antibody), before tumor inoculation, caused tumor regression[207, 208, 209, 210, 211, 212] whereas PC-61-mediated Treg depletion after tumor establishment had no effect in tumor growth[207, 213, 214]. The limited therapeutic efficacy of PC-61 antibody treatment is attributed to fact that the degree of depletion is not sufficient and PC-61 antibody also removes $CD25^+$ effector T cells. In some clinical trials, denileukin diftitox (ONTAK), which is a fusion protein between active domain of diphtheria toxin (DT)

and IL-2, is employed to reduce Treg number in cancer patients[215, 216, 217]. Although ONTAK was indeed able to decrease the number of Tregs in patients but the therapeutic efficacy was hampered, probably because of unwanted effects on tumor-specific T cells[218].

To test a more specific Treg ablation in pathological settings, including cancer, various groups have developed genetic models that allow selective depletion of Tregs by targeting only the cells expressing Foxp3, which is a transcription factor required for the development and function of Tregs. For this group, Alexander Rudensky's group has generated Foxp3^{DTR} mice harboring knock-in human diphtheria toxin receptor (DTR), and enhanced green fluorescent protein (eGFP) downstream of the internal stop codon of *foxp3* gene[219]. In this model, DT application results in transient depletion of almost all Tregs[219]. However, continuous DT administration in this model induces fatal autoimmunity[219]. Our group established Foxp3-LuciDTR4 mice, which contain a bacterial artificial chromosome (BAC) construct, composed of eGFP, human DTR and CBGr99 luciferase, which was inserted at the start codon of *foxp3* gene[220]. DT administration in these mice ablates DTR-expressing Tregs without inducing any autoimmune responses but DTR^{-} Tregs, which represent the very little portion of whole Treg population in mice, persist[220]. Another published Foxp3-DTR strain of mice, designated DEREG mice, also contains a BAC construct encoding human DTRand GFP[221].

Using the Foxp3-LuciDTR4 model, my group showed that Treg depletion induced activation of tumor-specific T cells and rejection of ovalbumin-expressing B16 (B16-OVA) tumors[222]. In the present study, I made use of Foxp3^{DTR} and Foxp3-LuciDTR4 mouse models to study anti-tumor immune responses against melanoma. I found that basophils are specifically enriched in melanomas following Treg depletion in Foxp3^{DTR} mice, enabling us to define a new role for basophils in anti-tumor immunity.

1.2.1 Basophils

Basophils are circulating basophilic granulocytes that comprise less than 1% of peripheral blood leukocytes. They were discovered by Paul Ehrlich in 1879 and named after their metachromatic granules that stain with basic dyes. Human basophils are 7-10 μm in size and have a segmented nucleus.

Basophils share several aspects with mast cells, such as expression of the high-affinity immunoglobulin E receptor FcεRI on cell surface and the secretion of chemical mediators that are associated with allergic responses[223, 224]. Therefore, they have often been mistakenly considered as minor and possibly redundant relatives of mast cells or as blood-circulating progenitors of mast cells. However, basophils can also be distinguished from mast cells by their segmented nuclei, mast cell protease 8 (mMCP8, also known as Basoph8) production and the lack of mast/stem cell growth factor receptor (c-Kit) expression[225]. Basophils enter the blood circulation in a steady state after they complete their maturation in the bone marrow. They infilrate into peripheral tissues upon various stimuli linked to pathological settings, including allergic reactions and parasitic infections[223, 224]. In contrast, mast cell circulate in the blood in an immature form and complete their maturation in the peripheral tissues in which they reside[223, 224]. Basophils do not proliferate after their maturation whereas mast cells can further proliferate in the periphery[223, 224]. In addition, the lifespan of basophils (~60 hour[226]) is much shorter than that of mast cells (weeks to months)[223, 224]. These differences between basophils and mast cells indicate that they may have distinct functions.

1.2.1.1 Basophil development

All blood cells emerge from hematopoietic stem cells (HSC) in the bone marrow. HSCs mature into common lymphoid progenitors (CLPs) that can give rise to T, B and NK cells or mature into common myeloid progenitors (CMPs) that are antecedents of erythrocytes, monocytes and granulocytes. Eosinophils, basophils and mast cells originate from the granulocyte-monocyte progenitor (GMP), descending from the CMP[227].

Commitment to eosinophil, basophil and mast cell lineages relies on the stimulation of specific transcriptional regulators in response to signals received from the cell surface. A model has been proposed that complex interplay between transcriptional factors GATA-2 and CEBP/α drives a GMP to specifically acquire eosinophil, basophil or mast cell properties, respectively[228]. Co-expression of GATA-2 and CEBP/α in GMPs leads to eosinophil development whereas GATA-2 expression in the absence of CEBP/α promotes GMPs to differentiate into basophil-mast cell common progenitors (BMCPs)[228]. BMCPs can then give rise to basophils by re-expression of CEBP/α or to mast cells if CEBP/α remains not expressed[228]. These findings indicate a tight developmental link between basophils, mast cells and eosinophils.

The precise extrinsic signals that guide timed expression of GATA-2 and CEBP/α and coordinated development of basophils, mast cells and eosinophils remain to be determined. It has been shown that IL-3, IL-5, granulocyte macrophage colony-stimulating factor (GM-CSF) and thymic stromal lymphopoietin (TSLP) are not necessary for basophil development in steady-state conditions because mice that lack receptors for these cytokines still harbor the same level of basophils compared to wild type mice[229].

1.2.1.2 Basophil homeostasis

Pathological conditions, such as parasitic infections, can induce a rise in basophil numbers. For instance, helminth infection of mice resulted in basophilia, which was shown to be dependent on IL-3[230]. Further studies demonstrated that T cells are a major source of IL-3 for induction of basophilia during helminth infection[231]. Direct evidence that IL-3 induces basophilia by augmenting differentiation of basophils in the bone marrow originates from in vitro studies where basophil precursors, purified from bone marrow of mice, were shown to develop into mature basophils in the presence of IL-3[229, 232]. In addition, survival of basophils can be enhanced by IL-3 via stimulation of NF-κB pathway[233, 234].

Another cytokine that has been described to cause basophilia is TSLP. Administration of recombinant TSLP into mice was shown to induce an increase in basophil numbers in the blood[235] and in the spleen[229], probably by enhancing the lifespan of basophils. TSLP-induced basophils differ from those stimulated with IL-3 in several aspects[229]. First of all, they are smaller in size compared to IL-3-elicited basophils[229]. They also express different array of genes and may assume different roles[229]. Studies are being carried out to analyze whether IL-3- and TSLP-stimulated basophils represent distinct subsets of basophils.

1.2.1.3 Tissue recruitment of basophils

Basophils can be selectively recruited to inflamed tissues in response to injury, assault or infection. Several human allergic diseases, including atopic dermatisis, asthma and rhinitis, are characterized by immense basophil infiltrates[236].

Tissue-specific recruitment of basophils is mediated by both activation and chemotactic factors. IL-3 was shown to induce infiltration basophils into lymph nodes after helminth infection[231, 237], whereas TSLP was observed to mediate accumulation of basophils in the skin in a model of atopic dermatitis[229]. Interestingly, IL-3 activation has been shown to enhance CD11b and CD18 expression on the surface of basophils, thereby augmenting adherence to endothelium[238, 239]. Besides, it was demonstrated that IL-3 stimulation of endothelial cells promotes selective adhesion and rolling of resting basophils in vitro[240]. The same study also showed that human basophils express CCR1, CCR2, CCR3, CCR7, CXCR1 and CXCR4 but only CCR7 is involved in IL-3 induced recruitment[240]. Other studies have shown that basophils can migrate in response to CCL2, CCL5, CCL7 and CCL11[241, 242].

After arriving in the tissue, basophils may receive several cues that enhance their survival and assume effector functions. These cues include cytokines, DAMPs, PAMPs and complement factors that originate from the tissue microenvironment itself, other infiltrating immune cells, or pathogens.

1.2.1.4 Basophil effector functions

Basophils have been shown to release histamine, proteoglycans (chondroitin and chondroitin sulphate etc.), several proteolytic enzymes, (elastase and lysophospholipase etc.) and lipid mediators such as leukotrienes and prostaglandins (LTC_4, PGD_2) from their cytoplasmic granules in a process called "degranulation"[224, 243]. Basophil degranulation usually takes place in response to crosslinking of immunoglobulin E (IgE) bound to FcεRI on their cell surface after exposure to allergens[224]. Moreover, the complement factors 3a (C3a) and C5a, bacterial peptide N-formyl-methionine-leucine-phenylanaline (fMLP) and IgD induce basophils to degranulate[244, 245]. The release of these preformed mediators has been linked to development of immediate hypersensitivity reactions[246].

Basophils also produce several cytokines in response to various stimuli, including FcεRI crosslinking and IL-3 stimulation. For example, basophils are a major source of Th2 cytokines, mainly IL-4 and IL-13, in several pathologic settings such as allergy and parasitic infections[226, 247, 248, 249]. Interestingly, they can synthesize more IL-4 and IL-13 per cell than other leukocytes[250, 251, 252, 253]. Moreover, it was demonstrated that IL-4, derived from basophils, induce Th2 polarization of $CD4^+$ T cells in vitro[254]. However, recent in vivo studies have shown that Th2 polarization in response to papain, alum/ovalbumin, or *nippostrongylus brasiliensis* is not dependent on basophils[255]. Recent studies have shown that, in the presence of IL-3, IL-33 and IL-18 can activate basophils to produce and secrete large amounts of cytokines and chemokines, including IL-4, IL-6, IL-9, IL-13, CCL2, CCL3, CCL4, CCL5 and GM-CSF, but bot IL-17, IL-5 and IFN-γ[256, 257, 258].

Basophils have been implicated in protective immunity against multicellular parasites such as helminthes and ticks, and in allergic reactions such as anaphylaxis, asthma and skin disorders[259, 260]. However, the real biological functions of basophils in these pathologic settings are not clear.

The precise role of basophils in cancer is also largely unclear. Several reports have demonstrated that patients diagnosed with myelodysplastic syndrome (MDS) harbor increased number of circulating basophils[261, 262, 263]. Moreover, a study

examining the prognostic significance of basophils showed that basophilia predicted reduced survival in MDS patients[264]. Basophilia is also common in patients with acute myeloid leukemia and accelerated chronic myeloid leukemia[265, 266]. The number of basophils and their activity was found to be augmented in some cohorts of patients with solid tumors. One group found increased degranulation of blood basophils in patients with stomach cancer[267], suggesting enhanced activity of basophils in those patients. Another group showed increased number of basophils in peripheral blood of lung cancer patients, but this basophilia in those lung cancer patients was also associated with increased levels of monocytes and eosinophils in the blood[268]. In mice, IL-4-transduced tumors exhibited marked infiltration of eosinophils, basophils, mast cells, macrophages[269], which, in turn, may initiate a pro-inflammatory cascade that favours influx of cytotoxic T cells and finally tumor rejection. Interestingly, immunohistochemical analysis of IL-4-transduced tumors showed that cells morphologically similar to basophils and mast cells produce TNF-α[269].

1.3 Rip1-Tag5 as A Model to Study Anti-Tumor Immune Responses

Preclinical tumor studies often utilize mouse tumor models that resemble the clinical situation as closely as possible. Rip1-Tag5 (RT5) mice is a transgenic mouse model of sponatenous pancreatic islet carcinogenesis, where the oncogene, simian virus 40 large T antigen (SV40-Tag) is specifically expressed in islet β cells under the control of the rat insulin promoter (RIP)[270]. RT5 mice exhibit multi-step carcinogenesis, which starts with hyperproliferation of pancreatic β cells in response to the induction of Tag oncogene expression at 10-12 weeks of age, continues with development of angiogenic islets and results in formation of highly vascularized, invasive solid tumors within 20 weeks[270]. This multi-step carcinogenesis precisely reflects clinical pancreatic neuroendocrine tumors (PanNET)[270]. Tag expression in transformed β cells leads to Tag antigen-specific immunity, characterized by T cell infiltrates in hyperproliferative islets[271, 272]. However, the T cell infiltration is lost during the transition from angiogenic islets to solid tumors[272].

The “angiogenic switch” during RT5 tumorigenesis induces conversion of the quiescent vasculature in early neoplastic lesions into an aberrant tumor vasculature which is characterized by dilated and tortous blood vessels[273]. Futhermore, adhesion of leukocytes to tumor endothelium is dramatically reduced in angiogenic islets and solid tumors and linked to changes in the tumor vasculature following induction of angioegenesis[272]. Treatment of RT5 tumors with antigen-based vaccination or adoptive T cell transfer causes only modest leukocyte infiltration into the tumors but with little effect on tumor progression[274], implying that aberrant tumor vasculature creates a physical barrier for T cell infiltration. The ultimate proof that an aberrant tumor vasculature indeed formed a barrier against T cell infiltration was provided in a recent from our laboratory, in which knock-out of *Rgs5* gene resulted in normalization of the tumor vasculature, that now permitted increased T cell infiltration and tumor rejection in the absence of additional danger signals[75].

Severeal years, our laboratory has attempted to design strategies to overcome the tumor endothelial barrier and to create permissive tumor microenvironment for effector T cells It was shown that whole body irradiation or application of a TLR9 ligand, cytosine-phosphorothioate-guanine (CpG) containing oligodeoxynucleotides (ODN), induced changes in the tumor microenvironment, which allowed the recruitment of T cells into the tumor[274, 275]. These changes included the normalization of the tumor vasculature and an increase in intratumoral expression of adhesion molecules, such as VCAM-1 and ICAM-1[274, 275]. These findings were further supported by a recent study conducted with collaborator Philip Beckhove (DKFZ, Heidelberg, Germany) where it was shown that local irradiation of RT5 tumors induces tumor vasculature normalization as well as VCAM-1 expression on tumor endothelium, resulting in strong infiltration of T cells into the tumors[276]. Interestingly, the study showed also that inducible nitric oxide synthase (iNOS) expression by macrophages is required for alterations in the tumor vasculature and subsequent T cell recruitment[276]. However, the precise role of $iNOS^{+}$ macrophages for tumor rejection remained unclear.

1.4 Aims of The Study

The success of clinical caner immunotherapy is hampered by many factors within the tumor microenvironment, including aberrant vasculature, Tregs and immunosuppressive tumor macrophages. The lack of T cell infiltration into tumors is a major limitation. For example, tumors usually exhibit an aberrant vasculature that prevents T cell infiltration. Another major obstacle is due by Tregs, which block generation of efficient T cell responses. Tumor macrophages promote many inportant characteristics of tumor progression, including supression of T cell responses, angiogenesis and tumor cell invasion.

Main aim of thesis was to define mechanisms of T cell infiltration into the tumor and the respective inhibitory mechanism, so that strategies for improved immunotherapy of cancer can be developed.

In a first approach, we set out to study the role of Tregs in tumor immunity. In previous studies, Our group has demonstrated that ~90% Treg depletion in tumor-bearing Foxp3.LuciDTR4 mice unleashed $CD8^+$ T cell responses against the tumor and resulted in complete rejection of melanomas expressing ovalbumin (OVA) as a surrogate tumor antigen whereas ~70% Treg depletion with anti-CD25 antibody was ineffective[222]. In the present study, I planned to investigate the effect of Treg depletion on the immune reaction against non-modified melanoma tumors, which were of lower immunogenicity than the OVA-modified B16 melanoma and, therefore, more difficult to reject. For this purpose, two different Foxp3DTR strains of mice were available, namely $Foxp3^{DTR}$ mice in which ~99% Tregs can be depleted, and Foxp3.LuciDTR4 mice in which ~90% of Tregs can be depleted. As in previous studies, Treg depletion was found to increase T cell infiltration into tumors, the precise composition of the infiltrating leukocyte subpopulations, status of tumor-associated macrophages (TAMs), presence of other innate subpopulations that may contribute to tumor rejection, and the underlying mechanism of leukocyte infiltration should be analyzed.

As a second model for the investigation of T cell infiltration, Rip1-Tag5 (RT5) mice were used, which develop spontaneous pancreatic islet tumors. These tumors are characterized by a typical aberrant tumor vasculature. In previous studies, our laboratory has found that this aberrant vasculature forms a barrier against infiltration of tumor-specific T cells[75].However, application of "danger signals" such as the TLR9 ligand CpG-ODN modified the aberrant vasculature in such a way that it became permissible for T cell infiltration[274]. CpG-ODN is known to bind to tumor macrophages[274]. The RT5 mice seemed to represent a promising model to explore the role of tumor macrophages for modulation of the tumor vasculature and T cell infiltration.

Finally, the two tumor models described here should be compared in order to see if there are common pathways for tumor rejection that could be exploited for novel therapeutic strategies.

2 MATERIALS AND METHODS

2.1 Materials

2.1.1 Mice

Mice (listed in **Table1**) were bred at the central animal facility of the German Cancer Research Center (DKFZ) and held under specific pathogen free conditions. Experiments were carried out according to governmental and institutional guidelines and regulations (Regierungspräsidium Karlsruhe, permit no. 35-9185.81/G98/08, 35-9185.81/G206/12 and 9185.81/G205/13).

Table 1: Mouse strains

Strain	**Source**
C57BL/6N (B6)	Charles River Laboratories
C3H/HeJ (C3H)	Charles River Laboratories
CD45.1 (B6 background)	Charles River Laboratories
Foxp3.LuciDTR4 (B6 background)	established in the laboratory
$Foxp3^{DTR}$ (B6 background)	provided by Alexander Rudensky (Memorial Sloan Kettering Cancer Center, New York, USA)
OT-I (B6 background)	Charles River Laboratories
Rip1-Tag5 (RT5) (C3H background)	Provided by Douglas Hanahan (Swiss Institute for Experimental Cancer Research, Lausanne, Switzerland)
TCR8 (C3H background)	Provided by Richard A Flavell (School of Medicine, Yale University, Yale, USA)

2.1.2 Tumor cell lines

HCmel 1274 melanoma, B16 melanoma and ovalbumin-expressing B16 melanoma (B16-OVA) were used. The HCmel 1274 melanoma cell line is derived from genetically modified HGF-CDK4 mice that spontaneously develop cutaneous melanoma[277].

2.1.3 Antibodies and reagents for cell depletion

Table 2: Antibodies and reagents used for cell depletion

Name	Clone	Company
α-CD4 antibody (Ab)	GK1.5	BioXCell
α-CD8 Ab	2.43	BioXCell
α-NK1.1 Ab	PK163-3-6	BioXCell
α-FcεRI Ab	MAR-1	eBiosciences
α-Siglec-F Ab	238047	R&D Systems
Diphtheria toxin (DT)		Sigma-Aldrich
Clodronate-loaded liposomes (CLIP)		Nico Van Rooijen, Vrije Universiteit, Netherlands

2.1.4 Antibodies and reagents for blocking experiments

Table 3: Antibodies and reagents used for blocking experiments

Name	Clone	Company
α-IFN-γ Ab	XMG1.2	BioXCell
α-CCL3 Ab	39626	R&D Systems
α-CCL4 Ab	46907	R&D Systems
N6-(1-iminoethyl)-L-lysine, dihydrochloride L-NIL		Cayman Chemical

2.1.5 Buffers and Solutions

Table 4: Buffers and solutions

Buffer/Solution	Composition
Phosphate buffered saline (PBS)	130 mM NaCl 2.6 mM KCl 1.5 mM KH_2PO_4 4 mM Na_2HPO_4 pH 7.2
Dulbecco's PBS (dPBS)	0.9 mM $CaCl_2$ 2.7 mM KCl 1.2 mM KH_2PO_4 0.5 mM $MgCl_2$ 137 mM NaCl 8.1 mM Na_2HPO_4 pH 7.4
PBS-Tween	PBS 0.01% Tween 20 (Sigma-Aldrich)
FACS buffer	dPBS 3% (v/v) Fetal calf serum (FCS) 0.01% (w/v) NaN_3
FACS blocking buffer	FACS buffer 1% Normal immunoglobulin (Privigen®, CSL Behring)
IF blocking buffer	PBS-Tween 5% (v/v) Goat serum (Sigma-Aldrich)
MACS buffer	dPBS 3% (v/v) FCS 2 mM EDTA
Heparin buffer	dPBS 2% (v/v) FCS 0.01% (w/v) NaN_3 5 U/ml Heparin (Ratiopharm)

ACK buffer	150 mM NH_4Cl 10 mM $KHCO_3$ 0.1 mM EDTA pH 7.2-7.4
Tissue digestion solution	dPBS 1 mg/ml Collagenase IV (Sigma-Aldrich) 50 U/ml DNase I (Sigma-Aldrich)
RT5 tumor digestion solution	dPBS 0.2 mg/ml Collagenase D (Roche) 0.025 mg/ml DNase I (Sigma-Aldrich) 0.08 mg/ml Dispase (Roche)
Trypsin-EDTA solution	0.025% (w/v) Trypsin (Sigma-Aldrich) 0.01% EDTA
StemPro® Accutase® cell dissociation solution (Life Technologies)	

2.1.6 Cytokines and NO donor

Table 5: Recombinant cytokines and NO donor

Name	**Company**
Mouse IL-2	eBiosciences
Mouse IL-3	PeproTech
Mouse IL-3	R&D Systems
Mouse IFN-γ	PeproTech
Mouse M-CSF	Sigma-Aldrich
Human IFN-γ	PeproTech
Human M-CSF	PeproTech
Human TNF	PeproTech
Glyceryl trinitrate (GTN)	Sigma-Aldrich

2.1.7 Commercial Kits

Table 6: Commercial kits

Kit name	Company
$CD4^+$ $CD25^+$ regulatory T cell isolation kit, mouse	Miltenyi
CD49b (DX5) microbeads, mouse	Miltenyi
Foxp3 staining kit, mouse/rat	eBiosciences
Griess reagent kit	Sigma-Aldrich
RNeasy mini kit	Qiagen
RNeasy micro kit	Qiagen
iScript™ cDNA synthesis kit	Bio-Rad
LightCycler® 480 SYBR Green I Master	Roche
Bio-Plex® Multiplex Assays	Bio-Rad

2.1.8 Cell culture media

Table 7: Cell culture media

Medium	Supplements
RPMI-1640 (Gibco®, Invitrogen) Roswell park memorial institute-1640	10% (v/v) FCS heat-inactivated 2 nM glutamine (Sigma-Aldrich) 100 U/ml penicilin (Sigma-Aldrich) 100 µg/ml streptomycin (Sigma-Aldrich) 0.05 mM 2-ME (Sigma-Aldrich)
DMEM (Gibco®, Invitrogen) Dulbecco's modified eagle's medium	10% (v/v) FCS heat-inactivated 2 nM glutamine (Sigma-Aldrich) 100 U/ml penicilin (Sigma-Aldrich) 100 µg/ml streptomycin (Sigma-Aldrich) 0.05 mM 2-ME (Sigma-Aldrich)
ENDOPAN-3 (Pan-BioTech)	3% (v/v) FCS FGF-2, VEGF, R3-IGF-1, ascorbic acid, heparin, gentamicin sulfate amphotericin B, hydrocortisone

2.1.9 Antibodies and reagents for flow cytometry

Table 8: Antibodies and reagents for flow cytometry
FITC, fluorescein isothiocyanate; PE, R-phycoerythrin; PerCP/Cy5.5, peridinin chlorophyll/cyanine (Cy5.5); PE/Cy7, PE/cyanine (Cy7); APC, allophycocyanin; AF647, Alexa Fluor 647; APC/Cy7, APC/cyanine (Cy7); APC/eF780, APC/eFluor® 780; PB, pacific blue; BV421, brilliant violet™ 421, BV650, brilliant violet™ 650

Name	Clone	Reactivity	Conjugate	Company
α-CD3ε Ab	145-2C11	Mouse	FITC	BDBiosciences
α-CD4 Ab	GK1.5	Mouse	APC/Cy7	BioLegend
α-CD4 Ab	GK1.5	Mouse	PB	BioLegend
α-CD8a Ab	53-6.7	Mouse	PE	BDBiosciences
α-CD8a Ab	53-6.7	Mouse	PE/Cy7	BDBiosciences
α-CD8a Ab	53-6.7	Mouse	AF647	BioLegend
α-CD11b Ab	M1/70	Mouse	PB	BioLegend
α-CD11c Ab	HL3	Mouse	PE/Cy7	BDBiosciences
α-CD19 Ab	1D3	Mouse	PE	BDBiosciences
α-CD45 Ab	30-F11	Mouse	PB	BioLegend
α-CD45 Ab	30-F11	Mouse	BV606	BioLegend
α-CD45.2 Ab	104	Mouse	APC/Cy7	BioLegend
α-CD49b Ab	DX5	Mouse	APC/eF780	eBiosciences
α-CD117 Ab (c-Kit)	2B8	Mouse	PE/Cy7	eBiosciences
α-CD200R3Ab	Ba13	Mouse	PE	BioLegend
α-CD206 Ab (MRC1)	C068C2	Mouse	PE	BioLegend
α-F4/80 Ab	BM8	Mouse	PerCP/Cy5.5	eBiosciences
α-F4/80 Ab	BM8	Mouse	PE/Cy7	eBiosciences
α-F4/80 Ab	BM8	Mouse	AF647	BioLegend
α-FcεRI Ab	MAR-1	Mouse	PE	eBiosciences
α-Gr-1 Ab	RB6-8C5	Mouse	FITC	BDBiosciences
α-Gr-1 Ab	RB6-8C5	Mouse	PE/Cy7	BioLegend
α-Gr-1 Ab	RB6-8C5	Mouse	APC	BDBiosciences
α-IgE Ab	R35-72	Mouse	FITC	BDBiosciences

α-iNOS Ab	CXNFT	Mouse	FITC	eBiosciences
α-MHC-II Ab (I-A/I-E)	M5/114.15.2	Mouse	FITC	BioLegend
α-MHC-II Ab (I-A/I-E)	M5/114.15.2	Mouse	APC/Cy7	BioLegend
α-NK1.1 Ab	PK136	Mouse	PE/Cy7	BDBiosciences
α-Siglec-F Ab	E50-2440	Mouse	PE	BDBiosciences
α-Siglec-F Ab	E50-2440	Mouse	APC	BDBiosciences
α-Ter119 Ab	TER119	Mouse	PerCP/Cy5.5	BioLegend
α-CD90.1 Ab (Thy1.1)	OX-7	Mouse	PB	BioLegend
α-CD62E Ab (E-Selectin)		Human		
α-CD54 Ab (ICAM-1)		Human		
α-CD106 Ab (VCAM-1)		Human		
α-vWF		Human		
Fixable viability dye			APC/eF780	eBiosciences
Propidium iodide (PI)				Fluka

2.1.10 Antibodies and reagents for immunofluorescene

Table 9 Antibodies and reagents for immunofluorescence

Name	**Clone**	**Conjugate**	**Company**
α-CD31 Ab	2H8		AbD Serotec
α-VCAM-1 (CD106) Ab	429		BD Biosciences
α-Armenian hamster IgG	Poly4055	DyLight™ 488	BioLegend
α-Armenian hamster IgG	Poly4055	DyLight™ 594	BioLegend
α-Rat IgG	Poly4054	DyLight™ 488	BioLegend

α-Rat IgG	Poly4054	Cy3	BioLegend
VectaShield® mounting medium with DAPI			Vector

2.1.11 Primers for quantitive real-time polymerase chain reaction (qRT-PCR)

Table 10: Primers for qRT-PCR

Gene	**Sequence (5'➔3')**
Angpt2	CCTCGACTACGACGACTCAGT TCTGCACCACATTCTGTTGGA
Ccl2	TTAAAAACCTGGATCGGAACCAA GCATTAGCTTCAGATTTACGGGT
Ccl3	TTCTCTGTACCATGACACTCTGC CGTGGAATCTTCCGGCTGTAG
Ccl4	TTCCTGCTGTTTCTCTTACACCT CTGTCTGCCTCTTTTGGTCAG
Ccl5	GCTGCTTTGCCTACCTCTCC TCGAGTGACAAACACGACTGC
Ccl7	GCTGCTTTCAGCATCCAAGTG CCAGGGACACCGACTACTG
Ccl11	GAATCACCAACAACAGATGCAC ATCCTGGACCCACTTCTTCTT
Ccl19	GGGGTGCTAATGATGCGGAA CCTTAGTGTGGTGAACACAACA
Ccl20	GCCTCTCGTACATACAGACGC CCAGTTCTGCTTTGGATCAGC
Ccl22	AGGTCCCTATGGTGCCAATGT CGGCAGGATTTTGAGGTCCA
Ccl24	ATTCTGTGACCATCCCCTCAT TGTATGTGCCTCTGAACCCAC
Cxcl9	TCCTTTTGGGCATCATCTTCC TTTGTAGTGGATCGTGCCTCG

Cxcl10	CCAAGTGCTGCCGTCATTTTC GGCTCGCAGGGATGATTTCAA
Fgf1	CCCTGACCGAGAGGTTCAAC GTCCCTTGTCCCATCCACG
Gapdh	AGGTCGGTGTGAACGGATTTG TGTAGACCATGTAGTTGAGGTCA
Gm-Csf	GGCCTTGGAAGCATGTAGAGG GGAGAACTCGTTAGAGACGACTT
Icam-1	GTGATGCTCAGGTATCCATCCA CACAGTTCTCAAAGCACAGCG
Ifn-α	TACTCAGCAGACCTTGAACCT CAGTCTTGGCAGCAAGTTGAC
Ifn-β	CAGCTCCAAGAAAGGACGAAC GGCAGTGTAACTCTTCTGCAT
Ifn-γ	ATGAACGCTACACACTGCATC CCATCCTTTTGCCAGTTCCTC
Il-1β	GCAACTGTTCCTGAACTCAACT ATCTTTTGGGGTCCGTCAACT
Il-2	TGAGCAGGATGGAGAATTACAGG GTCCAAGTTCATCTTCTAGGCAC
Il-3	GGGATACCCACCGTTTAACCA AGGTTTACTCTCCGAAAGCTCTT
Il-4	GGTCTCAACCCCCAGCTAGT GCCGATGATCTCTCTCAAGTGAT
Il-5	CTCTGTTGACAAGCAATGAGACG TCTTCAGTATGTCTAGCCCCTG
Il-6	TAGTCCTTCCTACCCCAATTTCC TTGGTCCTTAGCCACTCCTTC
Il-9	ATGTTGGTGACATACATCCTTGC TGACGGTGGATCATCCTTCAG
Il-10	GCTCTTACTGACTGGCATGAG CGCAGCTCTAGGAGCATGTG

Il-12	CTGTGCCTTGGTAGCATCTATG GCAGAGTCTCGCCATTATGATTC
Il-13	CCTGGCTCTTGCTTGCCTT GGTCTTGTGTGATGTTGCTCA
Il-18	GACTCTTGCGTCAACTTCAAGG CAGGCTGTCTTTTGTCAACGA
Il-25	ACAGGGACTTGAATCGGGTC TGGTAAAGTGGGACGGAGTTG
Il-33	TCCAACTCCAAGATTTCCCCG CATGCAGTAGACATGGCAGAA
Mcpt8	CCACTCCCGGCCCTATATG TGCTGTCATTACGATGTCTCTTG
Mhc-II (H2-2α)	TCAGTCGCAGACGGTGTTTAT GGGGGCTGGAATCTCAGGT
Nos2	GTTCTCAGCCCAACAATACAAGA GTGGACGGGTCGATGTCAC
Pdgf-α	GAGGAAGCCGAGATACCCC TGCTGTGGATCTGACTTCGAG
Rgs5	CGCACTCATGCCTGGAAAG TGAAGCTGGCAAATCCATAGC
Tnf	CCCTCACACTCAGATCATCTTCT GCTACGACGTGGGCTACAG
Tslp	ACGGATGGGGCTAACTTACAA AGTCCTCGATTTGCTCGAACT
Vcam-1	AGTTGGGGATTCGGTTGTTCT CCCCTCATTCCTTACCACCC
Vegf-α	CTGCCGTCCGATTGAGACC CCCCTCCTTGTACCACTGTC

2.1.12 Equipments

Table 11: Equipments

Name	Company
FACSCanto II	BD Biosciences
FACSAria II	BD Biosciences
Axio Observor.Z1	Zeiss
FastPrep® FP120 cell disrupter	Qbiogene
NanoDrop 2000™ spectrophotometer	Thermo Fisher Scientific
PTC-200 thermal cycler	MJ Research Inc.
Light Cycler® 480 II	Roche
Minifuge-2	Heraeus Christ
BB 6220 CO2 incubator	Heraeus Christ

2.1.13 Software

Table 12: Software

Name	Company
FACSDiva v. 6.1.2	BD Biosciences
FlowJo v. 9.8	Tree Star
ZEN 2011 lite (blue edition)	Zeiss
Light Cycler® 480 software v.1.5.0	Roche
Excel 2008 v. 12.3.6	Microsoft
Power Point 2008 v. 12.3.6	Microsoft
Prism 6 v. 6.0d	GraphPad Software
EndNote v. X7.2.1	Thomson Corporation

2.2 Methods

2.2.1 Mouse Studies

2.2.1.1 Tumor challenge

$1x10^6$ tumor cells were injected intradermally (i.d.) at the right flank of mice. Tumor sizes were measured with a caliper every 2-3 days and tumor volume was calculated according to the formula: $V= 0.5 \times Length \times Width^2$. Mice were sacrificed when tumors reached a size of 2000 mm^3.

2.2.1.2 Cell depletion

For Treg depletion, $Foxp3^{DTR}$ and Foxp3.LuciDTR4 mice received two consecutive injections with 20 ng/g DT (Sigma-Aldrich, Steinheim, Germany) intraperitoneally (i.p.). Treg depletion was initiated when the tumors displayed a volume of 250-500 mm^3.

For the depletion of $CD8^+$ T cells, mice were injected intraperitoneally (i.p.) with 500 µg anti-CD8 antibody (BioXCell, West Lebanon, USA, Clone 2.43) 0, 3, 6 days after Treg depletion. $CD4^+$ T cells were depleted by i.p. injection of 1 mg anti-CD4 antibody (BioXCell, West Lebanon, USA, Clone GK1.5) 0, 3, 6 days after Treg depletion. Natural killer (NK) cells were depleted by i.p. injection of 1 mg anti-NK1.1 antibody (BioXCell, West Lebanon, USA, Clone PK163-3-6) 0, 3, 6 days after Treg depletion.

Basophils were depleted by i.p. injection of 10 µg anti-FcεRI antibody (eBiosciences, Frankfurt am Main, Germany, Clone: MAR-1) 0, 2,3,4 and 6 days after Treg depletion for tumor growth experiments. For population analyses, MAR-1 was injected i.p. 0 and 2 days after Treg depletion.

For macrophage depletion in $Foxp3^{DTR}$ mice bearing intradermal HCmel 1274 tumors, clodronate-loaded liposomes (CLIP) (VUMC, Amsterdam, Netherlands)

were first injected 200 µl i.p and 100 µl intratumorally (i.t) 2 days following Treg depletion, then every 5 days 100 µl i.t until the end of the experiment. PBS-loaded liposomes (PLIP) (VUMC, Amsterdam, Netherlands) were used as control. For population analyses, CLIP or PLIP was injected 200 µl i.p and 100 µl i.t 2 days after Treg depletion.

Macrophages in Rip1-Tag5 (RT5) mice were depleted by i.p. injections of 100 µl CLIP every 5 days after an inital injection with 200 µl CLIP. PLIP was used as control.

2.2.1.3 Preparation of cell suspensions from mouse tissues

Cell suspension were prepared from tumor-draining lymph nodes (td-LN), spleen, lung, bone marrow and tumor. Tumor-draining lymph nodes were axillary, branchial and inguinal lymph nodes on the right flank of the mice.

For T cell preparations, spleens from OT-I or TCR8 mice were minced using a scalpel. Respective tissue fragments were meshed through 40 µm nylon cell strainer into a petri dish using the plunger end of the syringe. The cell strainer was then rinsed with ice-cold dPBS. The suspended cells were transferred into a 15 ml conical centrifugation tubes and spun at 4°C at 1200 rpm for 8 minutes and the supernatant was discarded. The cell pellet was resuspended in 2 ml of ACK buffer and incubated at room temperature for 3 minutes to lyse erythrocytes. After the incubation, 8 ml RPMI-1640 was added and the cells were centrifuged as mentioned above. The supernatant was again discarded and the pellet was resuspended in 2 ml RPMI-1640 medium.

For macrophage preparations, femurs and tibias were taken and both ends were cut with a scissor. Bone marrow cells were flushed out with a syringe and 25G needle using ice-cold dPBS. Cell suspension was next filtered into 50 ml falcon tubes through a 40 µm filter to remove crude tissue particles.

For flow cytometric stainings, tumors, td-LNs, spleens and lungs from mice were isolated from mice and placed in 3 ml of dPBS containing 1 mg/ml of

collagenase IV (Sigma-Aldrich, Steinheim, Germany) and 50 U/ml of Dnase I (Sigma-Aldrich, Steinheim, Germany). Tissue was disrupted using forceps and transferred into 5 ml round-bottom polystyrene tubes. Samples were then incubated at room temperature with gentle stirring by a magnet (100 rpm). Enzymatic digestion of the tissues was supported by mechanical disruption via pipetting up and down 10 times every 10 minutes. After 30 minutes, samples were filtered through a 40 µm nylon cell strainer. Erythrocytes were removed by incubating with ACK buffer for 2 minutes. After the centrifugation at 1400 rpm for 8 minutes, samples were incubated in FACS blocking buffer (FACS buffer with 1% normal immunoglobulin (Privigen®, CSL Berling, Hattersheim am Main, Germany) for 15 minutes. Finally, samples were stained for flow cytometry. RT5 tumors were first homogenized with small scissors and placed into 1.5 ml eppendorf tubes containing 1 ml of dPBS with 0.2 mg/ml of collagenase D (Roche, Mannheim, Germany), 0.08 mg/ml of dispase I (Roche, Mannheim, Germany) and 0.025 mg/ml of DNase I (Sigma-Aldrich, Steinheim, Germany). Samples were incubated at 37°C for 30 minutes. Samples were filtered through a 40 µm nylon cell strainer into a 5 ml round-bottom polystyrene tubes and then centrifuged at 1400 rpm for 8 minutes. The pellet was resuspended in FACS blocking buffer. After 15 minute-incubation, the samples were stained for flow cytometry.

2.2.1.4 Preparation of monouclear cells from whole blood

Whole blood was collected from the submandibular facial vein into dPBS including heparin in order to avoid clotting and then spun at 5000 rpm for 4 minutes. The supernatant was discarded and the cell pellet was resuspended in 1ml of ACK buffer to kill erythrocytes. After 7 minute-incubation at room temperature, samples were centrifuged at 5000 rpm for 4 minutes and the supernatant was discarded. The pellet was resuspended in FACS blocking buffer. Samples were then stained for flow cytometry analysis.

2.2.1.5 Adoptive transfer of $CD8^+$ T cells

Spleens were harvested from naive OT-I or TCR8 mice and disrupted to obtain single-cell suspensions as mentioned above. Splenic cells were resuspend at

$1x10^6$ cells/ml in RPMI-1640 medium supplemented with 10% FCS, 2 nM glutamine, 100 U/ml penicilin, 100 µg/ml streptomycin, 0.05 mM 2-ME, 10U/ml of recombinant IL-2 (eBiosciences, Frankfurt am Main, Germany). OT-I splenic cells were cultured in the presence of 25 nM SIINFEKL peptide (PSL, Heidelberg Germany). TCR8 splenic cells were cultured in the presence of 25 nM Tag peptide 560-568 (PSL, Heidelberg Germany). Cells were used for adoptive transfer 3 days after incubation at 37°C. B16-OVA-bearing mice received intravenous (i.v.) injections of $2.5x10^6$ activated OT-I $CD8^+$ T cells in 200 µl dPBS 1 day after macrophage transfer or 3 days after mouse recombinant IL-3 injection. RT5 mice were adoptively transferred with $2.5x10^6$ activated TCR8 $CD8^+$ T cells in 200 µl dPBS 1 day after CpG-ODN injection and 10 days after the first injection. For survival experiment, TCR8 $CD8^+$ T cell transfer was repeated every 10 days.

2.2.1.6 Adoptive transfer of macrophages

Bone marrow-derived cells were prepared from wild-type or $NOS2^{-/-}$ mice (received from Christian Bogdan, Universitätsklinikum, Erlangen) as mentioned above and cultured at $3.5x10^6$ cells/ml in RPMI-1640 medium supplemented with 10% FCS, 2 nM glutamine, 100 U/ml penicilin, 100 µg/ml streptomycin and 10 ng/ml mouse recombinant macrophage-colony stimulating factor (M-CSF) (Sigma-Aldrich, Steinheim, Germany). 5 days later, culture medium was changed to fresh medium with the same supplements. 3 days after the medium change, macrophages were activated with 20 ng/ml LPS (Sigma-Aldrich, Steinheim, Germany) and 20 ng/ml mouse recombinant IFN-γ (PeproTech, Hamburg, Germany) or left untreated. 18 hours later, macrophages were harvested using StemPro® Accutase® cell dissciation reagent (Life Technologies, Darmstadt Germany). For adoptive transfer, $5x10^6$ activated and non-activated macrophages in 200 µl dPBS were injected i.v. when tumors reached a size of 300-500 mm^3.

2.2.1.7 Adoptive transfer of Tregs

Spleens were harvested from naive wild-type mice and dissociated to obtain single-cell suspensions as mentioned above. Splenic cells were resuspend in MACS buffer and $CD4^+$ $CD25^+$ Tregs were sorted using the Treg magnetic isolation kit

(Miltenyi, Bergisch Gladbach, Germany) in a two-step procedure. First, $CD4^+$ T cells were negatively selected by depleting other cells over a MACS® column (LS column) with a cocktail of biotin-conjugated antibodies against CD8 (Ly-2), CD11b (Mac-1), CD45R (B220), CD49b (DX5), Ter-119 and anti-biotin magnetic microbeads. In the second step, negatively selected untouched $CD4^+$ T cells are labeled with CD25 microbeads, which allow positive selection of $CD4^+CD25^+$regulatory T cells. The magnetic cell sorting was performed on a Miltenyi MACS Multi Stand with MACS magnet (Miltenyi, Bergisch Gladbach, Germany) using LS columns. Purified $CD4^+$ $CD25^+$ Tregs were then injected i.t. into HCmel 1274-bearing $Foxp3^{DTR}$ mice 2 days after Treg depletion.

2.2.1.8 Oligonucleotide treatment

24 week-old RT5 mice were injected with phosphothioate-stabilized CpG-ODN 1668 (TCCATGACGTTCCTGATGCT) (TIB-MOLBIOL, Berlin, Germany) and 6 and 10 days after the first injection.

2.2.1.9 Cytokine injection

10 µg IL-3 (PeproTech, Hamburg, Germany) was mixed with 5 µg anti-IL-3 antibody (BD Biosciences, Heidelberg, Germany, Clone MP2-8F8) at room temperature for one minute. The cytokine and antibody mixture in 200 µl dPBS was injected into mice i.v. when tumors reached a size of 200-400 mm^3.

2.2.1.10 Cytokine, chemokine and inducible nitric oxide synthase (iNOS) blocking

For in vivo IFN-γ blockade, 500 µg anti- IFN-γ (BioXCell, West Lebanon, USA, Clone XMG1.2) or 500 µg isotype control, rat IgG1 (BioXCell, West Lebanon, USA), was injected into $Foxp3^{DTR}$ mice i.p. 2, 5 and 8 days after Treg depletion.

For in vivo blockade of CCL3 and CCL4, 250 µg of anti-CCL3 (R&D Systems, Abingdon, UK, Clone 39624) and anti-CCL4 (R&D Systems, Abingdon,

UK, Clone 46907) antibodies or appropriate isotype control, rat IgG2a, were injected into mice 0, 3, 6 days after OT-I $CD8^+$ T cell transfer.

iNOS activity in mice was blocked by 2 mM N6-(1-iminoethyl)-L-lysine, dihydrochloride (L-NIL) in the drinking water. The water bottles containing L-NIL was replaced every 2 days until the end of experiment.

2.2.2 Cell biology methods

2.2.2.1 Flow cytometric stainings and cell sorting

Antibodies used for flow cytometry are listed in **Table 8**. Single cell suspensions from the tissues were prepared as mentioned above and incubated with FACS blocking buffer for 15 minutes in 96-well plates with U-shaped wells to minimize non-specific binding. For extracellular staining, samples were incubated with a cocktail of fluorochrome-conjugated anti-mouse antibodies in FACS blocking buffer for 20 minutes at 4°C. Afterwards, samples were washed twice with FACS Buffer. To exclude dead cells, samples were then resuspended in 200 µl of FACS buffer containing 1 µg/ml propidium iodide (PI) (BD Biosciences, Heidelberg, Germany). For staining of intracellular molecules, samples were first stained with fixable viability dye (eBiosciences, Frankfurt am Main, Germany) for 15 minutes at 4°C and then fixed with fixation/permeabilization buffer from Foxp3-staining kit (eBiosciences, Frankfurt am Main, Germany) for 30-60 minutes. Samples were permeabilized with 1X permeabilization buffer from Foxp3-staining kit (eBiosciences, Frankfurt am Main, Germany) and then stained with a mixture of antibodies or isotype controls in 1X permeabilization buffer for 30 minutes at 4°C. After washing twice with 1X permeabilization buffer, samples were resuspended in FACS buffer. Stained samples were acquired using a BD FACSCanto II (BD Biosciences, Heidelberg, Germany) with BDFACSDiva software (BD Biosciences, Heidelberg, Germany). Data were analyzed with FlowJo software (Tree Star, Ashland, USA). For analysis of cells purified from tumors, $1\text{-}5x10^4$ cells were sorted with a FACSAria II (BD Biosciences, Heidelberg, Germany) running with FACSDiva Software (BD Biosciences, Heidelberg, Germany).

2.2.2.2 Cryosectioning and immunofluorescence analysis

Tumors were carefully excised from euthanized mice and placed into cryomolds containing OCT gel (Tissue-Tek®, Sakura, Staufen, Germany). Samples were first incubated in ice-cold isopentane for 10 minutes and then placed in liquid nitrogen-cooled isopentane for 10 minutes. Afterwards, samples were slowly exposed to liquid nitrogen. Frozen samples were stored at -80°C.

7 µm sections were prepared from OCT-embedded frozen tumors using Leica CM3050S cryotome (Wetzlar Germany) and placed onto silane-coated slides. After drying overnight, sections were fixed with 10 minute-incubation in ice-cold acetone. Samples were again air-dried for 20 minutes to allow acetone to evaporate from the tumor tissues. Sections were then used for immunofluorescent staining immediately or stored at -30°C for later use.

A hydrophobic wax pen used to create a boundary around the tissue sections on the slide. The immunofluorecent staining was performed in a humid chamber to prevent sections from drying. Sections were rehydrated in PBS containing 0.01% Tween20 (PBS-Tween) for 10 minutes and incubated in immunofluorescent (IF) blocking buffer (PBS-Tween containing 5% goat serum (Sigma-Aldrich, Steinheim, Germany) for 15 minutes. After draining off the blocking buffer from slides, the sections were incubated at room temperature for 60 minutes with 100 µl of primary antibodies in IF blocking buffer (listed in **Table 9**). Excess antibody was removed by washing the slides 3 times in PBS-Tween, 5 minutes each. 200 µl of secondary antibodies (listed in **Table 9**) in IF blocking buffer was added and samples were incubated in the dark at room temperature for 60 minutes. Excess antibody was removed by washing the slides 3 times in PBS-Tween, 5 minutes each. Thereafter, sections were mounted in VectaShield® mounting medium with DAPI (Vector, Peteborough, UK).

Stained sections were visualized under Zeiss Axio Observor.Z1 microscope (Zeiss, Jena, Germany). Zeiss blue software (Zeiss, Jena, Germany) was used to analyze the tumor vasculature.

2.2.2.3 Giemsa Staining

Morphology of sorted basophils was analyzed by Giemsa staining. Sorted basophils were first placed in a cuvette which was already assembled with a slide and a cardboard filter. After the centrifugation at 700 rpm for 4 minutes, cells on the slides were fixed with 100% methanol for 5 minutes. The slides were rinsed off in the water and allowed to air-dry. The cells were then stained with freshly prepared Giemsa solution (10% v/v Giemsa stain (Sigma-Aldrich, Steinheim, Germany) in deionized water) for 30 minutes. The slides were again rinsed in the water and air-dried. Thereafter, sections were mounted in Permount™ mounting medium (Thermo Fisher Scientific Karlsruhe, Germany). Giemsa-stained cells were then visualized under Zeiss Axioplan widefiled microscope (Zeiss, Jena, Germany). Zeiss blue software was used to analyze the tumor vasculature.

2.2.3 Cell culture methods

Cell culture was conducted under sterile conditions at 37°C in a CO_2 incubator (5%).

2.2.3.1 Culture of tumor cell lines

The growth medium for tumor cell lines, B16, B16-OVA and HCmel 1274, was DMEM supplemented with 10% FCS, 2 nM glutamine, 100 U/ml penicilin, 100 µg/ml streptomycin and 0.05 mM 2-ME. When the cells were 80-90% confluent, they were passaged.

2.2.3.2 Culture of human umbilical vein endothelial cells (HUVECs)

HUVECs were supplied from pooled donors (PromoCell, Heidelberg, Germany). Upon arrival, frozen HUVECs were immediately thawn and cultured in ENDOPAN 3 endothelial cell growth medium (Pan-Biotech, Aidenbach, Germany) supplemented with 3% FBS, 0.1% FGF-2, 0.1% VEGF, 0.1% R3-IGF-1, 0.1% ascorbic acid, 0.1% heparin, 0.12% gentamicin sulfate amphotericin B, 0.02%

hydrocortisone. Once they have reached 70-90% confluency, the cells were subcultured.

2.2.3.3 Isolation and culture of human macrophages

To obtain human macrophages, first of all, mononuclear cells were isolated from human peripheral blood by density gradient centrifugation using Ficoll-Paque™ (GE Healthcare, Freiburg, Germany). During centrifugation, erythrocytes and polynucleated cells pass through the Ficoll due to their higher density, while mononuclear cells accumulated as a white band on the top the Ficoll layer. This white band was carefully pipetted and washed twice with PBS. Isolated mononuclear cells were then plated at $2x10^8$/175 cm^2 in RPMI-1640 medium supplemented with 10% FCS, 2 nM glutamine, 100 U/ml penicilin, 100 µg/ml streptomycin and incubated for 90 minutes at 37°C. Thereafter, suspension cells were discarded and adherent cells, which mainly contains monocytes, were removed using StemPro® Accutase® cell dissociation reagent. Monocytes were next seeded at $2x10^6$ cells/ml in RPMI-1640 medium supplemented with 10% FCS, 2 nM glutamine, 100 U/ml penicilin, 100 µg/ml streptomycin and 25 ng/ml human recombinant M-CSF (PeproTech, Hamburg, Germany). After 6 day-incubation at 37°C, monocytes were differentiated into macrophages, confirmed by FACS staining with CD14 and CD68. Macrophages were left untreated (M0 macrophages) or activated in the presence of 100 ng/ml LPS and 20 ng/ml human recombinant IFN-γ (PeproTech, Hamburg, Germany) for 18 hours to generate M1 macrophages.

2.2.3.4 Co-culture of HUVECs and human macrophages

Human macrophages were isolated from circulating blood monocytes, and were left untreated (M0 macrophages) or activated (M1 macrophages) as mentioned above. Macrophages were then harvested using StemPro® Accutase® cell dissociation reagent. $1x10^6$ M1 or M0 macrophages were added to HUVECs, which had been cultured at $1x10^5$ cells/ml 3 days ago in 6-well plates, in the presence or absence of iNOS inhibitor L-NIL (1mM). 18 hours later, cells were harvested and the expression of adhesion molecules on HUVECs such as VCAM-1, ICAM-1 and E-

Selectin was measured by FACS. HUVECs were distinguished from macrophages by their expression of von willebrand factor (vWF).

2.2.3.5 Culture of HUVECs with NO donor

HUVECs were cultured at $1x10^5$ cells/ml into 6 well plates. 3 days later, NO donor, glycerel trinitrate (GTN) (Sigma-Aldrich, Steinheim, Germany) with different doses were added to the cultures. After 18 hour-incubation, cells were harvested and the expression of adhesion molecules on HUVECs such as VCAM-1, ICAM-1 and E-Selectin was measured by FACS.

2.2.3.6 Detection of nitric oxide (NO) as nitrite (NO_2^-)

The level of NO in the cell culture was measured by Griess reagent (Sigma-Aldrich, Steinheim, Germany) as NO_2^- according to manufacturer's instructions.

2.2.3.7 Generation and isolation of mouse basophils from bone marrow

Bone marrow cells were prepared as mentioned above and cultured RPMI-1640 medium supplemented with 10% FCS, 2 nM glutamine, 100 U/ml penicilin, 100 µg/ml streptomycin and 2 ng/ml mouse recombinant IL-3 (R&D Systems, Abingdon, UK) for 10 days to yield basophils and mast cells. Basophils were then purified by magnetic sorting based on CD49b expression. Sorted basophils were then activated by 50 ng/ml mouse recombinant IL-18 (R&D Systems, Abingdon, UK) and 100 ng/ml mouse recombinant IL-33 (R&D Systems, Abingdon, UK) in the presence of 2 ng/ml IL-3.

2.2.3.8 In vitro migration assay

Migration of activated OT-I $CD8^+$ T cells were analyzed using 96-well transwell plates with a 5 µm-pore size (Corning Life Sciences, Amsterdam, Netherlands). The lower chamber was loaded with 100 µl migration medium (RPMI-1640 supplemented with 0.2% FCS, 2 nM glutamine, 100 U/ml penicilin, 100 µg/ml streptomycin and 0.05 nM 2-ME) containing different doses ($1x10^5$-$1x10^6$) of

basophils. $1x10^5$ activated OT-I $CD8^+$ T cells were added in 50 µl to the upper chamber. As a positive control, OT-I $CD8^+$ T cells were placed directly into the lower chamber. As a negative control, migration medium alone was placed in the upper chamber. As a control group, OT-I $CD8^+$ T cells were added to the upper chamber and migration medium alone was added to the lower chamber. After 18 hour-incubation at 37°C, the transwell inserts were removed and the content of the lower compartment carefully pipetted and transferred into 96-well plates for FACS staining. The number of OT-I $CD8^+$ T cells were measured by flow cytometry in the presence of a particular number of microbeads. Migration rate was calculated using the formula: migration rate = 100 x (number of $CD8^+$ cells from lower chamber/number of beads) / (number of $CD8^+$ T cells from input sample/number of beads). For experiments with chemokine blockade, neutraziling antibodies against CCL3 (R&D Systems, Abingdon, UK) and CCL4 (R&D Systems, Abingdon, UK) were added to the lower chamber before the migration assay.

2.2.4 Molecular biology methods

2.2.4.1 Quantitive PCR (qRT-PCR)

Tumors were collected from mice and cut into samples of approximately 25 mg. Each sample was placed in a tube containing 450 µl of lysis buffer (RLT buffer) and 1.4 mm zirconium oxide beads (Peqlab, Erlangen, Germany). Samples were then mechanistically disrupted by FastPrep® FP120 cell disrupter (Qbiogene, Cedex, France) running at 6.5 m/s for 15 seconds. RNA was extracted using the RNeasy Mini Kit (Qiagen, Düsseldorf, Germany) according to manufacturer's instructions. RNA from sorted cells was isolated using the RNeasy Micro kit (Qiagen, Düsseldorf, Germany). The concentration of RNA was determined by a NanoDrop 2000™ spectrophotometer (Thermo Fischer Scientific, Karlsruhe, Germany). cDNA synthesis was performed using iScript cDNA synthesis kit (Bio-Rad, München, Germany) according to the protocol below.

Components	**Volume per reaction**
5x iScript reaction mix	4 µl
iScript reverse transcriptase	1 µl
Nuclease-free water	x µl
RNA template (100 fg to 1 µg total RNA)	x µl
Total volume	20 µl

Complete reaction mix was incubated at 25ºC for 5 minutes, at 42ºC for 30 minutes at 85ºC for 5 minutes in a thermal cycler.

Gene expression was determined using real-time PCR with LightCycler® 480 SYBR Green I Master (Roche, Mannheim, Germany) in a Light Cycler® 480 (Roche, Mannheim, Germany) according to the protocol below.

Components	**Volume per reaction**
SYBR Green I Master	5 µl
Primer mix (each 500nM)	1 µl
Nuclease-free water	1.5 µl
cDNA sample (100 fg to 1 µg)	2.5 µl
Total volume	10 µl

Pre incubation (1 cycle):	95°C 5 minutes
Amplification (45 cycles):	95°C 10 seconds
	60°C 15 seconds
	72°C 20 seconds
Melting curve (1 cycle):	95°C 5 seconds
	60°C 1 minutes
Cooling (1 cycle):	40°C 10 seconds

Dissociation curves were used to confrim specificity of the PCR. Results are expressed as $-\Delta\Delta Ct$. $-\Delta\Delta Ct = 2^{-\Delta Ctsample-\Delta Ctbiggest\ Ct}$, $\Delta Ct = Ct_{target\ mRNA} - Ct_{Gapdh}$. The primers used are shown in **Table 10**.

2.2.4.2 Protein level analysis

Tumor tissue and purified basophils were lysed using the Bio-Plex Cell Lysis Kit (Bio-Rad, München, Germany). Chemokines were quntified using the multiplex protein array system technology (Bio-Rad, München, Germany) according to manufacturer's instructions.

2.2.4.3 Microarray analysis

Total RNA was isolated from untreated HUVECs or from HUVECs treated with NO donor (GTN) or TNF, and hybridized to Human HT-12 v4 expression beadchip (Illumina, San Diego, USA) in DKFZ Genomics and Proteomics Facility. Normalized gene expression intensities were compared, and genes were considered to be differentially expressed between different groups if their fold change was greater than 2 or less than -2.

3 RESULTS

3.1 Treg Depletion as a Model to Study Immune Rejection of Tumors

Tumors harbor several mechanisms that impair the efficacy of cancer immunotherapy. One of the major obstacles is created by $CD4^+$ $CD25^+$ $Foxp3^+$ Tregs, which are known to promote tumor progression by limiting anti-tumor T cell response. Tregs are often found at elevated frequencies in the peripheral blood and tumors of cancer patients, and their accumulation is associated with poor disease outcome for many cancers[103, 104, 105, 106]. Various groups have established mouse models, which allow high-level depletion of Tregs. For example, Alexander Rudensky's group generated $Foxp3^{DTR}$ mutant mice, which express knocked-in human diptheria toxin receptor (DTR) and enhanced green fluorescent protein (eGFP) under the control of foxp3 locus[219]. In these mice, diptheria toxin (DT) administration results in almost complete Treg depletion[219]. In addition, our group established bacterial artificial chromosome (BAC)-transgenic Foxp3.LuciDTR4 mice, in which Tregs express luciferase and eGFP for the detection and human DTR for the depletion[220]. DT application in these mice led to about 90-95% depletion of Tregs[220]. The presence of these two mouse models displaying different degrees of Treg depletion allowed me to study whether the extent of Treg depletion would be important for anti-tumor immune responses.

3.1.1 Treg depletion in $Foxp3^{DTR}$ knock-in mice is more efficient than in BAC transgenic Foxp3.LuciDTR4 mice

The degree of Treg depletion in $Foxp3^{DTR}$ and Foxp3.LuciDTR4 models was compared one day after intraperitoneal DT (20 ng/g) application. For this purpose, Foxp3 expression in $CD4^+$ T cells was measured by flow cytometry in the tumor, tumor-draining lymph nodes (td-LNs), spleen and blood of wild type, $Foxp3^{DTR}$ and

Foxp3.LuciDTR4 mice. DT application in Foxp3.LuciDTR4 mice resulted in about 92% depletion in the tumor, 95% depletion in td-LNs, 92% depletion in spleen and 80% depletion in blood **(Figure 1A, B)**. DT treatment of $Foxp3^{DTR}$ mice led to about 99% depletion in the tumor, 99% depletion in td-LNs, 99% depletion in spleen and 90% depletion in blood **(Figure 1A, B)**. These findings show that Treg depletion is significantly more effective in $Foxp3^{DTR}$ mice as compared to Foxp3.LuciDTR4 mice, probably because in knock-in $Foxp3^{DTR}$ mice the DTR is expressed presumably in all $Foxp3^{+}$ Tregs. In contrast, BAC-transgenic Foxp3.LuciDTR4 mice contain a small percentage of $Foxp3^{+}$ Tregs that do not express DTR[220].

3.1.2 A small number of Tregs can obstruct the $CD8^{+}$ T cell-dependent complete rejection of tumors

To examine the role of differential Treg depletion in anti-tumor immune responses, HCmel 1274 and B16 melanomas were utilized. HCmel 1274 is a melanoma cell line recently derived from HGF-CDK4 mice which spontaneosuly develop melanoma due to transgenic overexpression of hepatocyte growth factor (HGF) and impaired $p16^{Ink4a}$-dependent cell cycle regulation resulting from an oncogenic CDK4 (R24C) germline mutation[277]. Similar to B16 cells, HCmel 1274 cells express natural melanoma antigens, including tyrosinase, tyrosine-related protein (TRP)-1, TRP-2 and glycoprotein 100 (gp100), which can induce T cell responses. The B16 cell line was isolated from a chemically induced melanoma in C57BL/6 mice more than 60 years ago. Although this cell line is still widely used by various laboratories, it should be noted that B16 can change within a laboratory due to continuous in vivo and in vitro passaging over time. Cell lines from genetic models of melanoma may better reflect the human disease when compared to B16 cells. Therefore, in the present study, mainly the HCmel 1274 melanoma was used.

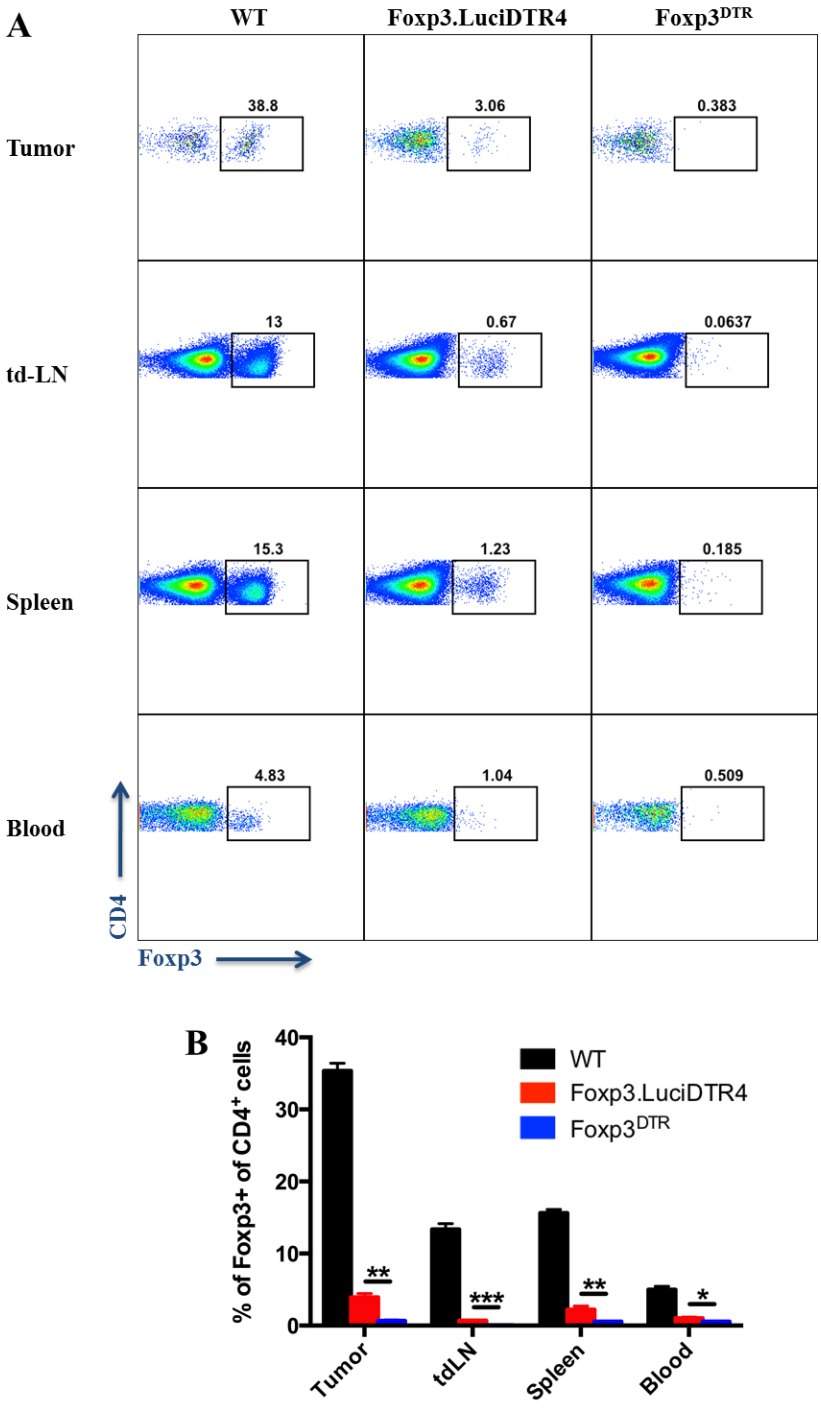

Figure 1: DT application in Foxp3^{DTR} and Foxp3.LuciDTR4 mice results in different degree of Treg depletion.
Wild-type (WT, C57BL/6N), Foxp3.LuciDTR4 and Foxp3DTR mice were injected with 1x106 HCmel 1274 cells i.d. When tumors reached a size of 250-500 mm3, Treg were depleted in Foxp3.LuciDTR4 and Foxp3DTR mice by i.p. injection of 20 ng/g bodyweight diphtheria toxin (DT). Analysis was performed 1 day after DT application. (A) Representative flow cytometric analysis of CD4+ Foxp3+ Treg in tumor, tumor draining-lymph nodes (td-LN), spleen and blood. (B) Summary of data presented in (A). Bars indicate mean±SEM of 6 mice per group. The experiment was repeated with similar results. *=p<0.05, *=p<0.01, *=p<0.001, ns=not statistically significant.

To analyze the effect of differential Treg depletion on the tumor growth, DT was injected twice into Foxp3^{DTR} and Foxp3.LuciDTR4 mice when tumors had reached a size of about 250-500 mm^3, usually on days 12-14. ~92% Treg depletion in Foxp3-LuciDTR4 mice resulted in partial regression of HCmel 1274 tumors **(Figure 2A)** and significantly prolonged the survival of tumor-bearing mice as compared to tumor-bearing wild type (WT) mice **(Figure 2B)**. Interestingly, ~99% Treg depletion in Foxp3^{DTR} mice led to complete regression of HCmel1274 tumors **(Figure 2A)** and, all of the tumor-bearing Foxp3^{DTR} mice were completely cured and survived until the experiment is terminated **(Figure 2B)**. In the case of B16 tumors, ~92% Treg depletion did not have an impact on tumor growth and survival **(Figure 2C, D)** whereas 99% Treg depletion improved the survival of tumor-bearing mice by inducing complete tumor rejection **(Figure 2C, D)**. These results show that the remaining ~8% Tregs in Foxp3.LuciDTR4 mice are able to prevent complete rejection of tumors.

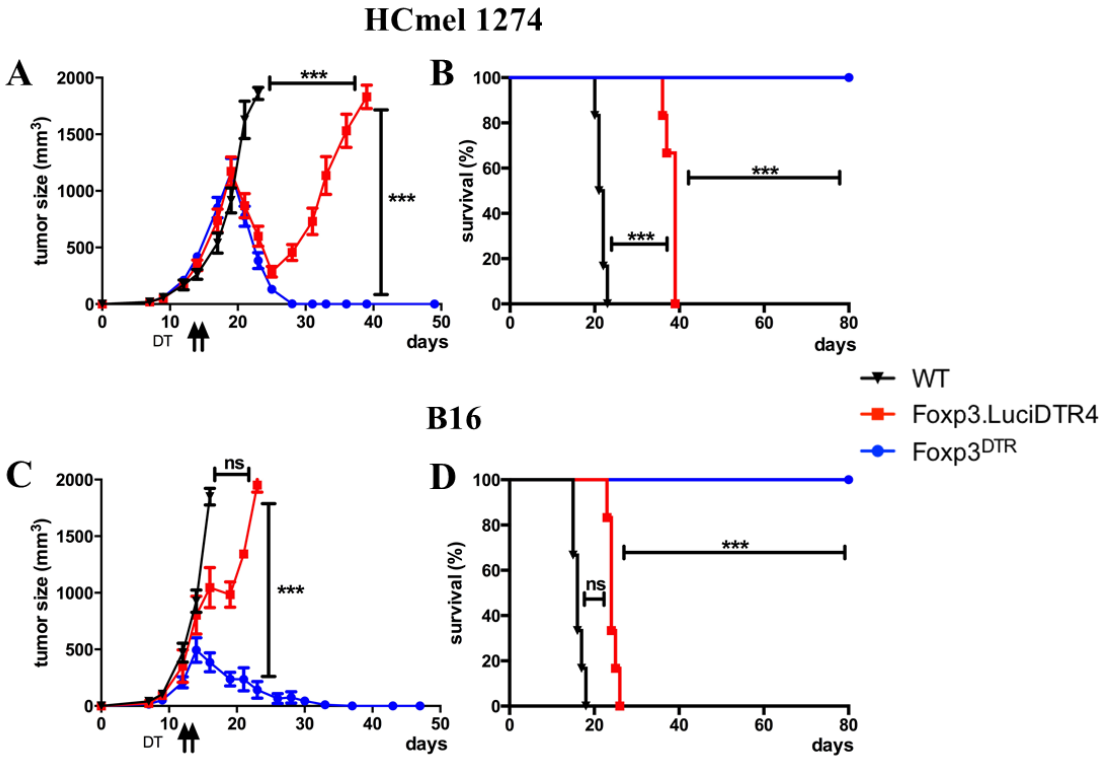

Figure 2: ~99% Treg depletion in Foxp3^{DTR} mice, but not ~92% Treg depletion in Foxp3.LuciDTR4 mice, induced complete rejection of established HCmel 1274 and B16 tumors.
(A) Growth of HCmel 1274 tumors in wild-type (WT, C57BL/6N), Foxp3.LuciDTR4 and Foxp3^{DTR} mice treated with diphtheria toxin (DT) on the indicated days. **(B)** Kaplan-Meier survival curves of mice shown in (A). **(C)** Growth of B16 tumors in wild-type (WT, C57BL/6N), Foxp3.LuciDTR4 and Foxp3^{DTR} mice treated with diphtheria toxin (DT) on the indicated days. **(D)** Kaplan-Meier survival curves of mice shown in (C). Results are shown as mean±SEM of 6 mice per group. Shown is 1 representative out of 3 independent experiments. *=p<0.05, *=p<0.01, *=p<0.001, ns=not statistically significant.

To identify the effector immune cell subpopulation that is required for HCmel 1274 tumor rejection after Treg depletion in Foxp3^{DTR} mice, CD8^{+} T, CD4^{+} T or NK cells were removed by depleting antibodies 2.43, GK1.5 or PK163-3-6, respectively. **Figure 3** shows that ablation of CD8^{+} T cells abolished Treg depletion-mediated tumor eradication, whereas CD4^{+} T cell and NK cell depletion had no effect on the tumor regression. These results indicate that CD8^{+} T cells are pivotal in HCmel 1274 rejection following Treg depletion, which is in agreement with a previous finding that the rejection of ovalbumin-expressing B16 in Foxp3.LuciDTR4 mice is dependent on CD8^{+} T cells[222].

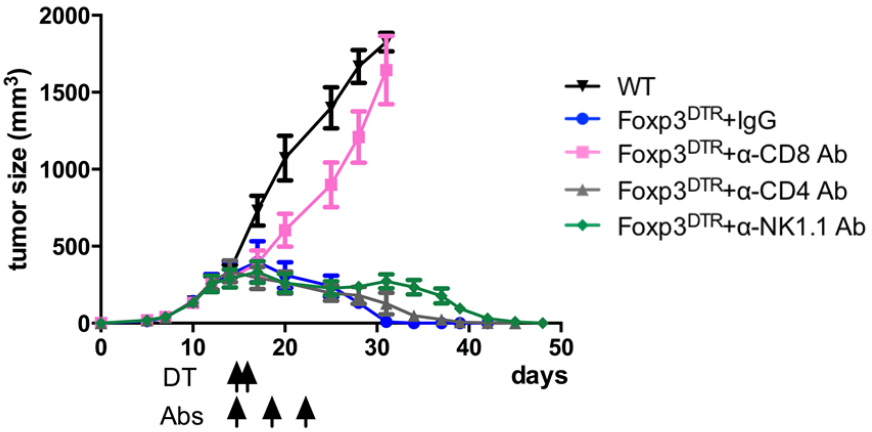

Figure 3: CD8^{+} T cells are responsible for HCmel 1274 tumor rejection following ~99% Treg depletion in Foxp3^{DTR} mice.

Growth of HCmel 1274 tumors in wild-type (WT, C57BL/6N), Foxp3.LuciDTR4 and Foxp3^{DTR} mice treated with diphtheria toxin (DT) and respective depleting antibodies on the indicated days. CD8^{+} T cells, CD4^{+} T cells and natural killer (NK) cells were depleted by i.p. injections of 0.5 mg anti-CD8 antibody 2.43, 1 mg anti-CD4 antibody GK1.5, 1 mg anti-NK1.1 antibody PK163, respectively. Rat IgG was used as isotype control antibody. Data are mean±SEM of 6 mice per group. Shown is 1 representative out of 2 independent experiments. *=p<0.05, *=p<0.01, *=p<0.001, ns=not statistically significant.

To confirm the observation that small numbers of Tregs can block complete rejection of tumors, Tregs were prepared from C57BL/6 splenic cells via magnetic sorting of CD4^{+} CD25^{+} cells and intratumorally transferred into Foxp3^{DTR} mice 2 days after DT treatment. The adoptive transfer of 2x10^{3} Tregs was found to prevent complete eradication of HCmel 1274 tumors following Treg depletion in 3 out of 6 mice **(Figure 4A)**, while the adoptive transfer of 2x10^{4} Tregs was found to impede complete tumor rejection in all 6 mice **(Figure 4A)**. In addition, all of the Foxp3^{DTR} mice, which had been injected with 2x10^{5} Tregs after DT application, exhibited tumor growth similar to WT mice without any sign of tumor rejection **(Figure 4A)**. Adoptive Treg reconstitution was also shown to reduce the surival of tumor-bearing

mice, depending on the number of tranferred cells **(Figure 4B)**. This data further verifies that small numbers of Tregs can still block the host's response against growing tumors, However, it should be noted that the transferred Tregs may expand rapidly due to homeostatic factors and that, therefore, transferred numbers do not reflect the actual Treg numbers in the tumor.

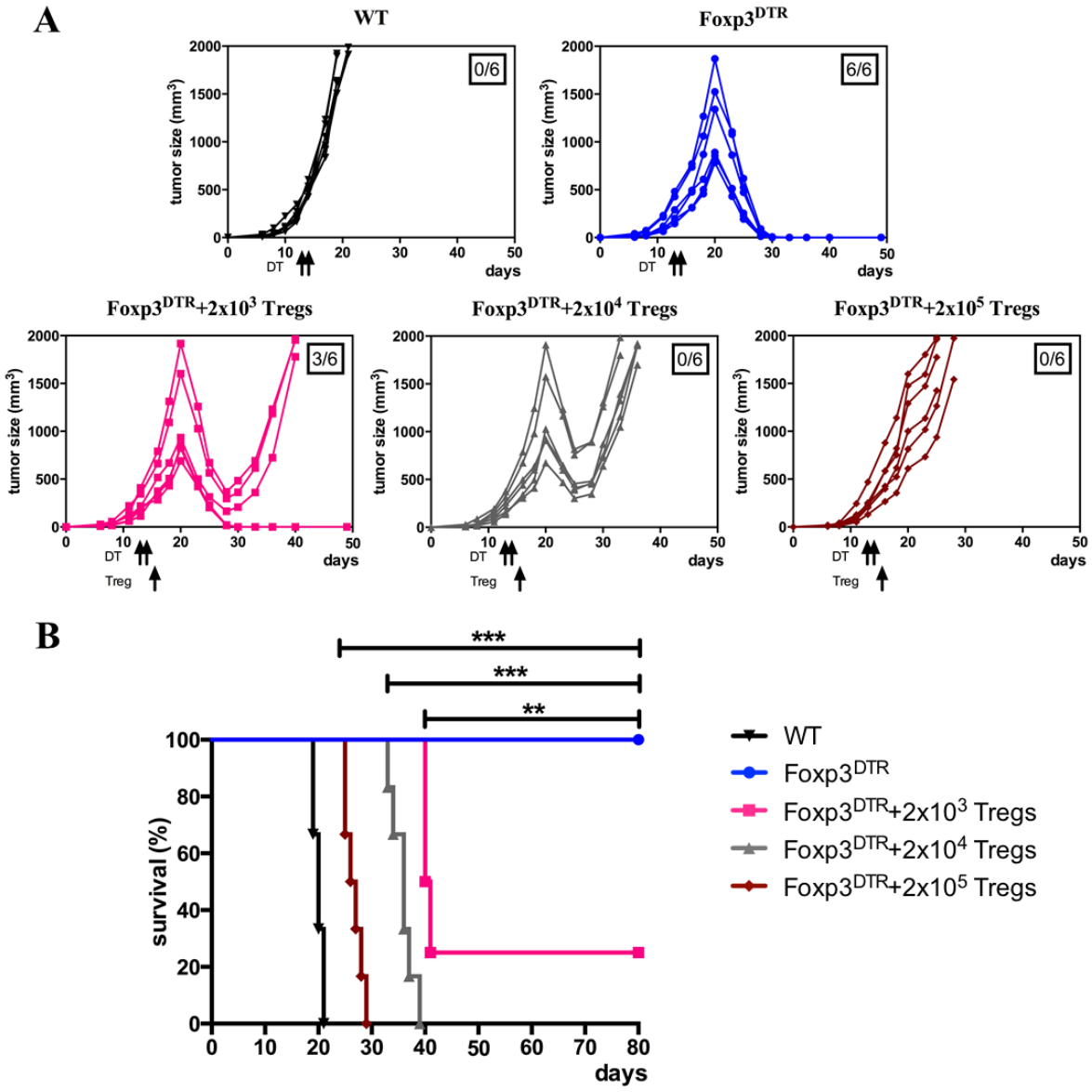

Figure 4: Adoptive cell reconstitution of Treg-depleted Foxp3^{DTR} mice with purified CD4^{+} CD25^{+} Tregs isolated from wild-type mice impaired rejection of HCmel1274 tumors.
(A) Growth of HCmel 1274 tumors in wild-type (WT, C57BL/6N), Foxp3^{DTR} mice treated with diphtheria toxin (DT) and Foxp3^{DTR} mice treated with DT and adoptively transferred with purified CD4^{+} CD25^{+} Tregs isolated from wild-type mice. 2x10^{3}, 2x10^{4} or 2x10^{5} purified Tregs were injected intratumorally into HCmel 1274-bearing mice 2 days after DT application. **(B)** Kaplan-Meier survival curves of mice shown in (A). Results are shown as mean±SEM of 6 mice per group. Shown is 1 representative out of 2 independent experiments. *=p<0.05, *=p<0.01, *=p<0.001, ns=not statistically significant.

3.1.3 Treg depletion in Foxp3^{DTR} mice promotes basophil recruitment into the tumor

Next, the immune cell infiltrates in HCmel 1274 tumors were investigated following Treg depletion in Foxp3^{DTR} and Foxp3.LuciDTR4 mice. Single-cell suspensions were prepared from tumors on day 16-18 (4 days after DT administration), when the size of tumors from wild-type (WT), Foxp3^{DTR} and Foxp3.LuciDTR4 mice were still in the same range, namely size of about 250-500 mm^3. Flow cytometric analysis showed that infiltration of CD45$^+$ leukocytes was enhanced in both models after Treg depletion **(Figure 5B)**. Among the leukoctye population in the tumor, CD8$^+$ T cells are specifically enriched in both Foxp3.LuciDTR4 and Foxp3^{DTR} models, but the level of infiltration was much stronger in the latter **(Figure 5C)**. Despite the fact that CD4$^+$ Tregs are removed after Treg depletion, it was found that the percentage of CD4$^+$ T cells in tumor-infiltrating leukocytes was similar between wild-type and Treg-depleted mice **(Figure 5C)**, indicating that conventional CD4$^+$ T cells infiltrated into the tumor after Treg depletion. In contrast to CD8$^+$ and CD4$^+$ T cells, the number of intratumoral B cells were reduced after Treg depletion **(Figure 5C)**. The percentage of innate cells, including natural killer (NK) cells, NKT cells, dendritic cells (DCs) and macrophages, in the intratumoral leukocytes were not changed following Treg depletion **(Figure 5D)** but it should be noted that the number of these cells is actually increased due to the general increase in leukocyte infiltration. Interestingly, Treg depletion induced tumor eosinophilia in both mouse models but tumor basophilia in only Foxp3^{DTR} mice **(Figure 5E)**. Treg depletion had no effect on the percentage of neutrophils in the leukocyte compartment of the tumor **(Figure 5E)**. In addition, tumors in wild-type, Foxp3.LuciDTR4 and Foxp3^{DTR} mice showed little mast cell infiltration **(Figure 5E)**. In conclusion, Treg depletion was found to induce infiltration of several leukocyte subpopulations in both mouse models, especially CD8$^+$ T cells, but basophils were only enriched in the tumors of Foxp^{DTR} mice.

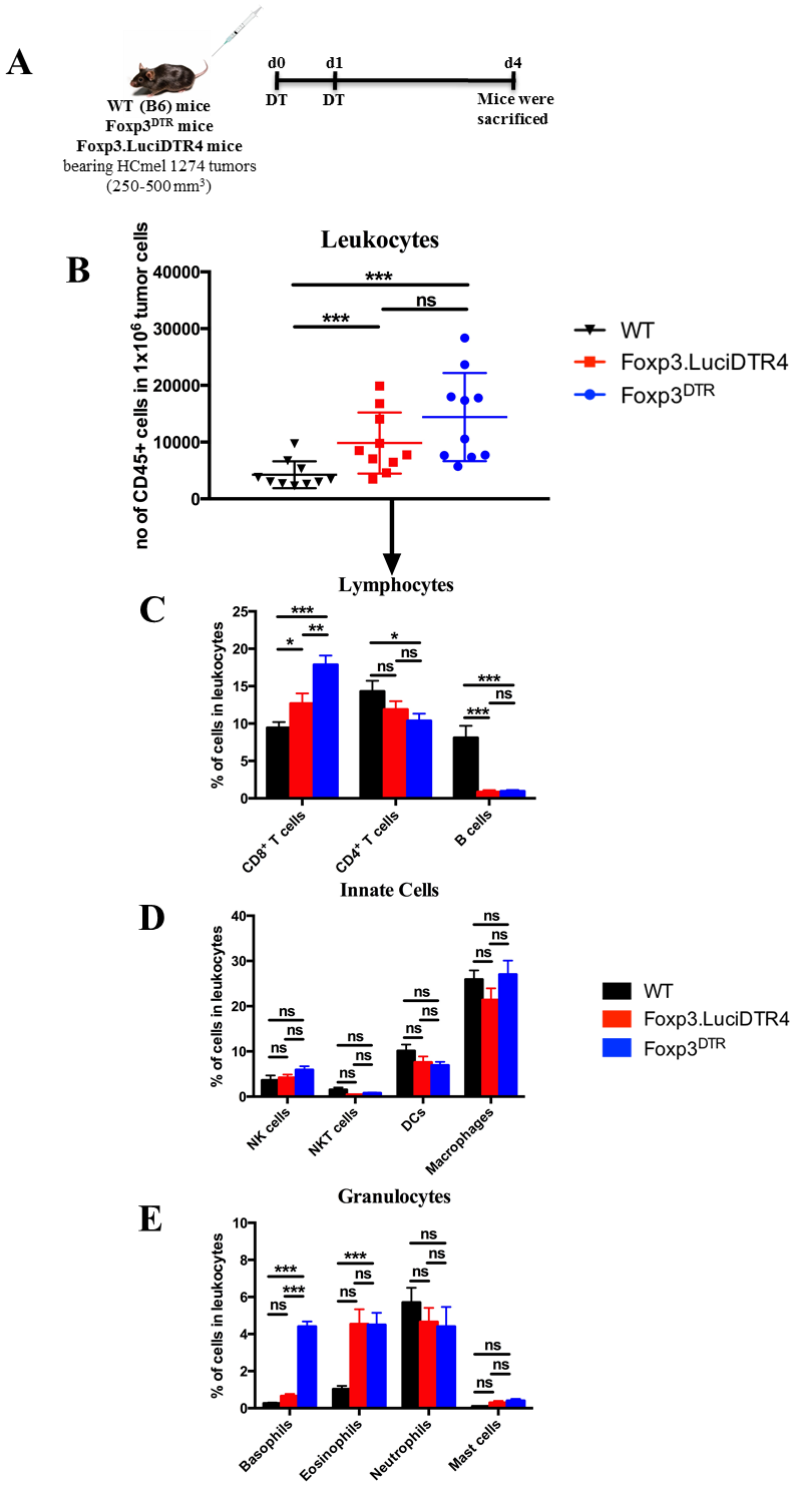

Figure 5: Treg depletion in Foxp3^{DTR} mice led to strong infiltration of leukocytes into tumors, notably CD8$^+$T cells and basophils.
(A) Wild-type (WT, C57BL/6N), Foxp3.LuciDTR4 and Foxp3^{DTR} mice were injected with 1x10^6 HCmel 1274 cells i.d. When tumors reached a size of 250-500 mm^3, Treg were depleted in Foxp3.LuciDTR4 and Foxp3^{DTR} mice by DT application on the indicated days. Analysis was performed 4 days after first DT application. **(B)** Quantification by flow cytometry of total CD45$^+$ leukocyte infiltration into HCmel 1274 tumors in the indicated mice treated with DT. **(C)** Percentage of lymphocytes in leukocytes infiltrating into HCmel 1274 tumors in the indicated mice treated with DT. **(D)** Percentage of innate cells in leukocytes infiltrating into HCmel 1274 tumors in the indicated mice treated with DT. **(E)** Percentage of granulocytes in leukocytes infiltrating into HCmel 1274 tumors in the indicated mice treated with DT. Analysis of tumor-infiltrating cells was performed by flow cytometry. Data are mean±SEM of 12 mice per group. Shown is all data from 2 independent experiments. *=p<0.05, *=p<0.01, *=p<0.001, ns=not statistically significant.

Basophils were identified in the tumor by dissecting the intratumoral $CD45^{int}$ population observed after Treg depletion in $Foxp3^{DTR}$ mice **(Figure 6B)**. Flow cytometric analysis showed that most of the $CD45^{int}$ cells in the tumor are characterized as $Fc\varepsilon RI^{+}$ (high affinity IgE receptor) $CD49b^{+}$ cells **(Figure 6B)**. These markers are expressed on both basophils and mast cells, but basophils can be differentiated from mast cells by the lack of c-Kit (CD117) expression **(Figure 6B)**. In addition, tumor-infiltrating basophils are IgE^{+} (**Figure 6B)**, indicating the activated status of basophils in Treg-depleted tumors because IgE is known to be a potent stimulator for effector functions of basophils. For a more comprenhensive characterization, The tumor-infiltrating $CD45^{+}$ $Fc\varepsilon RI^{+}$ $CD49b^{+}$ cells, $CD45^{+}$ $Fc\varepsilon RI^{-}$ $CD49b^{-}$ cells and $CD45^{-}$ cells were sorted by flow cytometry. RT-PCR analysis on sorted cells demonstrated that $CD45^{+}$ $Fc\varepsilon RI^{+}$ $CD49b^{+}$ cells expressed high levels of mast cell protease 8 (*Mcpt8*) mRNA, today also known as *Basoph8*, bacause it is a marker specific for basophils but not for mast cells. $CD45^{+}$ $Fc\varepsilon RI^{-}$ $CD49b^{-}$ cells and $CD45^{-}$ cells displayed no *Mcpt8/Basoph8* transcripts **(Figure 6C)**. Moreover, sorted intratumoral $CD45^{+}$ $Fc\varepsilon RI^{+}$ $CD49b^{+}$ cells showed characteristic basophil morphology with a lobulated nucleus and basophilic granules after Giemsa staining **(Figure 6D)**. In addition, after Treg depletion in $Foxp3^{DTR}$ mice, basophils were enriched only in the tumor, but not in the blood, spleen, td-LN and lung **(Figure 6E)**. The observation that basophils were only enriched in 99% Treg-depleted tumors suggested that basophils may be involved in tumor rejection in $Foxp3^{DTR}$ mice.

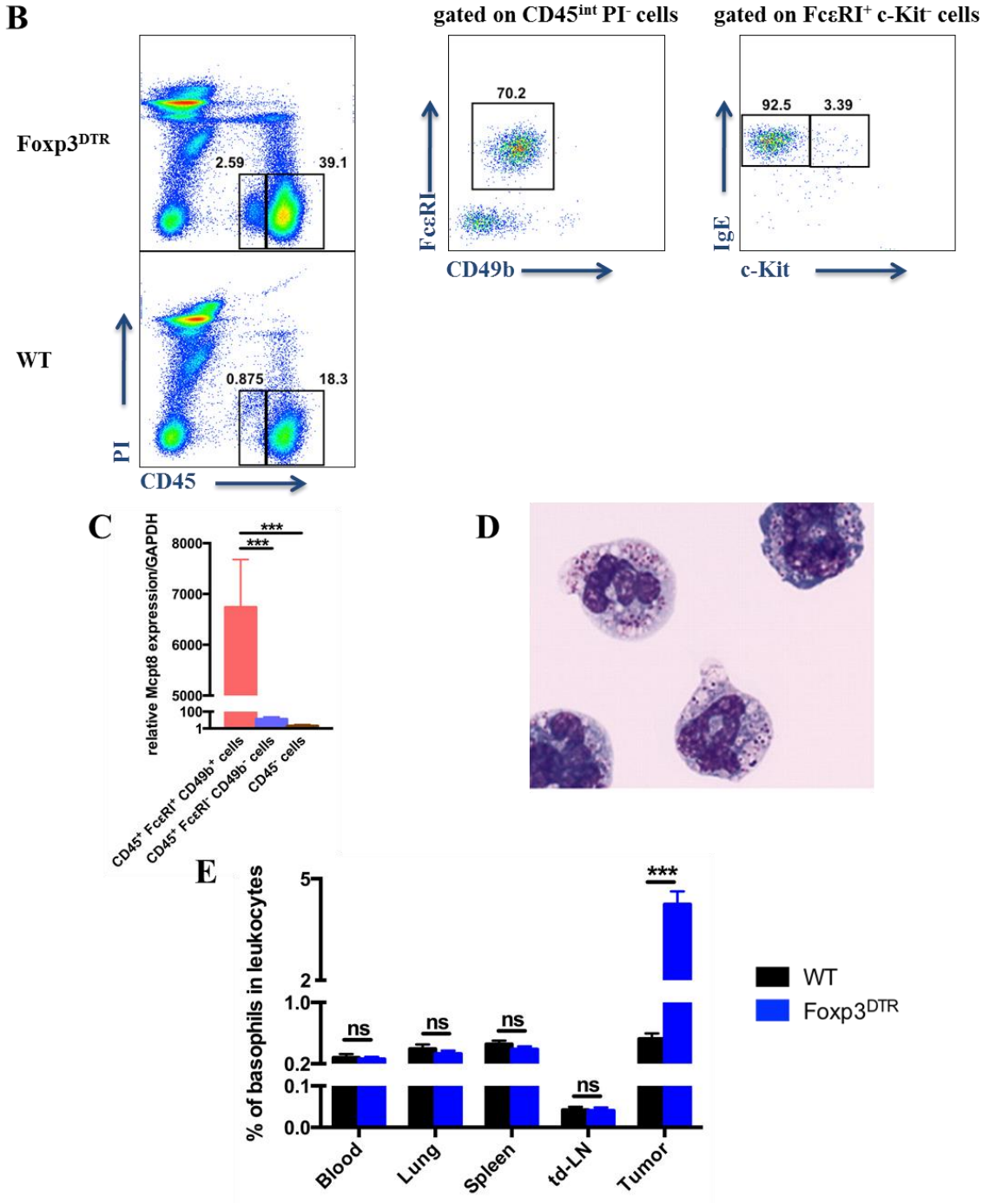

Figure 6: Characterization of tumor-infiltrating basophils after Treg depletion in Foxp3^{DTR} mice.

(A) Wild-type (WT, C57BL/6N) and Foxp3^{DTR} mice were injected with 1x10^{6} HCmel 1274 cells i.d. When tumors reached a size of 250-500 mm^{3}, Treg were depleted in Foxp3.LuciDTR4 and Foxp3^{DTR} mice by DT application on the indicated days. Analysis was performed 4 days after first DT application. **(B)** Flow cytometric analysis of HCmel 1274-infiltrating basophils which were characterized as CD45^{int} FcεRI^{+} CD49b^{+} IgE^{+} c-Kit^{-} cells. Results are shown as mean±SEM of 12 mice per group. Shown is all data from 2 independent experiments. **(C)** qRT-PCR analysis of CD45^{+} FcεRI^{+} CD49b^{+} cells sorted from HCmel 1274 tumors after Treg depletion for basophil-specific marker *Mcpt8*. Data are shown as mean±SEM of 12 mice per group. Shown all data from 2 independent experiments. **(D)** Representative giemsa staining of basophils (CD45^{+} FcεRI^{+} CD49b^{+} cells) sorted from HCmel 1274 tumors after Treg depletion. **(E)** Percentage of basophils (CD45^{+} FcεRI^{+} CD49b^{+} cells) in leukocytes in blood, lung, spleen, tumor draining-lymph nodes (td-LN) and tumor. Results are shown as mean±SEM of 12 mice per group. Shown is all data from 2 independent experiments. *=p<0.05, *=p<0.01, *=p<0.001, ns=not statistically significant.

3.1.4 Basophils are essential for efficient tumor rejection in Foxp3^{DTR} mice

The selective enrichment of basophils in Foxp3^{DTR} mice following Treg depletion prompted us to study the role of basophils in anti-tumor immune responses following Treg depletion, a FcεRI-specific monoclonal antibody (MAR-1) was employed, which is known to deplete basophils in mice[249]. Following intravenous injection (i.v.) of MAR-1, basophils were efficiently ablated in the tumor of Foxp3^{DTR} mice **(Figure 7B and C)**. Importantly, basophil depletion substantially impaired the rejection of HCmel 1274 tumors obtained by Treg depletion and reduced survival of tumor-bearing mice **(Figure 7D and E)**. These data exhibit that basophils are required for Treg depletion-mediated tumor eradication.

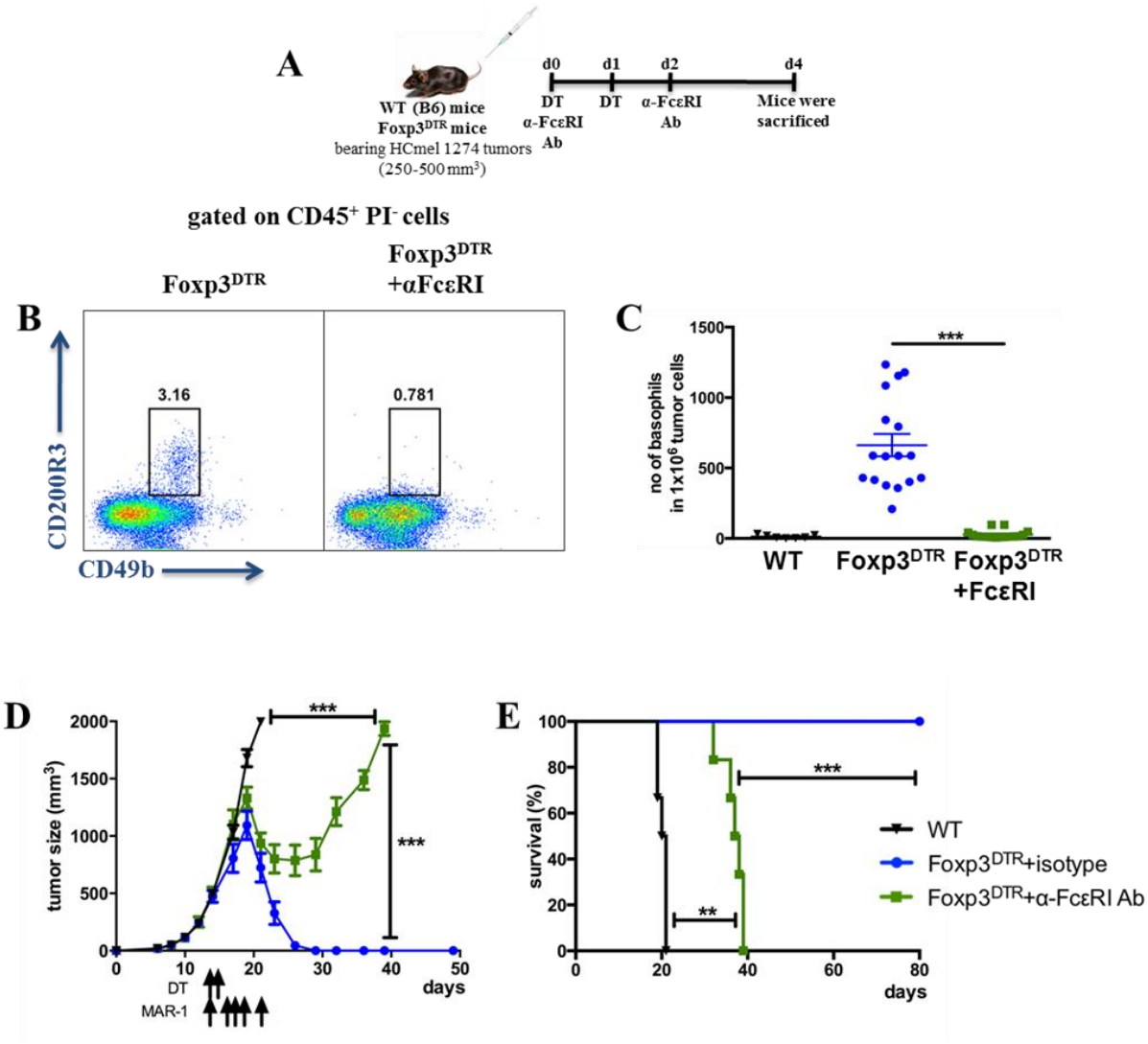

Figure 7: Basophil depletion curbs rejection of HCmel 1274 tumors obtained after Treg depletion in Foxp3^{DTR} mice.
(A) Wild-type (WT, C57BL/6N) and Foxp3^{DTR} mice were injected with 1x10^6 HCmel 1274 cells i.d. When tumors reached a size of 250-500 mm^3, Treg were depleted in Foxp3^{DTR} mice by DT on the indicated days. Basophils were depleted by i.p. injection of 10 µg/mice anti-FcεRI antibody MAR-1 on the indicated days. **(B)** Representative flow cytometric analysis of CD45$^+$ CD200R3$^+$ CD49b$^+$ basophils in the tumor before and after basophil depletion with anti-FcεRI antibody MAR-1. **(C)** Summary of data presented in (B). Results are mean±SEM of 17 mice per group. Shown is all data from 3 independent experiments. **(D)** Growth of HCmel 1274 tumors in wild-type (WT, C57BL/6N), Foxp3^{DTR} mice after Treg depletion with DT and Foxp3^{DTR} after Treg depletion combined with ablation of basophils by anti-FcεRI antibody MAR-1. Isotype indicates isotype-matched irrelevant antibody as control for anti-FcεRI antibody MAR-1 **(E)** Kaplan-Meier survival curves of mice shown in (D). Data are shown as mean±SEM of 6 mice per group. Shown is 1 representative out of 3 independent experiments. *=p<0.05, *=p<0.01, *=p<0.001, ns=not statistically significant.

Next, immune cell infiltrates in Treg-depleted HCmel 1274 tumors were analyzed before and after basophil depletion. Basophil depletion was found to lead to a marked reduction in infiltration of CD8$^+$ T cells **(Figure 8B)**. In addition, number of CD4$^+$ T cells, NK cells and macrophages in the tumor was significantly decreased after basophil depletion **(Figure 8B)**. In contrast, basophil ablation had no significant effect on the number of intratumoral B cells, DCs, eosinophils and neutrophils

(Figure 8B). These findings show that basophils play a role in anti-tumor immune responses, probably by promoting $CD8^+$ T cell infiltration into tumors.

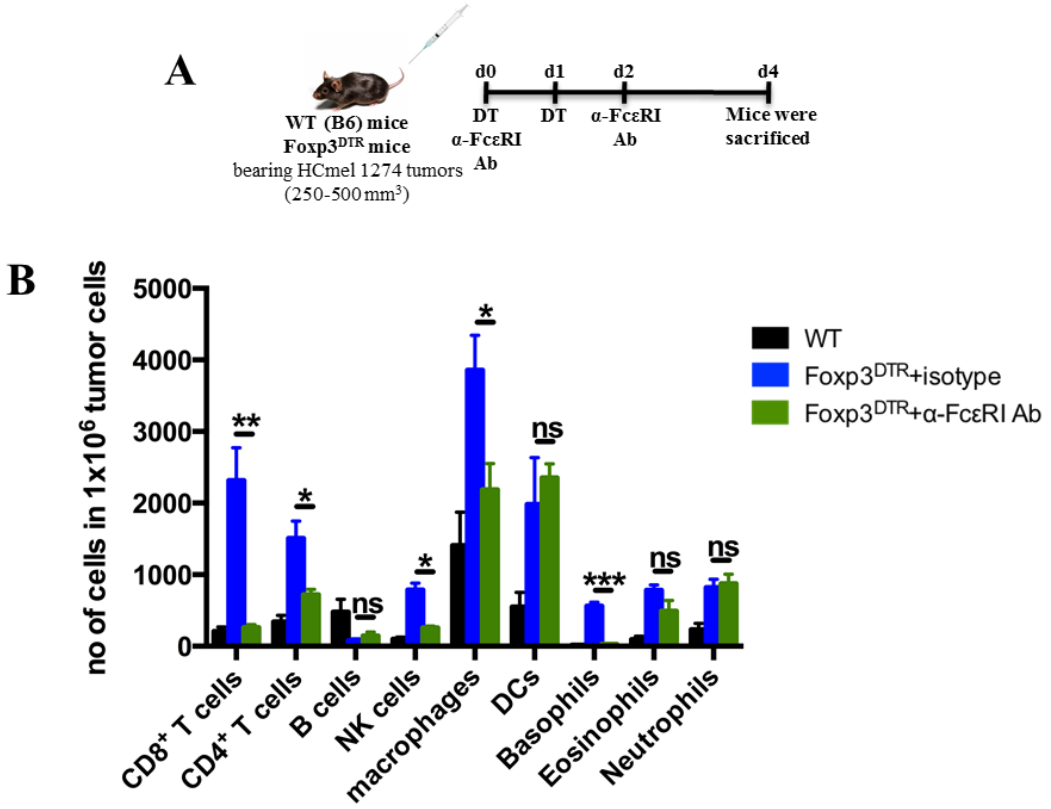

Figure 8: Basophil depletion hampered infiltration of several leukocyte subpopulations, including $CD8^+$ T cells, $CD4^+$ T cells, NK cells and macrophages, into Treg-depleted HCmel 1274 tumors in $Foxp3^{DTR}$ mice. **(A)** Wild-type (WT, C57BL/6N), Foxp3.LuciDTR4 and $Foxp3^{DTR}$ mice were injected with $1x10^6$ HCmel 1274 cells i.d. When tumors reached a size of 250-500 mm^3, Treg were depleted in Foxp3.LuciDTR4 and $Foxp3^{DTR}$ mice by DT application on the indicated days. Basophils were depleted by anti-FcεRI antibody MAR-1 on the indicated days. Analysis was performed 4 days after first DT application. **(B)** Quantification by flow cytometry of leukocyte subpopulation infiltration into HCmel 1274 tumors in the indicated mice. Results are shown as mean±SEM of 17 mice per group. Shown is all data from 3 independent experiments. *=p<0.05, *=p<0.01, *=p<0.001, ns=not statistically significant.

The effect of basophil depletion on tumor rejection was investigated at the molecular level. For this purpose, RT-PCR was performed on total RNA isolated from HCmel 1274 tumor lysates for analysis of the cytokine and chemokine profile of tumors in the presence and absence of basophils. Treg depletion was found to cause a cytokine storm in the tumor with strong upregulation of Th1 response-related cytokines, including *interferon (Ifn)-α*, *Ifn-β*, *Ifn-γ*, *tumor necrosis factor (Tnf)-α*, *Interleukin (Il)-1β*, *Il-12*, and Th2 response-related cytokines, such as *Il-3*, *Il-4*, *Il-5*, *Il-9*, *Il-10* and *Il-13* **(Figure 9B)**. These data suggest that Treg depletion induced both Th1 and Th2 responses against the tumor but Th1 cytokines seemed to be dominant over Th2 cytokines. Interestingly, with the exception of *Il-12*, *Il-5* and *Il-9*, the upregulation of these genes was remarkably curbed after basophil depletion **(Figure**

9B). This data suggests that basophils enhance the cytokine storm observed after Treg depletion.

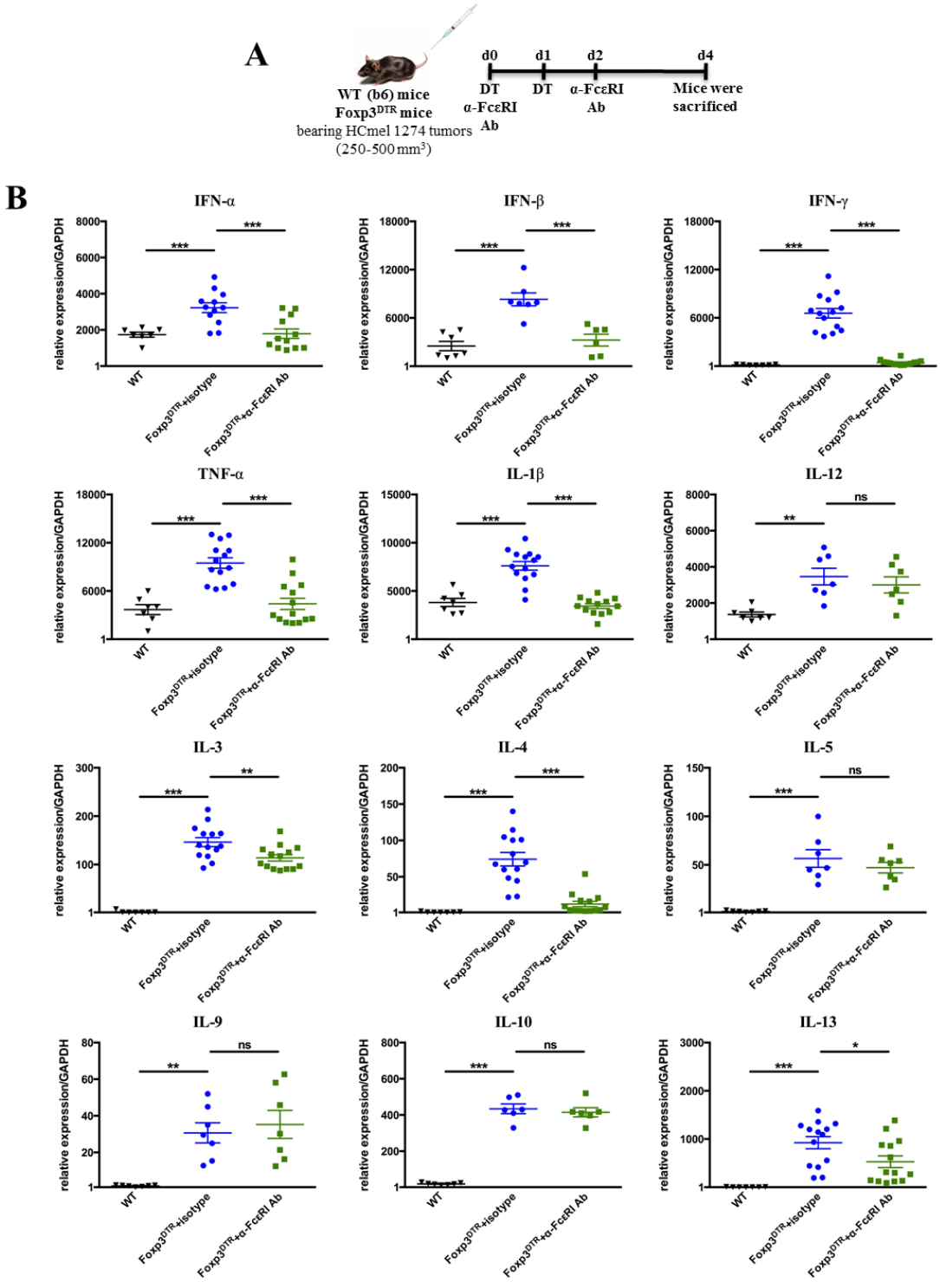

Figure 9: Changes in cytokine expression within the tumor microenvironment after Treg and basophil depletion.
(A) Wild-type (WT, C57BL/6N), Foxp3.LuciDTR4 and Foxp3^{DTR} mice were injected with 1x10^{6} HCmel 1274 cells i.d. When tumors reached a size of 250-500 mm^{3}, Treg were depleted in Foxp3.LuciDTR4 and Foxp3^{DTR} mice by DT application on the indicated days. Basophils were depleted by anti-FcεRI antibody MAR-1 on the indicated days. Analysis was performed 4 days after first DT application. **(B)** qRT-PCR analysis of proinflammatory cytokines in tumors of the indicated mice. Results are shown as mean±SEM of 17 mice per group. Shown is all data from 3 independent experiments. *=p<0.05, *=p<0.01, *=p<0.001, ns=not statistically significant.

Similar to cytokines, intratumoral expression of several chemokines such as *chemokine C-C motif ligand (Ccl)2*, *Ccl3*, *Ccl4*, *Ccl7*, *Ccl11*, *Ccl20*, *chemokine C-X-C motif ligand (Cxcl)9* and *Cxcl10* was augmented following Treg depletion **(Figure 10B)**. However, expression levels of *Ccl5*, *Ccl19*, *Ccl22* and *Ccl24* were not changed in the tumor after Treg depletion **(Figure 10B)**. CCL2, CCL3, CCL4, CCL5, CXCL9 and CXCL10 are known to be potent chemoattractants for tumor-infiltrating T and NK cells[62], thereby upregulation of the genes encoding CCL2, CCL3, CCL4, CXCL9 and CXCL10 may explain the increased infiltration of T and NK cells into HCmel 1274 tumors after Treg depletion. In addition, CCL2, CCL3, CCL4, CCL5 and CCL7 are implicated in infiltration of monocytes/macrophages into tumors[153], indicating that enhanced macrophage infiltration may result from the upregulation of the expression of CCL2, CCL3, CCL4 and CCL7 in the tumor microenvironment. CCL11 and CCL24 are powerful chemoattractants for eosinophils[278], strong activation of the gene encoding CCL11 could be the reason for enhanced infiltration of eosinophils into the tumor after Treg depletion. CCL20 and CCL22 has been shown to recruit Tregs into the tumor[105, 279], but CCL20 can also attract DCs into the tumors[280]. Importantly, basophil depletion resulted in a decreased expression of chemokines, *Ccl2*, *Ccl3*, *Ccl4*, *Cxcl9* and *Cxcl10* **(Figure 10B)**. These results indicate that basophils may a play a role in T cell migration into the tumor through chemokine production.

The requirement for basophils in Treg depletion-mediated tumor rejection was confirmed in an additional tumor system, B16 melanoma. Basophil depletion following DT treatment in B16-bearing mice was shown to yield comparable results **(Figure 11A, B, D and E)**. Basophils ablation impaired the rejection of B16 tumors obtained after Treg depletion **(Figure 11A)**, resulting in reduced survival of tumor-bearing mice **(Figure 11B)**. Basophil-depleted tumors displayed diminished infiltration of $CD8^+$ T cells, $CD4^+$ T cells and macrophages **(Figure 11D)** and decreased expression of *Ifn-γ*, *Ccl2*, *Ccl3*, *Ccl4*, *Cxcl9* and *Cxcl10* within the tumor microenvironment **(Figure 11E)**.

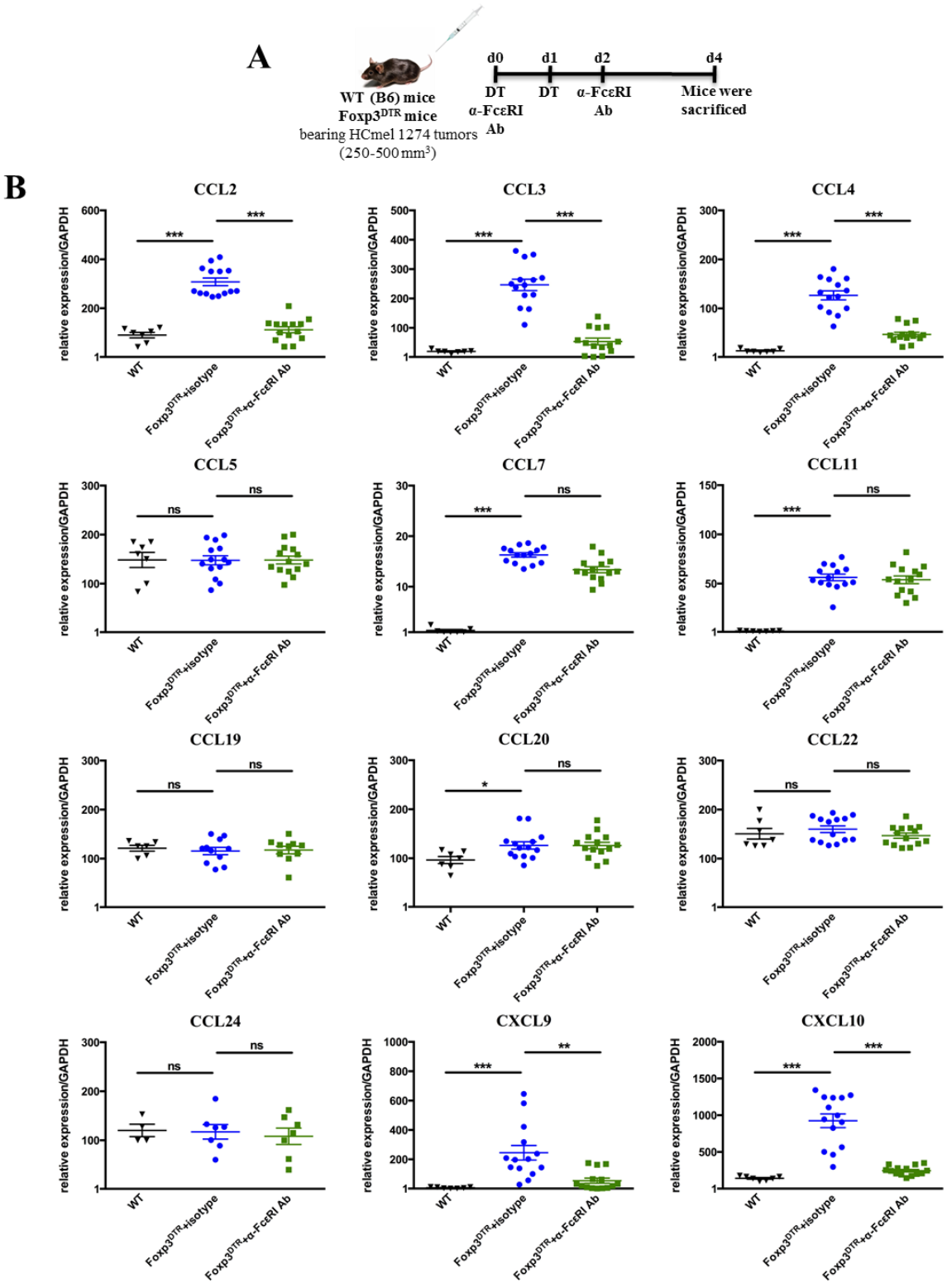

Figure 10: Changes in chemokine expression within the tumor microenvironment after Treg and basophil depletion.
(A) Wild-type (WT, C57BL/6N), Foxp3.LuciDTR4 and Foxp3^{DTR} mice were injected with 1x10^{6} HCmel 1274 cells i.d. When tumors reached a size of 250-500 mm^{3}, Treg were depleted in Foxp3.LuciDTR4 and Foxp3^{DTR} mice by DT application on the indicated days. Basophils were depleted by anti-FcεRI antibody MAR-1 on the indicated days. Analysis was performed 4 days after first DT application. **(B)** qRT-PCR analysis of chemoattractants in tumors of the indicated mice. Results are shown as mean±SEM of 17 mice per group. Shown is all data from 3 independent experiments. *=p<0.05, *=p<0.01, *=p<0.001, ns=not statistically significant.

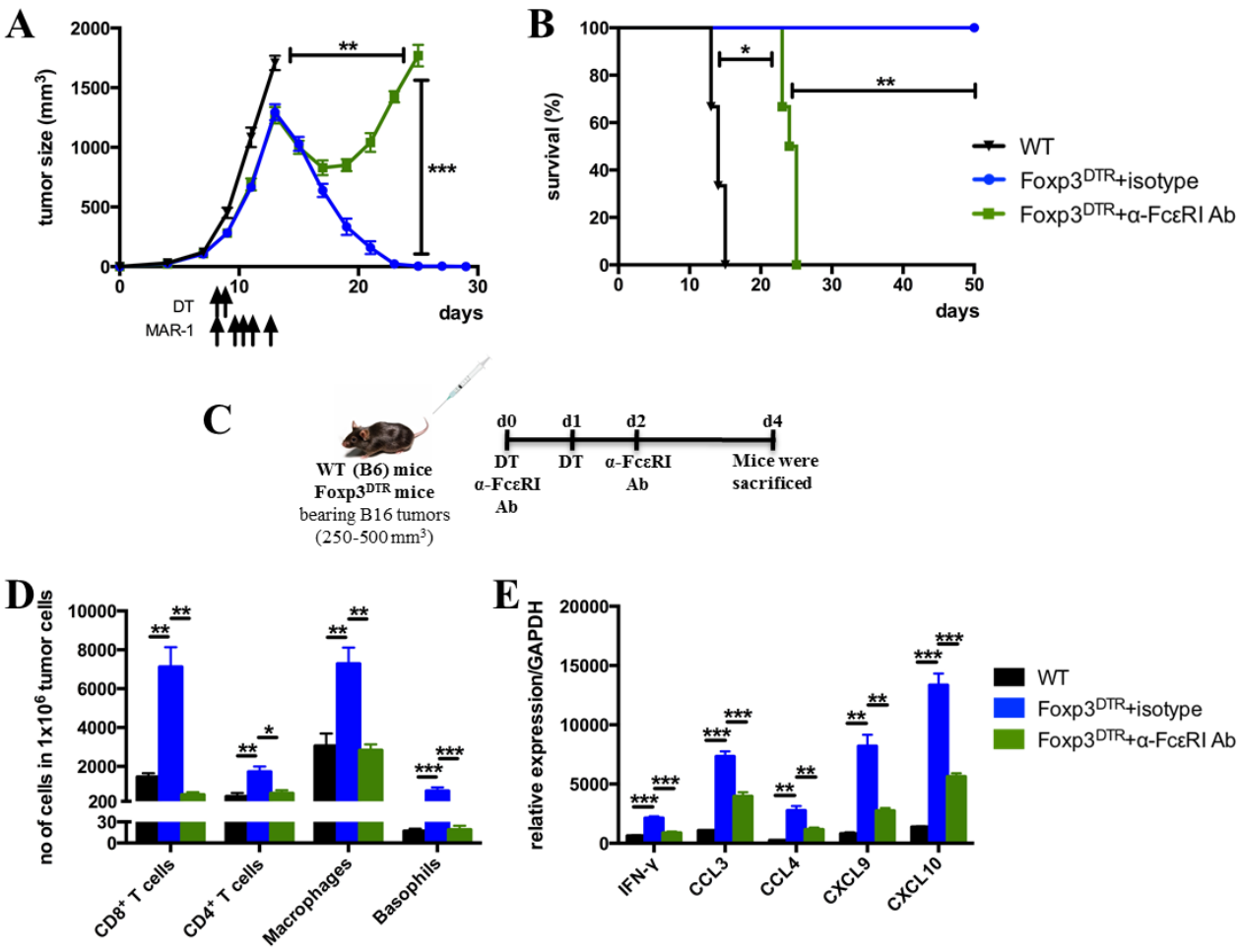

Figure 11: Basophil depletion impaired infiltration of leukocyte subpopulations into Treg-depleted B16 tumors and rejection of B16 tumors observed after Treg depletion in Foxp3^{DTR} mice.
(A) Growth of HCmel 1274 tumors in wild-type (WT, C57BL/6N), Foxp3^{DTR} mice after Treg depletion with DT and Foxp3^{DTR} after Treg depletion combined with ablation of basophils by anti-FcεRI antibody MAR-1. Isotype indicates isotype-matched irrelevant antibody as control for anti-FcεRI antibody MAR-1. DT and antibodies were injected on the indicated days **(B)** Kaplan-Meier survival curves of mice shown in (A). Data are shown as mean±SEM of 6 mice per group. Shown is 1 representative experiment. **(C)** Wild-type (WT, C57BL/6N), Foxp3.LuciDTR4 and Foxp3^{DTR} mice were injected with 1x10^6 HCmel 1274 cells i.d. When tumors reached a size of 250-500 mm^3, Treg were depleted in Foxp3.LuciDTR4 and Foxp3^{DTR} mice by DT application on the indicated days. Basophils were depleted by anti-FcεRI antibody MAR-1 on the indicated days. Analysis was performed 4 days after first DT application. **(D)** Quantification by flow cytometry of leukocyte subpopulation infiltration into HCmel 1274 tumors in the indicated mice. **(E)** qRT-PCR analysis of cytokines and chemokines in tumors of the indicated mice. Results are shown as mean±SEM of 6 mice per group. Shown is all data from 1 experiment. *=p<0.05, *=p<0.01, *=p<0.001, ns=not statistically significant.

3.1.5 Basophils promote $CD8^+$ T cell recruitment into the tumor through production of chemokines CCL3 and CCL4

So far analysis of tumor microenvironment was performed on day 4 after Treg depletion. In order to check whether basophils migrate into the tumor before $CD8^+$ T cells, immune cell infiltrates in HCmel 1274 tumors were analyzed by flow cytometry at an earlier time point, namely 2 days after DT treatment. Tumors in wild-type, Foxp3.LuciDTR4 and $Foxp3^{DTR}$ mice were found to exhibit similar level of $CD45^+$ leukocyte infiltration 2 days after DT application **(Figure 12B)**. Accordingly, similar $CD8^+$ T cell and B cell frequencies were observed in wild-type and Treg-ablated tumors **(Figure 12C)**. As expected, the density of $CD4^+$ T cells were reduced in the tumors of mice depleted of $CD4^+$ Tregs **(Figure 12C)**. In addition, the intratumoral infiltration of NK cells, NKT cells, DCs, macrophages, eosinophils, neutrophils and mast cells was not altered after Treg depletion **(Figure 12D and E)**. Strikingly, Treg-depleted tumors in $Foxp3^{DTR}$ mice were strongly infiltrated by basophils already 2 days after DT administration **(Figure 12E)**. These data show that basophils were the first immune cell population that infiltrated into the tumor following Treg depletion in $Foxp3^{DTR}$ mice.

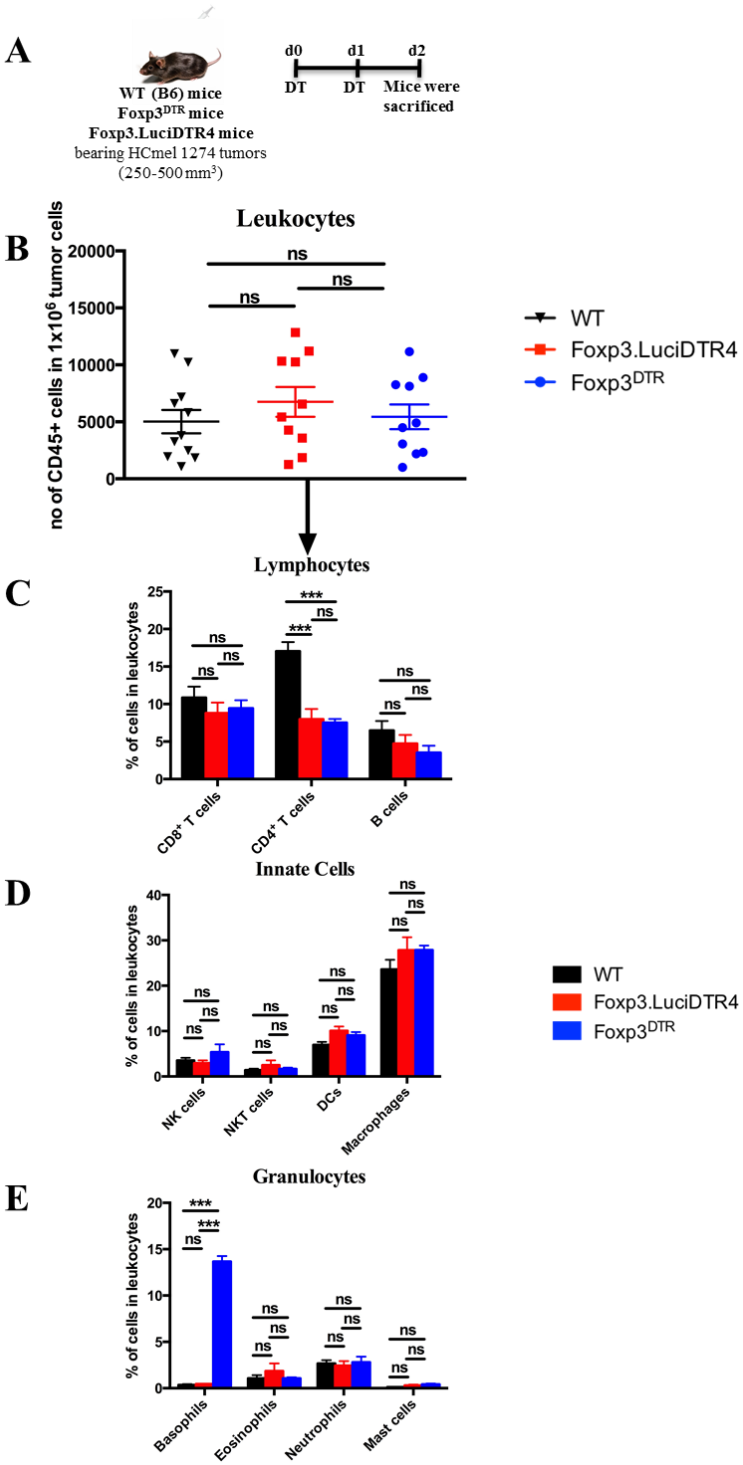

Figure 12: Basophils are the earliest leukocyte subpopulation that infiltrated HCmel 1274 tumors after Treg depletion in Foxp3^{DTR} mice.
(A) Wild-type (WT, C57BL/6N), Foxp3.LuciDTR4 and Foxp3^{DTR} mice were injected with 1x10^6 HCmel 1274 cells i.d. When tumors reached a size of 250-500 mm^3, Treg were depleted in Foxp3.LuciDTR4 and Foxp3^{DTR} mice by DT application on the indicated days. Analysis was performed 2 days after first DT application. **(B)** Quantification by flow cytometry of total CD45$^+$ leukocyte infiltration into HCmel 1274 tumors in the indicated mice treated with DT. **(C)** Percentage of lymphocytes in leukocytes infiltrating into HCmel 1274 tumors in the indicated mice treated with DT. **(D)** Percentage of innate cells in leukocytes infiltrating into HCmel 1274 tumors in the indicated mice treated with DT. **(E)** Percentage of granulocytes in leukocytes infiltrating into HCmel 1274 tumors in the indicated mice treated with DT. Analysis of tumor-infiltrating cells was performed by flow cytometry. Data are mean±SEM of 12 mice per group. Shown is all data from 2 independent experiments. *=p<0.05, *=p<0.01, *=p<0.001, ns=not statistically significant.

Kinetic studies on tumor infiltration by immune cell subpopulations confirmed that basophil infiltration preceded $CD8^+$ T cell infiltration **(Figure 13A and B)**. Basophils were enriched in the tumor 2 days after Treg depletion **(Figure 13A)** whereas the number of intratumoral $CD8^+$ T cells peaked 4 days after Treg depletion **(Figure 13B)**.

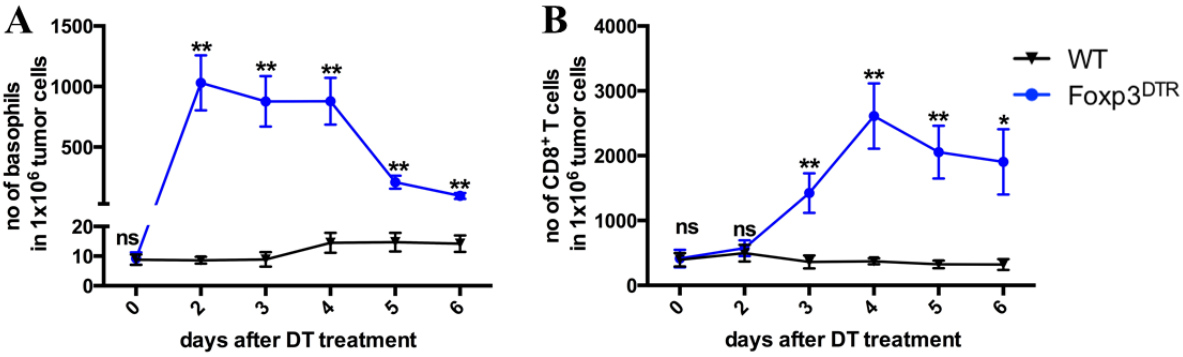

Figure 13: Basophil infiltration preceded $CD8^+$ T cell infiltration into Treg-depleted HCmel 1274 tumors. **(A)** Infiltration kinetics of basophils and **(B)** $CD8^+$ T cells into the tumor after Treg depletion in $Foxp3^{DTR}$ mice calculated by by flow cytometry. Results are mean±SEM of 12 mice per group. Shown is all data from 2 independent experiments. *=p<0.05, *=p<0.01, *=p<0.001, ns=not statistically significant.

Next, the chemokine profile of the tumor microenvironment was examined 2 days after Treg depletion, when basophil population peaked in the tumor. RT-PCR data revealed that the expression of chemokines *Ccl3* and *Ccl4* but not *Ccl2*, *Ccl5*, *Ccl7*, *Ccl11*, *Ccl12*, *Ccl19*, *Ccl20*, *Ccl22*, *Ccl24*, *Cxcl9* and *Cxcl10* was significantly upregulated 2 days following Treg depletion **(Figure 14B)**. Basophils ($CD45^+$ $Fc\varepsilon RI^+$ $CD49b^+$ cells) sorted from Treg-depleted tumor were found to express high levels of *Ccl3* and *Ccl4* but not *Ccl2*, *Cxcl9* and *Cxcl10* as compared with $CD45^+$ $Fc\varepsilon RI^-$ $CD49b^-$ cells and $CD45^-$ cells **(Figure 14C)**, suggesting that basophils are a critical source of CCL3 and CCL4 in the tumor microenvironment. Moreover, the production of CCL3 and CCL4 was observed only in tumoral basophils but not in splenic basophils (**Figure 14D)**. These observations show that basophils are a major source of chemokines CCL3 and CCL4 in the tumor microenvironment.

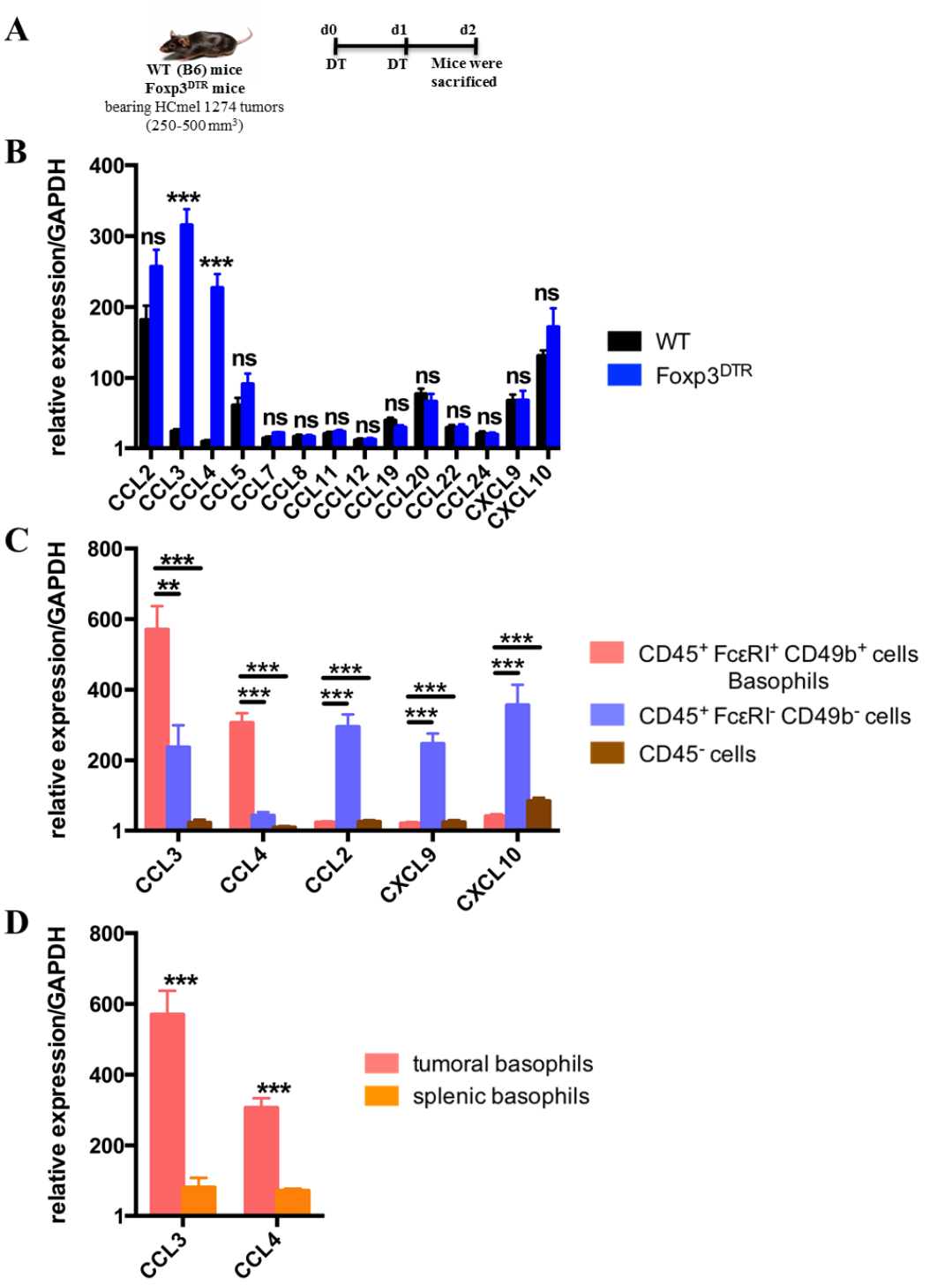

Figure 14: Basophils in Treg-depleted tumors produce CCL3 and CCL4 that are known to attract CD8$^+$ T cells.
(A) Wild-type (WT, C57BL/6N) and Foxp3^{DTR} mice were injected with 1x10^6 HCmel 1274 cells i.d. When tumors reached a size of 250-500 mm^3, Treg were depleted in Foxp3^{DTR} mice by DT application on the indicated days. Analysis was performed 2 days after first DT application. **(B)** qRT-PCR analysis of chemoattractants in tumors of the indicated mice 2 days after Treg depletion. **(C)** qRT-PCR analysis of chemokines in CD45$^+$ FcεRI$^+$ CD49b$^+$ basophils, CD45$^+$ FcεRI$^-$ CD49b$^-$ cells and CD45$^=$ cells sorted from HCmel 1274 tumors 2 days after Treg depletion. **(D)** qRT-PCR analysis of chemokines in CD45$^+$ FcεRI$^+$ CD49b$^+$ basophils sorted from the tumor or the spleen 2 days after Treg depletion. Results are mean±SEM of 12 mice per group. Shown is all data from 2 independent experiments. *=p<0.05, *=p<0.01, *=p<0.001, ns=not statistically significant.

Based on these results, I investigated the possibility that $CD8^+$ T cells were attracted into tumors by basophil-derived CCL3 and CCL4. Bone marrow-derived basophils were generated in the presence of IL-3. Fully differentiated basophils were shown to secrete elavated amounts of CCL3 and CCL4 but did not increase CCL2, CXCL9 and CXCL10 production when stimulated with a combination of IL-3, IL-18 and IL-33 **(Figure 15A)**, in agreement with previous findings[257, 258]. Using a two-chamber system in vitro, it was observed that basophils activated with IL-3+IL-18+IL-33 induced migration of activated $CD8^+$ T cells whereas basophils activated with IL-3 alone failed to do so **(Figure 15B)**. Blocking of CCL3 and CCL4 with a cocktail of specific antibodies markedly abrogated $CD8^+$ T cell migration **(Figure 15C)**. These findings demonstrate that basophils attract $CD8^+$ T cells by secreting CCL3 and CCL4, thereby providing an explanation for the decreased infiltration of $CD8^+$ T cells into Treg-depleted tumors in the absence of basophils.

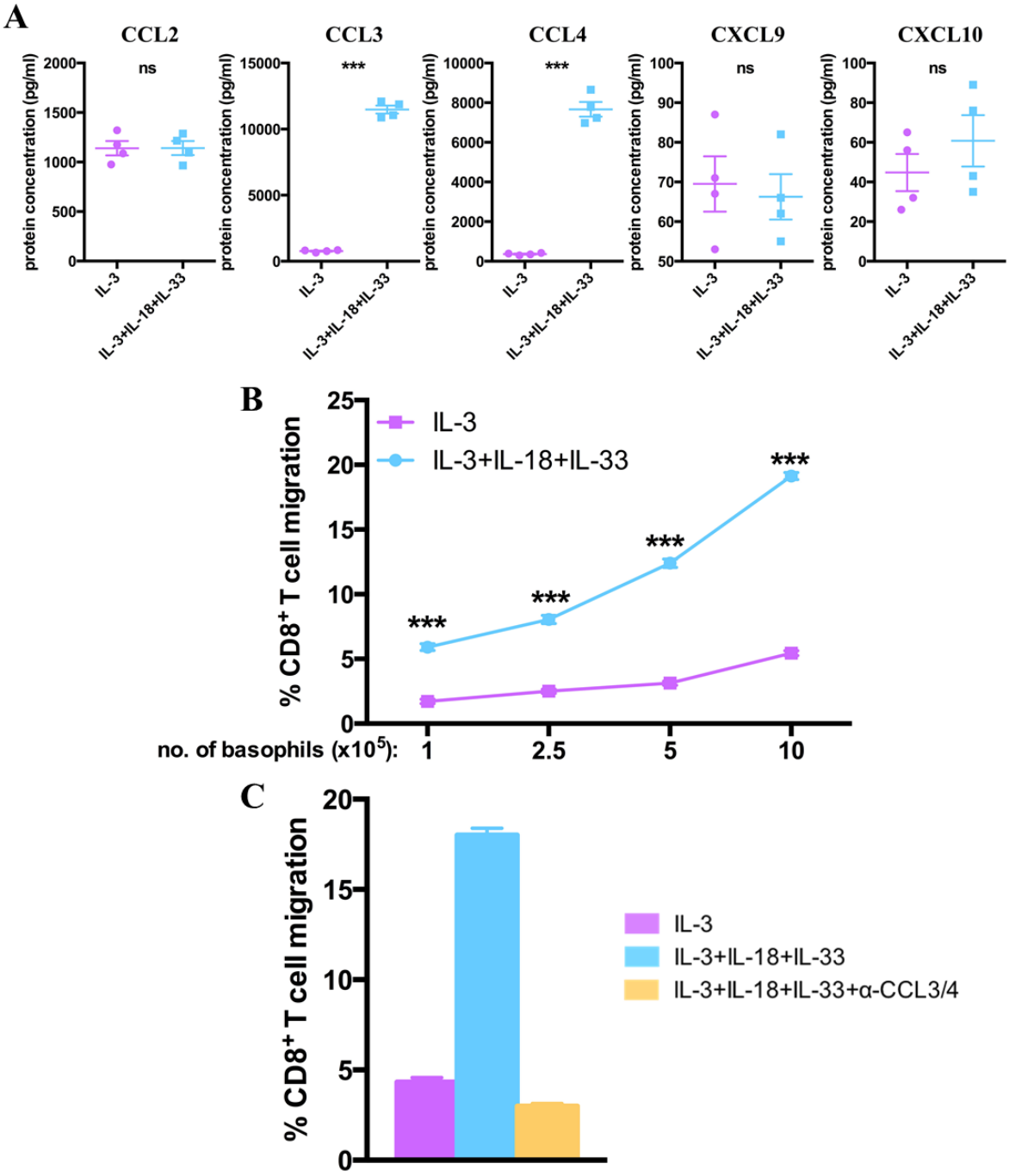

Figure 15: Basophil-derived chemokines induce CD8$^+$ T cell migration.
(A) Multiplex analysis of chemokines produced by basophils cultured *in vitro* with IL-3 only or with IL-3 plus IL-18 plus IL-33. Data are shown as mean±SEM of 4 samples. Shown is 1 representative experiment. **(B)** Basophils treated with IL-3 IL-18 plus IL-33 induce migration of CD8$^+$ T cells in a two-chamber system. **(C)** Inhibition of migration by specific antibodies against CCL3 and CCL4. Data are shown as mean±SEM of 6 samples. Shown is all data from 2 independent experiments. *=p<0.05, *=p<0.01, *=p<0.001, ns=not statistically significant.

3.1.6 Basophilia-induced $CD8^+$ T cell infiltration stimulates tumor-associated macrophages to produce chemokines CCL2, CXCL9 and CXCL10

As shown before, in addition to increased *Ccl3* and *Ccl4* levels, tumors displayed abundant *Ccl2*, *Cxcl9* and *Cxcl10* mRNAs 4 days after Treg depletion **(Figure 10B)**. Furthermore, basophil depletion was found to impair the upregulation of the genes encoding these chemokines **(Figure 10B)**. RT-PCR analysis revealed that sorted intratumoral basophils did not produce these chemokines **(Figure 14C)**. Thus, these findings suggested that basophils may act on other leukocyte subpopulations to stimulate production of these chemokines in the tumor microenvironment. Several studies have reported that CCL2, CXCL9 and CXCL10 are produced by macrophages, eosinophils or other myeloid cells in the tumor, mainly in response to IFN-γ and TNF-α[281, 282, 283]. Following Treg depletion in $Foxp3^{DTR}$ mice, the main source of these chemokines was shown to be macrophages sorted from the tumors (**Figure 16B)**. IFN-γ is known to be largely produced by $CD8^+$ T cells, indicating that activated $CD8^+$ T cells may control the production of CCL2, CXCL9 and CXCL10 by macrophages via IFN-γ. Indeed, basophil depletion, $CD8^+$ T cell depletion and IFN-γ blockade with respective antibodies were shown to cause a reduction in CCL2, CXCL9 and CXCL10 expression by intratumoral macrophages **(Figure 16D)**. These data indicate that decrease in intratumoral levels of CCL2, CXCL9 and CXCL10 after basophil depletion can be attributed to a reduced level of $CD8^+$ T cell infiltration and IFN-γ production by these $CD8^+$ T cells. Thus, it can be hypothesized that basophils first induce $CD8^+$ T cell migration into tumors through production of CCL3 and CCL4. The infiltrating $CD8^+$ T cells will polarize macrophages into M1-like CCL2-, CXCL9- and CXCL10- producing macrophages, which, in turn, are likely to amplify $CD8^+$ T cell trafficking into tumors.

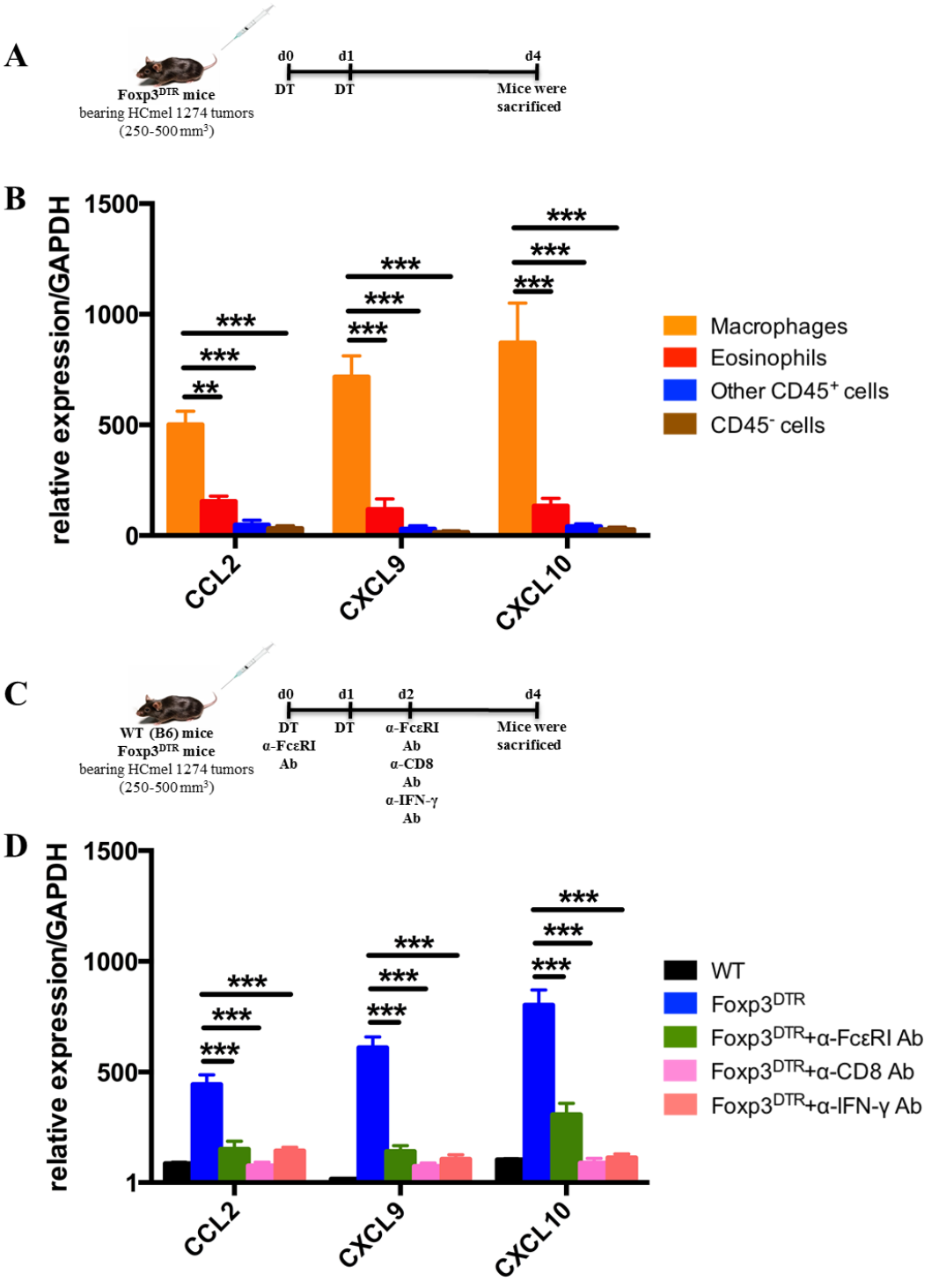

Figure 16: Tumor-associated macrophages produce CCL2, CXCL9 and CXCL10, which is dependent on IFN-γ produced by CD8$^+$ T cells.

(A) Foxp3^{DTR} mice were injected with 1x10^6 HCmel 1274 cells i.d. When tumors reached a size of 250-500 mm^3, Treg were depleted in Foxp3^{DTR} mice by DT application on the indicated days. Analysis was performed 4 days after first DT application. **(B)** qRT-PCR analysis of chemokines in CD45$^+$ CD11b$^+$ Gr-1^{low} F4/80$^+$ Siglec-F$^-$ macrophages, CD45$^+$ CD11b$^+$ Gr-1^{low} F4/80$^+$ Siglec-F$^+$ eosinophils, other CD45$^+$ cells and CD45$^=$ cells sorted from HCmel 1274 tumors 4 days after Treg depletion. **(C)** Wild-type (WT, C57BL/6N) and Foxp3^{DTR} mice were injected with 1x10^6 HCmel 1274 cells i.d. When tumors reached a size of 250-500 mm^3, Treg were depleted in Foxp3^{DTR} mice by DT application on the indicated days. Basophils and CD8$^+$ T cells were depleted by i.p. injections of 10 µg anti-FcεRI antibody MAR-1 and 0.5 mg anti-CD8 antibody 2.43, respectively, 2 days after DT application. IFN-γ was blocked by i.p. injection of 0.5 mg anti-IFN-γ antibody XMG1.2 2 days after first DT application. Analysis was performed 4 days after first DT application. **(D)** qRT-PCR analysis of chemokines in CD45$^+$ CD11b$^+$ Gr-1^{low} F4/80$^+$ Siglec-F$^-$ macrophages sorted from Treg-depleted HCmel 1274 tumors after basophil depletion, CD8$^+$ T cell depletion or IFN-γ blockade. Results are mean±SEM of 12 mice per group. Shown is all data from 2 independent experiments. *=p<0.05, *=p<0.01, *=p<0.001, ns=not statistically significant.

For examination of a role for M1-like polarization in tumor rejection, macrophages were depleted by administration of clodronate-loaded liposomes (CLIP), and IFN-γ activity was blocked by XMG1.2 antibody. Interestingly, tumor rejection after Treg depletion was shown to be completely abrogated by macrophage ablation and by IFN-γ blockade **(Figure 17A)**, indicating that macrophages are essential for Treg-mediated tumor rejection. Furthermore, macrophage ablation and IFN-γ blockade diminished the positive impact of Treg depletion on the survival of tumor-bearing mice **(Figure 17B)**. **Figure 17D** displayed that CLIP efficiently depleted the macrophages in the tumor whereas IFN- γ blockade did not have an effect on the number of macrophages. In addition, both macrophage depletion and IFN-γ blockade resulted in severely reduced $CD8^+$ and $CD4^+$ T cell infiltration into tumors concomitant with a dramatic decrease in expression of CCL2, CXCL9 and CXCL10 in the tumor **(Figure 17D and E)**.

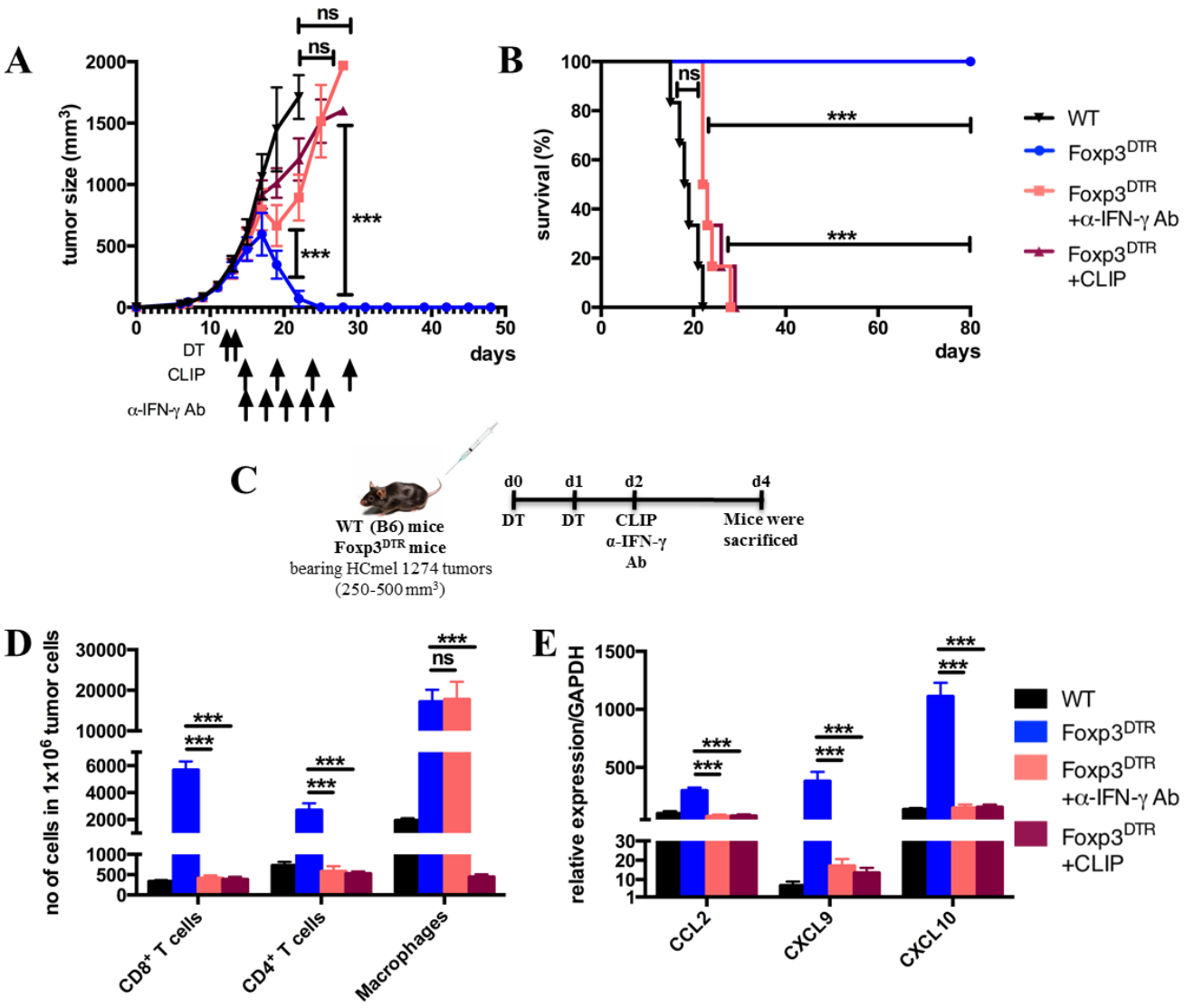

Figure 17: Macrophage depletion and IFN-γ blockade obstruct chemokine production within the Treg-depleted tumor microenvironment, thereby preventing T cell infiltration and tumor rejection observed after Treg depletion in Foxp3^{DTR} mice.
(A) Growth of HCmel 1274 tumors in wild-type (WT, C57BL/6N), Foxp3^{DTR} mice after Treg depletion with DT, Foxp3^{DTR} after Treg depletion combined with ablation of macrophages by 200 µl of clodronate-loaded liposomes (CLIP) and Foxp3^{DTR} after Treg depletion combined with blocking of IFN-γ by anti-IFN-γ antibody XMG1.2. DT, CLIP and antibody were injected on the indicated days. **(B)** Kaplan-Meier survival curves of mice shown in (A). Data are shown as mean±SEM of 6 mice per group. Shown is 1 representative out of 2 independent experiments. **(C)** Wild-type (WT, C57BL/6N) and Foxp3^{DTR} mice were injected with 1x10^6 HCmel 1274 cells i.d. When tumors reached a size of 250-500 mm^3, Treg were depleted in Foxp3^{DTR} mice by DT application on the indicated days. Macrophages were depleted by CLIP and IFN-γ was blocked by anti-IFN-γ antibody XMG1.2 2 days after Treg depletion. Analysis was performed 4 days after first DT application. **(D)** Quantification by flow cytometry of leukocyte subpopulation infiltration into HCmel 1274 tumors in the indicated mice. **(E)** qRT-PCR analysis of chemoattractants in tumors of the indicated mice. Results are shown as mean±SEM of 12 mice per group. Shown is all data from 2 independent experiments. *=p<0.05, *=p<0.01, *=p<0.001, ns=not statistically significant.

In a recent study, we have shown that depletion of Tregs in Foxp3.LuciDTR4 mice induced tumor eosinophilia, which were required for efficient rejection of ovalbumin-expressing B16 melanoma (B16-OVA) following Treg depletion[283]. In the present study, flow cytometry demonstrated that after Treg

depletion in Foxp3^{DTR} mice, infiltration of eosinophils into HCmel 1274 tumors was also enhanced **(Figure 5E)**. The potential role of eosinophils in rejection of HCmel 1274 tumors after Treg ablation was analyzed, using a Siglec-F specific monoclonal antibody that deplete eosinophils. However, in Foxp3^{DTR} mice, eosinophil depletion had no effect on tumor growth **(Figure 18A)**, showing that eosinophils are not essential for the regression of HCmel 1274 melanoma observed after Treg depletion. Kinetic studies of infiltration of tumors by leukocyte subpopulations revealed that after Treg depletion eosinophil and CD8^{+} T infiltration into HCmel 1274 tumors in Foxp3^{DTR} mice occured simultaneously **(Figure 13B and 18B)** whereas in Foxp3.LuciDTR4 mice eosinophil infiltration preceded CD8^{+} infiltration into B16-OVA tumors following ablation of Tregs[283].

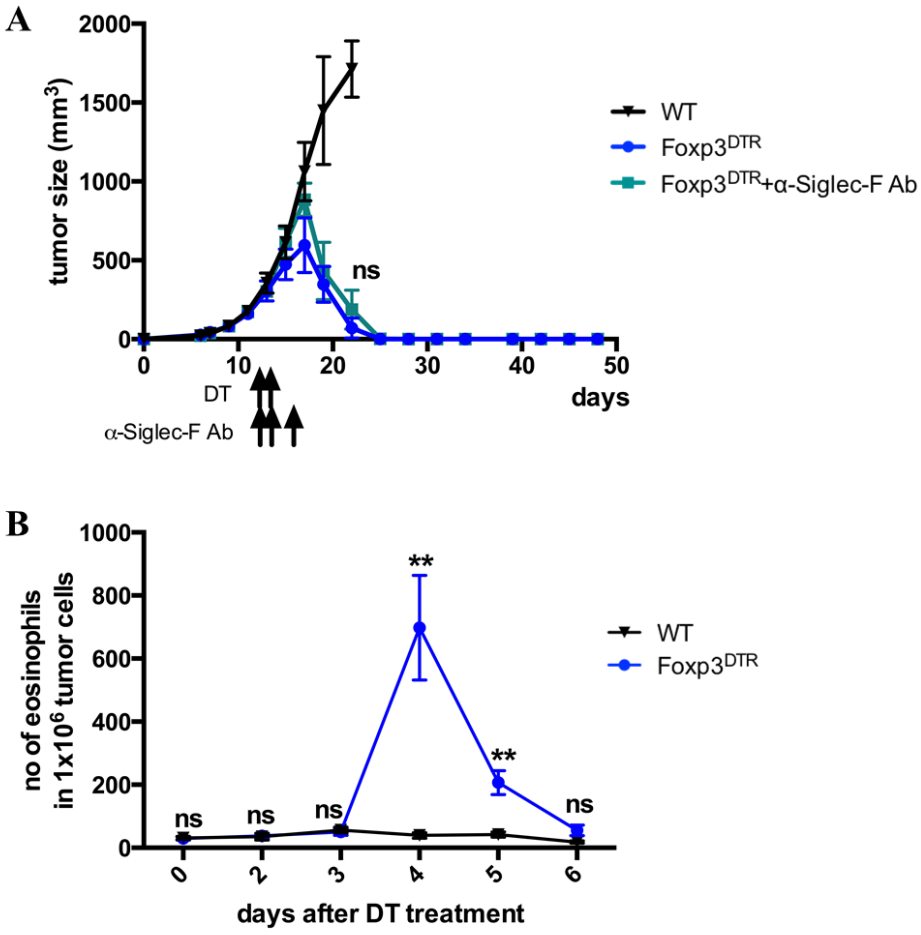

Figure 18: Eosinophil depletion has no effect on growth of HCmel 1274 tumors after Treg depletion in Foxp3^{DTR} mice.
(A) Growth of HCmel 1274 tumors in wild-type (WT, C57BL/6N), Foxp3^{DTR} mice after Treg depletion with DT and Foxp3^{DTR} after Treg depletion combined with ablation of eosinophils by anti-Siglec-F antibody (15 µg/mice). DT and antibodies were injected on the indicated days. Data are shown as mean±SEM of 6 mice per group. Shown is 1 representative experiment. **. (B)** Infiltration kinetics of eosinophils into the tumor after Treg depletion in Foxp3^{DTR} mice. Results are mean±SEM of 12 mice per group. Shown is all data from 2 independent experiments. *=p<0.05, *=p<0.01, *=p<0.001, ns=not statistically significant.

3.1.7 IL-3 mediates tumor-specific recruitment of basophils after Treg depletion

Next, the molecular mechanism of basophil infiltration into the tumor after Treg depletion in Foxp3^{DTR} mice was investigated. **Figure 12E** has shown that basophils were selectively recruited to the tumor 2 days after Treg depletion. Chemokine profiling on the same time point has revealed that the expression of CCL3 and CCL4 were strongly upregulated **(Figure 14B)**. However, further analysis demonstrated that these chemokines are actually produced by tumor-infiltrating basophils **(Figure 14C)**, indicating that the increase in the expression of CCL3 and CCL4 in the tumor resulted from basophil migration into the tumor. A large variety of cytokines, including IL-3, IL-5, IL-18, IL-25, IL-33, granulocyte macrophage colony-stimulating factor (GM-CSF) and thymic stromal lymphopoietin (TSLP), are implicated in the modulation of basophil development, homeostasis, recruitment and effector functions. Therefore, the intratumoral expression of these cytokines was analyzed by RT-PCR. The gene encoding IL-3 was strongly induced in tumors after Treg depletion in Foxp3^{DTR} mice but not after Treg depletion in Foxp3.LuciDTR4 mice **(Figure 19B)**. The expression level of other cytokines was not changed after Treg depletion in both models **(Figure 19B)**. A comprehensive analysis showed that intratumoral CD4^{+} T cells were a major source for IL-3 in the Treg-depleted tumor microenvironment in Foxp3^{DTR} mice **(Figure 19C)**. *Il-3* expression was only upregulated in the tumor but not in other organs such as spleen, td-LN and lung **(Figure 19D)**, indicating tumor-specific production of IL-3 correlated with tumor-specific recruitment of basophils. Together these findings suggest that Treg depletion causes tumor-infiltrating CD4^{+} T cells to secrete IL-3, which, in turn, attracts basophils into the tumor.

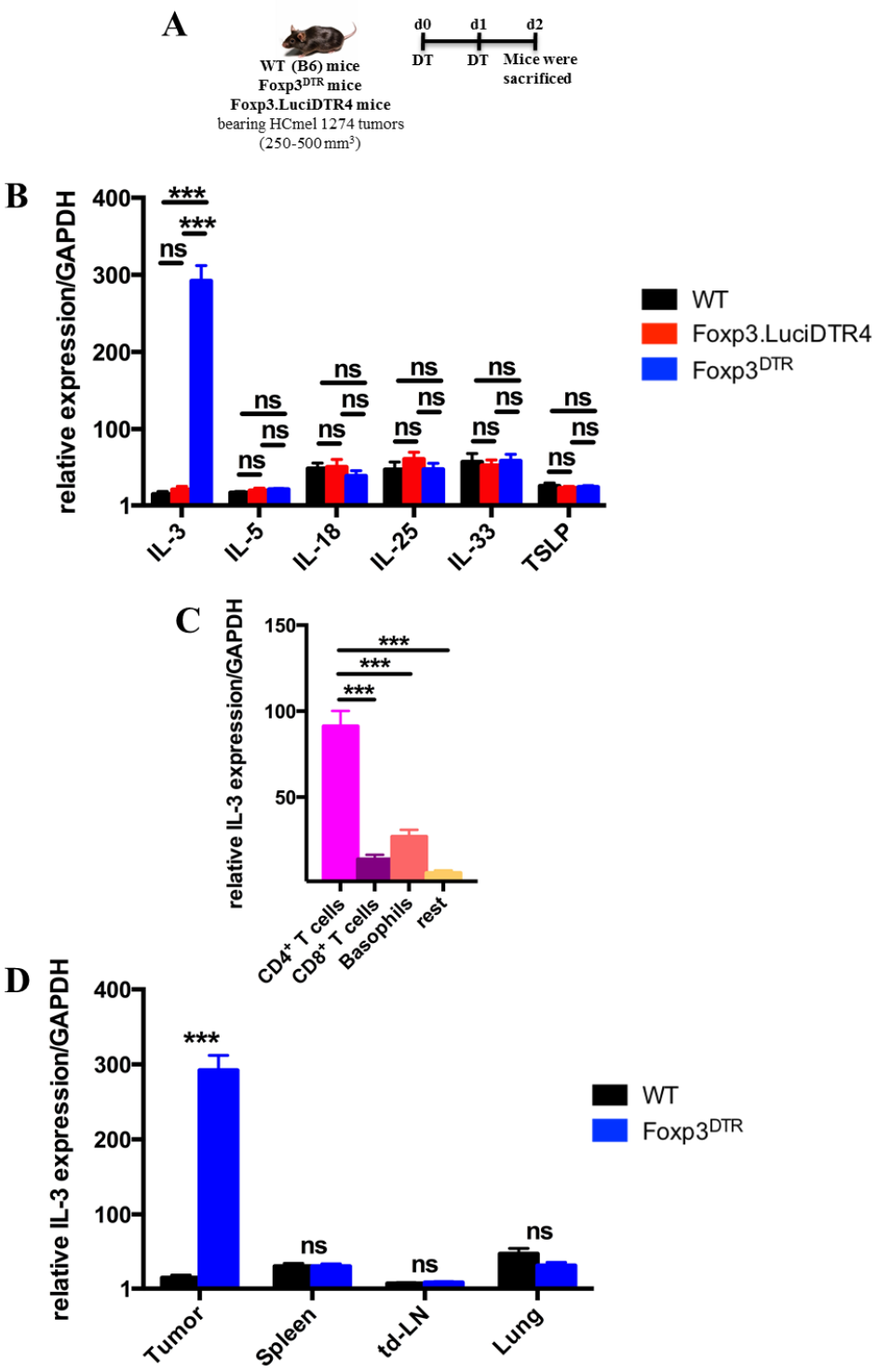

Figure 19: Tumor-specific recruitment of basophils after Treg depletion in Foxp3^{DTR} mice via IL-3.

(A) Wild-type (WT, C57BL/6N), Foxp3.LuciDTR4 and Foxp3^{DTR} mice were injected with 1x10^6 HCmel 1274 cells i.d. When tumors reached a size of 250-500 mm^3, Treg were depleted in Foxp3.LuciDTR4 and Foxp3^{DTR} mice by DT application on the indicated days. Analysis was performed 2 days after first DT application. **(B)** qRT-PCR analysis of cytokines, implicated in stimulation of basophil effector functions, within the HCmel 1274 tumor microenvironment 2 days after Treg depletion. Data are shown as mean±SEM of 12 mice per group. Shown is all data from 2 independent experiments **(C)** qRT-PCR analysis of IL-3 in CD45$^+$ CD3$^+$ CD4$^+$ T cells, CD45$^+$ CD3$^+$ CD8$^+$ T cells, CD45$^+$ FcεRI$^+$ CD49b$^+$ basophils and rest of the cells sorted from HCmel 1274 tumors 2 days after Treg depletion in Foxp3^{DTR} mice. Data are shown as mean±SEM of 6 mice per group. Shown is 1 representative experiment. **D)** qRT-PCR analysis of IL-3 in tumors, spleens, tumor-draining lymph nodes (td-LN) and lung. Data are shown as mean±SEM of 6 mice per group. Shown is 1 representative experiment. *=p<0.05, *=p<0.01, *=p<0.001, ns=not statistically significant.

3.1.8 Systemic administration of IL-3/antibody causes tumor-associated basophilia

In a study by Ohmori *et al*., it was reported that injection of IL-3/antibody complex (IL-3 + anti-IL-3 Ab) into mice facilitated expansion of basophils in vivo[232]. Consistent with these findings, intravenous administration of IL-3/antibody complex into tumor-bearing mice was found to induce basophilia in the blood, in the lung, in the spleen and in the tumor, but not in td-LNs **(Figure 20B)**. In addition, IL-3/antibody complex had no effect on the number of eosinophils and mast cells **(Figure 20B)**. As observed in the Treg depletion model, tumor-associated basophilia was correlated with an increased intratumoral expression of CCL3 and CCL4 **(Figure 20C)**. Since the IL-3/antibody complex mainly enhanced the levels of basophils, this approach enabled me to investigate more precisely the mechanism by which basophils support antitumor immunity.

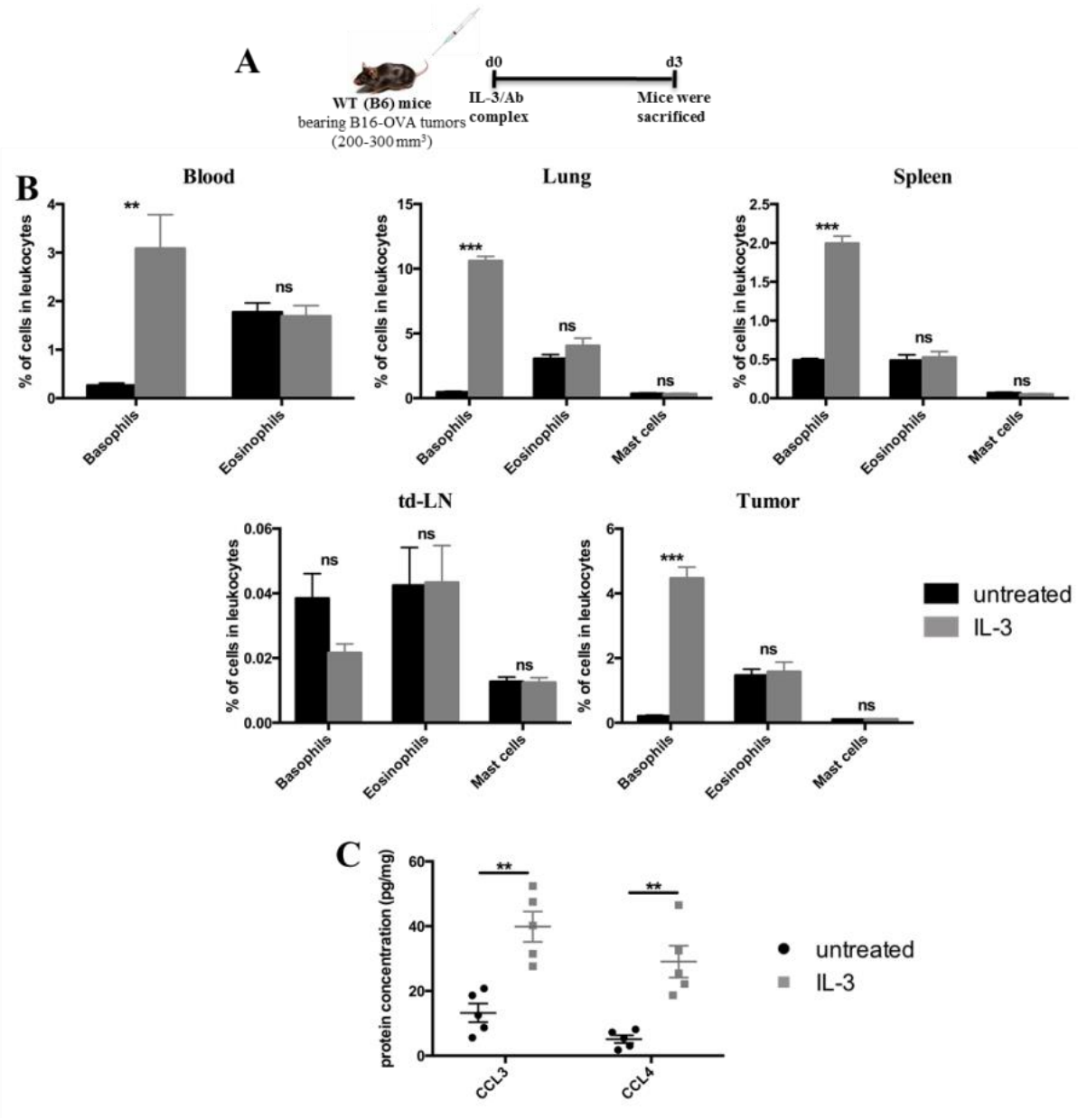

Figure 20: IL-3/antibody complex injection induces basophilia in B16-OVA tumor, which correlates with intratumoral CCL3 and CCL4 production.
(A) B16-OVA-bearing wild-type (WT, C57BL/6N) mice were injected i.v. with a mixture of mouse reombinant IL-3 (10 µg/mice) and anti-IL-3 antibody (5 µg/mice). 3 days later, mice were sacrificed for analysis. **(B)** Percentage of basophils and eosinophils in blood; percentage of basophils, eosinophils and mast cells in lung, spleen, tumor-draining lymph nodes (td-LN) and tumor in the indicated mice calculated by flow cytometry. Data are shown as mean±SEM of 10 mice per group. Shown is all data from 2 independent experiments. **(C)** Multiplex analysis of CC3 and CCL4 in tumor lysates of mice treated with IL-3/antibody complex or left untreated. Data are shown as mean±SEM of 5 mice. Shown is 1 representative experiment. *=p<0.05, *=p<0.01, *=p<0.001, ns=not statistically significant.

3.1.9 IL-3/antibody complex-induced basophilia enhances the infiltration of tumor-specific CD8$^+$ T cells

Immunotherapy based on the adoptive transfer of tumor-specific T cells is now a clinical therapy for cancer patients. However, its success is still limited[185]. Therefore, it was examined whether tumor-associated basophilia would be able to improve the efficacy of T cell therapy against B16 melanoma expressing ovalbumin as a surrogate tumor antigen (B16-OVA). As demonstrated in previous studies conducted in our laboratory, adoptive transfer of ovalbumin-specific CD8$^+$ T cells alone, which are derived from TCR-transgenic OT-I mice, resulted in limited control of B16-OVA tumor growth **(Figure 21A and B)**. Interestingly, when the transfer of OT-I CD8 T cells was combined with injection of IL-3/antibody complex, B16-OVA tumor growth was substantially inhibited and the survival of tumor-bearing mice prolonged **(Figure 21A and B)**. Moreover, in vivo blockade of CCL3 and CCL4 by injection of a combination of antibodies against these chemokines impaired the tumor rejection observed after IL-3/antibody complex+OT-I CD8$^+$ T cell therapy **(Figure 21A and B)**. These findings show that basophilia induced by the IL-3/antibody retarded tumor growth when combined with adoptive T cell therapy.

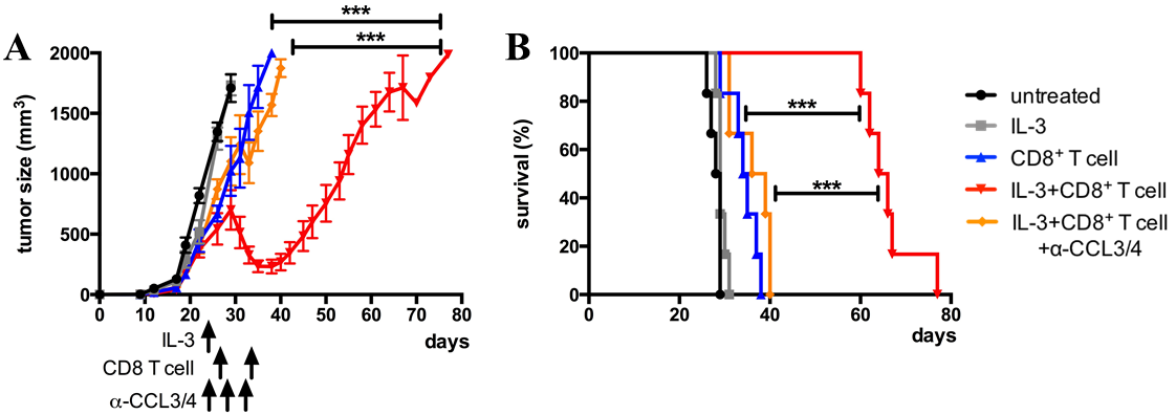

Figure 21: Adoptive transfer of tumor-specific CD8$^+$ T cells alone fails to control growth of B16-OVA tumors, whereas co-injection with IL-3/antibody complex leads to tumor rejection in a CCL3/4 dependent way.
(A) B16-OVA tumor growth curves in Wild-type (WT, C57BL/6N) mice after i.v. injection of IL-3/antibody complex alone, activated OT-I CD8$^+$ T cells alone, IL-3/antibody complex plus activated OT-I CD8$^+$ T cells and IL-3/antibody complex plus activated OT-I CD8$^+$ T cells in combination with a cocktail of antibodies against CCL3 and CCL4. **(B)** Kaplan-Meier survival curves of mice shown in (A). Data are shown as mean±SEM of 6 mice per group. Shown is 1 representative out of 2 independent experiments. *=p<0.05, *=p<0.01, *=p<0.001, ns=not statistically significant.

Analysis of the composition of immune cells revealed that $CD8^+$ T cells and $CD4^+$ T cells only scarcely infiltrated the tumors after OT-I $CD8^+$ T cell transfer alone **(Figure 22B)**. However, when combined with IL-3/antibody complex injection, tumors were strongly infiltrated by $CD8^+$ T cells and $CD4^+$ T cells **(Figure 22B)**, but not with B cells **(Figure 22B)**. In vivo blockade of basophil-derived chemokines CCL3 and CCL4 impaired the migration of $CD8^+$ T cells, mainly including transferred OT-I $CD8^+$ T cells, and $CD4^+$ T cells into the tumor **(Figure 22B and C)**. Combination therapy also led to a rise in the infiltration of innate immune cells into the tumor, including NK cells, DCs and macrophages but only the migration of NK cells and macrophages was affected by blocking of CCL3/4 **(Figure 22D)**. Among the tumor infiltrating-granulocytes, only basophils were enriched after combination therapy in the tumor but not eosinophils, neutrophils and mast cells **(Figure 22E)**. Importantly, CCL3/4 blocking was found to have no impact on IL-3/antibody complex-induced tumor-associated basophilia **(Figure 22E).** These results indicate that the IL-3/antibody complex-induced basophilia control recruitment of T cells and other leukocyte populations into tumors via production of CCL3 and CCL4.

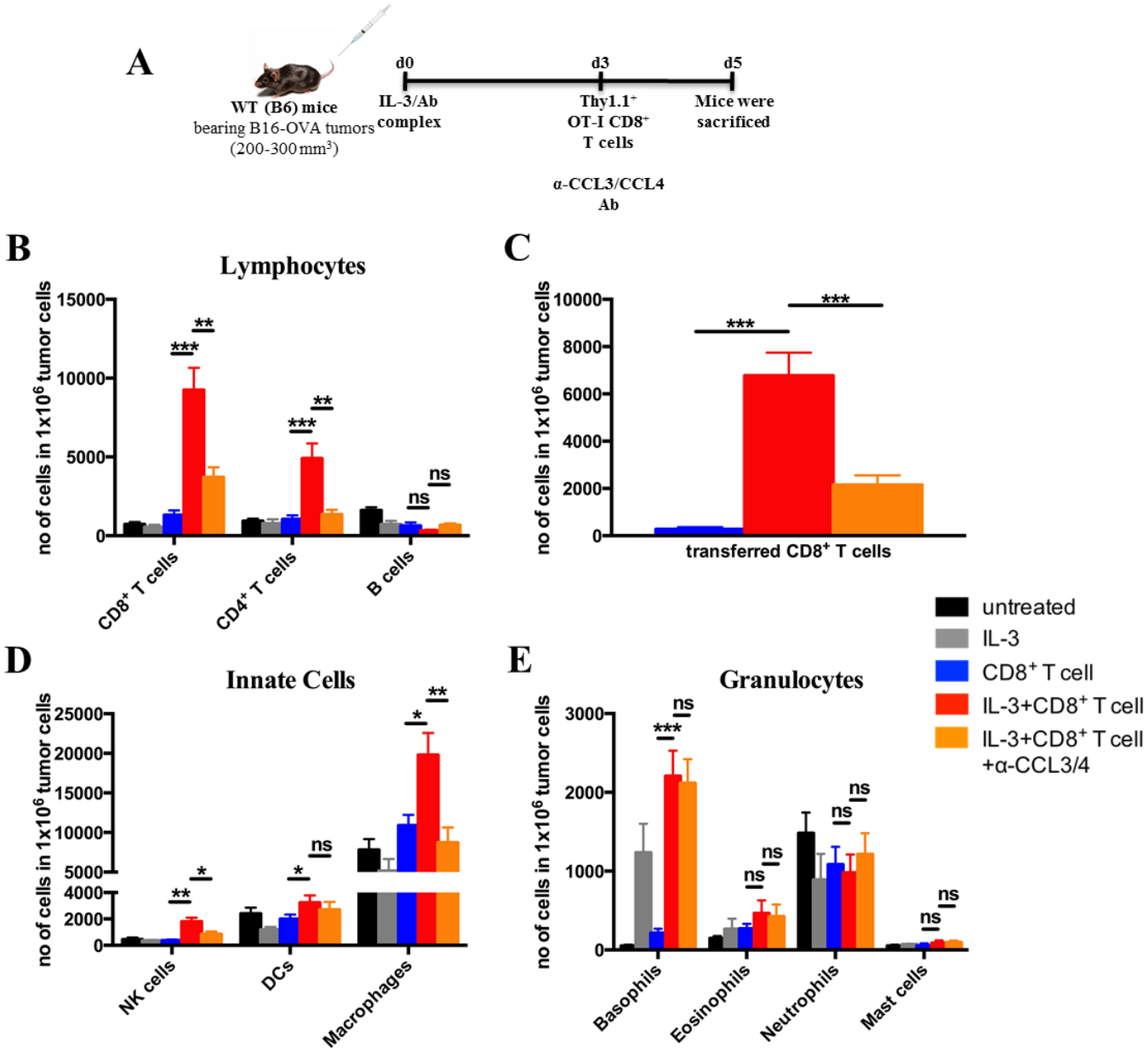

Figure 22: Combination of adoptive transfer of tumor-specific CD8$^+$ T cells with IL-3/antibody complex results in strong T cell infiltration into B16-OVA tumors in a CCL3/4 dependent way.
(A) B16-OVA-bearing wild-type (WT, C57BL/6N) mice were injected i.v. with IL-3/antibody complex 3 days before adoptive transfer of OT-I CD8$^+$ T cells. 2 days after CD8$^+$ T cell transfer, mice were sacrificed for analysis. Quantification by cytofluorometry of **(B)** lymphocyte infiltration, **(C)** transferred Thy1.1$^+$ OT-I CD8$^+$ T cell infiltration, **(D)** innate cell infiltration and **(E)** granulocyte infiltration into the tumor. Results are shown as mean±SEM of 10 mice per group. Shown is all data from 2 independent experiments. *=p<0.05, *=p<0.01, *=p<0.001, ns=not statistically significant.

3.1.10 IL-3/antibody complex+CD8 T cell transfer results in macrophage polarization and normalization of tumor vasculature

Macrophages are abundantly present in tumors of cancer patients. Tumor-associated macrophages (TAMs) usually present a protumoral M2 phenotype that depends on the cues in the tumor microenvironment[284]. M2 TAMs promote many critical aspects of tumor progression, including angiogenesis, tumor cell motility and invasion as well as suppression of antitumor immune responses[284]. Therefore, M2 TAMs represent a crucial target for cancer therapy. With appropriate therapeutic interventions, these cells might assume M1-like features. M1-like macrophages can induce direct killing of tumor cells, promote T cell-mediated inflammation, or decrease of angiogenesis[284]. Whereas TAMs isolated from untreated tumors displayed an M2-like phenotype, macrophages sorted from tumors after IL-3/antibody complex+$CD8^+$ T cell transfer were skewed towards an M1-like phenotype, as demonstrated by higher expression of the genes encoding CCL2, CXCL9, CXCL10, TNF-α, inducible nitric oxide synthase (iNOS), and lower expression of the M2 typical genes encoding arginase I (Arg1) and mannose receptor, c type 1 (MRC1) **(Figure 23B)**. These findings indicate that the combination therapy used here caused macrophage polarization towards M1 probably due to basophilia-induced infiltration of T cells. These T cells can secrete cytokines such as IFN-γ and TNF-α which can further skew tumor-associated M2 macrophages towards M1 macrophages and further enhance T cell infiltration through production of chemokines and cytokines such as CCL2, CXCL9, CXCL10 and TNF-α by M1-like macrophages.

In order to see if the combination of IL-3/antibody complex plus OT-I $CD8^+$ T cells is able to enhance normalization of the tumor vasculature, the tumor vessels were investigated by immunofluorescence. Results in **Figure 23C and D** show that untreated B16-OVA tumors were characterized by aberrant tumor vasculature and combination therapy, consisting of basophils induction by IL-3/antibody complex and OT-I $CD8^+$ T cells, promoted the normalization of tumor vasculature, as indicated by a reduction in the average $CD31^+$ vessel size. Moreover, the normalized vessels showed enhanced expression of VCAM-1 **(Figure 23C and D)**. In summary, combination therapy with IL-3/antibody complex and $CD8^+$ T cells induced tumor

vasculature normalization and tumor endothelium activation through M1 skewing of tumor associated macrophages.

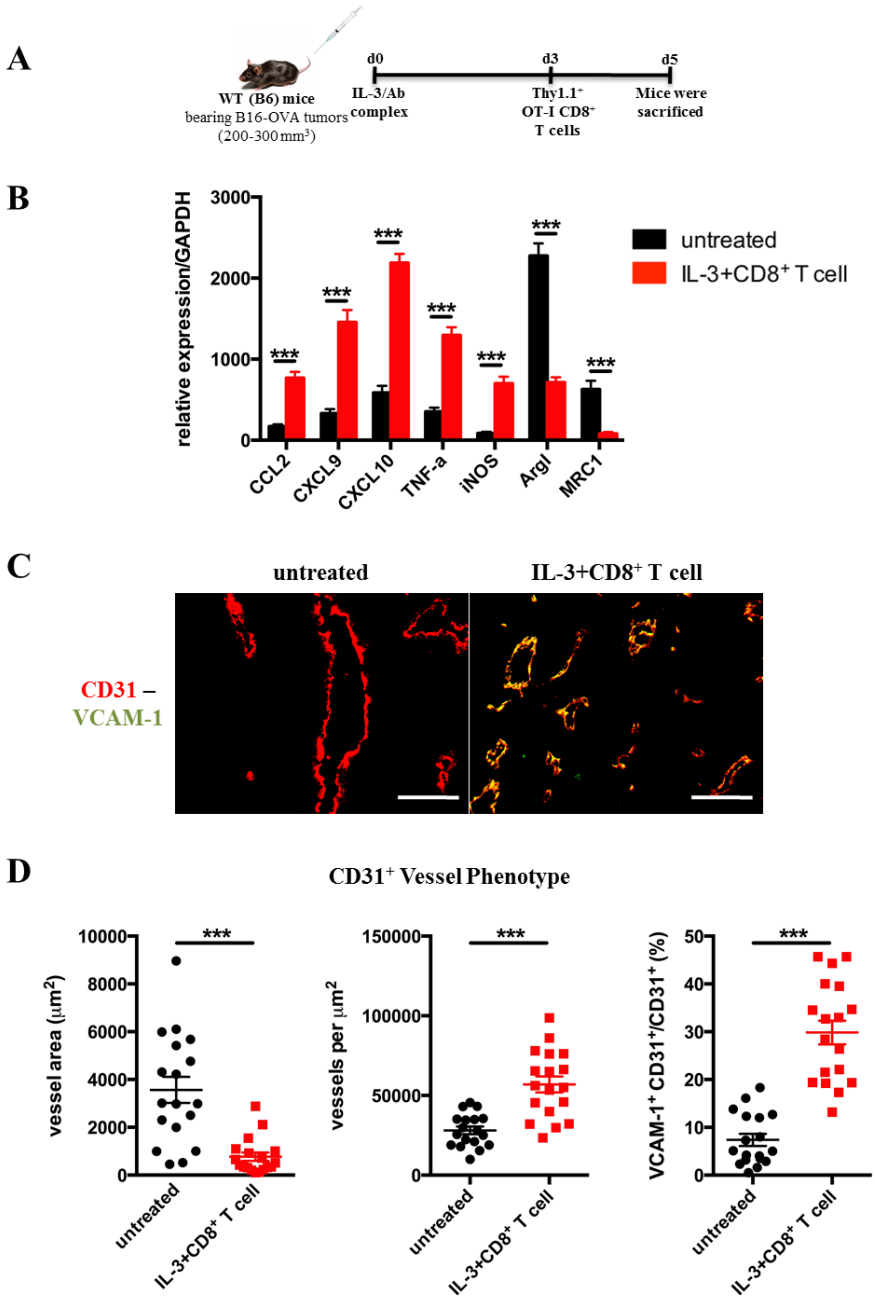

Figure 23: Combination of adoptive transfer of tumor-specific CD8⁺ T cells with IL-3/antibody complex induces M1-like polarization of tumor-associated macrophages and normalization of the tumor vasculature. **(A)** B16-OVA-bearing wild-type (WT, C57BL/6N) mice were injected i.v. with IL-3/antibody complex 3 days before adoptive transfer of OT-I CD8⁺ T cells. 2 days after CD8⁺ T cell transfer, mice were sacrificed for analysis. **(B)** qRT-PCR analysis of cytokines, chemokines and markers for M1- and M2-like macrophages from sorted CD45⁺ CD11b⁺ Gr-1^{low} F4/80⁺ Siglec-F⁻ tumor macrophages from untreated mice, and mice injected with IL-3/antibody complex and OT-I CD8⁺ T cells. Data are mean±SEM of 6 mice per group. Shown is 1 representative experiment. **(C)** Representative immunofluorescence microscopy analysis of tumor vessels of the indicated mice stained with antibodies against CD31 (red) and VCAM-1 (green). Yellow color shows colocalization. Size bar indicates 100 µm. **(D)** Quantification of individual CD31⁺ tumor vessel size, number of CD31⁺ tumor vessels and VCAM-1 expression on CD31⁺ tumor vessels. Tumors of comparable size were investigated. 3 random fields were analyzed from each tumor. Results are mean±SEM of 6 mice per group. Shown is 1 representative experiment. *=p<0.05, *=p<0.01, *=p<0.001, ns=not statistically significant.

3.2 Rip1-Tag5 (RT5) as a Model to Study Immune Rejection of Tumors

Previous studies have shown that treatment modalities such as vaccination against tumor antigens and adoptive T cell therapy failed to control tumor progression in RT5 mice due to inefficient T cell trafficking into tumors. This lack of T cell infiltration correlated with aberrant tumor vasculature[75, 274, 275]. However, the combination of adoptive T cell therapy with danger signals, such as irradiation and TLR9 agonist cytosine-phosphorothioate-guanine containing oligodeoxynucleotides (CpG-ODN), caused normalization of tumor vessels and recruitment of tumor-specific T cells into tumors. In the present study, the underlying mechasim how the combination of CpG-ODN with pre-activated tumor-specific $CD8^+$ T cells enhances T cell infiltration was investigated.

3.2.1 Combination of CpG-ODN with adoptive T cell transfer prolongs the survival of RT5 mice

Treatment of 24 week-old RT5 mice carrying large established pancreatic tumors with adoptive transfer of tumor antigen Tag-specific $CD8^+$ T cells alone led only to a slight improvement in survival but eventually all the mice succumbed to death **(Figure 24B)**. In contrast, treatment of mice with Tag-specific $CD8^+$ T cells in combination with CpG-ODN resulted in rejection of RT5 tumors and prolonged survival of tumor-bearing mice **(Figure 24B)**. CpG-ODN monotherapy had no impact on tumor growth in comparison with untreated mice **(Figure 24B)**.

In order to explore the mechanism underlying the successful combination therapy, tumor infiltration of 24 week-old RT5 mice by leukocyte subpopulations was examined by flow cytometry. It was observed that CpG-ODN alone was able to enhance tumor infiltration of $CD8^+$ T cells, composed of endogenous and transferred $CD8^+$ T cells, $CD4^+$ T cells, B cells and macrophages but not of NK cells and DCs whereas adoptive $CD8^+$ T cell therapy alone induced an increase only in the number of intratumoral $CD8^+$ T cells and $CD4^+$ T cells **(Figure 24C)**. Strikingly, combination therapy strongly enhanced infiltration of $CD8^+$ T cells, $CD4^+$ T cells, B cells and NK

cells, DCs and macrophages into the tumor **(Figure 24C)**, explaining the improved survival in RT5 mice treated with combination therapy.

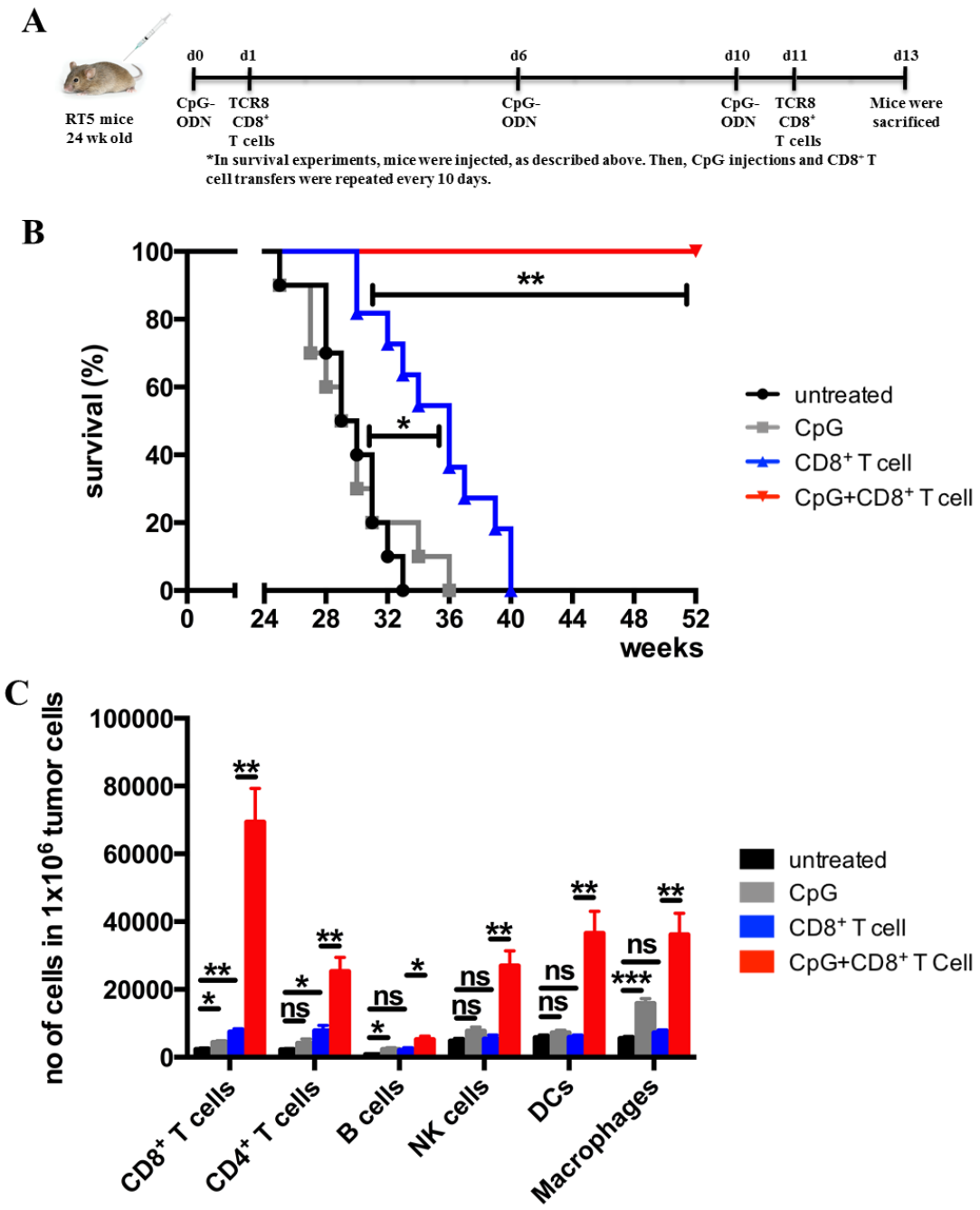

Figure 24: Combination of adoptive transfer of tumor-specific CD8$^+$ T cells with CpG-ODN results in strong infiltration of leukocyte subpopulations, notably CD8$^+$ T cells and macrophages, and tumor rejection.
(A) 24 week-old Rip1-Tag5 (RT5) mice were injected with 25 µg of CpG-ODN 1668 i.v. on days 0, 6 and 10. If indicated, the same group of mice received adoptive transfers of activated TCR8 CD8$^+$ T cells on day 1 and 11. Mice were sacrificed on day 13 and analyzed by flow cytometry. For survival experiments, mice were injected, as described above. CpG-ODN injection and adoptive transfers were repeated every 10 days until the end of experiment. **(B)** Kaplan-Meier survival curves of mice treated with CpG-ODN alone, adoptive transfer of TCR8 CD8$^+$ T cells alone and combination of CpG-ODN and adoptive transfer of TCR8 CD8$^+$ T cells. Data are shown as 10 mice per group. **(C)** Quantification by cytofluorometry of infiltration of leukocyte subpopulations into RT5 tumors. Results are shown as mean±SEM of 10 mice per group. Shown is all data from 2 independent experiments. *=p<0.05, *=p<0.01, *=p<0.001, ns=not statistically significant.

3.2.2 CpG-ODN polarizes tumor-associated macrophages into M1-like phenotype

In a previous study, systemically injected CpG-ODN, that was fluorochrome labeled, was found to bind to macrophages in the tumor[274]. Stimulated by this observation, the phenotype of tumor macrophages in RT5 mice was investigated for the expression of M1 marker iNOS and M2 marker CD206 (MRC1). In untreated tumors, the majority of macrophages were M2-like, as indicated by high level of CD206 expression and low level of iNOS expression **(Figure 25B and C)**. $CD8^+$ T cell transfer alone had no effect on the phenotype of macrophages whereas CpG-ODN polarized macrophages towards a M1-like phenotype, shown by an increase in iNOS production and a decrease in CD206 production **(Figure 25B and C)**. Combination of CpG-ODN with adoptive $CD8^+$ T cell transfer resulted in further augmented expression of iNOS in intratumoral macrophages **(Figure 25B and C)**.

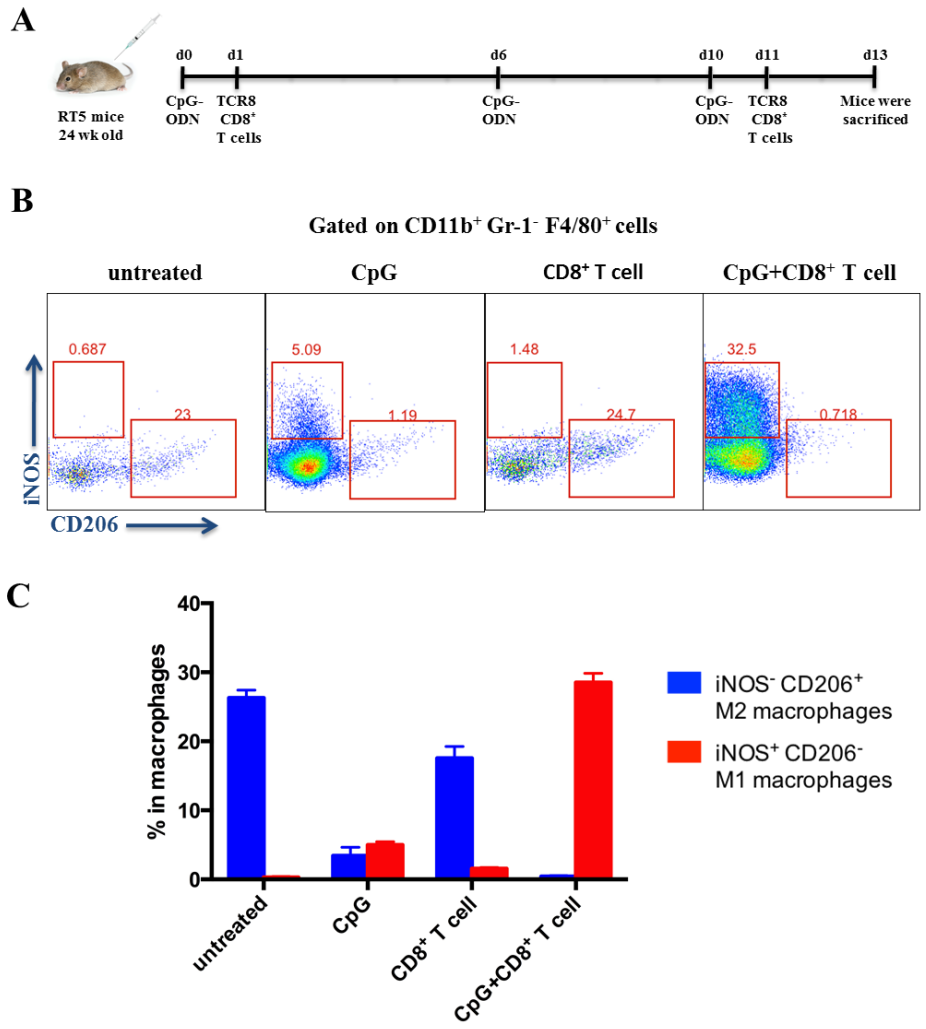

Figure 25: Combination therapy induces M1-like polarization of tumor-associated macrophages in RT5 mice.
(A) 24 week-old Rip1-Tag5 (RT5) mice were injected with 25 µg of CpG-ODN 1668 i.v. on days 0, 6 and 10. If indicated, the same group of mice received adoptive transfers of activated TCR8 $CD8^+$ T cells on day 1 and 11. Mice were sacrificed on day 13 and analyzed by flow cytometry. **(B)** Representative flow cytometric analysis of iNOS (M1 marker) and CD206 (MRC1) (M2 marker) expression on $CD11b^+$ $Gr\text{-}1^-$ $F4/80^+$ tumor macrophages. **(C)** Summary of data presented in (B). Bars indicate the percentage of respective population in total tumor-infiltrating macrophages. Data are mean±SEM of 10 mice per group. Shown is all data from 2 independent experiments.

3.2.3 iNOS-expressing macrophages are essential for tumor regression in RT5 mice

In order to investigate the potential role of $iNOS^+$ macrophages in tumor rejection after CpG-ODN plus adoptive $CD8^+$ T cell transfer, CLIP was employed for selective depletion of macrophages. In addition, L-N6-(1-iminoethyl)lysine (L-NIL), was used to selectively inhibit iNOS activity in RT5 mice. Interestingly, CLIP treatment abrogated the increased lifespan of tumor-bearing RT5 mice observed after

combination therapy **(Figure 26B)**. Flow cytometric analysis revealed that macrophages were efficiently depleted in the tumor by CLIP administration **(Figure 26C)**. Moreover, macrophage-depleted tumors displayed a reduced infiltration of $CD8^+$ T cells, $CD4^+$ T cells, NK cells and DCs **(Figure 26C)**. In contrast, iNOS blockade with L-NIL had a slight but not significant impact on the number of intratumoral macrophages, but also led to an reduction in the number of $CD8^+$ T cells, $CD4^+$ T cells, NK cells and DCs in the tumor (**Figure 26C)**. B cell infiltration is not significantly affected by either macrophage depletion or iNOS blockade **(Figure 26C)**. Notably, the inhibition of leukocyte infiltration by macrophage ablation was stronger than that by iNOS blockade, leaving open the possibility that other macrophage-derived factors are involved or that iNOS blockade was not complete. Overall, these findings indicate that iNOS macrophages extend the lifespan of RT5 mice by controlling T-cell trafficking into the tumor.

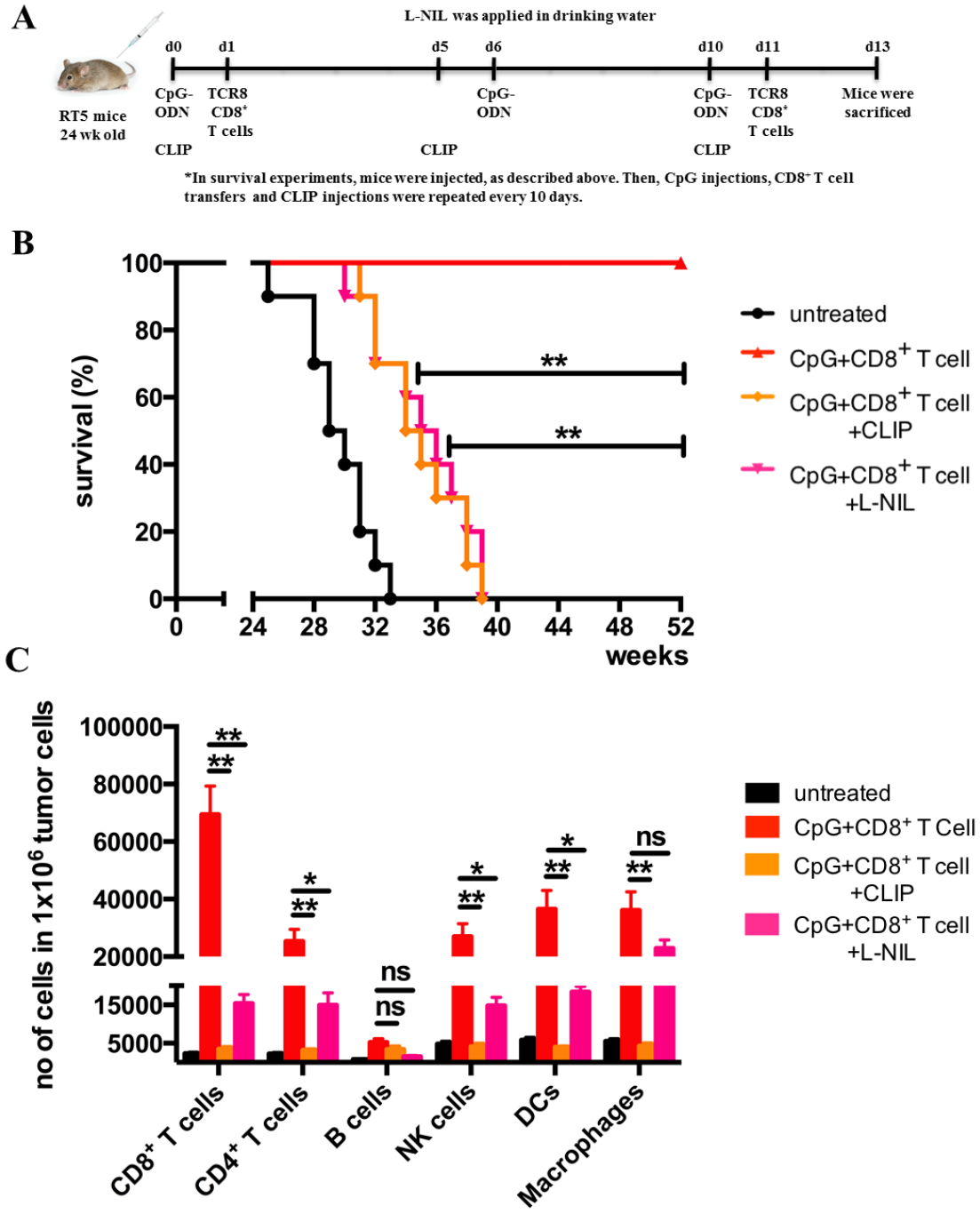

Figure 26: Macrophage depletion and iNOS blockade impairs T cell infiltration and RT5 tumor rejection
(A) 24 week-old Rip1-Tag5 (RT5) mice were injected with 25 µg of CpG-ODN 1668 i.v. on days 0, 6 and 10. If indicated, the same group of mice received adoptive transfers of activated TCR8 $CD8^+$ T cells on day 1 and 11. Mice were sacrificed on day 13 and analyzed by flow cytometry. Macrophages were depleted by i.p. injection of clodronate-loaded liposomes (CLIP) on day 0, 5 and 10. iNOS blockade was achieved by 2 mM L-NIL in the drinking water of mice. For survival experiments, mice were injected, as described above. CpG-ODN injection, adoptive transfers and CLIP injection were repeated every 10 days until the end of experiment. **(B)** Kaplan-Meier survival curves of mice treated with combination therapy, combination therapy accompanied with macrophage depletion by CLIP and combination therapy accompanied with iNOS blockade by L-NIL. Data are shown as 10 mice per group. **(C)** Quantification by cytofluorometry of infiltration of leukocyte subpopulations into RT5 tumors. Results are shown as mean±SEM of 10 mice per group. Shown is all data from 2 independent experiments. *=p<0.05, *=p<0.01, *=p<0.001, ns=not statistically significant.

3.2.4 iNOS activity in macrophages promotes normalization of the tumor vasculature

As mentioned above, late-stage RT5 tumors are characterized by abnormal tumor vessels, which form a pyhsical barrier against T cell penetration into the tumor. Therefore, it was studied whether iNOS macrophages can modulate the tumor vasculature and thereby allow T cell infiltration into tumors. Immunofluorescence analysis showed that untreated RT5 tumors harbor large dilated vessels **(Figure 27B and C)**, consistent with previous findings[75]. CpG-ODN alone or $CD8^+$ T cell transfer alone caused partial normalization of tumor vasculature, as indicated by replacement of large dilated vessels with smaller and more homogeneous vessels **(Figure 27b and C)**. Vessel normalization was further increased by combination of CpG-ODN and adoptive $CD8^+$ T cell transfer **(Figure 27B and C)**, suggesting that CpG-activated macrophages and pre-activated tumor-specific $CD8^+$ T cells act together to normalize the aberrant tumor vasculature. Moreover, CpG-ODN alone and $CD8^+$ T cell transfer alone induced vascular adhesion molecule-1 (VCAM-1) expression on the tumor endothelium, which was further enhanced by combination therapy **(Figure 27B and C)**. Importantly, macrophage depletion and iNOS blockade inhibited normalization of tumor vasculature and VCAM-1 expression on the tumor endothelium **(Figure 27B and C)**.

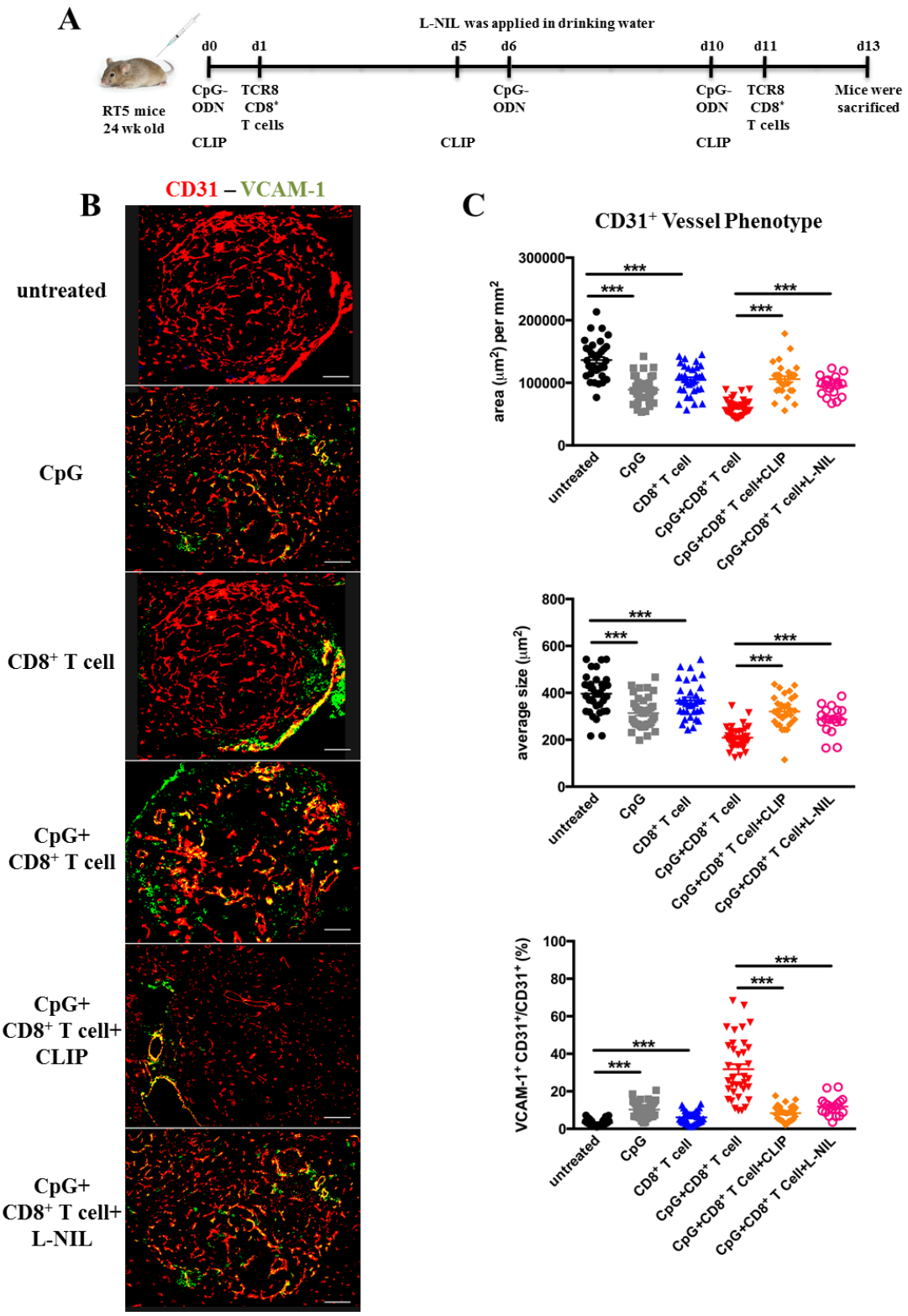

Figure 27: Combination therapy leads to normalization of the RT5 tumor vasculature, which is dependent on iNOS activity in tumor-associated macrophages

(A) 24 week-old Rip1-Tag5 (RT5) mice were injected with 25 µg of CpG-ODN 1668 i.v. on days 0, 6 and 10. If indicated, the same group of mice received adoptive transfers of activated TCR8 $CD8^+$ T cells on day 1 and 11. Mice were sacrificed on day 13 and analyzed by flow cytometry. Macrophages were depleted by i.p. injection of clodronate-loaded liposomes (CLIP) on day 0, 5 and 10. iNOS blockade was achieved by 2 mM L-NIL in the drinking water of mice. **(B)** Representative immunofluorescence microscopy analysis of tumor vessels of the indicated mice stained with antibodies against CD31 (red) and VCAM-1 (green). Yellow color shows colocalization. Size bar indicates 100 µm. **(C)** Quantification of $CD31^+$ tumor vessel area per square millimeter, average size of $CD31^+$ tumor vessels and VCAM-1 expression on $CD31^+$ tumor vessels. Tumors of comparable size were investigated. 3-6 random sections were analyzed from each tumor. Results are mean±SEM of 6 mice per group. Shown is all data from 2 independent experiments. *=p<0.05, *=p<0.01, *=p<0.001, ns=not statistically significant.

3.2.5 Adoptive transfer of iNOS-expressing macrophages promotes antitumor immunity

In order to study in more detail the mechanism by which iNOS activity in macrophages support T cell-mediated antitumor immune responses, *Nos2*$^{-/-}$ (iNOS-deficient) macrophages were utilized. First, macrophages derived from wild type and NOS2$^{-/-}$ bone marrow cells were activated lipopolysaccharide (LPS) and IFN-γ (M1) or left untreated (M0) compared for the expression of M1 and M2 markers. RT-PCR analysis showed that M1 polarization led to upregulation of the genes encoding Th1 cytokines TNF-α, IL-1β, IL-12, chemokines CCL2, CCL5, CXCL9, CXCL10, and other M1 markers, such as MHC-II in both wild type and NOS2 macrophages **(Figure 28A)**. Moreover, M1 wild type and M1 *Nos2*$^{-/-}$ macrophages displayed decreased expression of the genes encoding M2 markers, including Arginase I (ARGI), CD163, MRC1 and peroxisome-prolifeating receptor-γ (PPARG) and angiogenic factors, including vascular endothelial growth factor (VEGF)-α, angiopoeitin 2 (ANGPT2) and fibroblast growth factor 1 (FGF1) **(Figure 28A)**. As anticipated, *Nos2* expression is only induced in wt macrophages after LPS/IFN-γ-mediated polarization **(Figure 28A)**. This was further confirmed at the protein level by flow cytometry **(Figure 28B)**. In summary, wild type and NOS2$^{-/-}$ macrophages displayed similar gene expression profiles. This indicates that lack of iNOS activity does not affect the gene expression in macrophages.

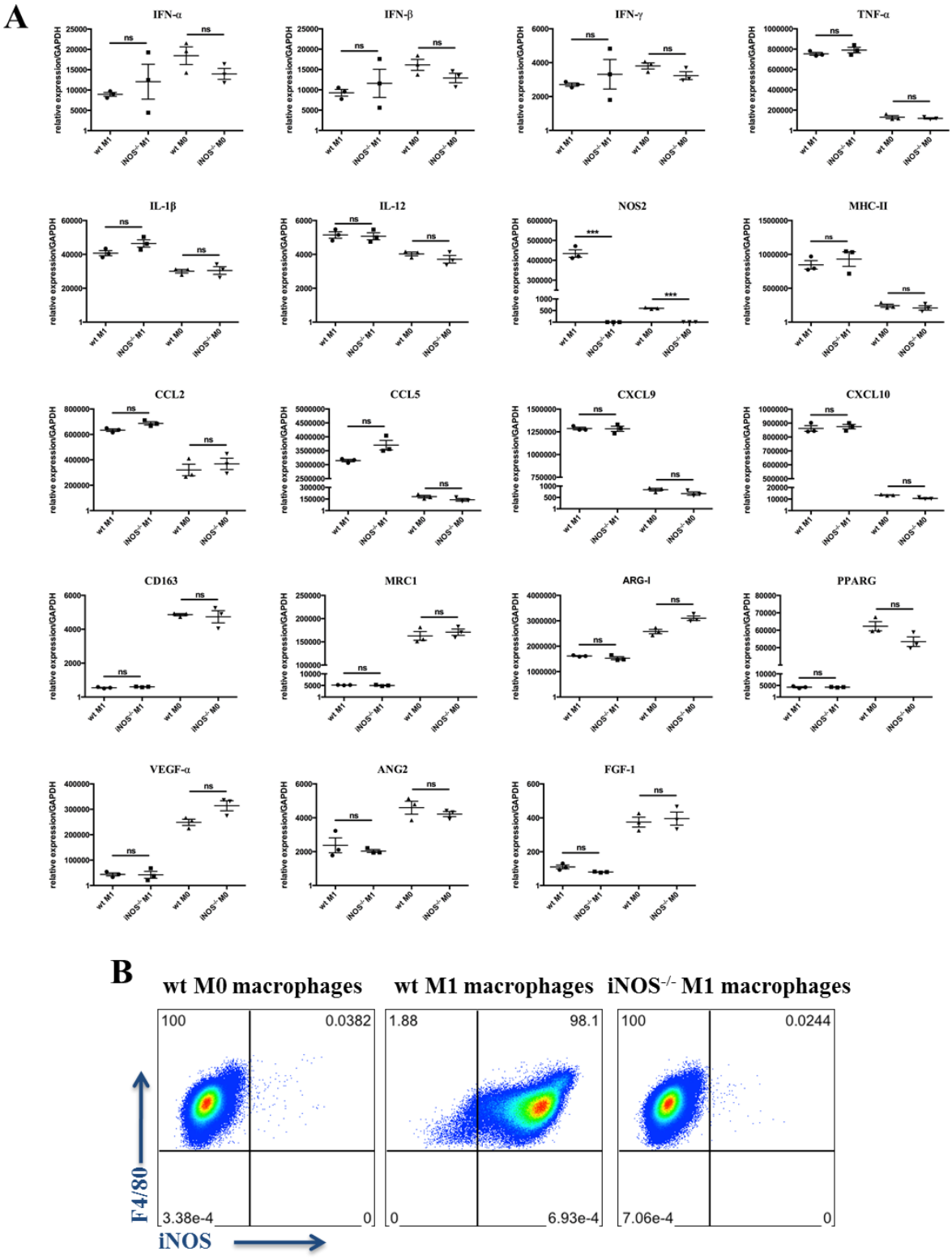

Figure 28: *In vitro*-activated wild-type (WT) and *Nos2*$^{-/-}$ macrophages displayed similar gene expression profiles.

(A) qRT-PCR analysis of cytokines, chemokines, proangiogenic factors, M1 and M2 markers expressed by WT and *Nos2*$^{-/-}$ macrophages cultured *in vitro* with our without LPS and IFN-γ (M1 macrophages and M0 macrophages, respectively). Data are shown as mean±SEM of 3 mice per group. Shown is 1 representative experiment. *=p<0.05, *=p<0.01, *=p<0.001, ns=not statistically significant **(B)** Representative flow cytometric analysis of iNOS expression on WT and *Nos2*$^{-/-}$ macrophages cultured *in vitro* with our without LPS and IFN-γ (M1 macrophages and M0 macrophages, respectively).

Next, it was studied whether transfer of pre-activated macrophages would be able to replace CpG-ODN treatment and enhance recruitment of tumor-specific $CD8^+$ T cells into the tumor. To this end, macrophages, which were isolated from CD45.2 congenic wt or *Nos2*$^{-/-}$ mice, were activated with LPS and IFN-γ (M1) or left untreated (M0), and then injected into CD45.1 congenic mice bearing B16-OVA one day before the adoptive transfer of tumor-specific OT-I $CD8^+$ T cells. The homing of adoptively transferred macrophages into the tumor was examined one day after macrophage transfer (before $CD8^+$ T cell transfer) by staining for CD4.2 marker on the transferred macrophages. Most of the transferred wt and *Nos2*$^{-/-}$ M1 macrophages reached the tumor whereas wt M0 macrophages showed lower migration capacity towards the tumor **(Figure 29B and C)**. The higher infiltration capacity of M1 macrophages probably resulted from increased chemokine receptor expression on activated macrophages. Of note, activated wt and *Nos2*$^{-/-}$ macrophages displayed the same level of infiltration into the tumor **(Figure 29B and C)**, suggesting that iNOS deficiency has no impact on migration capacity of macrophages.

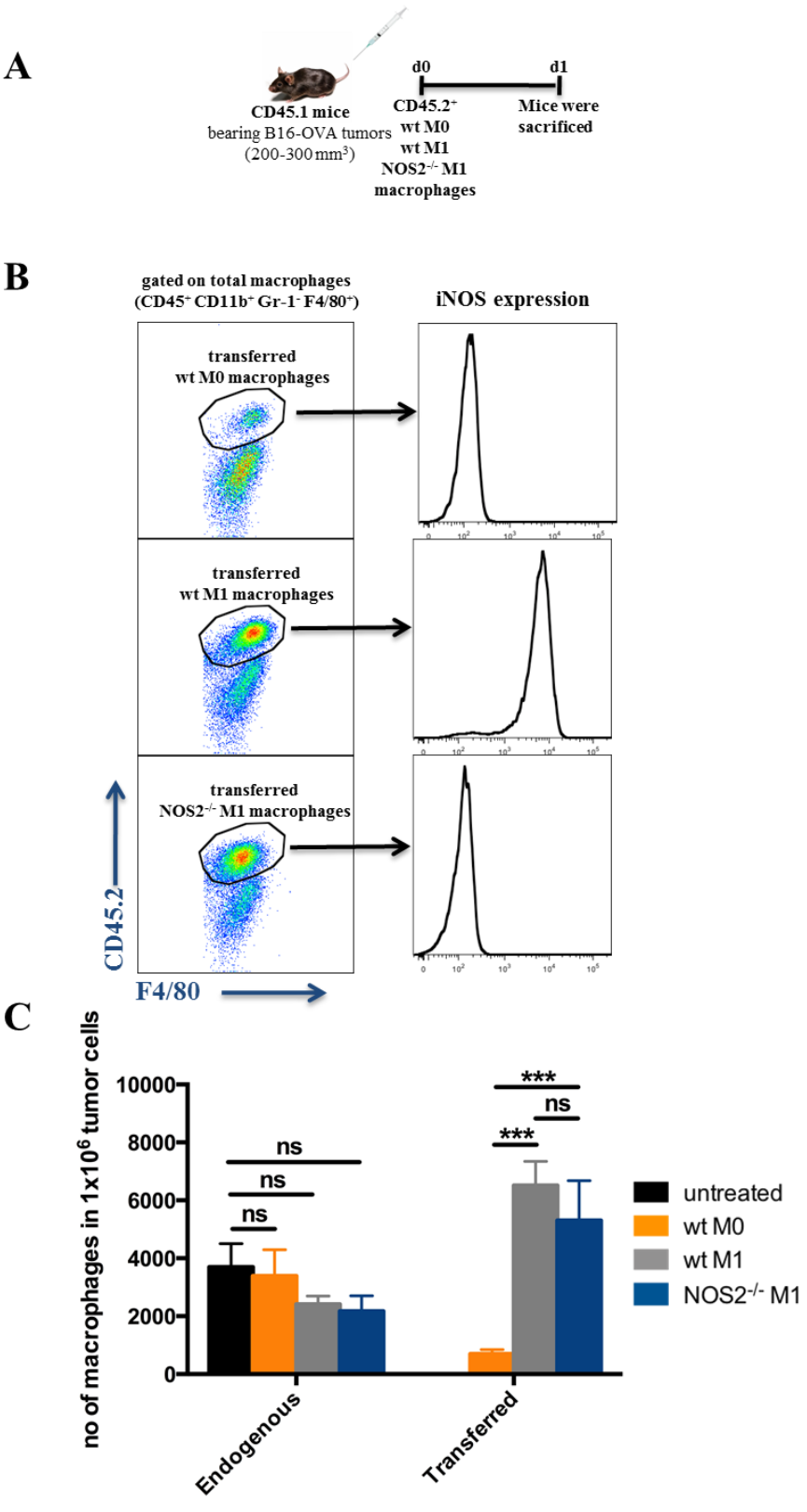

Figure 29: Transferred macrophages reached the tumor 1 day after adoptive transfer into tumor-bearing mice.

(A) CD45.2$^+$ macrophages were isolated from wild-type and *Nos2*$^{-/-}$ mice and activated with LPS and IFN-γ (M1) or left untreated (M0). B16-OVA-bearing CD45.1 mice were injected i.v. with CD45.2$^+$ macrophages as indicated. 1 day later, mice were sacrificed for analysis. **(B)** Representative flow cytometric analysis of CD45.2$^+$ transferred macrophages in tumors of CD45.1 mice. **(C)** Quantification by flow cytometry of CD45.2$^+$ transferred macrophages and CD45.1$^+$ endogenous macrophages in B16-OVA tumors. Results are shown as mean±SEM of 10 mice per group. Shown is all data from 2 independent experiments. *=p<0.05, *=p<0.01, *=p<0.001, ns=not statistically significant.

Examination of the subpopulations of immune cells in the tumor 2 days after $CD8^+$ T cell transfer revelaed that wt M1 macrophages alone and $CD8^+$ T cell alone were able to induce leukocyte infiltration into the tumor at low levels, which was strongly increased when the transfer of wt M1 macrophages were combined with the transfer of tumor-specific $CD8^+$ T cells **(Figure 30B)**. In contrast, co-transfer with M0 macrophages failed to enhance infiltration of leukocytes **(Figure 30B)**, demonstrating that macrophages must be polarized to M1-like macrophages in order to support leukocyte infiltration. Interestingly, co-transfer of *Nos2*$^{-/-}$ M1 macrophages with OT-I $CD8^+$ T cells resulted only in low level of leukocyte migration into the tumor **(Figure 30B)**. Analysis of respective leukocyte subpopulations showed that iNOS deficiency in the transferred macrophages led to an impaired migration of tumor-specific $CD8^+$ T and NK cells, and macrophages into the tumor **(Figure 30C, D and E)**.

Suprisingly, CD45.2+ transferred macrophages were not observed in tumors 3 days after macrophage transfer (Figure 31B), suggesting that transferred macrophages have short half-life. However, co-transfer of M1 macrophages with CD8+ T cells apparently induced polarization of CD45.1+ endogenous TAMs into M1-like phenotype, as characterized by high level of iNOS expression and low level of CD206 expression (Figure 31C and D). In contrast, M1 transfer alone, CD8+ T cell transfer alone or co-transfer with M0 macrophages had no effect on endogenous TAMs (Figure 31C and D). Co-transfer of Nos2-/- M1 macrophages with CD8+ T cells also resulted in substantially lower polarization of CD45.1+ endogenous macrophages towards M1-like macrophages (Figure 31C and D). In summary, iNOS+ macrophage co-transfer with CD8+ T cells increased the recruitment of tumor-specific CD8+ T cells into the tumor, as well as M1 skewing of endogenous macrophages.

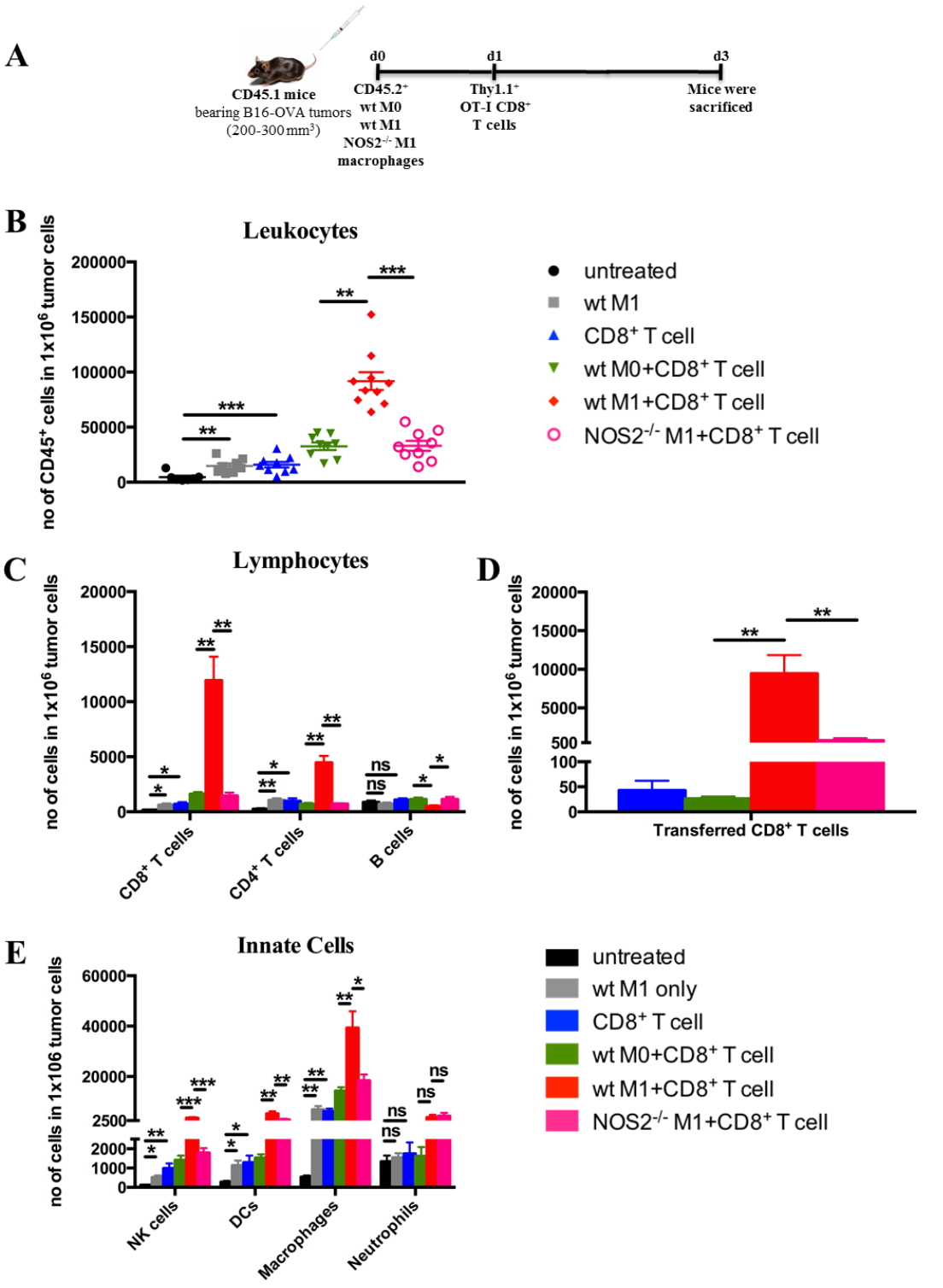

Figure 30: Co-transfer of iNOS$^+$ macrophages with tumor-specific CD8$^+$ T cells results in strong infiltration of leukocytes, notably tumor-specific CD8$^+$ T cells.
(A) CD45.2$^+$ macrophages were isolated from wild-type and *Nos2*$^{-/-}$ mice and activated with LPS and IFN-γ (M1) or left untreated (M0). B16-OVA-bearing CD45.1 mice were injected i.v. with CD45.2$^+$ macrophages 1 day before adoptive transfer of activated OT-I CD8$^+$ T cells. 2 days after CD8$^+$ T cell transfer, mice were sacrificed for analysis by flow cytometry. **(B)** Quantification of total CD45$^+$ leukocyte infiltration, **(C)** lypmhocyte infiltration**, (D)** Thy1.1$^+$ transferred OT-I CD8$^+$ T cell infiltration and **(E)** innate cell infiltration into B16-OVA tumors. Data are shown as mean±SEM of 10 mice per group. Shown is all data from 2 independent experiments. *=p<0.05, *=p<0.01, *=p<0.001, ns=not statistically significant.

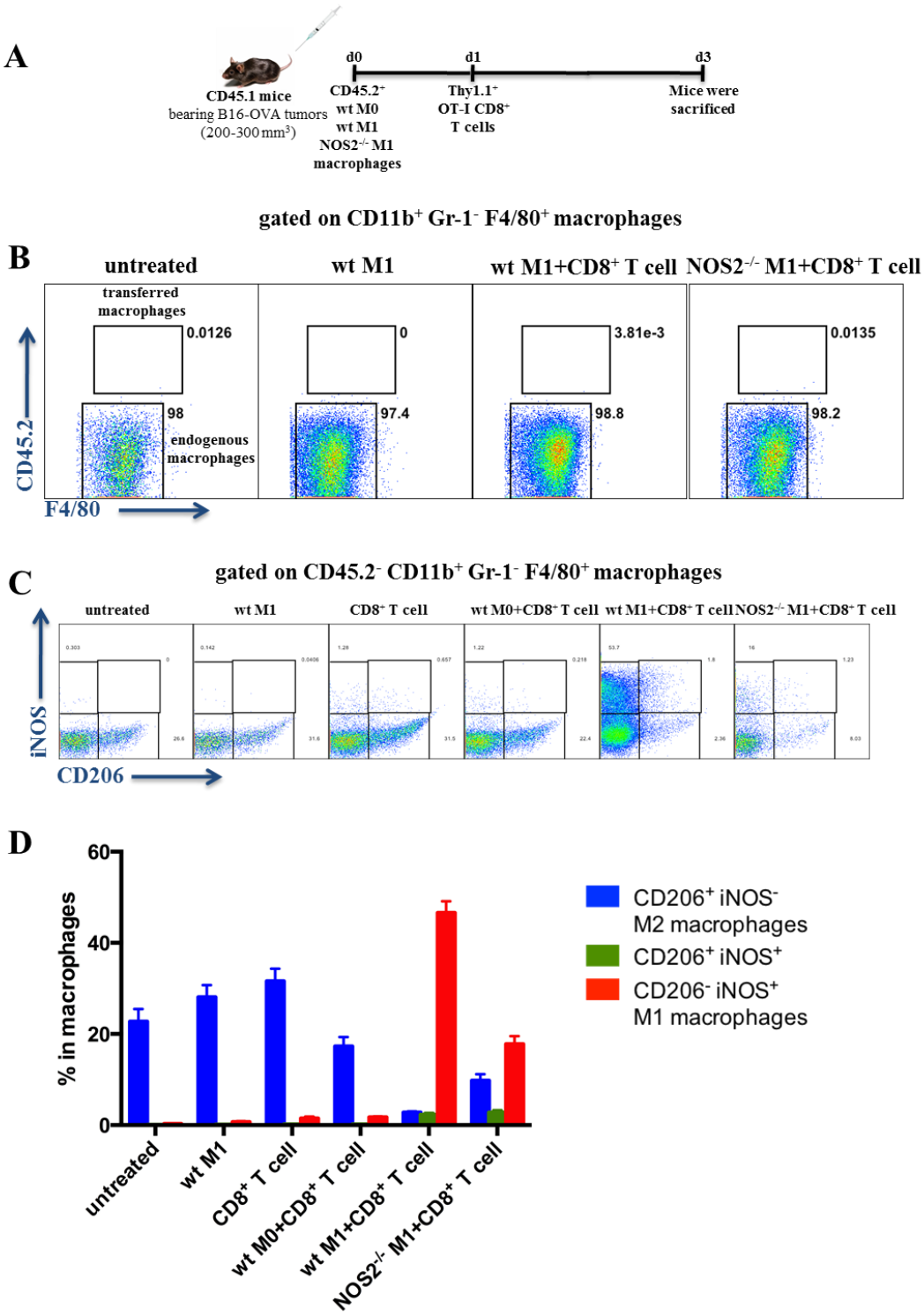

Figure 31: Co-transfer of iNOS$^+$ macrophages with tumor-specific CD8$^+$ T cells induces M1-like polarization of CD45.1$^+$ endogenous macrophages.
(A) CD45.2$^+$ macrophages were isolated from wild-type and *Nos2*$^{-/-}$ mice and activated with LPS and IFN-γ (M1) or left untreated (M0). B16-OVA-bearing CD45.1 mice were injected i.v. with CD45.2$^+$ macrophages 1 day before adoptive transfer of activated OT-I CD8$^+$ T cells. 2 days after CD8$^+$ T cell transfer, mice were sacrificed for analysis by flow cytometry.**(B)** Representative flow cytometric analysis of CD45.2$^+$ transferred macrophages in tumors of CD45.1 mice. (**C)** Representative flow cytometric analysis of iNOS (M1 marker) and CD206 (MRC1) (M2 marker) expression on CD45.2$^-$ endogenous tumor macrophages. **(D)** Summary of data presented in (B). Bars indicate the percentage of respective population in total tumor-infiltrating macrophages. Results are mean±SEM of 10 mice per group. Shown is all data from 2 independent experiments. *=p<0.05, *=p<0.01, *=p<0.001, ns=not statistically significant.

Next, tumors from mice treated with wt M1 macrophages or *Nos2*$^{-/-}$ M1 macrophages were examined by RT-PCR for the expression of the genes that take part in inflammation and angiogenesis. Co-transfer of CD8^{+} T cells with M1 macrophages was found to induce strong activation of the genes encoding Th1 response-related cytokines, IFN-α, IFN-β, IFN-γ, TNF-α, IL-12, IL-1, IL-2 and IL-6, Th2 response-related cytokines, IL-10, IL-4 and IL-13, chemokines, CCL2, CCL5, CXCL9 and CXCL10, adhesion molecules, VCAM-1 and intercellular adhesion molecule (ICAM)-1, and cytotoxic molecule Granzyme B **(Figure 32B)**. Interestingly, upregulation of these genes was significantly weaker when transferred macrophages lack iNOS activity **(Figure 32B)**. Furthermore, the intratumoral expression of angiogenic factors, such as *Vegf-α, Angpt2, regulator of G-protein signaling 5 (Rgs5), Fgf1, platelet-derived growth factor (Pdgf)-α* was substantially downregulated after the co-transfer of M1 macrophages with OT-I CD8^{+} T cells **(Figure 32B)**. In contrast, tumors, which were treated with combination of *Nos2*$^{-/-}$ macrophages and OT-I CD8 T cells, showed higher expression of these angiogenic genes **(Figure 32B)**. In summary, iNOS^{+} macrophages seem to control inflammation and angiogenesis in the tumor.

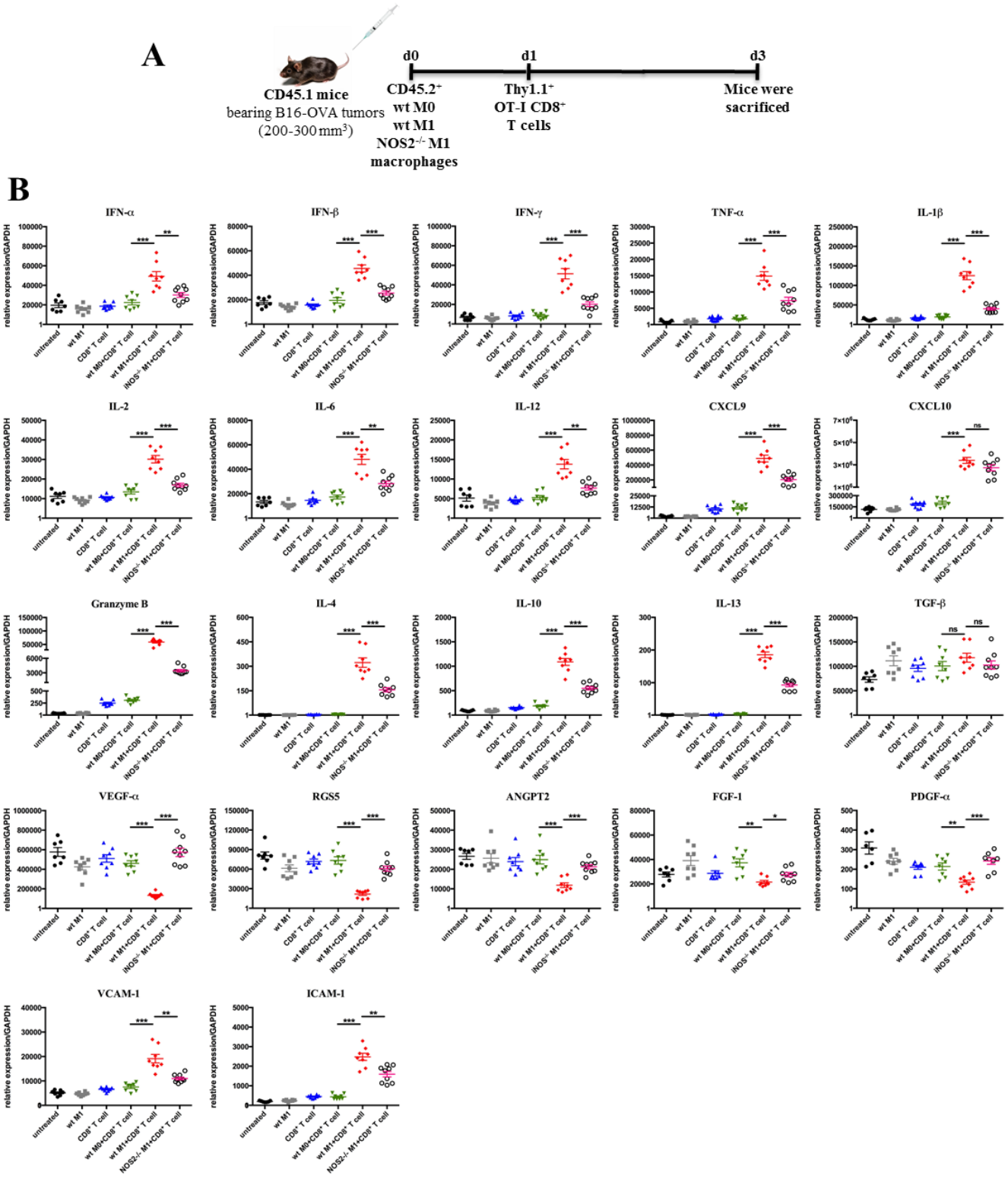

Figure 32: Changes in the B16-OVA tumor microenvironment after transfer of macrophages and OT-I CD8$^+$ T cells.

(A) CD45.2$^+$ macrophages were isolated from wild-type and *Nos2*$^{-/-}$ mice and activated with LPS and IFN-γ (M1) or left untreated (M0). B16-OVA-bearing CD45.1 mice were injected i.v. with CD45.2$^+$ macrophages 1 day before adoptive transfer of activated OT-I CD8$^+$ T cells. 2 days after CD8$^+$ T cell transfer, mice were sacrificed for analysis. **(B)** qRT-PCR analysis of cytokines, chemokines, proangiogenic factors, adhesion molcules in tumors of the indicated mice. Data are shown as mean±SEM of 10 mice per group. Shown is all data from 2 independent experiments. *=p<0.05, *=p<0.01, *=p<0.001, ns=not statistically significant.

3.2.6 Adoptive transfer of iNOS^{+} macrophages results in normalization of tumor vessels

The effect of macrophages on the tumor vasculature was analyzed one day after the macrophage transfer, when the transferred macrophages infiltrated the tumor. As shown before, untreated tumors are characterized by few but dilated vessels and low levels of VCAM-1 expression on CD31^{+} endothelial cells (ECs) **(Figure 33B and C)**. The transfer of wt M1 macrophages alone resulted in formation of smaller vessels and higher expression of VCAM-1 on ECs whereas wt M0 and *Nos2*$^{-/-}$ M1 macrophages had no effect on tumor vasculature at all **(Figure 33B and C)**. These findings demonstrate that activated macrophages can activate and normalize the tumor endothelium in an iNOS-dependent way.

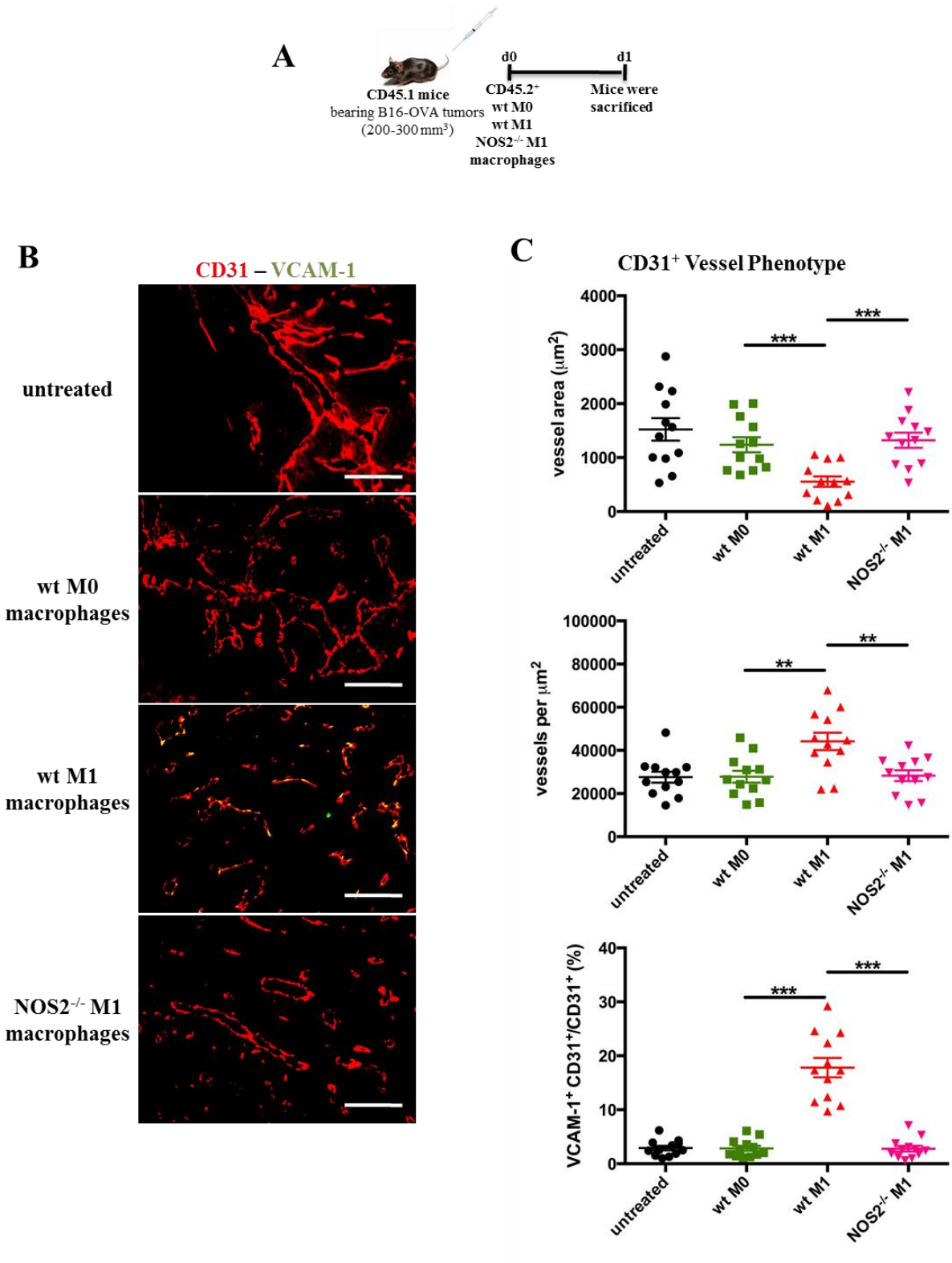

Figure 33: Adoptive transfer of iNOS$^+$ macrophages leads to normalization of the tumor vasculature.

(A) CD45.2$^+$ macrophages were isolated from wild-type and *Nos2*$^{-/-}$ mice and activated with LPS and IFN-γ (M1) or left untreated (M0). B16-OVA-bearing CD45.1 mice were injected i.v. with CD45.2$^+$ macrophages. 1 day later, mice were sacrificed for analysis. **(C)** Representative immunofluorescence microscopy analysis of tumor vessels of the indicated mice stained with antibodies against CD31 (red) and VCAM-1 (green). Yellow color shows colocalization. Size bar indicates 100 µm. **(D)** Quantification of individual CD31$^+$ tumor vessel size, number of CD31$^+$ tumor vessels and VCAM-1 expression on CD31$^+$ tumor vessels. Tumors of comparable size were investigated. 2 random fields were analyzed from each tumor. Results are mean±SEM of 6 mice per group. Shown is 1 representative experiment. *=p<0.05, *=p<0.01, *=p<0.001, ns=not statistically significant.

3.2.7 Macrophage-derived NO stimulates adhesion molecule expression on human umbilical vein endothelial cells (HUVECs)

The observed augmentation in VCAM-1 expression on tumor endothelial cells (ECs) only after the transfer of iNOS-expressing macrophages raised the possibility that macrophage-derived nitric oxide (NO) would directly act on ECs to stimulate the expression of the adhesion molecules. The effect of NO produced by macrophages on the expression of adhesion molecules on ECs was examined in preliminary experiments, in which HUVECs were co-cultured with human THP-1 macrophages, obtained after differentiation of THP-1 monocyte-like cell line by phorbol myristate acetate (PMA) treatment, in the presence or absence of iNOS inhibitor, L-NIL. Non-stimulated HUVECs displayed low expression of VCAM-1 **(Figure 34B and C)**. Co-culture with M1-polarized (by LPS and IFN-γ) THP-1 macrophages resulted in enhanced expression of VCAM-1 on HUVECs, whereas M0 macrophages failed to do so **(Figure 34B and C)**. Interestingly, iNOS blockade by L-NIL hampered the M1 macrophage-mediated increase in the expression of VCAM-1 **(Figure 34B and C)**.

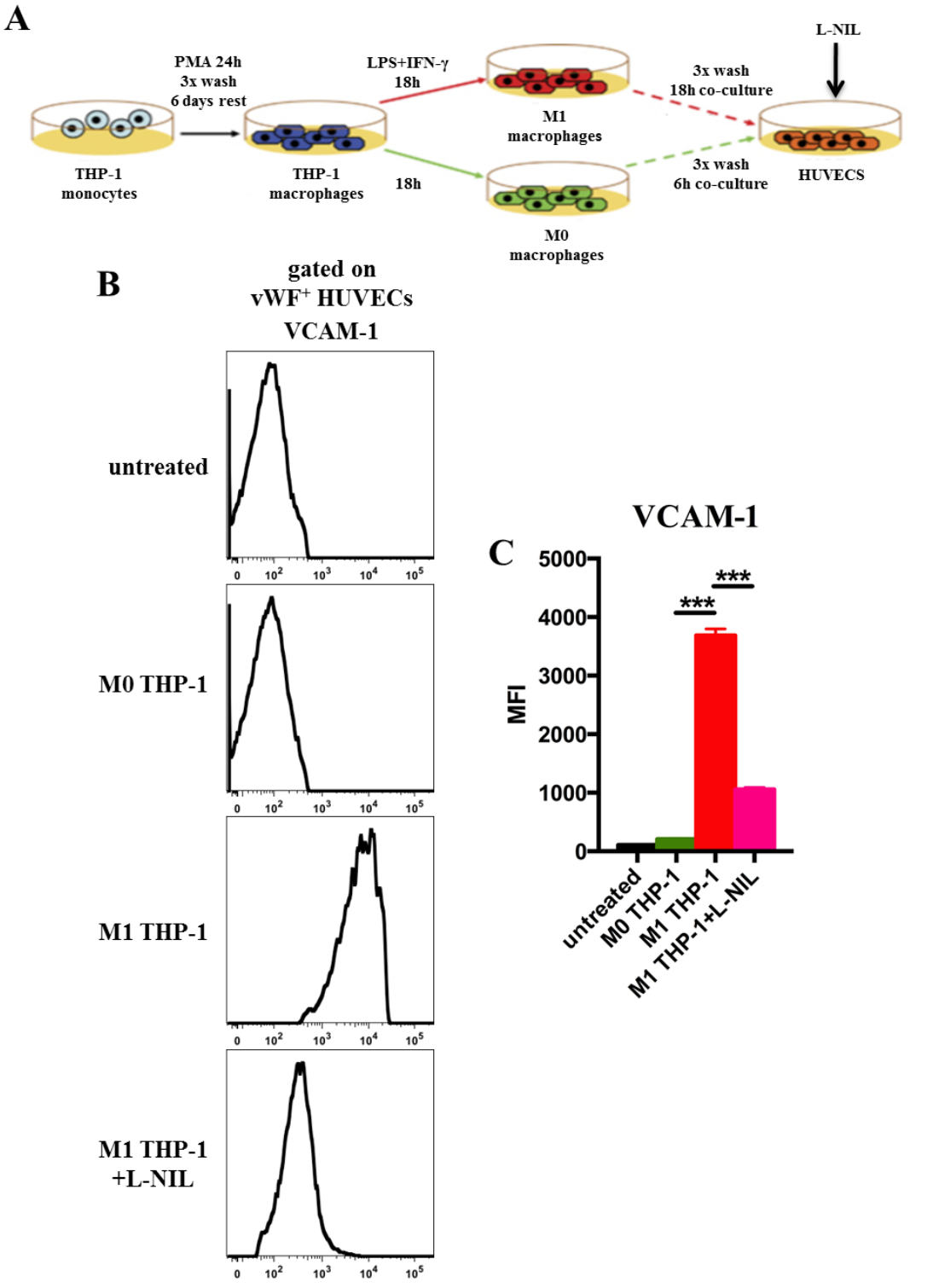

Figure 34: Co-culture with M1-polarized THP-1 human macrophages results in induction of VCAM-1 on human umbilical vein endothelial cells (HUVECs).
(A) THP-1 human monocytes were differentiated into THP-1 macrophages by phorbol 12-myristate 13-acetate (PMA) treatment for 24 hours. After 6 days in culture, THP-1 macrophages were activated by LPS and IFN-γ for 18 hours (M1) or left untreated (M0). THP-1 macrophages were washed 3 times and co-cultured with HUVECs in the presence or absence of N6-(1-iminoethyl)-L-lysine (L-NIL) for 18 hours. **(B)** Representative flow cytometric analysis of VCAM-1 expression on vWF^+ (von Willebrand Factor) HUVECs. **(C)** Quantification by flow cytometry of VCAM-1 expression on HUVECs as mean fluorescent intensity (MFI). Results are shown as mean±SEM of 6 samples per group. Shown is all data from 2 independent experiments. *=p<0.05, *=p<0.01, *=p<0.001, ns=not statistically significant.

In a more comprehensive study, HUVECs were co-cultured with human primary macrophages derived from blood monocytes. HUVECs co-cultured with M1 macrophages exhibited enhanced expression of adhesion molecules such as VCAM-1, ICAM-1 and E-Selectin whereas iNOS bloackade by L-NIL partially inhibited expression of these adhesion molecules **(Figure 35B and C)**. The incomplete inhibition obtained after L-NIL treatment suggests that additional factors are involved in the regulation of VCAM-1, ICAM-1 and E-Selectin expression on HUVECs. Together these data suggest that macrophages can directly regulate the expression of adhesion molecules on Ecs, probably through NO production.

In order to test if NO was directly able to induce adhesion molecules in endothelial cells, HUVECs were cultured in the presence of the NO donor glyceryl trinitrate (GTN). Low levels of NO (10.7 nM and 16.5 nM) were found to induce VCAM-1, ICAM-1 and E-selectin expression on HUVECs whereas higher level of NO (22.1 nM and 29.3 nM) failed to induce adhesion molecules **(Figure 36B)**. When HUVECs were stimulated by TNF, which is known to be potent inducer of adhesion molecule expression on HUVECs, the addition of NO at low concentrations enhanced VCAM-1, ICAM-1 and E-selectin expression **(Figure 36B)**. In contrast, NO at high higher concentrations suppressed the TNF-dependent expression of adhesion molecules **(Figure 36B)**. These findings show that NO at low levels is able to stimulate VCAM-1, ICAM-1 and E-selectin on HUVECs, explaining the observation that $iNOS^+$ macrophages, but not $iNOS^-$ macrophages, promotes VCAM-1 expression on the tumor endothelium.

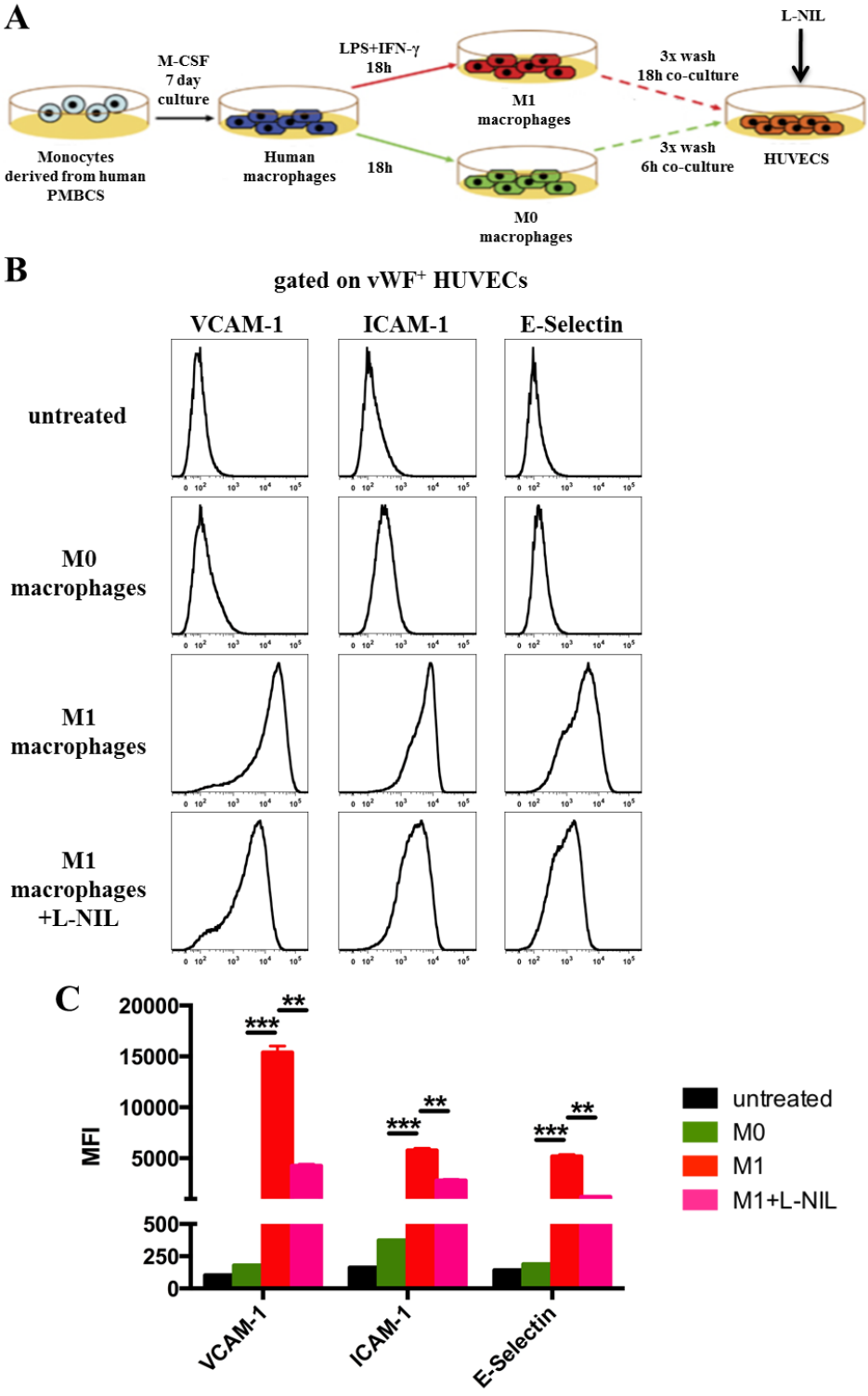

Figure 35: Co-culture with M1-polarized human primary macrophages leads to induction of VCAM-1, ICAM-1 and E-Selectin on human umbilical vein endothelial cells (HUVECs).
(A) Human macrophages were differentiated from blood monocytes in the presence of M-CSF. After 7 days in culture, fully differentiated macrophages were activated by LPS and IFN-γ for 18 hours (M1) or left untreated (M0). Macrophages were washed 3 times and co-cultured with HUVECs in the presence or absence of N6-(1-iminoethyl)-L-lysine (L-NIL) for 18 hours. **(B)** Representative flow cytometric analysis of VCAM-1, ICAM-1 and E-Selectin expression on vWF$^+$ HUVECs. **(C)** Quantification by flow cytometry of VCAM-1, ICAM-1 and E-Selectin expression on HUVECs as mean fluorescent intensity (MFI). Results are shown as mean±SEM of 6 samples per group. Shown is all data from 2 independent experiments. *=p<0.05, *=p<0.01, *=p<0.001, ns=not statistically significant.

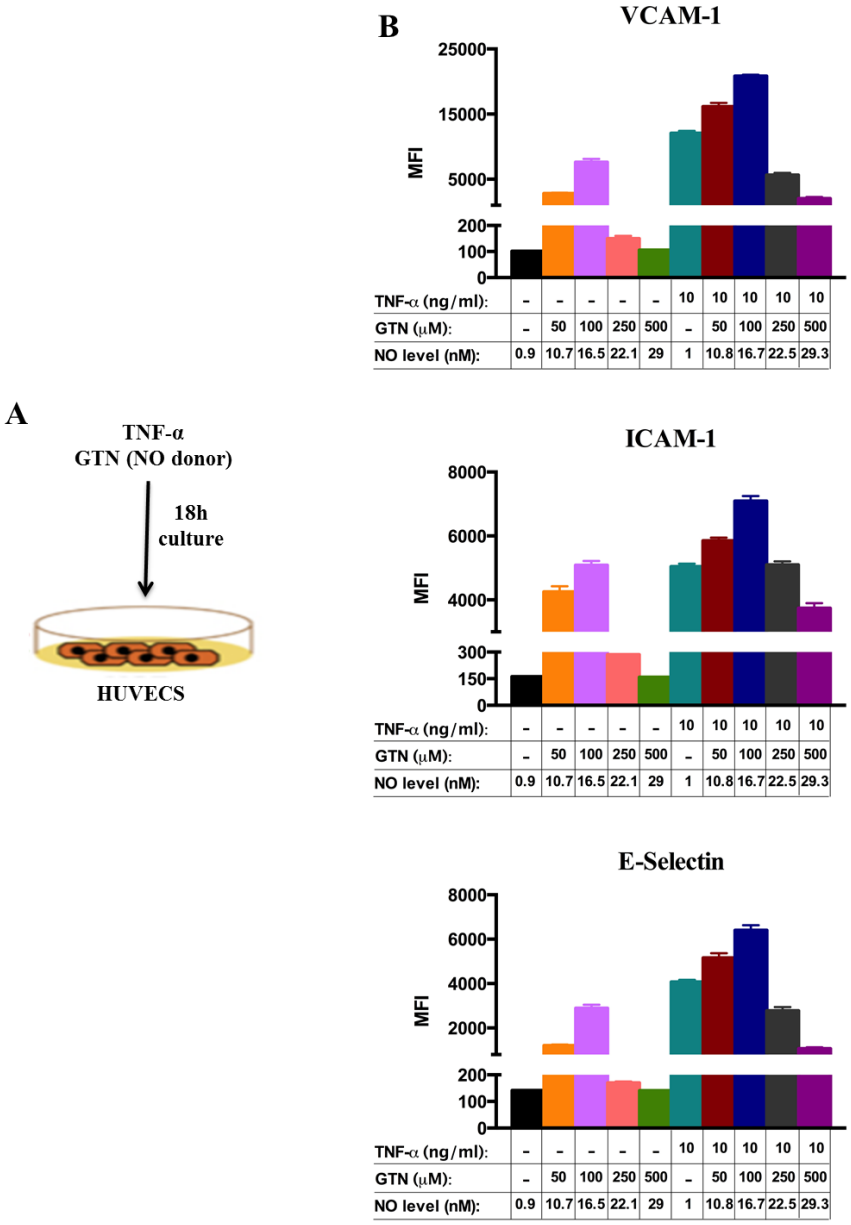

Figure 36: Treatment with low levels of NO donor glyceryl trinitrate (GTN) results in induction of VCAM-1, ICAM-1 and E-Selectin on human umbilical vein endothelial cells (HUVECs).
(A) HUVECs were cultured with indicated doses of NO donor glyceryl trinitrate (GTN) and TNF for 18 hours. **(B)** Quantification by flow cytometry of VCAM-1, ICAM-1 and E-Selectin expression on HUVECs as mean fluorescent intensity (MFI). Nitric oxide (NO) concentrations measured in the medium are shown. Results are shown as mean±SEM of 6 samples per group. Shown is all data from 2 independent experiments. *=p<0.05, *=p<0.01, *=p<0.001, ns=not statistically significant.

The transcriptional profile of HUVECs treated with low level of NO donor (GTN, 100 μM) was compared to HUVECs treated with TNF (10 ng/ml), which is known to be a potent inducer of adhesion molecule expression on endothelial cells, by microarray analysis using the HumanHT-12 expression beadchip. Analysis of more

than 47000 genes demonstrated that 572 genes were differentially expressed between NO-treated HUVECs and untreated HUVECs and 589 genes were differentially expressed between TNF-treated HUVECs and untreated HUVECs **(Figure 37)**. NO- and TNF-treated HUVECs displayed similar gene expression profiles, in which similar genes are upregulated or downregulated after both NO and TNF treatment compared to untreated samples. Many of the upregulated genes after both NO and TNF treatment were those that encode adhesion molecules, E-Selectin (*SELE*) and VCAM-1 (*VCAM1*), and chemokines, such as CX3CL1, CCL20 , CXCL10, CXCL5, CXCL2 and IL-8 (CXCL8) **(Table 13)**. Computer program analysis of microarray data showed that both NO and TNF activate an array of pathways that involve in granulocyte and agranulocyte extravasation and migration **(Table 14)**, probably by acting on NF-κB transcritption factor **(Table 15)**.

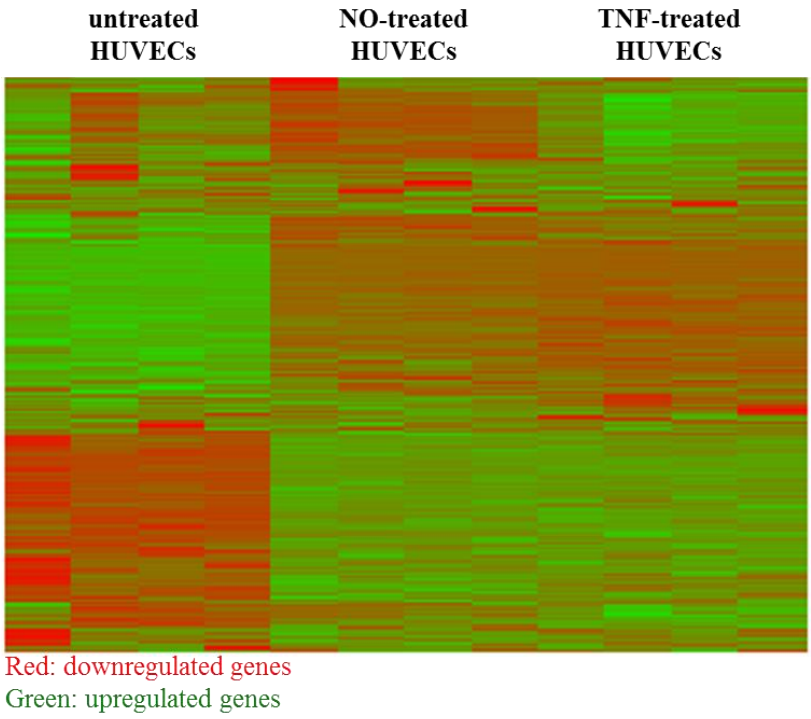

Figure 37: Microarray analysis of HUVECs treated with NO donor glyceryl trinitrate (GTN) and TNF.
Total RNA was isolated from untreated HUVECs or from HUVECs treated with NO donor (GTN) or TNF, and hybridized to Human HT-12 v4 expression beadchip. Normalized gene expression intensities were compared, and genes were considered to be differentially expressed between different groups if their fold change was greater than 2 or less than -2. Columns correspond to the experimental conditions (untreated, NO-treated and TNF-treated). 572 genes were differentially expressed between untreated and NO-treated HUVECs. 589 genes were differentially expressed between untreated and TNF-treated HUVECs. 221 genes were differentially expressed between NO-treated and TNF-treated HUVECs.

Table 13: Top upregulated molecules in HUVECs after NO and TNF treatment

NO-treated vs untreated

Top Molecules Fold change upregulated	
Molecules	Exp. Value
SELE	72.38
UBD	49.68
VCAM1	48.1
LTB	44.55
CX3CL1	30.57
CCL20	25.56
DARC	23.53
MMP10	22.4
SLC7A2	19.95
CXCL10	19.42
MX1	19.02
CXCL5	17.84
LAMC2	16.98
EBI3	16.59
SOD2	14.85
CXCL2	14.7
IL-8	14.49

TNF-treated vs untreated

Top Molecules Fold change upregulated	
Molecules	Exp. Value
SELE	102.32
VCAM1	64.14
UBD	49.33
LTB	42.26
CX3CL1	41.59
CCL20	34.34
SLC7A2	27.7
DARC	26.98
MMP10	26.615
CXCL10	25.953
MX1	25.26
CXCL5	22.59
CXCL6	21.82
CXCL2	20.89
SOD2	18.96
EBI3	18.45
IL-8	17.97

Table 14: Top activated pathways in HUVECs after NO and TNF treatment

NO-treated vs untreated

Top Canonical Pathways	
Name	p-value
Agranulocyte adhesion and diapedesis	2.04E-12
Granulocyte adhesion and diapedesis	3.50E-12
Activation of IRF by ctosolic pattern recognition receptors	6.05E-10
Interferon signaling	9.37E-10

TNF-treated vs untreated

Top Canonical Pathways	
Name	p- Value
Interferon signaling	6.18E-14
Granulocyte adhesion and diapedesis	2.01E-13
Agranulocyte adhesion and diapedesis	6.45E-12
Activation of IRF by ctosolic pattern recognition receptors	7.27E-12

Table 15: Top regulator effect networks in HUVECs after NO and TNF treatment

NO-treated vs untreated

Top Regulator Effect Networks		
ID regulators	Diseases&Functions	Consistency Score
NF-κB (complex)	Chemotaxis of myeloid cells	4.472
APP	Cell movement of neutrophils	4.359
APP	Cell movement of granulocytes	4.359
U0126	Inflammatory response	4.234
APP	Cell movement of myeloid cells	4.17

TNF-treated vs untreated

Top Regulator Effect Networks		
ID regulators	Diseases&Functions	Consistency Score
NF-κB (complex)	Chemotaxis of myeloid cells	4.364
APP	Cell movement of neutrophils	4.359
APP	Cell movement of granulocytes	4.359
APP	Cell movement of myeloid cells	4.287
TNF	Migration of tumor cells	4.264

4 DISCUSSION

4.1 Treg Depletion as a Model to Study Immune Rejection of Tumors

Regulatory T cells (Tregs) are abundantly present in a wide array of human tumors and a high density of Tregs is often associated with a poor clinical outcome. Tregs have been shown to potently block anti-tumor immune responses, mainly by impairing the efficacy of priming of tumor-specific T cells. Therefore, selective depletion of these cells is an emerging therapeutic strategy for cancer, with the aim of generating strong anti-tumor immune responses. In this study, the effect of Tregs in anti-tumor immunity was intensively analyzed using mouse models of Treg depletion.

4.1.1 Different levels of Treg depletion determine efficacy of tumor rejection

The main focus of this part of the study was to investigate whether the extent of Treg ablation would be important for the generation of immune responses against tumors. In this study, two mouse models were employed to selectively deplete Tregs upon diphtheria toxin (DT) administration. Foxp3^{DTR} mice were generated by targeted insertion of the construct encoding human diphtheria toxin receptor (DTR) and enhanced green fluorescent protein (eGFP) at *foxp3* locus[219]. This knock-in strategy allows depletion of almost all Foxp3^{+} Tregs because almost all Treg express the human DTR on their surface[219]. In previous studies, it was reported that persistent application of DT (every week) in these mice led to catastrophic autoimmune disease[219]. In contrast, limited DT application did not result in overt autoimmune responses, as performed in the present study probably due to an IL-2-dependent rapid proliferation of the remaining Tregs. Foxp.LuciDTR4 mice were generated by introduction of the transgene expressing human DTR, eGFP and luciferase into the mouse genome using bacterial artifical chromosome (BAC) technology[220]. BACs are large genomic DNA fragments theoretically containing all potential regulatory

elements of a gene[285], allowing tissue specific expression of the transgene. However, in BAC transgenic animals, the copy number and sites of genomic integration of the transgene are usually unknown[285]. In addition, the local chromatin structure may affect the transgene expression in BAC transgenic mice[285]. Thus, BAC transgenic mice may exhibit different degrees of transgene expression depending on the integration site of BAC construct. In Foxp3.LuciDTR4 mice, about 90% of Foxp3^{+} Tregs are ablated after DT application[220], indicating that about 90% of Tregs express DTR on their surface. In another BAC transgenic mouse line, Foxp3.LuciDTR3 mice, the level of depletion was about 70% after DT administration[220]. Importantly, both strains of Foxp3.LuciDTR4 BAC transgenic mice do not show any sign of autoimmunity[220] probably because remaining Tregs are sufficient to suppress autoimmune responses.

In a previous study, our group has shown that ~70% Treg depletion in Foxp3.LuciDTR3 mice, or ~70% Treg depletion obtained with anti-CD25 antibody (PC-61) in wild-type mice, had no effect on the growth of ovalbumin-expressing B16 melanoma (B16-OVA) and simian virus 40 large T antigen-expressing RMA lymphoma (RMA-Tag)[222]. In contrast, ~90% depletion resulted in complete rejection of these tumors[222]. In the present study, HCmel 1274 and B16 melanoma cell lines were utilized to analyze the effect of different degrees of Treg depletion on the growth of tumors displaying lower immunogenicity. Similar to B16-OVA and RMA-Tag, ~70% Treg depletion with PC-61 antibody in mice bearing HCmel 1274 or B16 melanoma failed to control tumor growth. Suprisingly, ~90% depletion in Foxp3.LuciDTR4 mice resulted in only partial regression of HCmel 1274 tumors and had little effect on the growth of B16 tumors. However, when the level of Treg depletion was raised to ~99% using Foxp3^{DTR} mice, complete rejection of HCmel1274 and B16 tumors was observed.

B16-OVA and RMA-Tag tumors present epitopes derived from OVA or Tag. These epitopes can be recognized as non-self antigens and induce robust T cell responses in the host. The ~10% Tregs, which are not depleted in Foxp3.LuciDTR4 mice, apparently fail to control such strong T cell responses, explaining the complete rejection of tumors expressing OVA or Tag. On the other hand, HCmel 1274 and B16 tumors produce self-proteins that may induce tolerance, thus expressing antigens that

can be recognized as "self" by the immune system. However, it is known that some melanocyte self antigens that are overexpressed in melanomas, including Melan-A/MART-1, gp100, tyrosinase, tyrosinase-related protein-1 (TRP-1) and TRP-2 can induce low-avidity T cell responses due to the mechanisms of central and peripheral tolerance. These low-avidity T cell responses less efficiently reject tumors than high-avidity T cell responses elicited against foreign antigens. It seems that the few remaining Tregs in Foxp3.LuciDTR4 mice can suppress such T cell responses directed against self antigens, in agreement with the observation that Foxp3.LuciDTR4 mice display no sign of autoimmunity after DT application. In contrast, when almost all Tregs are removed, peripheral tolerance mechanisms against self antigens appear to collapse, resulting in efficient regression of HCmel 1274 and B16 tumors. In agreement with this, Treg-depleted Foxp3^{DTR} mice displayed vitiligo-like depigmentation in the tumor rejection area, similar to the depigmentation observed in melanoma patients receiving immunotherapy. In fact, in the clinic vitiligo is regarded as a positive parameter for an anti-tumor response.

Adoptive reconstitution of Tregs in Foxp3^{DTR} mice after Treg depletion further supported the notion that few numbers of Tregs are able to control immune responses against tumors of lower immunogenicity. In agreement with this notion, intratumoral injection of low numbers of CD4^{+} CD25^{+} splenic Tregs (2x10^{3} cells) caused inhibition of tumor rejection. However, it should be emphasized that transferred Tregs may rapidly expand in Treg-depleted mice due to IL-2 dependent homeostatic proliferation which has been observed in Treg-depleted mice[220].

4.1.2 Treg depletion induces drastic changes in the tumor microenvironment

Treg depletion-mediated regression of HCmel 1274 tumors was accompanied by a massive infiltration of leukocytes into the tumor 4 days after Treg depletion. Notably, CD8^{+} T cells were particularly enriched in both Foxp3.LuciDTR4 and Foxp3^{DTR} mice after Treg depletion but the level of CD8^{+} T cell infiltration was higher in Foxp3^{DTR} mice than in Foxp3.LuciDTR4 mice. Higher level of CD8^{+} T cell infiltration may explain why complete tumor rejection was achieved in Foxp3^{DTR}, but

not in Foxp3.LuciDTR4 mice, since tumor rejection obtained in Foxp3^{DTR} mice after Treg depletion was shown to be dependent on CD8^{+} T cells. Suprisingly, Treg-depleted tumors in Foxp3^{DTR} displayed strong infiltration of basophils, which represented 4% of total tumor-infiltrating leukocytes 4 days after Treg depletion. Tumor-infiltrating basophils were characterized as CD45^{int} FcεRI^{+} CD49b^{+} CD200R3^{+} c-Kit^{-} cells by flow cytometry. They were also shown to be IgE^{+}, indicating an activated phenotype of tumor-associated basophils since IgE is a potent stimulator for effector functions of basophils. Sorted intratumoral CD45^{+} FcεRI^{+} CD49b^{+} cells displayed high levels of Mcpt8 mRNA, which encodes basophil-specific mast cell protease 8, a granzyme B-like protease stored in the granules of basophils, now designated as Basoph8). Giemsa staining showed that the sorted cells exhibited a typical basophil morphology with a lobulated nucleus and basophilic granules.

The cytokine and chemokine profile of HCmel 1274 tumors was measured 4 days after Treg depletion in Foxp3^{DTR} mice and showed that Treg depletion resulted in a pro-inflammatory tumor microenvironment. The enhanced expression of genes encoding IFN-γ, IFN-α, IFN-β, TNF, IL-12, IL-1β in the tumor microenvironment indicated strong activation of both innate and adaptive immune cells. For instance, these cytokines are known to activate DCs and to skew macrophages towards a M1-like phenotype, which, may promote the activation and infiltration of tumor-specific T cells. Expression of genes encoding Th2 response-related cytokines, such as IL-3, IL-4, IL-5, IL-10 and IL-13 was also upregulated after Treg depletion. The elevated levels of Th2 cytokines may be explained byincreased infiltration of basophils and eosinophils into the tumor because these cells are known to be potent producers of Th2 cytokines upon activation with an appropriate stimuli.

Similar to cytokines, intratumoral levels of chemokines such as CCL2, CCL3, CCL4, CCL7, CCL11, CCL20, CXCL9 and CXCL10 were substantially augmented 4 days following Treg depletion, Of note, the expression of CCL2, CCL3, CCL4, CXCL9 and CXCL10 in tumors of melanoma patients was found to correlate with the presence of intratumoral CD8^{+} T cells[62]. Consistently, enhanced expression of these chemokines in murine models of cancer has been shown to be associated with infiltration of tumor-specific CD8^{+} T cells[281, 286, 287, 288, 289, 290, 291, 292, 293]. Thus, the

observed increase in the production of these chemokines may provide an explanation for the particular enrichment of $CD8^+$ T cells and tumor rejection after Treg depletion. Further analysis was carried out to identify the cell types producing these chemokines within the tumor microenvironment. Gene expression profiling data with cells sorted from Treg-depleted tumors revealed that CCL3 and CCL4 were mainly produced by tumor-associated basophils whereas CCL2, CXCL9 and CXCL10 were mostly produced by tumor-associated macrophages. In several in vitro studies, basophils were shown to produce CCL3 and CCL4 in response to activation by IgE[294] or by a combination of IL-3, IL-18 and IL-33[257, 258]. In the present study, I confirmed that activation of basophils with a combination of IL-3, IL-18 and IL-33 results in enhanced production of CCL3 and CCL4 but not of CCL2, CXCL9 and CXCL10. Moreover, using a two-chamber system, activated basophils were found to induce migration of activated $CD8^+$ T cells via production of CCL3 and CCL4. This finding is novel, because so far, it has not been known that basophils can induce $CD8^+$ T cell migration.

The observed production of chemokines CCL3 and CCL4 by tumor-associated basophils raised the possibility that $CD8^+$ T cells could be attracted in vivo to the tumor by these chemokines. The examination of early immune responses (2 days after Treg depletion) demonstrated that basophils were the first immune cell population that infiltrated the tumor after Treg depletion, thereby preceding infiltration by $CD8^+$ T cells. Basophil infiltration resulted in an increase in the intratumoral expression of CCL3 and CCL4 2 days following Treg depletion, explaining the enhanced infiltration of $CD8^+$ T cells on the next day.

In order to understand the mechanism underlying the selective tumor recruitment of basophils, gene expression profiling was performed for the presence of potential chemokine transcripts that are important for migration of basophils into tissues. 2 days after Treg depletion, the expression of basophil-derived chemokines CCL3 and CCL4 was found to be upregulated but not expression of other chemokines, suggesting that other mechanism may be involved in the recruitment basophils into the tumor. It has been shown that selective tissue recruitment of basophils can be mediated by a variety of cytokines that are implicated in homeostatis and activation of basophils. For example, IL-3 has been demonstrated to be a critical

factor for infiltration of basophils into lymph nodes following infection of mice with helminth[237]. Consistent with this finding, intratumoral expression of IL-3 was shown to be upregulated only in Foxp^{DTR} mice after Treg depletion, but not in Foxp3.LuciDTR4 mice. In conclusion, IL-3 seems to play a crucial role in the recruitment of basophils into the tumor ~99% after Treg depletion.

4.1.3 Basophils play an essential role in tumor rejection after Treg depletion in Foxp3^{DTR} mice

MAR-1, a monoclonal antibody specific to FcεRIα, was employed to study the role of basophils in Treg depletion-mediated tumor rejection. MAR-1 could be used because there was very little intratumoral infiltration of mast cells and FcεRI^{+} DCs after Treg depletion.

The rejection of HCmel 1274 and B16 tumors following Treg depletion was drastically hampered in the absence of basophils, resulting in severely reduced survival of tumor-bearing mice. Analysis of the immune cell composition in Treg-depleted HCmel 1274 and B16 tumors showed that the intratumoral infiltration of tumor-rejector CD8^{+} T cells was markedly decreased after basophil ablation, explaining the impaired tumor regression after basophil depletion. Interestingly, in addition to reduction in CCL3 and CCL4 expression, basophil depletion resulted in the diminished expression of CCL2, CXCL9 and CXCL10. The curbed expression of CCL3 and CCL4 is the most likely mechanism underlying reduced migration of CD8^{+} T cells after basophil ablation.

4.1.4 Basophils act on tumor-associated macrophages via induction of CD8^{+} T cell infiltration into the tumor

Among myeloid cells, macrophages are the most prominent cell population in the tumor. Tumor-associated macrophages often exhibit an M2-like phenotype, which is characterized by low expression of the chemokines that are important for T cell infiltration into the tumor. Consistently, macrophages sorted from untreated HCmel 1274 tumors displayed low levels of CCL2, CXCL9 and CXCL10 mRNA.

Macrophages are amenable to changes in the tumor microenvironment and exhibit functional plasticity depending on the nature of environmental cues. After Treg depletion, macrophages underwent a change in their phenotype and produced increased amounts of CCL2, CXCL9 and CXCL10, thereby enhancing $CD8^+$ T cell infiltration into the tumor. However, basophil depletion impaired the increase in the expression of these chemokines obtained by Treg depletion. Interestingly, these chemokines are IFN-γ-inducible chemokines[295]. IFN-γ is known to be one of the key effector molecules for tumor-specific $CD8^+$ T cells[185]. Indeed, both $CD8^+$ T cell depletion and IFN-γ blockade resulted in decreased expression of CCL2, CXCL9 and CXCL10 in Treg-depleted tumors, suggesting that reduced number of intratumoral $CD8^+$ T cells and reduced intratumoral expression of IFN-γ are responsible for the reduced intratumoral expression of these chemokines after basophil depletion. These observations indicate a feedback mechanism in which basophils first induce $CD8^+$ T cell migration into the tumor via production of CCL3 and CCL4, These tumor-infiltrating IFN-γ^+ $CD8^+$ T cells caused polarization of macrophages towards M1-like macrophages that secrete CCL2, CXCL9 and CXCL10. These chemokines further enhance $CD8^+$ T cell infiltrationand macrophage polarization. This feedback loop is further supported by the kinetic studies showing that the expression of CCL3 and CCL4, and the infiltration by basophils, preceded the expression of CCL2, CXCL9 and CXCL10 and the infiltration by $CD8^+$ T cells.

The observed expression of the $CD8^+$ T cell-chemoattractants CCL2, CXCL9 and CXCL10 by tumor-associated macrophages indicate an essential role of macrophages in Treg depletion-mediated tumor rejection. This hypothesis was supported by the finding that depletion of macrophages with CLIP impeded the basophil-dependent rejection of HCmel 1274 tumors. Specifically, macrophage depletion resulted in decreased expression levels of the chemokines within the tumor microenvironment, such as CCL2, CXCL9 and CXCL10, and impaired the infiltration of $CD8^+$ T cell infiltration into the tumor, demonstrating that macrophages serve as critical accessory cells for the attraction of tumor-specific $CD8^+$ T cells. The blockade of IFN-γ yielded comparable results, indicating that IFN-γ production within the tumor microenvironment is crucial for anti-tumoral functions of macrophages.

In a recent study, we have reported that eosinophils were essential for the rejection of ovalbumin-expressing B16 tumors after Treg depletion in Foxp3.LuciDTR4 mice[283]. Therefore, the role of eosinophils was also investigated in the rejection of HCmel 1274 tumors after Treg depletion in Foxp3^{DTR} mice. However, depletion of eosinophils with anti-Siglec-F antibody had no influence in the rejection of HCmel 1274 tumors. These results show that eosinophils do not play a vital role in the tumor rejection in Foxp3^{DTR} mice. Comparitive studies revealed that the level of infiltration by eosinophils was 20-fold higher in B16-OVA tumors in Foxp3.LuciDTR4 mice as compared to eosinophil infiltration in HCmel 1274 tumors after 99% Treg depletion in Foxp3^{DTR} mice. Moreover, infiltration of CD8^{+} T cells into B16-OVA tumors occured 6 days after Treg depletion and 2 days after eosinophil infiltration[283]. In contrast, in Foxp3^{DTR} mice infiltration of CD8^{+} T cells and eosinophils into HCmel 1274 tumors occurred simultaneously on day 4 after Treg depletion, suggesting that eosinophils do not play an important role in CD8^{+} T cell migration into HCmel 1274 tumors.

4.1.5 IL-3/antibody complex-induced basophilia improves the efficacy of adoptive T cell therapy in melanoma-bearing mice

In the clinic, adoptive T cell therapy has emerged as a promising immunotherapy but its success is limited[185]. Therefore, I investigated whether or not experimentally induced tumor-associated basophilia would improve the efficacy of T cell therapy. For this purpose, I attempted to expand the number of basophils in the tumor. One approach was to adoptively transfer activated bone marrow-derived basophils into tumor-bearing mice. However, since in vitro generation of basophils from bone marrow is laborious and yields only small number of mature basophils, another method was chosen, namely injection of IL-3, which is a important differentiation and homeostatic factor for basophils. In a previous study, injection of IL-3 complexed with anti-IL-3 antibody into mice was shown to selectively increase the number of basophils[232]. The IL-3/antibody complex is more efficient than IL-3 alone because the antibody will protect IL-3 from rapid degradation. B16-OVA was used as tumor model because OT-I TCR transgenic mice were available in the laboratory. These mice contain ovalbumin specific CD8^{+} T cells that can be used for

T cell transfer studies. 3 days after the injection of IL-3/antibody complex , basophilia, but not eosinophilia or mastocytosis, was observed in the tumor, lung, spleen and blood of B16-OVA-bearing mice. Basophilia in the tumor resulted in enhanced production of CCL3 and CCL4, which induced recruitment of leukocytes into B16-OVA tumors, notably the transferred tumor-specific OT-I $CD8^+$ T cells. This combination therapy resulted in tumor rejection and prolonged survival of tumor-bearing mice. Macrophages sorted from the mice treated with a combination of IL-3/antibody complex and tumor-specific $CD8^+$ T cells displayed an M1-like phenotype with higher expression of M1 markers such as CCL2, CXCL9, CXCL10, TNF-α and iNOS, and lower expression of M2 markers such as MRC1 and ArginaseI. In addition, the basophil combination therapy induced normalization of the tumor vasculature and increased expression of adhesion molecules such as VCAM-1 on tumor endothelium. The observed normalization of the vasculature and increase in the expression of chemokines such as CCL2, CXCL9 and CXCL10 by macrophages apparently further augment the infiltration of tumor-specific $CD8^+$ T cells into the tumor.

Together these studies show that, under particular conditions, basophils play a critical role in T cell mediated-tumo rejection. Basophils are usually associated with poor clinical outcome in cancer patients, however, our results indicate that the mere presence of basophils should not be used a prognostic factor for cancer patients without detemination of the precise activation status of basophils, as well as the status of T cell infiltration.

4.2 Rip1-Tag5 (RT5) Model as a Model to Study Immune Rejection of Tumors

Inefficient T cell trafficking to the tumor represents a critical problem for efficient cancer immunotherapy. A major barrier for T cell migration into the tumor is the establishment of an aberrant vasculature by tumors that is characterized by dilated and tortous vessels and by low-level expression of adhesion molecules which are required for T cell extravasation. The effect of an aberrant tumor vasculature on T cell infiltration was extensively studied in our laboratory using the RT5 mouse model

of spontaneous pancreatic islet tumors. Adoptive T cell therapy with tumor-specific $CD8^+$ and $CD4^+$ T cells has limited effects on tumor progression in RT5 mice since these cells fail to penetrate into the tumor due to the presence of aberrant tumor vessels. In previous studies, our group has shown that induction of vasculature normalization with danger signals such as irradiation[275, 276] and TLR ligands[274] resulted in efficient infiltration of tumor-reactive T cells into the tumor.

4.2.1 CpG-ODN improves the efficacy of adoptive T cell therapy in RT5 mice

Animal studies and clinical trials have demonstrated that CpG-ODN can have potent immunostimulatory effects on the immune cells and enhance the efficacy of a variety of immunotherapies[296]. CpG-ODN can activate innate immune cells, including DCs, NK cells and macrophages cells through binding to TLR9[297], resulting in secretion of pro-inflammatory cytokines that promote T cell responses[298, 299]. Especially, the prominent effect of CpG-ODN on DCs indicates that it might be an useful adjuvant for vaccination strategies against cancer. Several studies have reported that anti-tumor vaccination with CpG-ODN was able to induce immune responses but was only effective in prophylactic setting[300, 301, 302, 303]. In contrast, Intra- and peritumoral injection of CpG-ODN was found by us and other groups to lead to rejection of established tumors[304, 305, 306]. This rejection was dependent on the activation of cytotoxic T cells and NK cells[305]. However, these studies have not investigated whether CpG acts as an adjuvant that enhance the priming and activation of T cells, or as a danger signal that directly induces changes within the tumor microenvironment. In a recent study, our group has shown that systemic CpG-ODN application can indeed function as a potent danger signal that renders RT5 tumors permissive for tumor-specific $CD8^+$ T cells[274].

In this thesis, I have observed that systemic application of CpG-ODN in combination with adoptive transfer of tumor-specific $CD8^+$ T cells prolonged the survival of RT5 mice. This combination therapy induced massive infiltration of leukocytes into RT5 tumors, including $CD8^+$ T cells, $CD4^+$ T cells, NK cells, DCs and macrophages. Of note, CpG-ODN was found to bind to intratumoral macrophages in

RT5 tumors[274]. Further analysis demonstrated that CpG-ODN ploarized tumor-resident macrophages towards a M1-like phenotype, which is characterized by high-level expression of the M1 marker iNOS and low-level expression of the M2 marker CD206 (MRC1). The combination of CpG-ODN with tumor-specific $CD8^+$ T cells led also to normalization of the tumor vasculature and enhanced expression of VCAM-1 on the tumor endothelium. Both processes are known to promote T cell infiltration into the tumor.

4.2.2 iNOS activity in tumor-infiltrating macrophages is required for normalization of tumor vasculature, T cell recruitment and RT5 tumor regression

The present data showed that depletion of the M1-polarized macrophages with CLIP inhibited T cell recruitment and tumor rejection obtained by combination therapy. Macrophage depletion also prevented normalization of the tumor vasculature and diminished VCAM-1 expression on the tumor endothelium, thereby explaining the impaired recruitment of tumor-specific $CD8^+$ T cells into the tumor. Importantly, blockade of iNOS with L-NIL treatment impeded normalization of the tumor vasculature, expression of VCAM-1 on the tumor endothelium, infiltration of tumor-specific $CD8^+$ T cells and tumor regression, indicating that iNOS expression in macrophages is critical for anti-tumoral effects of macrophages. These observations were suprising and puzzling, because after NO was mainly regarded as a toxic molecule and iNOS, therefore, as an immunosuppressive moeity[307].

In order to study in more detail the mechanim by which iNOS activity by macrophages support tumor immunity, macrophages from wild-type and iNOS-deficient mice ($NOS2^{-/-}$ mice) were compared for their capacity to induce inflammation, normalization of the tumor vasculature and migration of $CD8^+$ T cells into the tumor. After activtion with LPS and IFN-γ, wild-type and iNOS-deficient macrophages exhibited no difference in the expression of inflammatory cytokines and chemokines, including TNF-α, IL-12 and IL-1β, CCL2, CCL5, CXCL9 and CXCL10. In addition, both wild-type and iNOS-deficient macrophages displayed decreased expression of pro-angiogenic molecules, such as VEGF-α, ANG2 and FGF1. Overall,

these findings indicate that the lack of iNOS had no major effects on the phenotype of activated macrophages. When injected into tumor-bearing mice, activated wild-type and $NOS2^{-/-}$ macrophages were found to migrate into the tumor with the same efficacy. However, only $iNOS^{+}$ wild-type macrophages were able to induce vascular changes in the tumor, such as replacement of dilated vessels with a high number of small vessels and induction of VCAM-1 expression on $CD31^{+}$ endothelial cells. Co-transfer of activated wild-type M1 macrophages with tumor-specific $CD8^{+}$ T cells resulted in extensive infiltration by leukocytes, including tumor-specific $CD8^{+}$ T cells, NK cells, DCs and macrophages. In contrast, tumors of mice treated by co-transfer of iNOS-deficient M1 macrophages with tumor-specific $CD8^{+}$ T cells displayed restricted infiltration of leukocytes, notably tumor-specific $CD8^{+}$ T cells. Furthermore, gene expression profiling of the tumor micronenvironment revealed that co-transfer of $iNOS^{+}$ macrophages with $CD8^{+}$ T cells caused strong activation of the genes encoding pro-inflammatory molecules, including IFN-α, IFN-β, IFN-γ, TNF-α, IL-12, IL-1, IL-2 and IL-6, chemokines, including CCL2, CCL5, CXCL9 and CXCL10, and adhesion molecules, including VCAM-1 and ICAM-1 and strong suppression of the genes encoding pro-angiogenic molecules, including VEGF-α, ANG2, RGS5, FGF1, PDGF-α. Apparently, the lack of iNOS expression in macrophages hindered the augmented expression of pro-inflammatory cytokines, chemokines and adhesion molecules achieved after co-transfer of $iNOS^{+}$ macrophages with $CD8^{+}$ T cells. Conversely, iNOS deficiency in macrophages led to partial reversion of the suppression of the genes encoding proangiogenic molecules. These findings show that adoptive transfer of pre-activated macrophages can promote infiltration of T cells into the tumor in the absence of additional danger signal such as CpG-ODN.

Suprisingly, there were no transferred macrophages left in the tumor 3 days after the injection, suggesting that transferred macrophages have short half-life. However, after co-transfer of wild-type M1 macrophages and tumor-specific $CD8^{+}$ T cells, endogenous intratumoral macrophages exhibited potent M1-like phenotype with high expression of iNOS. On the contrary, iNOS deficieny in transferred macrophages resulted in impaired polarization of endogenous macrophages towards a $iNOS^{+}$ phenotype, suggesting that iNOS expression in transferred macrophages play a role in polarization of endogenous macrophages probably via induction of infiltration of

IFN-γ-producing $CD8^+$ T cells into the tumor. Skewing of endogenous macrophages is interesting and deserves further investigation.

The precise mechanisms of normalization of tumor vessels after macrophage transfer and the sequence of events are still elusive. Unlike normal vessels, tumor vessels display structural and functional abnormalities due to the incessant production of proangiogenic factors such as VEGF within the tumor microenvironment. Tumor-associated macrophages (TAMs) seem to be an important source of VEGF in many cancers. Targeted-deletion of VEGF in macrophages was demonstrated to cause normalization of tumor vasculature in animal models[73]. These observations indicate that the level of VEGF production by macrophages is vital for formation of aberrant tumor vessels. Thus, macrophage skewing from a M2-like phenotype towards a M1-like phenotype apparently plays a critical role in normalization of tumor vasculature. In addition, M1-like macrophages may produce anti-angiogenic molecules, such as TNF, CXCL9, CXCL10 and IL-12, representing another mechanism by which M1-like macrophages induce vascular nomalization.

4.2.3 NO regulates the expression of adhesion molecules on human umbilical endothelial cells (HUVECs)

Nitric oxide is produced from of L-arginine and molecular oxygen through activity of NO synthases. Neuronal NO synthase (nNOS) is found in neurons, endothelial NO synthase (eNOS) is expressed by endotheial cells, and inducible NO synthase (iNOS) is produced by myeloid cells, mainly macrophages. NO has diverse effects on the immune system but it is best known for its inhibitory activity on T cells[307].

The process of T cell extravasation involves the migration of T cells from the blood stream through vascular endothelium into the target tissue, where they exercise their effector functions. ICAM-1, VCAM-1 and E-selectin expressed on endothelial cells mediate the adhesion of T cells to the wall of blood vessels through interactions with a variety of ligands found on T cells[308]. In steady-state conditions, quiescent endothelial cells poorly interact with circulating T cells due to the low-level

expression of adhesion molecules on their surface. However, in the case of inflammation or infection, a variety of pro-inflammatory molecules, such as TNF, IFN-γ and IL-1β, are produced, which induce expression of adhesion molecules lining the inflammed tissue, thereby promoting T cell infiltration. Since trafficking T cells to the tumor is of prime importance, a better understanding of T cell extravasation through tumor vessels is important for the development of effective immunotherapies against cancer.

In this thesis, iNOS expression in macrophages was found to correlate with enhanced expression of VCAM-1 on the tumor endothelium in RT5 mice. In order to study the underlying mechanism, as well as the relevance of these findings for human endothelial cells, HUVECs were co-cultured with the human THP-1 macrophage-like cell line or with primary human macrophages, which were derived from blood monocytes. After activation with LPS and IFN-γ, the resulting M1-polarized macrophages were found to stimulate the expression of adhesion molecules, including VCAM-1, ICAM-1 and E-Selectin on HUVECs. Blocking of iNOS with L-NIL inhibited the induction of adhesion molecules obtained during co-culture with M1 macrophages. The incomplete inhibition suggested that additional factors, such as TNF, are involved in regulation of adhesion molecules on endothelial cells. HUVECs were treated with the NO donor glyceryl trinitrate (GTN). Interestingly, NO alone at low levels were able to augment the expression of above-mentioned adhesion molecules, indicating that the level of NO is a critical parameter for the expression of adhesion molecules. Our study also that low concentrations of NO was observed to potentiate TNF-induced expression of VCAM-1, ICAM-1 and E-selectin on HUVECs whereas high concentrations blocked TNF-induced expression of these molecules.

Microarray analysis of revealed that the genes encoding adhesion molecules, such as VCAM-1 and E-Selectin, and chemokines, such as CX3CL1, CCL20, CXCL10, CXCL5, CXCL2 and IL-8 (CXCL8), are highly upregulated in HUVECs treated with low level of NO. TNF-treated HUVECs displayed comparable gene expression pattern with increased expression of above-mentioned molecules. NO treatment resulted in activation of diapedesis pathways in HUVECs, indicating that NO-treated HUVECs exhibit enhanced capaticity for transendothelial migration of leukocytes. Moreover, NO acts on a variety of signaling transduction pathways in

HUVECs for the regulation of gene expression. Similar gene expression profiling of NO- and TNF-treated HUVECs suggests that NO works via NF-κB activation. Umansky *et al.*'s findings, where low level of NO was found to enhance TNF-induced activation of NF-κB, reinforces this hypothesis. However, more analysis should be carried out to identify the mechanism by which NO modulates the process of NF-κB activation.

The role of NO in normalization of tumor vasculature and leukocyte extravasation is unclear. A previous study reported that inhibition of NO production by glioblastomas via blockade of nNOS caused normalization of the tumor vasculature, resulting in enhanced oxygenation of tumors and improved efficacy of radiation therapy[309]. Another study showed that endothelin B receptor (ET_BR) induced upregulation of NO synthases, resulting in NO release from the endothelium[310]. NO in turn impeded the expression of ICAM-1 on the tumor endothelium, impairing T cell adhesion and, consequently, preventing T cell infiltration into the tumor[311]. In addition, several groups have examined the influence of NO on adhesion molecules expressed by HUVECs using a variety of NO donors[312, 313, 314, 315]. In these studies, NO was found to downregulate the endothelial expression of VCAM-1, ICAM-1 and E-Selectin[312, 313, 314, 315]. In contrast to these findings, this study demonstrated that low level of NO induced the expression of adhesion molecules on HUVECs. In addition, iNOS activity in M1-like macrophages led to normalization of the tumor vasculature and increased expression of VCAM-1 on the tumor endothelium, indicating that M1-polarized macrophages produce low amounts of NO that are required for induction of adhesion molecules on endothelial cells. These contradictory data suggest that the source or amount of NO are key factors for its inhibitory or stimulatory properties within the tumor microenvironment. It seems that, in order to establish the conditions under which NO upregulate or downregulate endothelial expression of adhesion molecules, NO levels within the immediate environment of endothelial cells should be determined.

4.3 Conclusions

The results obtained in two different systems revealed a unifying mechanism of tumor rejection, in which M1 skewing of intratumoral macrophages plays a central role in T cell-mediated rejection of tumors (**summarized in Figure 38)**.

Tumor-infiltrating macrophages are mainly of an M2-like phenotype characterized by high-level expression of immunosuppressive molecules and pro-angiogenic factors such as VEGF that are known to cause abnormal morphology of tumor vessels. The present study shows that polarization of tumor-associated macrophages towards an M1-like phenotype by danger signals such as CpG-ODN or basophilia-induced $CD8^+$ T cell infiltration play a central for tumor rejection. M1-skewed macrophages produce only low amounts of VEGF, leading to the removal of key driver of tumor angiogenesis and promoting normalization of the tumor vasculature, which is known to enhance T cell infiltration. In addition, M1-polarization leads to production of NO by macrophages, which can enhance expression of adhesion molecules such as VCAM-1 on the tumor endothelium, thereby augmenting T cell infiltration into the tumor. M1-polarized macrophages also produce large amounts of CXCL9 and CXCL10, which attract tumor-reactive T cells into the tumor. Then, in a feedback mechanism, infiltrating T cells lead to more M1 skewing, normalization and VCAM-1 expression, thereby to more T cell infiltration and tumor eradication.

Despite the fact that increasing our understanding of the tumor microenvironment has accelerated the progress in the development of effective immunotherapies, including vaccination, adoptive T therapy and immune checkpoint inhibitors, against cancer, the clinical success is still limited. One of the major limitations of cancer immunotherapy is failure of T cell trafficking to the tumor due to low levels of inflammation and chemokines, and aberrant tumor vasculature. Based on the present study, targeted modulation of Tregs, basophils or macrophages represents a promising strategy for promoting the recruitment of tumor-specific $CD8^+$ T cells into the tumor. Moreover, adoptive transfer of pre-activated macrophages emerges as a promising tool for improvement of clinical cancer therapy.

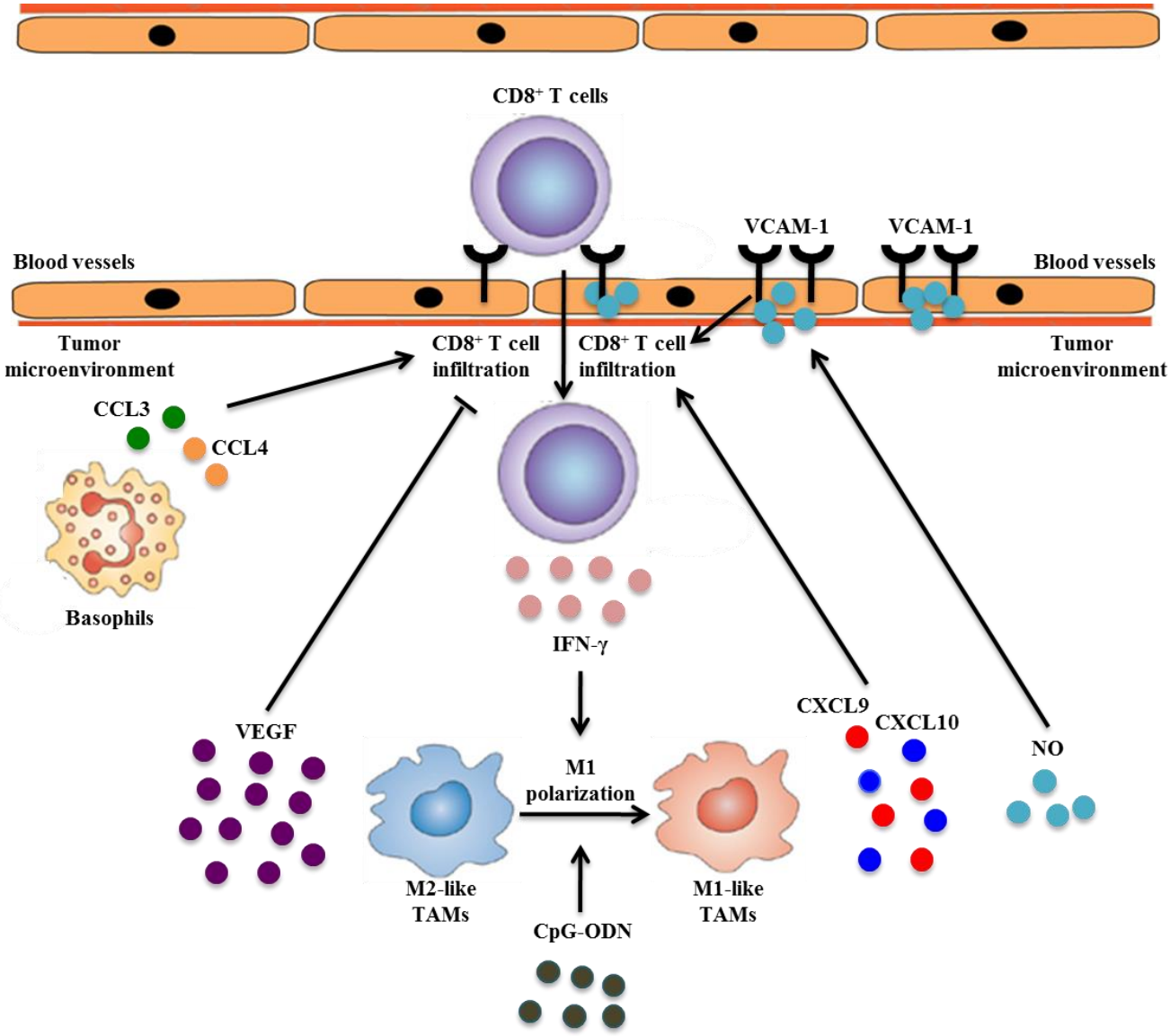

Figure 38: Polarization of M2-like macrophages into M1-like macrophages play a central in tumor rejection.
Tumor-associated macrophages (TAMs) with M2-like phenotype lead to abnormal tumor vasculature by producing angiogenic factors, such as VEGF, thereby impairing $CD8^+$ T cell infiltration into the tumor. Basophill-derived CCL3 and CCL4 induces migration of IFN-γ-producing $CD8^+$ T cells into the tumor. Elevated levels of IFN-γ polarize TAMs from M2-like phenotype to M1-like phenotype. M1 skweing of TAMs can also be achieved by systemic administration of CpG-ODN. M1-skewed macrophages enhance $CD8^+$ infiltration into the tumor by several mechanisms: M1-like macrophages produce only little amount of VEGF, leading to removal of the most potent proangiogenic factor and promoting normalization of the tumor vasculaturecell infiltration. M1-polarized macrophages produce nitric oxide (NO), which enhances expression of adhesion molecules, such as VCAM-1, on tumor endothelial cells. M1-skewed macrophages also produce large amounts of CXCL9 and CXCL10, which are known to be potent chemoattractants for $CD8^+$ T cells.

5 BIBLIOGRAPHY

1. Stewart BW, Wild CP. *World cancer report 2014.*

2. Burnet M. Cancer: a biological approach. III. Viruses associated with neoplastic conditions. IV. Practical applications. *British medical journal* 1957, **1**(5023)**:** 841-847.

3. Burnet FM. The concept of immunological surveillance. *Progress in experimental tumor research* 1970, **13:** 1-27.

4. Thomas L. On immunosurveillance in human cancer. *The Yale journal of biology and medicine* 1982, **55**(3-4)**:** 329-333.

5. Street SE, Trapani JA, MacGregor D, Smyth MJ. Suppression of lymphoma and epithelial malignancies effected by interferon gamma. *The Journal of experimental medicine* 2002, **196**(1)**:** 129-134.

6. Shankaran V, Ikeda H, Bruce AT, White JM, Swanson PE, Old LJ, *et al.* IFNgamma and lymphocytes prevent primary tumour development and shape tumour immunogenicity. *Nature* 2001, **410**(6832)**:** 1107-1111.

7. Girardi M, Oppenheim DE, Steele CR, Lewis JM, Glusac E, Filler R, *et al.* Regulation of cutaneous malignancy by gammadelta T cells. *Science* 2001, **294**(5542)**:** 605-609.

8. Dunn GP, Bruce AT, Sheehan KC, Shankaran V, Uppaluri R, Bui JD, *et al.* A critical function for type I interferons in cancer immunoediting. *Nature immunology* 2005, **6**(7)**:** 722-729.

9. Kaplan DH, Shankaran V, Dighe AS, Stockert E, Aguet M, Old LJ, *et al.* Demonstration of an interferon gamma-dependent tumor surveillance system in immunocompetent mice. *Proceedings of the National Academy of Sciences of the United States of America* 1998, **95**(13)**:** 7556-7561.

10. Smyth MJ, Thia KY, Street SE, MacGregor D, Godfrey DI, Trapani JA. Perforin-mediated cytotoxicity is critical for surveillance of spontaneous lymphoma. *The Journal of experimental medicine* 2000, **192**(5)**:** 755-760.

11. Kinlen LJ, Webster AD, Bird AG, Haile R, Peto J, Soothill JF, *et al.* Prospective study of cancer in patients with hypogammaglobulinaemia. *Lancet* 1985, **1**(8423)**:** 263-266.

12. Mueller BU, Pizzo PA. Cancer in children with primary or secondary immunodeficiencies. *The Journal of pediatrics* 1995, **126**(1)**:** 1-10.

13. Hayward AR, Levy J, Facchetti F, Notarangelo L, Ochs HD, Etzioni A, *et al.* Cholangiopathy and tumors of the pancreas, liver, and biliary tree in boys with X-linked immunodeficiency with hyper-IgM. *Journal of immunology* 1997, **158**(2)**:** 977-983.

14. Galon J, Costes A, Sanchez-Cabo F, Kirilovsky A, Mlecnik B, Lagorce-Pages C, *et al.* Type, density, and location of immune cells within human colorectal tumors predict clinical outcome. *Science* 2006, **313**(5795)**:** 1960-1964.

15. Zhang L, Conejo-Garcia JR, Katsaros D, Gimotty PA, Massobrio M, Regnani G, *et al.* Intratumoral T cells, recurrence, and survival in epithelial ovarian cancer. *The New England journal of medicine* 2003, **348**(3)**:** 203-213.

16. Al-Shibli KI, Donnem T, Al-Saad S, Persson M, Bremnes RM, Busund LT. Prognostic effect of epithelial and stromal lymphocyte infiltration in non-small cell lung cancer. *Clinical cancer research : an official journal of the American Association for Cancer Research* 2008, **14**(16)**:** 5220-5227.

17. Kawai O, Ishii G, Kubota K, Murata Y, Naito Y, Mizuno T, *et al.* Predominant infiltration of macrophages and CD8(+) T Cells in cancer nests is a significant predictor of survival in stage IV nonsmall cell lung cancer. *Cancer* 2008, **113**(6)**:** 1387-1395.

18. Mahmoud SM, Paish EC, Powe DG, Macmillan RD, Grainge MJ, Lee AH, *et al.* Tumor-infiltrating CD8+ lymphocytes predict clinical outcome in breast cancer. *Journal of clinical oncology : official journal of the American Society of Clinical Oncology* 2011, **29**(15)**:** 1949-1955.

19. Naito Y, Saito K, Shiiba K, Ohuchi A, Saigenji K, Nagura H, *et al.* CD8+ T cells infiltrated within cancer cell nests as a prognostic factor in human colorectal cancer. *Cancer research* 1998, **58**(16)**:** 3491-3494.

20. Cho Y, Miyamoto M, Kato K, Fukunaga A, Shichinohe T, Kawarada Y, *et al.* CD4+ and CD8+ T cells cooperate to improve prognosis of patients with esophageal squamous cell carcinoma. *Cancer research* 2003, **63**(7)**:** 1555-1559.

21. Hiraoka K, Miyamoto M, Cho Y, Suzuoki M, Oshikiri T, Nakakubo Y, *et al.* Concurrent infiltration by CD8+ T cells and CD4+ T cells is a favourable prognostic factor in non-small-cell lung carcinoma. *British journal of cancer* 2006, **94**(2)**:** 275-280.

22. Fridman WH, Pages F, Sautes-Fridman C, Galon J. The immune contexture in human tumours: impact on clinical outcome. *Nature reviews Cancer* 2012, **12**(4)**:** 298-306.

23. Budhu A, Forgues M, Ye QH, Jia HL, He P, Zanetti KA, *et al.* Prediction of venous metastases, recurrence, and prognosis in hepatocellular carcinoma

based on a unique immune response signature of the liver microenvironment. *Cancer cell* 2006, **10**(2)**:** 99-111.

24. Kristensen VN, Vaske CJ, Ursini-Siegel J, Van Loo P, Nordgard SH, Sachidanandam R, *et al.* Integrated molecular profiles of invasive breast tumors and ductal carcinoma in situ (DCIS) reveal differential vascular and interleukin signaling. *Proceedings of the National Academy of Sciences of the United States of America* 2012, **109**(8)**:** 2802-2807.

25. Forssell J, Oberg A, Henriksson ML, Stenling R, Jung A, Palmqvist R. High macrophage infiltration along the tumor front correlates with improved survival in colon cancer. *Clinical cancer research : an official journal of the American Association for Cancer Research* 2007, **13**(5)**:** 1472-1479.

26. Kim DW, Min HS, Lee KH, Kim YJ, Oh DY, Jeon YK, *et al.* High tumour islet macrophage infiltration correlates with improved patient survival but not with EGFR mutations, gene copy number or protein expression in resected non-small cell lung cancer. *British journal of cancer* 2008, **98**(6)**:** 1118-1124.

27. Shimura S, Yang G, Ebara S, Wheeler TM, Frolov A, Thompson TC. Reduced infiltration of tumor-associated macrophages in human prostate cancer: association with cancer progression. *Cancer research* 2000, **60**(20)**:** 5857-5861.

28. Welsh TJ, Green RH, Richardson D, Waller DA, O'Byrne KJ, Bradding P. Macrophage and mast-cell invasion of tumor cell islets confers a marked survival advantage in non-small-cell lung cancer. *Journal of clinical oncology : official journal of the American Society of Clinical Oncology* 2005, **23**(35)**:** 8959-8967.

29. Redmond WL, Sherman LA. Peripheral tolerance of CD8 T lymphocytes. *Immunity* 2005, **22**(3)**:** 275-284.

30. Khan IS, Mouchess ML, Zhu ML, Conley B, Fasano KJ, Hou Y, *et al.* Enhancement of an anti-tumor immune response by transient blockade of central T cell tolerance. *The Journal of experimental medicine* 2014, **211**(5)**:** 761-768.

31. Trager U, Sierro S, Djordjevic G, Bouzo B, Khandwala S, Meloni A, *et al.* The immune response to melanoma is limited by thymic selection of self-antigens. *PloS one* 2012, **7**(4)**:** e35005.

32. Itano AA, Jenkins MK. Antigen presentation to naive CD4 T cells in the lymph node. *Nature immunology* 2003, **4**(8)**:** 733-739.

33. Albert ML, Pearce SF, Francisco LM, Sauter B, Roy P, Silverstein RL, *et al.* Immature dendritic cells phagocytose apoptotic cells via alphavbeta5 and CD36, and cross-present antigens to cytotoxic T lymphocytes. *The Journal of experimental medicine* 1998, **188**(7)**:** 1359-1368.

34. Kurts C, Kosaka H, Carbone FR, Miller JF, Heath WR. Class I-restricted cross-presentation of exogenous self-antigens leads to deletion of autoreactive CD8(+) T cells. *The Journal of experimental medicine* 1997, **186**(2)**:** 239-245.

35. Forster I, Lieberam I. Peripheral tolerance of CD4 T cells following local activation in adolescent mice. *European journal of immunology* 1996, **26**(12)**:** 3194-3202.

36. Adler AJ, Marsh DW, Yochum GS, Guzzo JL, Nigam A, Nelson WG, *et al.* CD4+ T cell tolerance to parenchymal self-antigens requires presentation by bone marrow-derived antigen-presenting cells. *The Journal of experimental medicine* 1998, **187**(10)**:** 1555-1564.

37. Janeway CA, Jr. The immune system evolved to discriminate infectious nonself from noninfectious self. *Immunology today* 1992, **13**(1)**:** 11-16.

38. Pulendran B, Palucka K, Banchereau J. Sensing pathogens and tuning immune responses. *Science* 2001, **293**(5528)**:** 253-256.

39. Palucka K, Banchereau J. How dendritic cells and microbes interact to elicit or subvert protective immune responses. *Current opinion in immunology* 2002, **14**(4)**:** 420-431.

40. Matzinger P. Tolerance, danger, and the extended family. *Annual review of immunology* 1994, **12:** 991-1045.

41. Chen GY, Nunez G. Sterile inflammation: sensing and reacting to damage. *Nature reviews Immunology* 2010, **10**(12)**:** 826-837.

42. Krysko DV, Agostinis P, Krysko O, Garg AD, Bachert C, Lambrecht BN, *et al.* Emerging role of damage-associated molecular patterns derived from mitochondria in inflammation. *Trends in immunology* 2011, **32**(4)**:** 157-164.

43. Kroemer G, Galluzzi L, Kepp O, Zitvogel L. Immunogenic cell death in cancer therapy. *Annual review of immunology* 2013, **31:** 51-72.

44. Ueno H, Schmitt N, Klechevsky E, Pedroza-Gonzalez A, Matsui T, Zurawski G, *et al.* Harnessing human dendritic cell subsets for medicine. *Immunological reviews* 2010, **234**(1)**:** 199-212.

45. Cheng P, Zhou J, Gabrilovich D. Regulation of dendritic cell differentiation and function by Notch and Wnt pathways. *Immunological reviews* 2010, **234**(1)**:** 105-119.

46. Cella M, Scheidegger D, Palmer-Lehmann K, Lane P, Lanzavecchia A, Alber G. Ligation of CD40 on dendritic cells triggers production of high levels of interleukin-12 and enhances T cell stimulatory capacity: T-T help via APC activation. *The Journal of experimental medicine* 1996, **184**(2)**:** 747-752.

47. Ridge JP, Di Rosa F, Matzinger P. A conditioned dendritic cell can be a temporal bridge between a CD4+ T-helper and a T-killer cell. *Nature* 1998, **393**(6684)**:** 474-478.

48. Diehl L, den Boer AT, Schoenberger SP, van der Voort EI, Schumacher TN, Melief CJ, *et al.* CD40 activation in vivo overcomes peptide-induced peripheral cytotoxic T-lymphocyte tolerance and augments anti-tumor vaccine efficacy. *Nature medicine* 1999, **5**(7)**:** 774-779.

49. French RR, Chan HT, Tutt AL, Glennie MJ. CD40 antibody evokes a cytotoxic T-cell response that eradicates lymphoma and bypasses T-cell help. *Nature medicine* 1999, **5**(5)**:** 548-553.

50. Almand B, Resser JR, Lindman B, Nadaf S, Clark JI, Kwon ED, *et al.* Clinical significance of defective dendritic cell differentiation in cancer. *Clinical cancer research : an official journal of the American Association for Cancer Research* 2000, **6**(5)**:** 1755-1766.

51. Gabrilovich DI, Chen HL, Girgis KR, Cunningham HT, Meny GM, Nadaf S, *et al.* Production of vascular endothelial growth factor by human tumors inhibits the functional maturation of dendritic cells. *Nature medicine* 1996, **2**(10)**:** 1096-1103.

52. Della Porta M, Danova M, Rigolin GM, Brugnatelli S, Rovati B, Tronconi C, *et al.* Dendritic cells and vascular endothelial growth factor in colorectal cancer: correlations with clinicobiological findings. *Oncology* 2005, **68**(2-3)**:** 276-284.

53. Takahashi A, Kono K, Ichihara F, Sugai H, Fujii H, Matsumoto Y. Vascular endothelial growth factor inhibits maturation of dendritic cells induced by lipopolysaccharide, but not by proinflammatory cytokines. *Cancer immunology, immunotherapy : CII* 2004, **53**(6)**:** 543-550.

54. Steinbrink K, Jonuleit H, Muller G, Schuler G, Knop J, Enk AH. Interleukin-10-treated human dendritic cells induce a melanoma-antigen-specific anergy in CD8(+) T cells resulting in a failure to lyse tumor cells. *Blood* 1999, **93**(5)**:** 1634-1642.

55. Geissmann F, Revy P, Regnault A, Lepelletier Y, Dy M, Brousse N, *et al.* TGF-beta 1 prevents the noncognate maturation of human dendritic Langerhans cells. *Journal of immunology* 1999, **162**(8)**:** 4567-4575.

56. Elia AR, Cappello P, Puppo M, Fraone T, Vanni C, Eva A, *et al.* Human dendritic cells differentiated in hypoxia down-modulate antigen uptake and change their chemokine expression profile. *Journal of leukocyte biology* 2008, **84**(6)**:** 1472-1482.

57. Gottfried E, Kunz-Schughart LA, Ebner S, Mueller-Klieser W, Hoves S, Andreesen R, *et al.* Tumor-derived lactic acid modulates dendritic cell activation and antigen expression. *Blood* 2006, **107**(5)**:** 2013-2021.

58. Gabrilovich DI, Ostrand-Rosenberg S, Bronte V. Coordinated regulation of myeloid cells by tumours. *Nature reviews Immunology* 2012, **12**(4)**:** 253-268.

59. Kalinski P, Hilkens CM, Snijders A, Snijdewint FG, Kapsenberg ML. IL-12-deficient dendritic cells, generated in the presence of prostaglandin E2, promote type 2 cytokine production in maturing human naive T helper cells. *Journal of immunology* 1997, **159**(1)**:** 28-35.

60. Braun D, Longman RS, Albert ML. A two-step induction of indoleamine 2,3 dioxygenase (IDO) activity during dendritic-cell maturation. *Blood* 2005, **106**(7)**:** 2375-2381.

61. Menetrier-Caux C, Montmain G, Dieu MC, Bain C, Favrot MC, Caux C, *et al.* Inhibition of the differentiation of dendritic cells from CD34(+) progenitors by tumor cells: role of interleukin-6 and macrophage colony-stimulating factor. *Blood* 1998, **92**(12)**:** 4778-4791.

62. Harlin H, Meng Y, Peterson AC, Zha Y, Tretiakova M, Slingluff C, *et al.* Chemokine expression in melanoma metastases associated with CD8+ T-cell recruitment. *Cancer research* 2009, **69**(7)**:** 3077-3085.

63. Loos T, Mortier A, Proost P. Chapter 1. Isolation, identification, and production of posttranslationally modified chemokines. *Methods in enzymology* 2009, **461:** 3-29.

64. Proost P, Mortier A, Loos T, Vandercappellen J, Gouwy M, Ronsse I, *et al.* Proteolytic processing of CXCL11 by CD13/aminopeptidase N impairs CXCR3 and CXCR7 binding and signaling and reduces lymphocyte and endothelial cell migration. *Blood* 2007, **110**(1)**:** 37-44.

65. Molon B, Ugel S, Del Pozzo F, Soldani C, Zilio S, Avella D, *et al.* Chemokine nitration prevents intratumoral infiltration of antigen-specific T cells. *The Journal of experimental medicine* 2011, **208**(10)**:** 1949-1962.

66. Boon T, Coulie PG, Van den Eynde BJ, van der Bruggen P. Human T cell responses against melanoma. *Annual review of immunology* 2006, **24:** 175-208.

67. Lurquin C, Lethe B, De Plaen E, Corbiere V, Theate I, van Baren N, *et al.* Contrasting frequencies of antitumor and anti-vaccine T cells in metastases of a melanoma patient vaccinated with a MAGE tumor antigen. *The Journal of experimental medicine* 2005, **201**(2)**:** 249-257.

68. Dudley ME, Wunderlich JR, Robbins PF, Yang JC, Hwu P, Schwartzentruber DJ, *et al.* Cancer regression and autoimmunity in patients after clonal repopulation with antitumor lymphocytes. *Science* 2002, **298**(5594)**:** 850-854.

69. Jain RK. Normalization of tumor vasculature: an emerging concept in antiangiogenic therapy. *Science* 2005, **307**(5706)**:** 58-62.

70. Boocock CA, Charnock-Jones DS, Sharkey AM, McLaren J, Barker PJ, Wright KA, *et al.* Expression of vascular endothelial growth factor and its receptors flt and KDR in ovarian carcinoma. *Journal of the National Cancer Institute* 1995, **87**(7)**:** 506-516.

71. Itakura J, Ishiwata T, Shen B, Kornmann M, Korc M. Concomitant over-expression of vascular endothelial growth factor and its receptors in pancreatic cancer. *International journal of cancer Journal international du cancer* 2000, **85**(1)**:** 27-34.

72. Sunderkotter C, Steinbrink K, Goebeler M, Bhardwaj R, Sorg C. Macrophages and angiogenesis. *Journal of leukocyte biology* 1994, **55**(3)**:** 410-422.

73. Stockmann C, Doedens A, Weidemann A, Zhang N, Takeda N, Greenberg JI, *et al.* Deletion of vascular endothelial growth factor in myeloid cells accelerates tumorigenesis. *Nature* 2008, **456**(7223)**:** 814-818.

74. Facciabene A, Peng X, Hagemann IS, Balint K, Barchetti A, Wang LP, *et al.* Tumour hypoxia promotes tolerance and angiogenesis via CCL28 and T(reg) cells. *Nature* 2011, **475**(7355)**:** 226-230.

75. Hamzah J, Jugold M, Kiessling F, Rigby P, Manzur M, Marti HH, *et al.* Vascular normalization in Rgs5-deficient tumours promotes immune destruction. *Nature* 2008, **453**(7193)**:** 410-414.

76. Berger M, Bergers G, Arnold B, Hammerling GJ, Ganss R. Regulator of G-protein signaling-5 induction in pericytes coincides with active vessel remodeling during neovascularization. *Blood* 2005, **105**(3)**:** 1094-1101.

77. Piali L, Fichtel A, Terpe HJ, Imhof BA, Gisler RH. Endothelial vascular cell adhesion molecule 1 expression is suppressed by melanoma and carcinoma. *The Journal of experimental medicine* 1995, **181**(2)**:** 811-816.

78. Griffioen AW, Damen CA, Martinotti S, Blijham GH, Groenewegen G. Endothelial intercellular adhesion molecule-1 expression is suppressed in human malignancies: the role of angiogenic factors. *Cancer research* 1996, **56**(5)**:** 1111-1117.

79. Noman MZ, Buart S, Van Pelt J, Richon C, Hasmim M, Leleu N, *et al.* The cooperative induction of hypoxia-inducible factor-1 alpha and STAT3 during hypoxia induced an impairment of tumor susceptibility to CTL-mediated cell lysis. *Journal of immunology* 2009, **182**(6)**:** 3510-3521.

80. Noman MZ, Janji B, Kaminska B, Van Moer K, Pierson S, Przanowski P, *et al.* Blocking hypoxia-induced autophagy in tumors restores cytotoxic T-cell activity and promotes regression. *Cancer research* 2011, **71**(18)**:** 5976-5986.

81. Doedens AL, Stockmann C, Rubinstein MP, Liao D, Zhang N, DeNardo DG, *et al.* Macrophage expression of hypoxia-inducible factor-1 alpha suppresses

T-cell function and promotes tumor progression. *Cancer research* 2010, **70**(19)**:** 7465-7475.

82. Frebel H, Nindl V, Schuepbach RA, Braunschweiler T, Richter K, Vogel J, *et al.* Programmed death 1 protects from fatal circulatory failure during systemic virus infection of mice. *The Journal of experimental medicine* 2012, **209**(13)**:** 2485-2499.

83. Mazanet MM, Hughes CC. B7-H1 is expressed by human endothelial cells and suppresses T cell cytokine synthesis. *Journal of immunology* 2002, **169**(7)**:** 3581-3588.

84. Rodig N, Ryan T, Allen JA, Pang H, Grabie N, Chernova T, *et al.* Endothelial expression of PD-L1 and PD-L2 down-regulates CD8+ T cell activation and cytolysis. *European journal of immunology* 2003, **33**(11)**:** 3117-3126.

85. Zang X, Sullivan PS, Soslow RA, Waitz R, Reuter VE, Wilton A, *et al.* Tumor associated endothelial expression of B7-H3 predicts survival in ovarian carcinomas. *Modern pathology : an official journal of the United States and Canadian Academy of Pathology, Inc* 2010, **23**(8)**:** 1104-1112.

86. Huang X, Bai X, Cao Y, Wu J, Huang M, Tang D, *et al.* Lymphoma endothelium preferentially expresses Tim-3 and facilitates the progression of lymphoma by mediating immune evasion. *The Journal of experimental medicine* 2010, **207**(3)**:** 505-520.

87. Hernandez GL, Volpert OV, Iniguez MA, Lorenzo E, Martinez-Martinez S, Grau R, *et al.* Selective inhibition of vascular endothelial growth factor-mediated angiogenesis by cyclosporin A: roles of the nuclear factor of activated T cells and cyclooxygenase 2. *The Journal of experimental medicine* 2001, **193**(5)**:** 607-620.

88. Pirtskhalaishvili G, Nelson JB. Endothelium-derived factors as paracrine mediators of prostate cancer progression. *The Prostate* 2000, **44**(1)**:** 77-87.

89. Motz GT, Santoro SP, Wang LP, Garrabrant T, Lastra RR, Hagemann IS, *et al.* Tumor endothelium FasL establishes a selective immune barrier promoting tolerance in tumors. *Nature medicine* 2014, **20**(6)**:** 607-615.

90. Liotta LA, Kohn EC. The microenvironment of the tumour-host interface. *Nature* 2001, **411**(6835)**:** 375-379.

91. Li H, Fan X, Houghton J. Tumor microenvironment: the role of the tumor stroma in cancer. *Journal of cellular biochemistry* 2007, **101**(4)**:** 805-815.

92. De Wever O, Demetter P, Mareel M, Bracke M. Stromal myofibroblasts are drivers of invasive cancer growth. *International journal of cancer Journal international du cancer* 2008, **123**(10)**:** 2229-2238.

93. Singh S, Ross SR, Acena M, Rowley DA, Schreiber H. Stroma is critical for preventing or permitting immunological destruction of antigenic cancer cells. *The Journal of experimental medicine* 1992, **175**(1)**:** 139-146.

94. Kraman M, Bambrough PJ, Arnold JN, Roberts EW, Magiera L, Jones JO, *et al.* Suppression of antitumor immunity by stromal cells expressing fibroblast activation protein-alpha. *Science* 2010, **330**(6005)**:** 827-830.

95. Garin-Chesa P, Old LJ, Rettig WJ. Cell surface glycoprotein of reactive stromal fibroblasts as a potential antibody target in human epithelial cancers. *Proceedings of the National Academy of Sciences of the United States of America* 1990, **87**(18)**:** 7235-7239.

96. Hagood JS, Prabhakaran P, Kumbla P, Salazar L, MacEwen MW, Barker TH, *et al.* Loss of fibroblast Thy-1 expression correlates with lung fibrogenesis. *The American journal of pathology* 2005, **167**(2)**:** 365-379.

97. Koumas L, Smith TJ, Feldon S, Blumberg N, Phipps RP. Thy-1 expression in human fibroblast subsets defines myofibroblastic or lipofibroblastic phenotypes. *The American journal of pathology* 2003, **163**(4)**:** 1291-1300.

98. Di Tommaso L, Pasquinelli G, Damiani S. Smooth muscle cell differentiation in mammary stromo-epithelial lesions with evidence of a dual origin: stromal myofibroblasts and myoepithelial cells. *Histopathology* 2003, **42**(5)**:** 448-456.

99. Ladanyi A, Mohos A, Somlai B, Liszkay G, Gilde K, Fejos Z, *et al.* FOXP3+ cell density in primary tumor has no prognostic impact in patients with cutaneous malignant melanoma. *Pathology oncology research : POR* 2010, **16**(3)**:** 303-309.

100. Woo EY, Chu CS, Goletz TJ, Schlienger K, Yeh H, Coukos G, *et al.* Regulatory CD4(+)CD25(+) T cells in tumors from patients with early-stage non-small cell lung cancer and late-stage ovarian cancer. *Cancer research* 2001, **61**(12)**:** 4766-4772.

101. Liyanage UK, Moore TT, Joo HG, Tanaka Y, Herrmann V, Doherty G, *et al.* Prevalence of regulatory T cells is increased in peripheral blood and tumor microenvironment of patients with pancreas or breast adenocarcinoma. *Journal of immunology* 2002, **169**(5)**:** 2756-2761.

102. Somasundaram R, Jacob L, Swoboda R, Caputo L, Song H, Basak S, *et al.* Inhibition of cytolytic T lymphocyte proliferation by autologous CD4+/CD25+ regulatory T cells in a colorectal carcinoma patient is mediated by transforming growth factor-beta. *Cancer research* 2002, **62**(18)**:** 5267-5272.

103. Sasada T, Kimura M, Yoshida Y, Kanai M, Takabayashi A. CD4+CD25+ regulatory T cells in patients with gastrointestinal malignancies: possible involvement of regulatory T cells in disease progression. *Cancer* 2003, **98**(5)**:** 1089-1099.

104. Bates GJ, Fox SB, Han C, Leek RD, Garcia JF, Harris AL, *et al.* Quantification of regulatory T cells enables the identification of high-risk breast cancer patients and those at risk of late relapse. *Journal of clinical oncology : official journal of the American Society of Clinical Oncology* 2006, **24**(34)**:** 5373-5380.

105. Curiel TJ, Coukos G, Zou L, Alvarez X, Cheng P, Mottram P, *et al.* Specific recruitment of regulatory T cells in ovarian carcinoma fosters immune privilege and predicts reduced survival. *Nature medicine* 2004, **10**(9)**:** 942-949.

106. Sato E, Olson SH, Ahn J, Bundy B, Nishikawa H, Qian F, *et al.* Intraepithelial CD8+ tumor-infiltrating lymphocytes and a high CD8+/regulatory T cell ratio are associated with favorable prognosis in ovarian cancer. *Proceedings of the National Academy of Sciences of the United States of America* 2005, **102**(51)**:** 18538-18543.

107. Ishida T, Ishii T, Inagaki A, Yano H, Komatsu H, Iida S, *et al.* Specific recruitment of CC chemokine receptor 4-positive regulatory T cells in Hodgkin lymphoma fosters immune privilege. *Cancer research* 2006, **66**(11)**:** 5716-5722.

108. Valzasina B, Piconese S, Guiducci C, Colombo MP. Tumor-induced expansion of regulatory T cells by conversion of CD4+CD25- lymphocytes is thymus and proliferation independent. *Cancer research* 2006, **66**(8)**:** 4488-4495.

109. Liu VC, Wong LY, Jang T, Shah AH, Park I, Yang X, *et al.* Tumor evasion of the immune system by converting CD4+CD25- T cells into CD4+CD25+ T regulatory cells: role of tumor-derived TGF-beta. *Journal of immunology* 2007, **178**(5)**:** 2883-2892.

110. Seo N, Hayakawa S, Takigawa M, Tokura Y. Interleukin-10 expressed at early tumour sites induces subsequent generation of CD4(+) T-regulatory cells and systemic collapse of antitumour immunity. *Immunology* 2001, **103**(4)**:** 449-457.

111. Chen W, Jin W, Hardegen N, Lei KJ, Li L, Marinos N, *et al.* Conversion of peripheral CD4+CD25- naive T cells to CD4+CD25+ regulatory T cells by TGF-beta induction of transcription factor Foxp3. *The Journal of experimental medicine* 2003, **198**(12)**:** 1875-1886.

112. Zarek PE, Huang CT, Lutz ER, Kowalski J, Horton MR, Linden J, *et al.* A2A receptor signaling promotes peripheral tolerance by inducing T-cell anergy and the generation of adaptive regulatory T cells. *Blood* 2008, **111**(1)**:** 251-259.

113. Chappert P, Leboeuf M, Rameau P, Lalfer M, Desbois S, Liblau RS, *et al.* Antigen-specific Treg impair CD8(+) T-cell priming by blocking early T-cell expansion. *European journal of immunology* 2010, **40**(2)**:** 339-350.

114. McNally A, Hill GR, Sparwasser T, Thomas R, Steptoe RJ. CD4+CD25+ regulatory T cells control CD8+ T-cell effector differentiation by modulating IL-2 homeostasis. *Proceedings of the National Academy of Sciences of the United States of America* 2011, **108**(18)**:** 7529-7534.

115. Vignali DA, Collison LW, Workman CJ. How regulatory T cells work. *Nature reviews Immunology* 2008, **8**(7)**:** 523-532.

116. Facciabene A, Motz GT, Coukos G. T-regulatory cells: key players in tumor immune escape and angiogenesis. *Cancer research* 2012, **72**(9)**:** 2162-2171.

117. Loser K, Apelt J, Voskort M, Mohaupt M, Balkow S, Schwarz T, *et al.* IL-10 controls ultraviolet-induced carcinogenesis in mice. *Journal of immunology* 2007, **179**(1)**:** 365-371.

118. Strauss L, Bergmann C, Szczepanski M, Gooding W, Johnson JT, Whiteside TL. A unique subset of CD4+CD25highFoxp3+ T cells secreting interleukin-10 and transforming growth factor-beta1 mediates suppression in the tumor microenvironment. *Clinical cancer research : an official journal of the American Association for Cancer Research* 2007, **13**(15 Pt 1)**:** 4345-4354.

119. Grossman WJ, Verbsky JW, Tollefsen BL, Kemper C, Atkinson JP, Ley TJ. Differential expression of granzymes A and B in human cytotoxic lymphocyte subsets and T regulatory cells. *Blood* 2004, **104**(9)**:** 2840-2848.

120. Gondek DC, Lu LF, Quezada SA, Sakaguchi S, Noelle RJ. Cutting edge: contact-mediated suppression by CD4+CD25+ regulatory cells involves a granzyme B-dependent, perforin-independent mechanism. *Journal of immunology* 2005, **174**(4)**:** 1783-1786.

121. Ren X, Ye F, Jiang Z, Chu Y, Xiong S, Wang Y. Involvement of cellular death in TRAIL/DR5-dependent suppression induced by CD4(+)CD25(+) regulatory T cells. *Cell death and differentiation* 2007, **14**(12)**:** 2076-2084.

122. Garin MI, Chu CC, Golshayan D, Cernuda-Morollon E, Wait R, Lechler RI. Galectin-1: a key effector of regulation mediated by CD4+CD25+ T cells. *Blood* 2007, **109**(5)**:** 2058-2065.

123. Pandiyan P, Zheng L, Ishihara S, Reed J, Lenardo MJ. CD4+CD25+Foxp3+ regulatory T cells induce cytokine deprivation-mediated apoptosis of effector CD4+ T cells. *Nature immunology* 2007, **8**(12)**:** 1353-1362.

124. Deaglio S, Dwyer KM, Gao W, Friedman D, Usheva A, Erat A, *et al.* Adenosine generation catalyzed by CD39 and CD73 expressed on regulatory T cells mediates immune suppression. *The Journal of experimental medicine* 2007, **204**(6)**:** 1257-1265.

125. Bopp T, Becker C, Klein M, Klein-Hessling S, Palmetshofer A, Serfling E, *et al.* Cyclic adenosine monophosphate is a key component of regulatory T cell-mediated suppression. *The Journal of experimental medicine* 2007, **204**(6)**:** 1303-1310.

126. Fallarino F, Grohmann U, Hwang KW, Orabona C, Vacca C, Bianchi R, *et al.* Modulation of tryptophan catabolism by regulatory T cells. *Nature immunology* 2003, **4**(12)**:** 1206-1212.

127. Cederbom L, Hall H, Ivars F. CD4+CD25+ regulatory T cells down-regulate co-stimulatory molecules on antigen-presenting cells. *European journal of immunology* 2000, **30**(6)**:** 1538-1543.

128. Liang B, Workman C, Lee J, Chew C, Dale BM, Colonna L, *et al.* Regulatory T cells inhibit dendritic cells by lymphocyte activation gene-3 engagement of MHC class II. *Journal of immunology* 2008, **180**(9)**:** 5916-5926.

129. Murray PJ, Allen JE, Biswas SK, Fisher EA, Gilroy DW, Goerdt S, *et al.* Macrophage activation and polarization: nomenclature and experimental guidelines. *Immunity* 2014, **41**(1)**:** 14-20.

130. Mantovani A, Sozzani S, Locati M, Allavena P, Sica A. Macrophage polarization: tumor-associated macrophages as a paradigm for polarized M2 mononuclear phagocytes. *Trends in immunology* 2002, **23**(11)**:** 549-555.

131. Biswas SK, Sica A, Lewis CE. Plasticity of macrophage function during tumor progression: regulation by distinct molecular mechanisms. *Journal of immunology* 2008, **180**(4)**:** 2011-2017.

132. Pucci F, Venneri MA, Biziato D, Nonis A, Moi D, Sica A, *et al.* A distinguishing gene signature shared by tumor-infiltrating Tie2-expressing monocytes, blood "resident" monocytes, and embryonic macrophages suggests common functions and developmental relationships. *Blood* 2009, **114**(4)**:** 901-914.

133. Sica A, Bronte V. Altered macrophage differentiation and immune dysfunction in tumor development. *The Journal of clinical investigation* 2007, **117**(5)**:** 1155-1166.

134. Finak G, Bertos N, Pepin F, Sadekova S, Souleimanova M, Zhao H, *et al.* Stromal gene expression predicts clinical outcome in breast cancer. *Nature medicine* 2008, **14**(5)**:** 518-527.

135. Beck AH, Espinosa I, Edris B, Li R, Montgomery K, Zhu S, *et al.* The macrophage colony-stimulating factor 1 response signature in breast carcinoma. *Clinical cancer research : an official journal of the American Association for Cancer Research* 2009, **15**(3)**:** 778-787.

136. Steidl C, Lee T, Shah SP, Farinha P, Han G, Nayar T, *et al.* Tumor-associated macrophages and survival in classic Hodgkin's lymphoma. *The New England journal of medicine* 2010, **362**(10)**:** 875-885.

137. Kamper P, Bendix K, Hamilton-Dutoit S, Honore B, Nyengaard JR, d'Amore F. Tumor-infiltrating macrophages correlate with adverse prognosis and Epstein-Barr virus status in classical Hodgkin's lymphoma. *Haematologica* 2011, **96**(2)**:** 269-276.

138. Niino D, Komohara Y, Murayama T, Aoki R, Kimura Y, Hashikawa K, *et al.* Ratio of M2 macrophage expression is closely associated with poor prognosis for Angioimmunoblastic T-cell lymphoma (AITL). *Pathology international* 2010, **60**(4)**:** 278-283.

139. Zhang W, Wang L, Zhou D, Cui Q, Zhao D, Wu Y. Expression of tumor-associated macrophages and vascular endothelial growth factor correlates with poor prognosis of peripheral T-cell lymphoma, not otherwise specified. *Leukemia & lymphoma* 2011, **52**(1)**:** 46-52.

140. Lenz G, Wright G, Dave SS, Xiao W, Powell J, Zhao H, *et al.* Stromal gene signatures in large-B-cell lymphomas. *The New England journal of medicine* 2008, **359**(22)**:** 2313-2323.

141. Hammes LS, Tekmal RR, Naud P, Edelweiss MI, Kirma N, Valente PT, *et al.* Macrophages, inflammation and risk of cervical intraepithelial neoplasia (CIN) progression--clinicopathological correlation. *Gynecologic oncology* 2007, **105**(1)**:** 157-165.

142. Bronkhorst IH, Ly LV, Jordanova ES, Vrolijk J, Versluis M, Luyten GP, *et al.* Detection of M2-macrophages in uveal melanoma and relation with survival. *Investigative ophthalmology & visual science* 2011, **52**(2)**:** 643-650.

143. Zhang BC, Gao J, Wang J, Rao ZG, Wang BC, Gao JF. Tumor-associated macrophages infiltration is associated with peritumoral lymphangiogenesis and poor prognosis in lung adenocarcinoma. *Medical oncology* 2011, **28**(4)**:** 1447-1452.

144. Leek RD, Harris AL. Tumor-associated macrophages in breast cancer. *Journal of mammary gland biology and neoplasia* 2002, **7**(2)**:** 177-189.

145. Onita T, Ji PG, Xuan JW, Sakai H, Kanetake H, Maxwell PH, *et al.* Hypoxia-induced, perinecrotic expression of endothelial Per-ARNT-Sim domain protein-1/hypoxia-inducible factor-2alpha correlates with tumor progression, vascularization, and focal macrophage infiltration in bladder cancer. *Clinical cancer research : an official journal of the American Association for Cancer Research* 2002, **8**(2)**:** 471-480.

146. Lin EY, Nguyen AV, Russell RG, Pollard JW. Colony-stimulating factor 1 promotes progression of mammary tumors to malignancy. *The Journal of experimental medicine* 2001, **193**(6)**:** 727-740.

147. Lin EY, Li JF, Gnatovskiy L, Deng Y, Zhu L, Grzesik DA, *et al.* Macrophages regulate the angiogenic switch in a mouse model of breast cancer. *Cancer research* 2006, **66**(23)**:** 11238-11246.

148. Zhang W, Zhu XD, Sun HC, Xiong YQ, Zhuang PY, Xu HX, *et al.* Depletion of tumor-associated macrophages enhances the effect of sorafenib in metastatic liver cancer models by antimetastatic and antiangiogenic effects. *Clinical cancer research : an official journal of the American Association for Cancer Research* 2010, **16**(13)**:** 3420-3430.

149. Burke B, Tang N, Corke KP, Tazzyman D, Ameri K, Wells M, *et al.* Expression of HIF-1alpha by human macrophages: implications for the use of macrophages in hypoxia-regulated cancer gene therapy. *The Journal of pathology* 2002, **196**(2)**:** 204-212.

150. Lewis CE, Pollard JW. Distinct role of macrophages in different tumor microenvironments. *Cancer research* 2006, **66**(2)**:** 605-612.

151. Lewis C, Murdoch C. Macrophage responses to hypoxia: implications for tumor progression and anti-cancer therapies. *The American journal of pathology* 2005, **167**(3)**:** 627-635.

152. Lin EY, Li JF, Bricard G, Wang W, Deng Y, Sellers R, *et al.* Vascular endothelial growth factor restores delayed tumor progression in tumors depleted of macrophages. *Molecular oncology* 2007, **1**(3)**:** 288-302.

153. Dirkx AE, Oude Egbrink MG, Wagstaff J, Griffioen AW. Monocyte/macrophage infiltration in tumors: modulators of angiogenesis. *Journal of leukocyte biology* 2006, **80**(6)**:** 1183-1196.

154. Fischer C, Jonckx B, Mazzone M, Zacchigna S, Loges S, Pattarini L, *et al.* Anti-PlGF inhibits growth of VEGF(R)-inhibitor-resistant tumors without affecting healthy vessels. *Cell* 2007, **131**(3)**:** 463-475.

155. Conrotto P, Valdembri D, Corso S, Serini G, Tamagnone L, Comoglio PM, *et al.* Sema4D induces angiogenesis through Met recruitment by Plexin B1. *Blood* 2005, **105**(11)**:** 4321-4329.

156. Pollard JW. Tumour-educated macrophages promote tumour progression and metastasis. *Nature reviews Cancer* 2004, **4**(1)**:** 71-78.

157. Liu J, Zhang N, Li Q, Zhang W, Ke F, Leng Q, *et al.* Tumor-associated macrophages recruit CCR6+ regulatory T cells and promote the development of colorectal cancer via enhancing CCL20 production in mice. *PloS one* 2011, **6**(4)**:** e19495.

158. Savage ND, de Boer T, Walburg KV, Joosten SA, van Meijgaarden K, Geluk A, *et al.* Human anti-inflammatory macrophages induce Foxp3+ GITR+

CD25+ regulatory T cells, which suppress via membrane-bound TGFbeta-1. *Journal of immunology* 2008, **181**(3)**:** 2220-2226.

159. Sharda DR, Yu S, Ray M, Squadrito ML, De Palma M, Wynn TA, *et al.* Regulation of macrophage arginase expression and tumor growth by the Ron receptor tyrosine kinase. *Journal of immunology* 2011, **187**(5)**:** 2181-2192.

160. Rodriguez PC, Zea AH, DeSalvo J, Culotta KS, Zabaleta J, Quiceno DG, *et al.* L-arginine consumption by macrophages modulates the expression of CD3 zeta chain in T lymphocytes. *Journal of immunology* 2003, **171**(3)**:** 1232-1239.

161. Rodriguez PC, Quiceno DG, Zabaleta J, Ortiz B, Zea AH, Piazuelo MB, *et al.* Arginase I production in the tumor microenvironment by mature myeloid cells inhibits T-cell receptor expression and antigen-specific T-cell responses. *Cancer research* 2004, **64**(16)**:** 5839-5849.

162. Nagaraj S, Gupta K, Pisarev V, Kinarsky L, Sherman S, Kang L, *et al.* Altered recognition of antigen is a mechanism of CD8+ T cell tolerance in cancer. *Nature medicine* 2007, **13**(7)**:** 828-835.

163. Marincola FM, Jaffee EM, Hicklin DJ, Ferrone S. Escape of human solid tumors from T-cell recognition: molecular mechanisms and functional significance. *Advances in immunology* 2000, **74:** 181-273.

164. Chang CC, Campoli M, Ferrone S. Classical and nonclassical HLA class I antigen and NK Cell-activating ligand changes in malignant cells: current challenges and future directions. *Advances in cancer research* 2005, **93:** 189-234.

165. Wallich R, Bulbuc N, Hammerling GJ, Katzav S, Segal S, Feldman M. Abrogation of metastatic properties of tumour cells by de novo expression of H-2K antigens following H-2 gene transfection. *Nature* 1985, **315**(6017)**:** 301-305.

166. Garrido F, Algarra I, Garcia-Lora AM. The escape of cancer from T lymphocytes: immunoselection of MHC class I loss variants harboring structural-irreversible "hard" lesions. *Cancer immunology, immunotherapy : CII* 2010, **59**(10)**:** 1601-1606.

167. Momburg F, Moller P, Moldenhauer G, Hammerling GJ. Loss of HLA-A,B,C in colorectal carcinoma is related to the degree of de-differentiation. *Journal of immunogenetics* 1986, **13**(2-3)**:** 195-199.

168. Whiteside TL. Tumor-induced death of immune cells: its mechanisms and consequences. *Seminars in cancer biology* 2002, **12**(1)**:** 43-50.

169. Hamanishi J, Mandai M, Iwasaki M, Okazaki T, Tanaka Y, Yamaguchi K, *et al.* Programmed cell death 1 ligand 1 and tumor-infiltrating CD8+ T lymphocytes are prognostic factors of human ovarian cancer. *Proceedings of*

the National Academy of Sciences of the United States of America 2007, **104**(9)**:** 3360-3365.

170. Hirano F, Kaneko K, Tamura H, Dong H, Wang S, Ichikawa M, *et al.* Blockade of B7-H1 and PD-1 by monoclonal antibodies potentiates cancer therapeutic immunity. *Cancer research* 2005, **65**(3)**:** 1089-1096.

171. Curiel TJ, Wei S, Dong H, Alvarez X, Cheng P, Mottram P, *et al.* Blockade of B7-H1 improves myeloid dendritic cell-mediated antitumor immunity. *Nature medicine* 2003, **9**(5)**:** 562-567.

172. Belai EB, de Oliveira CE, Gasparoto TH, Ramos RN, Torres SA, Garlet GP, *et al.* PD-1 blockage delays murine squamous cell carcinoma development. *Carcinogenesis* 2014, **35**(2)**:** 424-431.

173. Duraiswamy J, Freeman GJ, Coukos G. Therapeutic PD-1 pathway blockade augments with other modalities of immunotherapy T-cell function to prevent immune decline in ovarian cancer. *Cancer research* 2013, **73**(23)**:** 6900-6912.

174. Dubensky TW, Jr., Reed SG. Adjuvants for cancer vaccines. *Seminars in immunology* 2010, **22**(3)**:** 155-161.

175. Schwartzentruber DJ, Lawson DH, Richards JM, Conry RM, Miller DM, Treisman J, *et al.* gp100 peptide vaccine and interleukin-2 in patients with advanced melanoma. *The New England journal of medicine* 2011, **364**(22)**:** 2119-2127.

176. Kenter GG, Welters MJ, Valentijn AR, Lowik MJ, Berends-van der Meer DM, Vloon AP, *et al.* Vaccination against HPV-16 oncoproteins for vulvar intraepithelial neoplasia. *The New England journal of medicine* 2009, **361**(19)**:** 1838-1847.

177. Leffers N, Lambeck AJ, Gooden MJ, Hoogeboom BN, Wolf R, Hamming IE, *et al.* Immunization with a P53 synthetic long peptide vaccine induces P53-specific immune responses in ovarian cancer patients, a phase II trial. *International journal of cancer Journal international du cancer* 2009, **125**(9)**:** 2104-2113.

178. Schuster SJ, Neelapu SS, Gause BL, Janik JE, Muggia FM, Gockerman JP, *et al.* Vaccination with patient-specific tumor-derived antigen in first remission improves disease-free survival in follicular lymphoma. *Journal of clinical oncology : official journal of the American Society of Clinical Oncology* 2011, **29**(20)**:** 2787-2794.

179. Lizee G, Overwijk WW, Radvanyi L, Gao J, Sharma P, Hwu P. Harnessing the power of the immune system to target cancer. *Annual review of medicine* 2013, **64:** 71-90.

180. Rosenberg SA, Yang JC, Restifo NP. Cancer immunotherapy: moving beyond current vaccines. *Nature medicine* 2004, **10**(9)**:** 909-915.

181. Rosenberg SA, Sherry RM, Morton KE, Scharfman WJ, Yang JC, Topalian SL, *et al.* Tumor progression can occur despite the induction of very high levels of self/tumor antigen-specific CD8+ T cells in patients with melanoma. *Journal of immunology* 2005, **175**(9)**:** 6169-6176.

182. Rosenberg SA, Yang JC, Sherry RM, Kammula US, Hughes MS, Phan GQ, *et al.* Durable complete responses in heavily pretreated patients with metastatic melanoma using T-cell transfer immunotherapy. *Clinical cancer research : an official journal of the American Association for Cancer Research* 2011, **17**(13)**:** 4550-4557.

183. Itzhaki O, Hovav E, Ziporen Y, Levy D, Kubi A, Zikich D, *et al.* Establishment and large-scale expansion of minimally cultured "young" tumor infiltrating lymphocytes for adoptive transfer therapy. *Journal of immunotherapy* 2011, **34**(2)**:** 212-220.

184. Besser MJ, Shapira-Frommer R, Treves AJ, Zippel D, Itzhaki O, Hershkovitz L, *et al.* Clinical responses in a phase II study using adoptive transfer of short-term cultured tumor infiltration lymphocytes in metastatic melanoma patients. *Clinical cancer research : an official journal of the American Association for Cancer Research* 2010, **16**(9)**:** 2646-2655.

185. Restifo NP, Dudley ME, Rosenberg SA. Adoptive immunotherapy for cancer: harnessing the T cell response. *Nature reviews Immunology* 2012, **12**(4)**:** 269-281.

186. Davila ML, Riviere I, Wang X, Bartido S, Park J, Curran K, *et al.* Efficacy and toxicity management of 19-28z CAR T cell therapy in B cell acute lymphoblastic leukemia. *Science translational medicine* 2014, **6**(224)**:** 224ra225.

187. Lamers CH, Sleijfer S, Vulto AG, Kruit WH, Kliffen M, Debets R, *et al.* Treatment of metastatic renal cell carcinoma with autologous T-lymphocytes genetically retargeted against carbonic anhydrase IX: first clinical experience. *Journal of clinical oncology : official journal of the American Society of Clinical Oncology* 2006, **24**(13)**:** e20-22.

188. Park JR, Digiusto DL, Slovak M, Wright C, Naranjo A, Wagner J, *et al.* Adoptive transfer of chimeric antigen receptor re-directed cytolytic T lymphocyte clones in patients with neuroblastoma. *Molecular therapy : the journal of the American Society of Gene Therapy* 2007, **15**(4)**:** 825-833.

189. Grupp SA, Kalos M, Barrett D, Aplenc R, Porter DL, Rheingold SR, *et al.* Chimeric antigen receptor-modified T cells for acute lymphoid leukemia. *The New England journal of medicine* 2013, **368**(16)**:** 1509-1518.

190. Porter DL, Levine BL, Kalos M, Bagg A, June CH. Chimeric antigen receptor-modified T cells in chronic lymphoid leukemia. *The New England journal of medicine* 2011, **365**(8)**:** 725-733.

191. Huang Y, Goel S, Duda DG, Fukumura D, Jain RK. Vascular normalization as an emerging strategy to enhance cancer immunotherapy. *Cancer research* 2013, **73**(10)**:** 2943-2948.

192. Motz GT, Coukos G. Deciphering and reversing tumor immune suppression. *Immunity* 2013, **39**(1)**:** 61-73.

193. Willett CG, Boucher Y, di Tomaso E, Duda DG, Munn LL, Tong RT, *et al.* Direct evidence that the VEGF-specific antibody bevacizumab has antivascular effects in human rectal cancer. *Nature medicine* 2004, **10**(2)**:** 145-147.

194. Willett CG, Duda DG, di Tomaso E, Boucher Y, Ancukiewicz M, Sahani DV, *et al.* Efficacy, safety, and biomarkers of neoadjuvant bevacizumab, radiation therapy, and fluorouracil in rectal cancer: a multidisciplinary phase II study. *Journal of clinical oncology : official journal of the American Society of Clinical Oncology* 2009, **27**(18)**:** 3020-3026.

195. Fischer I, Cunliffe CH, Bollo RJ, Raza S, Monoky D, Chiriboga L, *et al.* High-grade glioma before and after treatment with radiation and Avastin: initial observations. *Neuro-oncology* 2008, **10**(5)**:** 700-708.

196. Manning EA, Ullman JG, Leatherman JM, Asquith JM, Hansen TR, Armstrong TD, *et al.* A vascular endothelial growth factor receptor-2 inhibitor enhances antitumor immunity through an immune-based mechanism. *Clinical cancer research : an official journal of the American Association for Cancer Research* 2007, **13**(13)**:** 3951-3959.

197. Shrimali RK, Yu Z, Theoret MR, Chinnasamy D, Restifo NP, Rosenberg SA. Antiangiogenic agents can increase lymphocyte infiltration into tumor and enhance the effectiveness of adoptive immunotherapy of cancer. *Cancer research* 2010, **70**(15)**:** 6171-6180.

198. Rolny C, Mazzone M, Tugues S, Laoui D, Johansson I, Coulon C, *et al.* HRG inhibits tumor growth and metastasis by inducing macrophage polarization and vessel normalization through downregulation of PlGF. *Cancer cell* 2011, **19**(1)**:** 31-44.

199. Chambers CA, Kuhns MS, Egen JG, Allison JP. CTLA-4-mediated inhibition in regulation of T cell responses: mechanisms and manipulation in tumor immunotherapy. *Annual review of immunology* 2001, **19:** 565-594.

200. Hodi FS, O'Day SJ, McDermott DF, Weber RW, Sosman JA, Haanen JB, *et al.* Improved survival with ipilimumab in patients with metastatic melanoma. *The New England journal of medicine* 2010, **363**(8)**:** 711-723.

201. Robert C, Thomas L, Bondarenko I, O'Day S, Weber J, Garbe C, *et al.* Ipilimumab plus dacarbazine for previously untreated metastatic melanoma. *The New England journal of medicine* 2011, **364**(26)**:** 2517-2526.

202. Dong H, Strome SE, Salomao DR, Tamura H, Hirano F, Flies DB, *et al.* Tumor-associated B7-H1 promotes T-cell apoptosis: a potential mechanism of immune evasion. *Nature medicine* 2002, **8**(8)**:** 793-800.

203. Iwai Y, Ishida M, Tanaka Y, Okazaki T, Honjo T, Minato N. Involvement of PD-L1 on tumor cells in the escape from host immune system and tumor immunotherapy by PD-L1 blockade. *Proceedings of the National Academy of Sciences of the United States of America* 2002, **99**(19)**:** 12293-12297.

204. Brahmer JR, Tykodi SS, Chow LQ, Hwu WJ, Topalian SL, Hwu P, *et al.* Safety and activity of anti-PD-L1 antibody in patients with advanced cancer. *The New England journal of medicine* 2012, **366**(26)**:** 2455-2465.

205. Topalian SL, Hodi FS, Brahmer JR, Gettinger SN, Smith DC, McDermott DF, *et al.* Safety, activity, and immune correlates of anti-PD-1 antibody in cancer. *The New England journal of medicine* 2012, **366**(26)**:** 2443-2454.

206. Duraiswamy J, Kaluza KM, Freeman GJ, Coukos G. Dual blockade of PD-1 and CTLA-4 combined with tumor vaccine effectively restores T-cell rejection function in tumors. *Cancer research* 2013, **73**(12)**:** 3591-3603.

207. Onizuka S, Tawara I, Shimizu J, Sakaguchi S, Fujita T, Nakayama E. Tumor rejection by in vivo administration of anti-CD25 (interleukin-2 receptor alpha) monoclonal antibody. *Cancer research* 1999, **59**(13)**:** 3128-3133.

208. Shimizu J, Yamazaki S, Sakaguchi S. Induction of tumor immunity by removing CD25+CD4+ T cells: a common basis between tumor immunity and autoimmunity. *Journal of immunology* 1999, **163**(10)**:** 5211-5218.

209. Sutmuller RP, van Duivenvoorde LM, van Elsas A, Schumacher TN, Wildenberg ME, Allison JP, *et al.* Synergism of cytotoxic T lymphocyte-associated antigen 4 blockade and depletion of CD25(+) regulatory T cells in antitumor therapy reveals alternative pathways for suppression of autoreactive cytotoxic T lymphocyte responses. *The Journal of experimental medicine* 2001, **194**(6)**:** 823-832.

210. Jones E, Dahm-Vicker M, Simon AK, Green A, Powrie F, Cerundolo V, *et al.* Depletion of CD25+ regulatory cells results in suppression of melanoma growth and induction of autoreactivity in mice. *Cancer immunity* 2002, **2:** 1.

211. Li J, Hu P, Khawli LA, Epstein AL. Complete regression of experimental solid tumors by combination LEC/chTNT-3 immunotherapy and CD25(+) T-cell depletion. *Cancer research* 2003, **63**(23)**:** 8384-8392.

212. Teng MW, Swann JB, von Scheidt B, Sharkey J, Zerafa N, McLaughlin N, *et al.* Multiple antitumor mechanisms downstream of prophylactic regulatory T-cell depletion. *Cancer research* 2010, **70**(7)**:** 2665-2674.

213. Ko K, Yamazaki S, Nakamura K, Nishioka T, Hirota K, Yamaguchi T, *et al.* Treatment of advanced tumors with agonistic anti-GITR mAb and its effects on tumor-infiltrating Foxp3+CD25+CD4+ regulatory T cells. *The Journal of experimental medicine* 2005, **202**(7)**:** 885-891.

214. Quezada SA, Peggs KS, Simpson TR, Shen Y, Littman DR, Allison JP. Limited tumor infiltration by activated T effector cells restricts the therapeutic activity of regulatory T cell depletion against established melanoma. *The Journal of experimental medicine* 2008, **205**(9)**:** 2125-2138.

215. Dannull J, Su Z, Rizzieri D, Yang BK, Coleman D, Yancey D, *et al.* Enhancement of vaccine-mediated antitumor immunity in cancer patients after depletion of regulatory T cells. *The Journal of clinical investigation* 2005, **115**(12)**:** 3623-3633.

216. Mahnke K, Schonfeld K, Fondel S, Ring S, Karakhanova S, Wiedemeyer K, *et al.* Depletion of CD4+CD25+ human regulatory T cells in vivo: kinetics of Treg depletion and alterations in immune functions in vivo and in vitro. *International journal of cancer Journal international du cancer* 2007, **120**(12)**:** 2723-2733.

217. Morse MA, Hobeika AC, Osada T, Serra D, Niedzwiecki D, Lyerly HK, *et al.* Depletion of human regulatory T cells specifically enhances antigen-specific immune responses to cancer vaccines. *Blood* 2008, **112**(3)**:** 610-618.

218. Barnett B, Kryczek I, Cheng P, Zou W, Curiel TJ. Regulatory T cells in ovarian cancer: biology and therapeutic potential. *American journal of reproductive immunology* 2005, **54**(6)**:** 369-377.

219. Kim JM, Rasmussen JP, Rudensky AY. Regulatory T cells prevent catastrophic autoimmunity throughout the lifespan of mice. *Nature immunology* 2007, **8**(2)**:** 191-197.

220. Suffner J, Hochweller K, Kuhnle MC, Li X, Kroczek RA, Garbi N, *et al.* Dendritic cells support homeostatic expansion of Foxp3+ regulatory T cells in Foxp3.LuciDTR mice. *Journal of immunology* 2010, **184**(4)**:** 1810-1820.

221. Lahl K, Loddenkemper C, Drouin C, Freyer J, Arnason J, Eberl G, *et al.* Selective depletion of Foxp3+ regulatory T cells induces a scurfy-like disease. *The Journal of experimental medicine* 2007, **204**(1)**:** 57-63.

222. Li X, Kostareli E, Suffner J, Garbi N, Hammerling GJ. Efficient Treg depletion induces T-cell infiltration and rejection of large tumors. *European journal of immunology* 2010, **40**(12)**:** 3325-3335.

223. Galli SJ. Mast cells and basophils. *Current opinion in hematology* 2000, **7**(1)**:** 32-39.

224. Stone KD, Prussin C, Metcalfe DD. IgE, mast cells, basophils, and eosinophils. *The Journal of allergy and clinical immunology* 2010, **125**(2 Suppl 2)**:** S73-80.

225. Falcone FH, Haas H, Gibbs BF. The human basophil: a new appreciation of its role in immune responses. *Blood* 2000, **96**(13)**:** 4028-4038.

226. Ohnmacht C, Voehringer D. Basophil effector function and homeostasis during helminth infection. *Blood* 2009, **113**(12)**:** 2816-2825.

227. Iwasaki H, Akashi K. Myeloid lineage commitment from the hematopoietic stem cell. *Immunity* 2007, **26**(6)**:** 726-740.

228. Iwasaki H, Mizuno S, Arinobu Y, Ozawa H, Mori Y, Shigematsu H, *et al.* The order of expression of transcription factors directs hierarchical specification of hematopoietic lineages. *Genes & development* 2006, **20**(21)**:** 3010-3021.

229. Siracusa MC, Saenz SA, Hill DA, Kim BS, Headley MB, Doering TA, *et al.* TSLP promotes interleukin-3-independent basophil haematopoiesis and type 2 inflammation. *Nature* 2011, **477**(7363)**:** 229-233.

230. Lantz CS, Boesiger J, Song CH, Mach N, Kobayashi T, Mulligan RC, *et al.* Role for interleukin-3 in mast-cell and basophil development and in immunity to parasites. *Nature* 1998, **392**(6671)**:** 90-93.

231. Shen T, Kim S, Do JS, Wang L, Lantz C, Urban JF, *et al.* T cell-derived IL-3 plays key role in parasite infection-induced basophil production but is dispensable for in vivo basophil survival. *International immunology* 2008, **20**(9)**:** 1201-1209.

232. Ohmori K, Luo Y, Jia Y, Nishida J, Wang Z, Bunting KD, *et al.* IL-3 induces basophil expansion in vivo by directing granulocyte-monocyte progenitors to differentiate into basophil lineage-restricted progenitors in the bone marrow and by increasing the number of basophil/mast cell progenitors in the spleen. *Journal of immunology* 2009, **182**(5)**:** 2835-2841.

233. Didichenko SA, Spiegl N, Brunner T, Dahinden CA. IL-3 induces a Pim1-dependent antiapoptotic pathway in primary human basophils. *Blood* 2008, **112**(10)**:** 3949-3958.

234. Zheng X, Karsan A, Duronio V, Chu F, Walker DC, Bai TR, *et al.* Interleukin-3, but not granulocyte-macrophage colony-stimulating factor and interleukin-5, inhibits apoptosis of human basophils through phosphatidylinositol 3-kinase: requirement of NF-kappaB-dependent and -independent pathways. *Immunology* 2002, **107**(3)**:** 306-315.

235. Perrigoue JG, Saenz SA, Siracusa MC, Allenspach EJ, Taylor BC, Giacomin PR, *et al.* MHC class II-dependent basophil-CD4+ T cell interactions promote T(H)2 cytokine-dependent immunity. *Nature immunology* 2009, **10**(7)**:** 697-705.

236. Ito Y, Satoh T, Takayama K, Miyagishi C, Walls AF, Yokozeki H. Basophil recruitment and activation in inflammatory skin diseases. *Allergy* 2011, **66**(8)**:** 1107-1113.

237. Kim S, Prout M, Ramshaw H, Lopez AF, LeGros G, Min B. Cutting edge: basophils are transiently recruited into the draining lymph nodes during helminth infection via IL-3, but infection-induced Th2 immunity can develop without basophil lymph node recruitment or IL-3. *Journal of immunology* 2010, **184**(3)**:** 1143-1147.

238. Suzukawa M, Hirai K, Iikura M, Nagase H, Komiya A, Yoshimura-Uchiyama C, *et al.* IgE- and FcepsilonRI-mediated migration of human basophils. *International immunology* 2005, **17**(9)**:** 1249-1255.

239. Bochner BS, McKelvey AA, Sterbinsky SA, Hildreth JE, Derse CP, Klunk DA, *et al.* IL-3 augments adhesiveness for endothelium and CD11b expression in human basophils but not neutrophils. *Journal of immunology* 1990, **145**(6)**:** 1832-1837.

240. Lim LH, Burdick MM, Hudson SA, Mustafa FB, Konstantopoulos K, Bochner BS. Stimulation of human endothelium with IL-3 induces selective basophil accumulation in vitro. *Journal of immunology* 2006, **176**(9)**:** 5346-5353.

241. Uguccioni M, Mackay CR, Ochensberger B, Loetscher P, Rhis S, LaRosa GJ, *et al.* High expression of the chemokine receptor CCR3 in human blood basophils. Role in activation by eotaxin, MCP-4, and other chemokines. *The Journal of clinical investigation* 1997, **100**(5)**:** 1137-1143.

242. Iikura M, Ebisawa M, Yamaguchi M, Tachimoto H, Ohta K, Yamamoto K, *et al.* Transendothelial migration of human basophils. *Journal of immunology* 2004, **173**(8)**:** 5189-5195.

243. Schwartz LB. Enzyme mediators of mast cells and basophils. *Clinical reviews in allergy* 1983, **1**(3)**:** 397-416.

244. Klos A, Tenner AJ, Johswich KO, Ager RR, Reis ES, Kohl J. The role of the anaphylatoxins in health and disease. *Molecular immunology* 2009, **46**(14)**:** 2753-2766.

245. Guo RF, Ward PA. Role of C5a in inflammatory responses. *Annual review of immunology* 2005, **23:** 821-852.

246. Schneider E, Thieblemont N, De Moraes ML, Dy M. Basophils: new players in the cytokine network. *European cytokine network* 2010, **21**(3)**:** 142-153.

247. Schroeder JT. Basophils: emerging roles in the pathogenesis of allergic disease. *Immunological reviews* 2011, **242**(1)**:** 144-160.

248. Denzel A, Maus UA, Rodriguez Gomez M, Moll C, Niedermeier M, Winter C, *et al.* Basophils enhance immunological memory responses. *Nature immunology* 2008, **9**(7)**:** 733-742.

249. Sokol CL, Barton GM, Farr AG, Medzhitov R. A mechanism for the initiation of allergen-induced T helper type 2 responses. *Nature immunology* 2008, **9**(3)**:** 310-318.

250. Gessner A, Mohrs K, Mohrs M. Mast cells, basophils, and eosinophils acquire constitutive IL-4 and IL-13 transcripts during lineage differentiation that are sufficient for rapid cytokine production. *Journal of immunology* 2005, **174**(2)**:** 1063-1072.

251. Gibbs BF, Haas H, Falcone FH, Albrecht C, Vollrath IB, Noll T, *et al.* Purified human peripheral blood basophils release interleukin-13 and preformed interleukin-4 following immunological activation. *European journal of immunology* 1996, **26**(10)**:** 2493-2498.

252. Schroeder JT, MacGlashan DW, Jr., Kagey-Sobotka A, White JM, Lichtenstein LM. IgE-dependent IL-4 secretion by human basophils. The relationship between cytokine production and histamine release in mixed leukocyte cultures. *Journal of immunology* 1994, **153**(4)**:** 1808-1817.

253. Min B, Prout M, Hu-Li J, Zhu J, Jankovic D, Morgan ES, *et al.* Basophils produce IL-4 and accumulate in tissues after infection with a Th2-inducing parasite. *The Journal of experimental medicine* 2004, **200**(4)**:** 507-517.

254. Oh K, Shen T, Le Gros G, Min B. Induction of Th2 type immunity in a mouse system reveals a novel immunoregulatory role of basophils. *Blood* 2007, **109**(7)**:** 2921-2927.

255. Ohnmacht C, Schwartz C, Panzer M, Schiedewitz I, Naumann R, Voehringer D. Basophils orchestrate chronic allergic dermatitis and protective immunity against helminths. *Immunity* 2010, **33**(3)**:** 364-374.

256. Falcone FH, Knol EF, Gibbs BF. The role of basophils in the pathogenesis of allergic disease. *Clinical and experimental allergy : journal of the British Society for Allergy and Clinical Immunology* 2011, **41**(7)**:** 939-947.

257. Kroeger KM, Sullivan BM, Locksley RM. IL-18 and IL-33 elicit Th2 cytokines from basophils via a MyD88- and p38alpha-dependent pathway. *Journal of leukocyte biology* 2009, **86**(4)**:** 769-778.

258. Kondo Y, Yoshimoto T, Yasuda K, Futatsugi-Yumikura S, Morimoto M, Hayashi N, *et al.* Administration of IL-33 induces airway hyperresponsiveness and goblet cell hyperplasia in the lungs in the absence of adaptive immune system. *International immunology* 2008, **20**(6)**:** 791-800.

259. Karasuyama H, Mukai K, Obata K, Tsujimura Y, Wada T. Nonredundant roles of basophils in immunity. *Annual review of immunology* 2011, **29:** 45-69.

260. Voehringer D. Protective and pathological roles of mast cells and basophils. *Nature reviews Immunology* 2013, **13**(5)**:** 362-375.

261. Matsushima T, Handa H, Yokohama A, Nagasaki J, Koiso H, Kin Y, *et al.* Prevalence and clinical characteristics of myelodysplastic syndrome with bone marrow eosinophilia or basophilia. *Blood* 2003, **101**(9)**:** 3386-3390.

262. Fureder W, Schernthaner GH, Ghannadan M, Hauswirth A, Sperr WR, Semper H, *et al.* Quantitative, phenotypic, and functional evaluation of basophils in myelodysplastic syndromes. *European journal of clinical investigation* 2001, **31**(10)**:** 894-901.

263. Shibata K, Watanabe M, Yano H, Matsuzaki M, Funai N, Sano M. Importance of basophilia in haematopoietic disorders. *Haematologia* 1998, **29**(3)**:** 241-253.

264. Wimazal F, Germing U, Kundi M, Noesslinger T, Blum S, Geissler P, *et al.* Evaluation of the prognostic significance of eosinophilia and basophilia in a larger cohort of patients with myelodysplastic syndromes. *Cancer* 2010, **116**(10)**:** 2372-2381.

265. Denburg JA, Browman G. Prognostic implications of basophil differentiation in chronic myeloid leukemia. *American journal of hematology* 1988, **27**(2)**:** 110-114.

266. Kantarjian HM, Dixon D, Keating MJ, Talpaz M, Walters RS, McCredie KB, *et al.* Characteristics of accelerated disease in chronic myelogenous leukemia. *Cancer* 1988, **61**(7)**:** 1441-1446.

267. Sergeev SI, Gracheva ZA, Bergut FA, Sokolova, II. [Degranulation and intracellular heparin of basophilic granulocytes in patients with stomach cancer]. *Sovetskaia meditsina* 1977(2)**:** 29-33.

268. Anthony HM. Blood basophils in lung cancer. *British journal of cancer* 1982, **45**(2)**:** 209-216.

269. Di Carlo E, Modesti A, Coletti A, Colombo MP, Giovarelli M, Forni G, *et al.* Interaction between endothelial cells and the secreted cytokine drives the fate of an IL4- or an IL5-transduced tumour. *The Journal of pathology* 1998, **186**(4)**:** 390-397.

270. Hanahan D. Heritable formation of pancreatic beta-cell tumours in transgenic mice expressing recombinant insulin/simian virus 40 oncogenes. *Nature* 1985, **315**(6015)**:** 115-122.

271. Forster I, Hirose R, Arbeit JM, Clausen BE, Hanahan D. Limited capacity for tolerization of CD4+ T cells specific for a pancreatic beta cell neo-antigen. *Immunity* 1995, **2**(6)**:** 573-585.

272. Ryschich E, Schmidt J, Hammerling GJ, Klar E, Ganss R. Transformation of the microvascular system during multistage tumorigenesis. *International journal of cancer Journal international du cancer* 2002, **97**(6)**:** 719-725.

273. Hanahan D, Folkman J. Patterns and emerging mechanisms of the angiogenic switch during tumorigenesis. *Cell* 1996, **86**(3)**:** 353-364.

274. Garbi N, Arnold B, Gordon S, Hammerling GJ, Ganss R. CpG motifs as proinflammatory factors render autochthonous tumors permissive for infiltration and destruction. *Journal of immunology* 2004, **172**(10)**:** 5861-5869.

275. Ganss R, Ryschich E, Klar E, Arnold B, Hammerling GJ. Combination of T-cell therapy and trigger of inflammation induces remodeling of the vasculature and tumor eradication. *Cancer research* 2002, **62**(5)**:** 1462-1470.

276. Klug F, Prakash H, Huber PE, Seibel T, Bender N, Halama N, *et al.* Low-dose irradiation programs macrophage differentiation to an iNOS(+)/M1 phenotype that orchestrates effective T cell immunotherapy. *Cancer cell* 2013, **24**(5)**:** 589-602.

277. Landsberg J, Kohlmeyer J, Renn M, Bald T, Rogava M, Cron M, *et al.* Melanomas resist T-cell therapy through inflammation-induced reversible dedifferentiation. *Nature* 2012, **490**(7420)**:** 412-416.

278. Rothenberg ME. Eotaxin. An essential mediator of eosinophil trafficking into mucosal tissues. *American journal of respiratory cell and molecular biology* 1999, **21**(3)**:** 291-295.

279. Chen KJ, Lin SZ, Zhou L, Xie HY, Zhou WH, Taki-Eldin A, *et al.* Selective recruitment of regulatory T cell through CCR6-CCL20 in hepatocellular carcinoma fosters tumor progression and predicts poor prognosis. *PloS one* 2011, **6**(9)**:** e24671.

280. He S, Wang L, Wu Y, Li D, Zhang Y. CCL3 and CCL20-recruited dendritic cells modified by melanoma antigen gene-1 induce anti-tumor immunity against gastric cancer ex vivo and in vivo. *Journal of experimental & clinical cancer research : CR* 2010, **29:** 37.

281. Peng W, Liu C, Xu C, Lou Y, Chen J, Yang Y, *et al.* PD-1 blockade enhances T-cell migration to tumors by elevating IFN-gamma inducible chemokines. *Cancer research* 2012, **72**(20)**:** 5209-5218.

282. Haabeth OA, Lorvik KB, Hammarstrom C, Donaldson IM, Haraldsen G, Bogen B, *et al.* Inflammation driven by tumour-specific Th1 cells protects against B-cell cancer. *Nature communications* 2011, **2:** 240.

283. Carretero R, Sektioglu IM, Garbi N, Salgado OC, Beckhove P, Hammerling GJ. Eosinophils orchestrate cancer rejection by normalizing tumor vessels and enhancing infiltration of CD8 T cells. *Nature immunology* 2015.

284. Noy R, Pollard JW. Tumor-associated macrophages: from mechanisms to therapy. *Immunity* 2014, **41**(1)**:** 49-61.

285. Sparwasser T, Eberl G. BAC to immunology--bacterial artificial chromosome-mediated transgenesis for targeting of immune cells. *Immunology* 2007, **121**(3)**:** 308-313.

286. Gonzalez-Martin A, Gomez L, Lustgarten J, Mira E, Manes S. Maximal T cell-mediated antitumor responses rely upon CCR5 expression in both CD4(+) and CD8(+) T cells. *Cancer research* 2011, **71**(16)**:** 5455-5466.

287. Iida N, Nakamoto Y, Baba T, Nakagawa H, Mizukoshi E, Naito M, *et al.* Antitumor effect after radiofrequency ablation of murine hepatoma is augmented by an active variant of CC Chemokine ligand 3/macrophage inflammatory protein-1alpha. *Cancer research* 2010, **70**(16)**:** 6556-6565.

288. Gough M, Crittenden M, Thanarajasingam U, Sanchez-Perez L, Thompson J, Jevremovic D, *et al.* Gene therapy to manipulate effector T cell trafficking to tumors for immunotherapy. *Journal of immunology* 2005, **174**(9)**:** 5766-5773.

289. Nakasone Y, Fujimoto M, Matsushita T, Hamaguchi Y, Huu DL, Yanaba M, *et al.* Host-derived MCP-1 and MIP-1alpha regulate protective anti-tumor immunity to localized and metastatic B16 melanoma. *The American journal of pathology* 2012, **180**(1)**:** 365-374.

290. Lanca T, Costa MF, Goncalves-Sousa N, Rei M, Grosso AR, Penido C, *et al.* Protective role of the inflammatory CCR2/CCL2 chemokine pathway through recruitment of type 1 cytotoxic gammadelta T lymphocytes to tumor beds. *Journal of immunology* 2013, **190**(12)**:** 6673-6680.

291. Guirnalda P, Wood L, Goenka R, Crespo J, Paterson Y. Interferon gamma-induced intratumoral expression of CXCL9 alters the local distribution of T cells following immunotherapy with. *Oncoimmunology* 2013, **2**(8)**:** e25752.

292. Tannenbaum CS, Tubbs R, Armstrong D, Finke JH, Bukowski RM, Hamilton TA. The CXC chemokines IP-10 and Mig are necessary for IL-12-mediated regression of the mouse RENCA tumor. *Journal of immunology* 1998, **161**(2)**:** 927-932.

293. Hong M, Puaux AL, Huang C, Loumagne L, Tow C, Mackay C, *et al.* Chemotherapy induces intratumoral expression of chemokines in cutaneous melanoma, favoring T-cell infiltration and tumor control. *Cancer research* 2011, **71**(22)**:** 6997-7009.

294. Li H, Sim TC, Grant JA, Alam R. The production of macrophage inflammatory protein-1 alpha by human basophils. *Journal of immunology* 1996, **157**(3)**:** 1207-1212.

295. Groom JR, Luster AD. CXCR3 ligands: redundant, collaborative and antagonistic functions. *Immunology and cell biology* 2011, **89**(2)**:** 207-215.

296. Jahrsdorfer B, Weiner GJ. CpG oligodeoxynucleotides for immune stimulation in cancer immunotherapy. *Current opinion in investigational drugs* 2003, **4**(6)**:** 686-690.

297. Hemmi H, Takeuchi O, Kawai T, Kaisho T, Sato S, Sanjo H, *et al.* A Toll-like receptor recognizes bacterial DNA. *Nature* 2000, **408**(6813)**:** 740-745.

298. Krieg AM, Hartmann G, Yi AK. Mechanism of action of CpG DNA. *Current topics in microbiology and immunology* 2000, **247:** 1-21.

299. Krieg AM. CpG motifs: the active ingredient in bacterial extracts? *Nature medicine* 2003, **9**(7)**:** 831-835.

300. Brunner C, Seiderer J, Schlamp A, Bidlingmaier M, Eigler A, Haimerl W, *et al.* Enhanced dendritic cell maturation by TNF-alpha or cytidine-phosphate-guanosine DNA drives T cell activation in vitro and therapeutic anti-tumor immune responses in vivo. *Journal of immunology* 2000, **165**(11)**:** 6278-6286.

301. Davila E, Kennedy R, Celis E. Generation of antitumor immunity by cytotoxic T lymphocyte epitope peptide vaccination, CpG-oligodeoxynucleotide adjuvant, and CTLA-4 blockade. *Cancer research* 2003, **63**(12)**:** 3281-3288.

302. Weiner GJ, Liu HM, Wooldridge JE, Dahle CE, Krieg AM. Immunostimulatory oligodeoxynucleotides containing the CpG motif are effective as immune adjuvants in tumor antigen immunization. *Proceedings of the National Academy of Sciences of the United States of America* 1997, **94**(20)**:** 10833-10837.

303. Baral RN, Saha A, Chatterjee S, Foon KA, Krieg A, Weiner GJ, *et al.* Immunostimulatory CpG oligonucleotides enhance the immune response of anti-idiotype vaccine that mimics carcinoembryonic antigen. *Cancer immunology, immunotherapy : CII* 2003, **52**(5)**:** 317-327.

304. Carpentier AF, Chen L, Maltonti F, Delattre JY. Oligodeoxynucleotides containing CpG motifs can induce rejection of a neuroblastoma in mice. *Cancer research* 1999, **59**(21)**:** 5429-5432.

305. Kawarada Y, Ganss R, Garbi N, Sacher T, Arnold B, Hammerling GJ. NK- and CD8(+) T cell-mediated eradication of established tumors by peritumoral injection of CpG-containing oligodeoxynucleotides. *Journal of immunology* 2001, **167**(9)**:** 5247-5253.

306. Heckelsmiller K, Rall K, Beck S, Schlamp A, Seiderer J, Jahrsdorfer B, *et al.* Peritumoral CpG DNA elicits a coordinated response of CD8 T cells and innate effectors to cure established tumors in a murine colon carcinoma model. *Journal of immunology* 2002, **169**(7)**:** 3892-3899.

307. Bogdan C. Regulation of lymphocytes by nitric oxide. *Methods in molecular biology* 2011, **677:** 375-393.

308. Bevilacqua MP. Endothelial-leukocyte adhesion molecules. *Annual review of immunology* 1993, **11:** 767-804.

309. Kashiwagi S, Tsukada K, Xu L, Miyazaki J, Kozin SV, Tyrrell JA, *et al.* Perivascular nitric oxide gradients normalize tumor vasculature. *Nature medicine* 2008, **14**(3)**:** 255-257.

310. Tsukahara H, Ende H, Magazine HI, Bahou WF, Goligorsky MS. Molecular and functional characterization of the non-isopeptide-selective ETB receptor in endothelial cells. Receptor coupling to nitric oxide synthase. *The Journal of biological chemistry* 1994, **269**(34)**:** 21778-21785.

311. Buckanovich RJ, Facciabene A, Kim S, Benencia F, Sasaroli D, Balint K, *et al.* Endothelin B receptor mediates the endothelial barrier to T cell homing to tumors and disables immune therapy. *Nature medicine* 2008, **14**(1)**:** 28-36.

312. Spiecker M, Darius H, Kaboth K, Hubner F, Liao JK. Differential regulation of endothelial cell adhesion molecule expression by nitric oxide donors and antioxidants. *Journal of leukocyte biology* 1998, **63**(6)**:** 732-739.

313. Lefer AM, Lefer DJ. The role of nitric oxide and cell adhesion molecules on the microcirculation in ischaemia-reperfusion. *Cardiovascular research* 1996, **32**(4)**:** 743-751.

314. Khan BV, Harrison DG, Olbrych MT, Alexander RW, Medford RM. Nitric oxide regulates vascular cell adhesion molecule 1 gene expression and redox-sensitive transcriptional events in human vascular endothelial cells. *Proceedings of the National Academy of Sciences of the United States of America* 1996, **93**(17)**:** 9114-9119.

315. Takahashi M, Ikeda U, Masuyama J, Funayama H, Kano S, Shimada K. Nitric oxide attenuates adhesion molecule expression in human endothelial cells. *Cytokine* 1996, **8**(11)**:** 817-821.

6 ABBREVIATIONS

A

ACT adoptive cell therapy
AIRE autoimmune regulator
ANGPT2 angiopoeitin 2
APC antigen presenting cell
ARG1 arginase 1

B

B16-OVA ovalbumin-expressing B16
BAC bacterial artificial chromosome
b-FGF basic-fibroblast growth factor
BMCP basophil-mast cell common progenitor

C

C3a complement factor 3a
C5a complement factor 5a
CAF carcinoma-associated fibroblast
CAR chimeric antigen receptor
CCL2 chemokine C-C motif ligand 2
CCL3 chemokine C-C motif ligand 3
CCL4 chemokine C-C motif ligand 4
CCL5 chemokine C-C motif ligand 5
CCL7 chemokine C-C motif ligand 7
CCL11 chemokine C-C motif ligand 11
CCL19 chemokine C-C motif ligand 19
CCL20 chemokine C-C motif ligand 20
CCL22 chemokine C-C motif ligand 22
CCL24 chemokine C-C motif ligand 24
CCL28 chemokine C-C motif ligand 28
CCR1 chemokine C-C motif receptor 1
CCR2 chemokine C-C motif receptor 2
CCR3 chemokine C-C motif receptor 3
CCR4 chemokine C-C motif receptor 4
CCR7 chemokine C-C motif receptor 7
CCR10 chemokine C-C motif receptor 10
cDNA complementary deoxyribonucleic acid
c-Kit mast/stem cell growth factor receptor
CLIP clodronate-loaded liposomes
CLP common lymphoid progenitor
CMP common myeloid progenitor
CpG cytosine-phosphorothioate-guanine
CTLA4 cytotoxic T lymphocyte antigen-4

CVID common variable immunodeficiency
CX3CL1 chemokine C-X3-C motif ligand 1
CXCL2 chemokine C-X-C motif ligand 2
CXCL5 chemokine C-X-C motif ligand 5
CXCL6 chemokine C-X-C motif ligand 6
CXCL9 chemokine C-X-C motif ligand 9
CXCL10 chemokine C-X-C motif ligand 10
CXCR1 chemokine C-X-C motif receptor 1
CXCR4 chemokine C-X-C motif receptor 1

D

DAMP danger-associated molecular pattern
DARC duffy antigen/chemokine receptor
DC dendritic cell
DT diphtheria toxin
DTR diphtheria toxin receptor

E

EBI3 Epstein-Barr virus induced gene 3
EC endothelial cell
ECM extracellular matrix
eGFP enhanced green fluorescent protein
eNOS endothelial nitric oxide synthase

F

FAP fibroblast-activating protein
FasL fas ligand
FcεRI high-affinity immunoglobulin E receptor
FDA United States Food and Drug Administration
FGF fibroblast growth factor
FGF1 fibroblast growth factor 1
fMLP N-formyl-methionine-leucine-phenylanaline
Foxp3 forkhead box P_3

G

GIST gastrointestinal stromal tumors
GM-CSF granulocyte macrophage colony-stimulating factor
GMP granulocyte-monocyte progenitor
gp100 glycoprotein 100
GTN glyceryl trinitrate

H

HB-EGF heparin-binding epidermal growth factor
HIF-1 hypoxia-inducible factor-1
HIF-2 hypoxia-inducible factor-2

HSC hematopoietic stem cell
HUVEC human umbilical vein endothelial cell

I

ICAM-1 intracellular adhesion molecule-1
ICAM-2 intracellular adhesion molecule-2
IDO indoleamine 2,3-dioxygenase
IFN-α interferon-alpha
IFN-β interferon-beta
IFN-γ interferon-gamma
IgA immunoglobulin A
IgD immunoglobulin D
IgE immunoglobulin E
IL-1β interleukin-1beta
IL-2 interleukin-2
IL-3 interleukin-3
IL-4 interleukin-4
IL-5 interleukin-5
IL-6 interlukin-6
IL-8 interleukin-8
IL-9 interleukin-9
IL-10 interleukin-10
IL-12 interleukin-12
IL-13 interleukin-13
IL-17 interleukin-17
IL-18 interleukin-18
IL-25 interleukin-25
IL-33 interleukin-33
IL-35 interleukin-35
iNOS inducible nitric oxide synthase
iTreg inducible regulatory T cell

L

LAG-3 lymphocyte-activation gene-3
LAMC2 laminin, gamma 2
L-NIL N6-(1-iminoethyl)-L-lysine
LPS lipopolysaccharide
LTB lymphotoxin beta
LTC_4 leukotriene C_4

M

M-CSF macrophage colony-stimulating factor
MDS myelodysplastic syndrome
MDSC myeloid-derived suppressor cell
MHC major histocompatibility complex
MIF macrophage inhibitory factor
mMCP8 mast cell protease 8

MMP10 matrix metallopeptidase 10
MRC1 mannose receptor 1, c type 1
mRNA messenger ribonucleic acid
mTEC medullary thymic epithelial cells
MX1 myxovirus resistance 1

N

NK natural killer
NO nitric oxide
nNOS neuronal nitric oxide synthase
nTreg natural regulatory T cell

O

ODN oligodeoxynucleotide
OVA ovalbumin

P

PAF platelet activating factor
PAMP pathogen-associated molecular pattern
PanNET pancreatic neuroendocrine tumor
PDGF platelet-derived growth factor
PDGF-α platelet-derived growth factor-alpha
PD-1 programmed death receptor-1
PD-L1 programmed death ligand-1
PD-L2 programmed death ligand-2
PGD_2 prostagladin D_2
PGE_2 prostagladin E_2
PlGF placental growth factor
PLIP PBS-loaded liposomes
PMA phorbol myristate acetate
PPARG peroxisome-proliferating receptor-γ

Q

qRT-PCR quantitative real time-polymerase chain reaction

R

RAG2 recombination activating gene 2
RGS5 regulator of G-protein signaling 5
RIP rat insulin promoter
RMA-Tag simian virus 40 large T antigen-expressing RMA
RNA ribonucleic acid
RNS reactive nitrogen species
RT5 Rip1-Tag5
RT-PCR real time-polymerase chain reaction

S

SELE E-Selectin
SEMA4D semaphoring 4D
SLC7A2 solute carrier family 7(cationic amino acid transporter,y+system), member 2
SOD2 superoxide dismutase 2
SV40-Tag simian virus 40 large T antigen

T

TAM tumor-associated macrophage
TCR T cell receptor
Th-1 T-helper 1
Th-2 T-helper 2
TGF-β transforming growth factor-beta
TIM-3 T cell immunoglobulin mucin-3
TLR toll-like receptor
TLR9 toll-like receptor 9
TNF tumor necrosis factor
TNF-α tumor necrosis factor-alpha
TRAIL tumor necrosis factor-related apoptosis-inducing ligand
Treg regulatory T cell
TRP-1 tyrosinase related protein-1
TRP-2 tyrosinase related protein-2
TSLP thymic stromal lymphopoietin

U

UBD ubiquitin D

V

VCAM-1 vascular cell adhesion molecule-1
VEGF vascular endothelial growth factor
VEGF-α vascular endothelial growth factor-alpha